Modeling Simple Epithelium Tissue Using Tensegrity Structures

by

Susan Jane Crawford-Young

A Thesis submitted to the Faculty of Graduate Studies of

The University of Manitoba

In partial fulfilment of the requirements of the degree of

MASTER OF SCIENCE

Graduate Program in Biomedical Engineering

University of Manitoba

Winnipeg, Manitoba

Abstract

The mechanical contribution to tissue behaviour is an important part of tissue development, homeostasis, and disease. Mechanical models of tissues are used in many areas of study including simulations, tissue engineering and the development of replacement parts for the body, and Optical Coherence Elastography where models are used for verification. Discovering some of the behaviors of tissue due to the structure alone will give more insight into the mechanics and behavior tissues. Structures that have tension as a main component of their architecture are called tensegrities and have different behaviors from normal structures that are mainly built to withstand compression.

A model consisting of a single layer of three cells and their attachments was developed using simple tensegrities as a base structure. Tensegrities are formed of a truss structure of strings and bars where the tensioned strings hold the structure upright. Having only two base parameters of elasticity one for the strings and one for the bars make the model more efficient computationally. The model was made into three forms representing squamish tissue – short model, cuboidal tissue – medium sized model, and columnar tissue – tall model. These models were then tested using physiological ranges of size, force, attachments and prestrains in both tension and compression. The resulting force-distance and stress-strain curves were evaluated and found to have both linear and non-linear slopes. The stress-strain curves were shown to model real tissue in tension and compression. The models developed were compared to data from tissue and found to closely match the data for the tissue. The factors that influence the mechanics of the tissue model are the cytoskeleton, the cell attachments and the base attachments, and these are the known factors that influence the mechanics of cell sheets. The models are adjustable by modifying the values of the strings and bars of the tensegrity models and the test conditions.

Acknowledgements

I would like to thank the University of Manitoba, Department of Biomedical Engineering, Dr. S. Sherif, Dr. Q. Zhang and my family for giving me the opportunity to create this study and thesis.

List of Tables Page

List of Equations Page

List of Figures Page

Table of Contents Page

1.0 Introduction

Epithelia are a main animal tissue type in the body and are the covering for organs and form skin and other diverse tissues such as the alveolar sacks of the lung. They are the tissue that protects our body from the exterior environment.

Epithelial tissue has a distinctive mechanical form where cells are attached to each other with a tight – adherens junction complex connecting cells through trijunctions at the corners of three cells and more junctions as necessary. There is an actomyosin ring at the apical side of the cells which connects through the tight-adherens junctions creating a connected confluent tissue that can tighten with contraction of the actomyosin complex. The cells basal side is connected to a basement membrane using integrin complexes which are also composed of cell cytoskeleton components.

The structure is kept in tension and is considered to be a tensegrity structure with the cell cytoskeleton acting as the parts of the tensegrity. Knowing what the mechanics of the structure is important in understanding the overall mechanical behavior of epithelial tissue.

The mechanical properties of tissues are important to their form and function in living systems. Epithelial tissues are on the exterior of the body or body parts. They separate the organs, line the digestive tract and lungs and are our skin or integumentary system.

Discoveries of the effect the mechanics of cells and tissues, on cell morphology and genetic expression have been shown to be an integral part of cell physiology (Kalukula et al., 2022). Modeling the mechanics of cells is becoming an important part of studying cell mechanics and many models of epithelial cells have been made in the past. Most of the epithelial tissues have been modeled as single cells (Smallwood, 2009). Cells in a tissue behave differently than those of a single cell due to their interactions with each other (Gjorevski and Nelson, 2012). Being able to extrapolate the viscoelasticity and other measures such as the elasticity, shear, creep, and mechanical property of relaxation gives insight into the whole cell and tissue physiology.

The mechanical properties of epithelia tissue allow them to act as barriers tissue and it is important to be able to model the tissue in order to study their over all mechanics, different mechanics for healthy and diseased state, design artificial tissue and assist in imaging tissue properties. Tissue including epithelial tissue are viscoelastic with non-linear stress-strain curves. The stress strain curves are produced by

measuring the amount a tissue stretches as force is applied to the tissue. A typical stress-strain curve is shown in Figure 1.1.

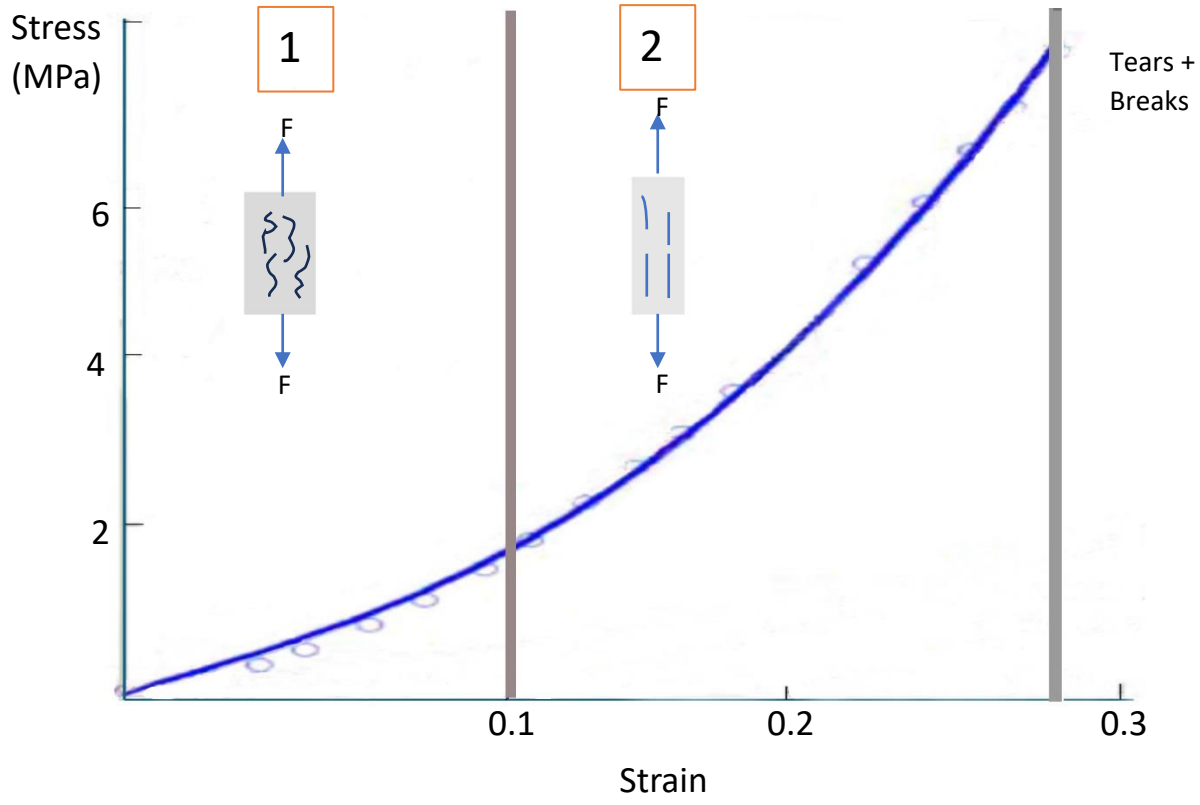

Figure 1.1 *Stress-strain curve for skin under tension. The boxes in areas 1 and 2 show the alignment of the collagen fibers in skin as they are loaded. Collagen aligns with the direction of stretch (Dwivedi et al., 2022; Fernades et al., 2019).*

The curve in Figure 1 is J shaped and shows a change of state in the tissue-material where the fibers go from unaligned to aligned. This shape of stress-strain curve is common in all tissue types.

There is a wide variety of modeling created to model cells and tissues. Some are commercially available and open source software whole others are in house programming for specific purposes (Glazner, 2024 In conversation). Some modeling is for molecular the molecular scale and some is for macroscale tissue level models and everything in-between.

For mechanical modeling continuum mechanics is often used with tissues represented by spring-dashpot models to model their behavior. Tissues are viscoelastic and are a tensioned soft matter material therefore the spring-dashpot model works for individual situations within a limited range. The models have different arrangements of the spring and dashpots to match the materials that are being studied.

Another common use model is to curve fit the observed behavior with hyperelastic curves such as the Ogden model. (Lohr et al., 2022). The Ogden model measures isotropic tissue well and usually combines shear measurements with compression and tension measurements to obtain mechanical parameters. The model measurements in tension are between 0.0 and 2.0 strain. The Ogden model is often used in time dependent studies and is often implemented in finite element studies. The model is insensitive to some loading conditions and shear in tissues like epithelial tissue because epithelial tissue tends to fluidize in shear (Atia and Fredberg, 2023).

A general model that is used for epithelial tissue is the vertex model which can be used in 3D but is mostly used in 2D to model the behavior of cell sheets. Using CompuCell3D as an example does not give precise forces involved in the observed process that are modeled (Glazner 2024 in conversation). This model gives insights into cell behavior but do not precisely model the forces involved.

Models available usually don't cover the range of strain that tissues operate under which usually occur between 0.0 and 0.5 strain and beyond. Some examples of this are given in Fernades et al., 2019; Wozniak et al., 2009; Xu et al., 2022; and Dwivedi et al., 2022.

Tensegrity models show non-linear stress-strain or force-displacement curves in many instances (Fraternali, 2015). Tissues show nonlinearity in their elasticity which is the elastic modulus calculated from the stress-strain curves they produce under load. The structure of cells and tissues are structures in tension and are thought to be tensegrities (Ingber, 2014) and therefore it is worthwhile to investigate tensegrity builds for use in tissue modeling. These models cover a larger range of strain than conventional models.

Objectives

Build a tensegrity model of mammalian tissue. Find the direct value of the changing Modulus of Elasticity for a simplified tensegrity model of tissue that will be measured using stress-strain or similar force-displacement curves. Then compare the modulus of elasticity to real tissue measurements.

2.0 Literature Review

2.1 Epithelial Tissue

Epithelial tissue has a different structure from internal body animal tissue. It is attached to a fibrous thin film and the cells have an actomyosin belt usually at their apex of their cells and are attached to each other at the belt to form a network. The actin and myosin complex that is incorporated into the belt acts in a similar way to muscle and can tighten or pre-strain the belt. Epithelial tissue is a confluent or connected

tissue that is exterior or interior to the body. There are four basic types of cells Squamous, cuboidal, columnar and pseudostratified. There are many single layered epithelial tissues but many are also many layered – called stratified epithelia. See Figure 2. (Lemki and Nelson, 2021). Epithelia tissue has been studied and imaged both in-vivo and in-vitro in embryology, cell physiology, wound healing and cancer. The structure of this tissue has been mapped and cells of the epithelia are bound together with junctions at an actomyosin ring around the circumference of the cell. This gives the tissue a unique structure.

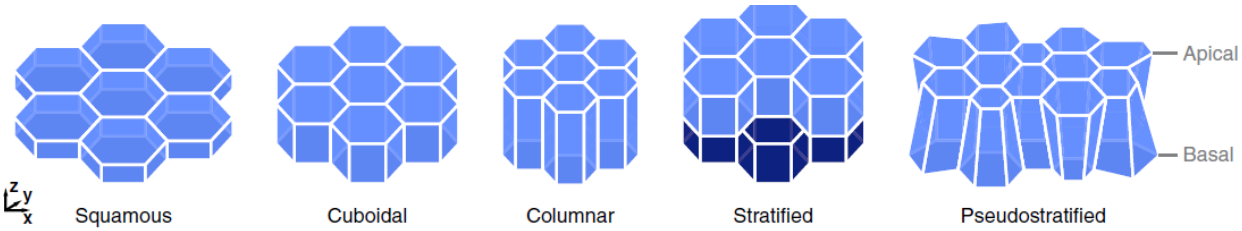

Figure 2.1 *Illustration of the different cell shapes in epithelial tissue (Lemki and Nelson, 2021)*

The different shapes allow for different functions in epithelial tissue with squamous cells used for diffusion (ling alveoli), cuboidal secretion (ducts and glands), columnar absorption (intestine) and pseudostratified mixed function (bronchial tubes). Epithelial cells are all attached to a basement Membrane or extracellular matrix (ECM) at the basal part of the cell. Cells in epithelial tissue are attached on all sides except the top or apical side with cellular junctions.

Epithelial cells are all between the width of 10 - 30 µm and are of varying heights:

- Squamous 0.2 – 0.5 µm
- Cuboidal 5 – 10 µm
- Columnar 20-30 µm

The size of cells depends on the species of the animal, their location in the body, and their function. A squamous cell is defined as height/width << 1, cuboidal height/width ~ 1, and columnar height/width>>1 (Puliafito, 2017).

2.1.1 Cell cytoskeleton

Cells and tissues have a cytoskeleton with three main categories: microfilaments, intermediate filaments, and microtubules as seen in Figure 2.2.

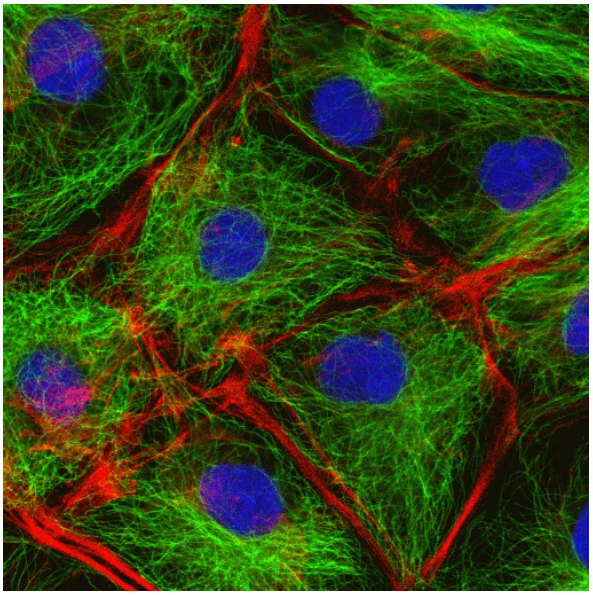

Figure 2.2 *Animal cells stained with fluorescent labels microtubules (green), actin (red), and the nucleus (blue) (Shipman et al., 2020)*

The intermediate filaments are not show in Figure 3 as this is an image of the apical part of the cell and the intermediate filaments are often associated with the nucleus.

Microfilaments mostly consist of actin and are found at the periphery of cells (Ni et al., 2022). In epithelial and endothelial cells the actin fibers form a belt around the circumference of the cell (Dufort et al., 2011; Kokkinos et al., 2010; Saraswathibhatla, 2023). The actin is often bundled into linear fibers and is often associated with non muscle myosin at the attachment or junctions between cells called adherens junctions (Kaunas et al., 2011; Vanderleest et al., 2018). The adherens junctions and actomyosin belt are often at the top or apical part of the cell but on stiffer substrates the belt and adherens junction can be at the bottom or basal part of the cell (Vanderleest et al., 2018). The myosin and actin work together to move the actin fibers in a similar way to what occurs in muscle with the ratcheting head on the myosin moving along the actin (Kaunas et al., 2011). This tightens the junctions between cells and shifts their boundaries (Morris, 2021). Myosin also forms in a matt at the apical part of the cell and this can affect the cell mechanics (Bieling, 2016). The actomyosin belt is made up of bundled fibers with other molecules such as actinin that attach the fibers together (Kaunas et a., 2011). The elasticity of the actin is one Giga Pascal (Ingber et al., 2014) and actin bundles are 10 nm in diameter (Pegoraro et al., 2017)

The intermediate filaments are actually a group of filaments with two of the filaments being vimentin and keratin. The keratin intermediate filament is most prominent in epithelial cells with vimentin expressed in motile or crawling cells (mesenchyme) cells (Schepers, 2022; Lorenz et al., 2023). Intermediate filaments

are more elastic than actin filaments and are thought to work with actin under some conditions of large strain (Schepers, 2022). Keratin is linear until a strain of 0.7 and then they stiffen, also during cyclic strain they elongate but keep their original strain value (Lorenz et al., 2023). Intermediate filaments are 1 µm in diameter and have elasticity that ranges form 1 to 10 MPa (Ingber et al., 2014). Networks of filaments form due to crosslinking which are transient and affect the network value of the shear modulus. The crosslinking unbinds more commonly at low frequencies changing the shear value (Schepers, 2022).

Microtubules are the larger and stiffer cytoskeleton element with a persistence length Lp > 1 mm (Ingber et al., 2014; Pegoraro et al. 2017). This persistence length makes microtubules a candidate for bars in a tensegrity structure. For microtubules to act as bars they need to be stiffened and this can occur when microfilaments attached to the sides of microtubules pull on the microtubule in the same way a flag pole is stiffened by guide wires. Microtubules stabilize the apical part of cells. Microtubules are stiffened by strain. Compression can stabilise cell cytoskeleton and align microtubules with actin (Purta et al., 2023).

The combination of actin belts with adherens junctions attachments forms a network of actomyosin in tissues. Tissue is a combined network that acts together. Cells in a tissue are not the same as the individual cells that are taken out of that tissue. This is most striking in circulatory endothelial cells which need to experience blood pressure, flow, and curvature to maintain their structure and function (Dessallis et al., 2021). Cells will often undergo apoptosis if removed from their tissue and epithelial tissue can change into motile mesenchyme tissue in what is referred to as epithelial to mesenchyme transition (Putra et al., 2023). The model of tissue should therefore include the concept of cable networks (Coughlin and Stamenovic, 2003). The networks include actin filaments that are prestressed and attached to a substrate. The confluency of the tissue is an important property of tissue mechanics. Kidney cells grown in a monolayer had lower stiffness that the same cells grown as single cells or in a wound healing assay (Efremov et al., 2013).

Filament Type	**D (nm)**	**Lp (µm)**	**E (MPa)**	**E_{max}(MPa)**	**F_{max} (nN)**	**ε_{max} (%)**	**B ($pN.\mu m^2$)**
Actin microfilaments	5 - 10	10 - 20	2600	*	0.4	0.9	0.073
Microtubules	25/12	5000	1700	*	*	*	22 - 44
Intermediate filaments	10	1	6.4	80	14	220	0.003
Stress fibers	200-1000	*	1.45	100	380	275	$\geq$100

D – filament diameter; Lp – persistence length; E – elastic modulus; $\mathbf{E_{max}}$ – elastic modulus associated with F_{max}; F_{max} – tensile force at which the filament breaks; $\boldsymbol{\varepsilon_{max}}$ - strain corresponding to Fmax; B –bending rigidity; * no data available. Data for microtubules include inner/outer diameters.

Table 1 *Types of cell cytoskeleton and their properties (Stamenovic and Wang, 2011).*

The actin microfilaments and microtubules are in bundles in cells making the representative bundled actin and microtubules at least a magnitude larger than their representative single filament. The mechanical properties are determined by the actomyosin and other molecules that bind the bundles together (Rodriguez et al., 2013).

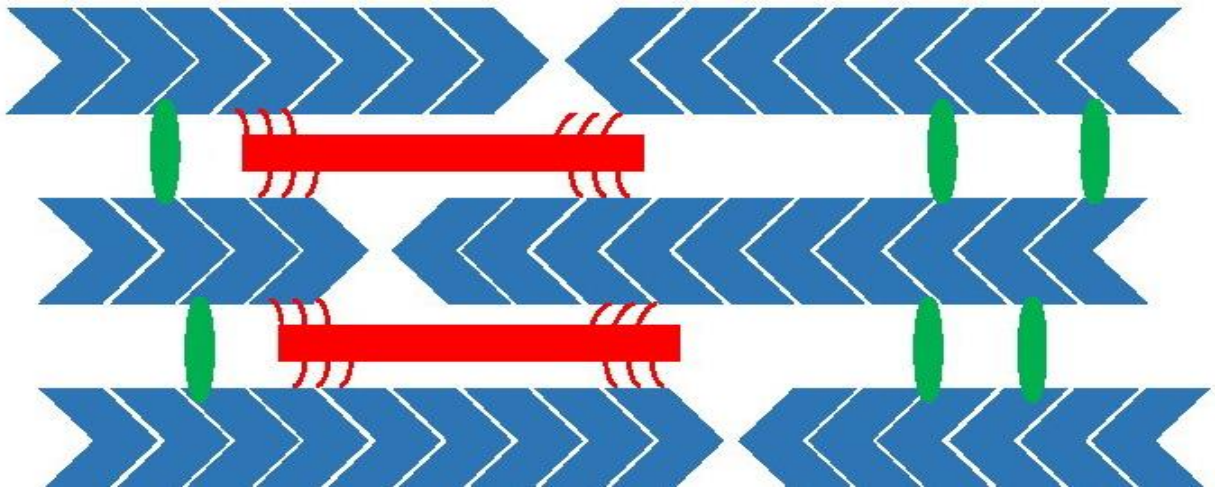

Figure 2.3 *Actomyosin stress fibers. F-actin - blue , myosin – red, and actinin – green (Kassianidou et al., 2015)*

There are other molecular cross-linkers such as a-actinin (Rodriguez et al., 2013).

The cytoskeleton components are thought to be tensegrity structures. The concept of tensegrity structures scales from cytoskeleton components at the cellular level to larger structures in the body such as muscle - tendon and bone. Using tensegrity structures to model tissue fits with this concept and should be scalable to bulk tensegrity representations to be computational efficient. Scalability of tensegrity structures is a problem that needs to be carefully studied and finding equivalent structures may have to be modeled experimentally rather than analytically (Gilewski and Al Sabouni-Zawadzka, 2021).

2.1.2 Cell Attachments

The actinomycin belt that circles epithelial cells is attached to adjacent cells in tissue by tight junctions, adherens junctions, and desmosomes in vertebrates (Higashi, 2017).

A side view of epithelial tissue shows the connections of the cytoskeleton to the next cell, to the basement membrane and to the nucleus inside the cell (Figure 5). The change of attachments and shape of the cell will affect the nucleus and can cause genetic change (Kalukula et al., 2022).

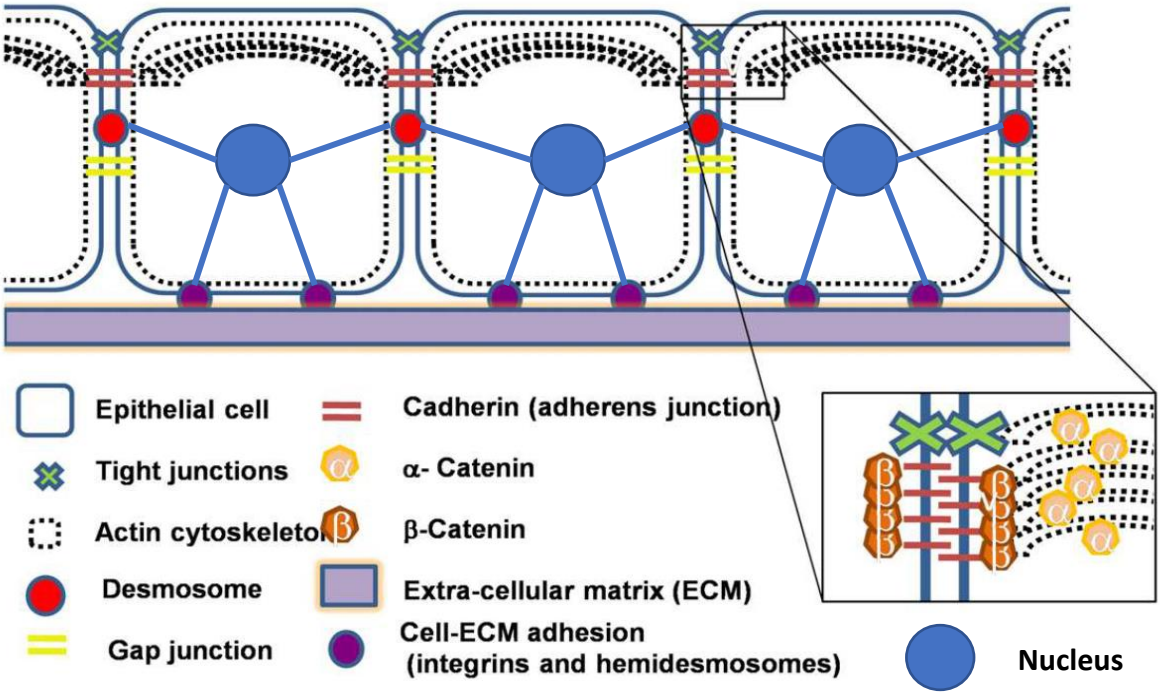

Figure 2.4 *Side view of epithelial cells showing their attachments (Kokkinos, 2010 – modified)*

The tight junctions help the tissue repel external substances from entering the tissue or any of the tissue that is below the epithelial cells.

The Cadherin - adherens junctions are associated with non-muscle myosin and the actin-myosin complex tightens the actin or actomyosin belt around the apical part of the cell.

The desmosomes attach the nucleus to the cell junctions and come into play when the cell has large mechanical forces applied to it (Schepers, 2022)

Gap junctions allow cell cytosol contents to flow from one cell to another allowing for exchange of water and other substances between cells in a tissue.

The attachments of the cells are to the other cells and to the substrate – Extra-cellular matrix (ECM). The main attachments that force is transmitted through are the tight junctions, adherens junctions and the Cell – ECM integrins.

The Tight Junctions are usually between 200-500 nm long and 11 – 15 nm wide with intermediate space between cells at 10 nm giving the junction size at an average of 300 nm long by around 35 nm in width. The Adherens Junctions are 200 to 300 nm long and up to 100 nm wide with intermediate space of 20 to 25 nm giving the junctions at an average of 250 nm long and 220 nm wide (Vanslembrouck et al, 2022).

Adding these two junctions together to give depth and width the whole complex situated around the actomyosin belt gives a distance in length from apical to basal of 400 to 800 nm long and width using adherens junction width of 220 to 225 nm. Assuming longer columnar cells have longer junctions for modeling. In summary the length of the junctions used for the model are a length 0.2 for squamish cells and 0.5 µm for the cuboidal and columnar cells. The width of the membrane around each cell is half the width of the adherens junction at 110 nm and approximately 0.1 µm.

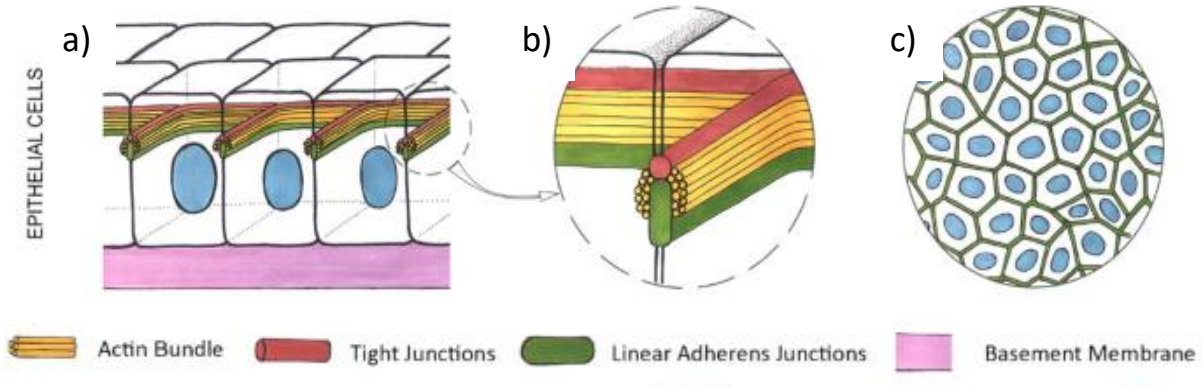

Figure 2.5 *Epithelial cell apical belt structure a) epithelial cells in a monolayer b) close-up area of stable cell-cell adhesion in epithelial cells c) a top view of a monolayer of epithelial cells, connected by stable linear adherens junctions (Rubtsova et al., 2021).*

2.1.3 Trijunctions

The most important and complicated of the junctions in tissue is the tricellular junction where three cells meet. The tricellular junction is the width of the actomyosin belt. There are also bicellular junctions along the length of the cell interface with the adjacent cells as shown in Figure 2.6 (Cartagena-Rivera, 2017; Higashi and Miller, 2017).

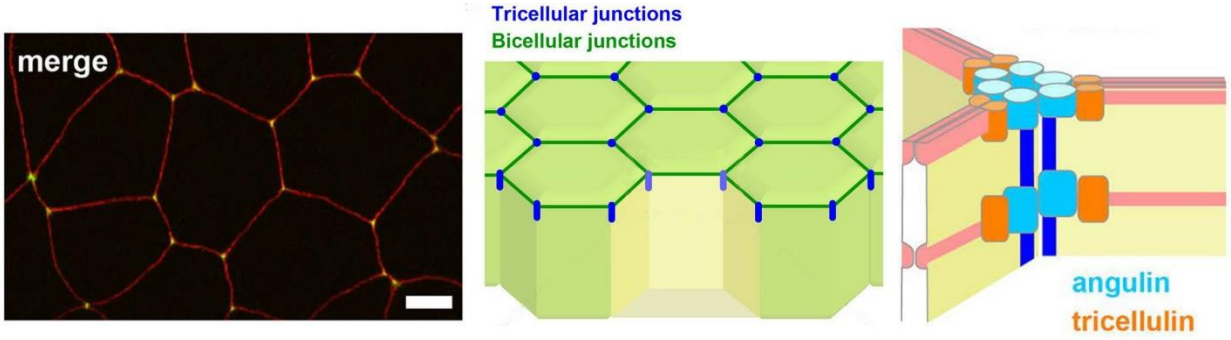

Figure 2.6 *Tricellular Junctions are at the corners of the packed cells and are a complex that includes the actin belt and the tight and adherens junctions. There are bicellular junctions around the periphery of cells. Scale bar 10 µm (Higashi and Miller, 2017).*

The cellular junctions in combination with the actomyosin belt adjusts the prestress in epithelial cells. Prestress or the stiffness in tissue is an important mechanical property that affects overall cell stiffness (Gu et al., 2023). The prestress comes from the actomyosin complexes in cells. In epithelial cells the actin in the actomyosin belt is associated with non-muscle myosin and force is transmitted through the adherens and tight junctions and the actomyosin belt(Cartagena-Rivera et al. 2017).

Epithelial tissue models can be formed using hexagon tiling over a surface. In confluent tissue the hexagons change shape and can be other shapes including octagons to squares and sometimes triangular depending on the balance of the forces within the tissue (Boyd et al., 2017). These shapes all form a mesh like continuous tiling. They act as a barrier between the environment and other tissues or between organs (Higashi and Miller, 2017).

In summary the apical end of epithelial cells are exposed to the environment and this means they are exposed to air or water type material. The basal bottom layer is attached to a thin film which is the Extracellular Matrix or basement membrane. There is an ring around the exterior of the cell made of actin bundles which can be tightened with the non-muscle myosin.

The distance between the actomyosin belts in cells and the gap where the junctions attached is the width of the cell membrane and some extracellular space. The total thickness across the cell membrane is about 10 nm x 2 = 0.02 um (Naser et al. 2022). The distance between epithelial cells range from 10 to 200 nm depending on the type of epithelial cell (Peckham et al., 2003)

2.1.4 Extracellular Matrix (ECM)

The substrate that cells attach to also determine the mechanical properties of tissue (Saraswathibhatla et al., 2023). The substrate in epithelial cells is a thin network called the Extracellular Matrix (ECM) or Basement Membrane. It varies in stiffness from soft approximately 100 Pa to hard approximately 10 KPa and varies in thickness from hundreds of nanometers to microns (Saraswathibhatla et al., 2023) . The cellular attachments are called integrins and they adhere to complexes in the cell that attach to the cytoskeleton of the cell and to the basement membrane. The extracellular matrix has a large effect on development or cell differentiation with harder ECM of 50 KPa producing bone, medium stiffness 10 KPa producing muscle and soft ECM 50 Pa producing neural tissue (Engler et al., 2006). It has been noted that the ECM in tension has a J-shaped – non-linear stress-strain curve (Guimaraes et al., 2020). The cellular processes that the ECM affects are cell spreading, migration, differentiation, division, apoptosis, tumor phenotype, morphogenesis, and matrix secretion (Saraswathibhatla et al., 2023). Cells create the ECM

that they attach to and in turn the ECM influences how the cells create the ECM and this feedback is a major influence on cell mechanical response (Guimardes et al., 2020). The amount of water in a cell changes the cytoskeleton dynamics. As ECM or basement membrane stiffness increases the cell volume decreases mainly due to efflux of water (Atia and Fredberg, 2023). This also slows the relaxation rate.

2.1.5 Cell Shape

Cell shapes also have influence on the mechanics of cells and their rearrangements or transitions (Sahu et al., 2019). Different cell types have a variety of cell cytoskeleton structures that are specific to the cell type and the orientation of microtubules in cells is important to their shape and function (Iwanski, 2024). The cell substrate or basement membrane is a part of the forces shaping the nucleus.

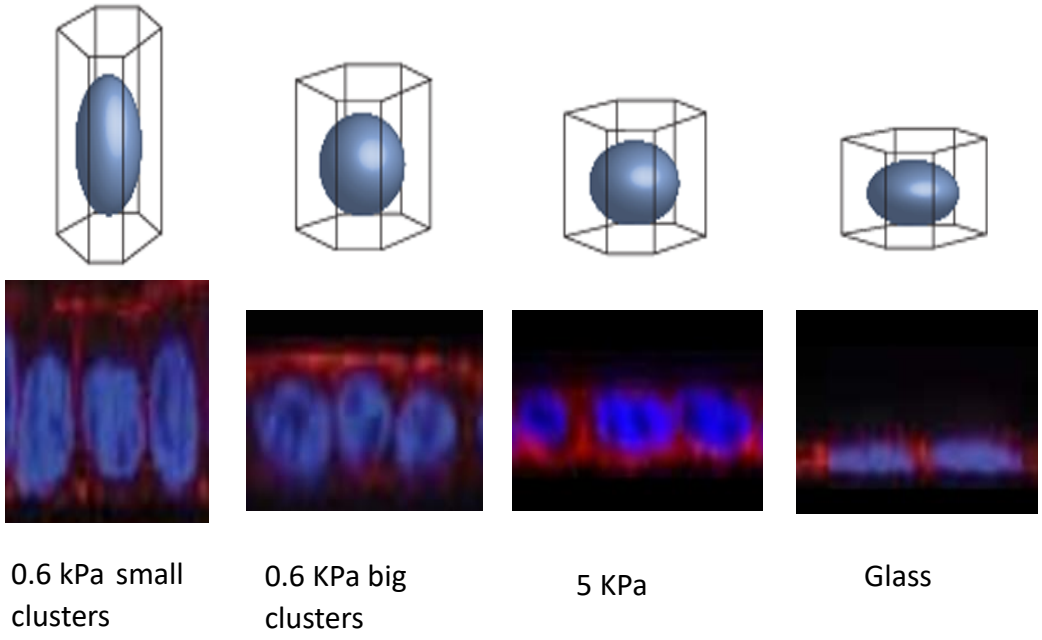

Figure 2.7 *Shape of cells and their nucleus due to substrate stiffness* ***Top*** *Shape of the tissue as a function of the substrate stiffness.* ***Bottom*** *Length of the rectangular boxes is 20um. The nucleus of the cells is in blue, Actin is in red (Kaliman et al., 2021).*

When the nucleus is compressed some of the nuclear pores are opened and the nuclear material is rearranged. This rearranges the DNA in the cell causing a genetic shift in the cell (Kalukula, 2022).

In the x-y or cross section shape is an important measurement as well and is the main parameter measured for the vertex model (Staddon et al., 2023). For large cross-section cells cross cell actin filaments will often form across the top of the cell (Lopez-Gay et al., 2020. A cell does not usually have a hexagon shape even

though that is the configuration that will tile a flat sheet. The epithelium cell's apex shape shift as forces change on the cell sheet. The basal portion of the cell is more stationary.

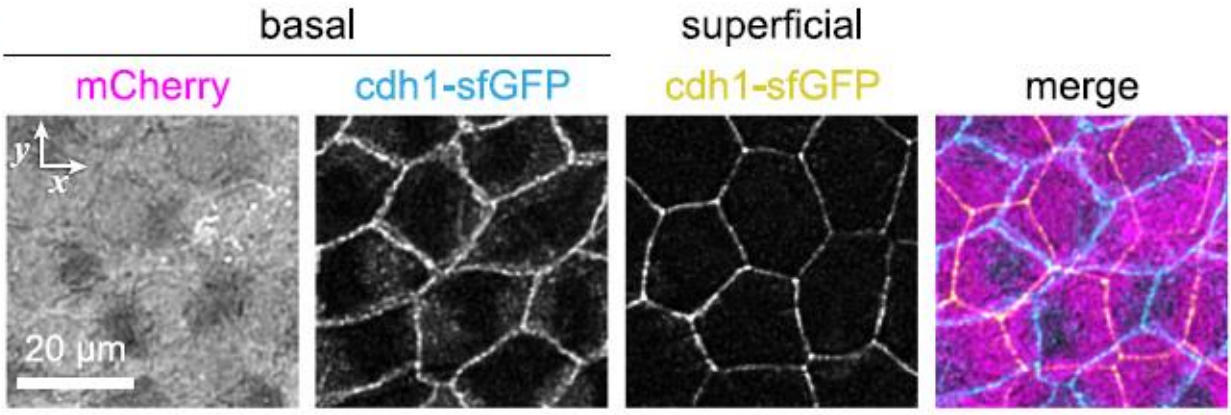

Figure 2.8 *Shapes of epithelial cells Left to right - Layers of cells shown with dyes: mCherry in basal cells and E-cadherin in basal and superficial cells - blue in basal and yellow in superficial cells. E-cadherin remains localized at the cell periphery in both layers (Kennard et al., 2023).*

The cells in Figure 9 are partly hexagon shaped and the apical or superficial parts of the cells do not align with each other. These shapes also affect the nucleus. The apical portion of cells change shape due to forces on the surface of the tissue and the amount of shape change from the hexagon shape are considered to be defects or disordered tilling (Tong et al., 2022). The defects are one of the main parameters that determine tissue mechanical properties (Staddon et al., 2023). Shape change can occur if the sides of the cell are shortened or there is more force applied to parts of the surface than in the other directions (Armengol-Collado et al., 2023; Morris, 2021).

Cells in the epithelial layer are confluent and in steady state are considered to be in a jammed or solid phase where cells are trapped by their neighbours. Sometimes due to perturbations the cells can become unjammed and form a fluidized sheet of cells that migrates. This is called unjamming transition (UJT) and is different from the epithelial to mesenchyme cell transition that occurs when epithelial cells are unattached from each other and become mobile crawling cells (Atia and Fredberg, 2023).

2.1.6 Chirality in Cells and tissue

Chirality exists in eukaryotic cells and organisms and is the foundation of left-right asymmetry (Inaki et al., 2016). The main cause of the asymmetry is in the actin cytoskeleton and the actin chirality is due to its cross-linking molecules such as alpha-actinin and myosin II. A crosslinker called Fascin is also a cross-linker but this molecule is not in mature epithelial cells (Zhang et al., 3023).

2.1.7 Other factors

Other factors in finding the stress-strain relationship in tissue are the rate of the applied force (Ünal et al., 2016) and the amount of ATP available in the tissue (Ebata et al., 2023). This includes the tissue's normal living physiological range as well as abnormal situations such as fast acting forces (Ünal et al., 2016) or cells deprived of oxygen-ATP in hypoxia (Cortes et al., 2019). Intermediate filaments act as a protection for cells when they are over 70% deformed (Pensalfini et al., 2023; Schepers, 2022). The intermediate filaments are attached to desmosomes on the sides of the cells and are attached to the nucleus (Chifflet and Hernandez, 2012; Balda and Matter. 2003). Cells can fine tune their mechanics with a change in pH as well (Schepers, 2022). The water and salt balance in tissue also changes the Force – Compression curve in cells (Sugimura et al., 2016). Cell reproduction and death will also change the mechanics of tissue (Ambrosini, 2017). Stretch fluidizes the cytoskeleton therefore stretching and then returning to normal configuration allows the cells to adapt to their mechanical environment. Breaking the bonds of both actin and microtubules are part of an active cells life (Atia and Fredberg, 2023; Ermakov, 2018). Cell membranes are reinforced with actin and sometimes keratin. This outer shell can also have a major influence on the stiffness of cells and tissue (Shepers, 2022).

2.1.8 Measuring Force Deformation Behavior of Epithelial Tissue

Individual cells are measured in Atomic Force Microscopy (AFM) by indenting the cells and the forces of indentation are in the nano-Newtons (nN) (Sim et al., 2015). This magnitude of force nN is observed in cells using micro-posts (Rodriguez et al., 2013). Measuring the forces quantitatively in the epithelial layer is an unsolved problem. Mapping the curvature of single cell layer epithelia due to known stress has been measured using controlled geometry (Marin-Llaurado et al., 2023).

2.1.9 Stress-Strain Curves of Cells and Tissues

There are many ways to measure the stress and strain in tissue and some of them are mainly compression measurements and others are mainly tension measurements. Some of the methods for cells are; Atomic Force Microscopy (AFM) (compression, frequency), Micropipette aspiration (tension), Rhinometry (frequency application), optical tweezers, laser ablation, micro pressure probes and magnetic beads plus various lab made devices (Schwayer and Bruckner, 2023). Different resulting curves are obtained from each type of measurement. Compression and tension curves are normally different in materials and there are different methods of applying frequence for material measurement (Polio et al. 2018). For AFM the frequency of the force was converted in FDC Micro-rheology for a tip velocity of 10 µm s−1 equivalent

frequency of 166 Hz, Tip velocity of 60 µm s−1 (1 kHz), tip velocity of 150 µm s−1 (2.5 kHz) and tip velocity of 300 µm s−1 (5 kHz) (Garcia et al., 2020).

The rate of the applied force changes the Stress-Strain or Force-Displacement curve as does the amount of oxygen and other necessary parts of the cell such as actin, myosin, calcium, cadherin, catenin, vinculin, actinin and Microtubules.

There is a difference in the stress-strain curve for two cell attachment depending on the strain rate shown in Figure 2.9.

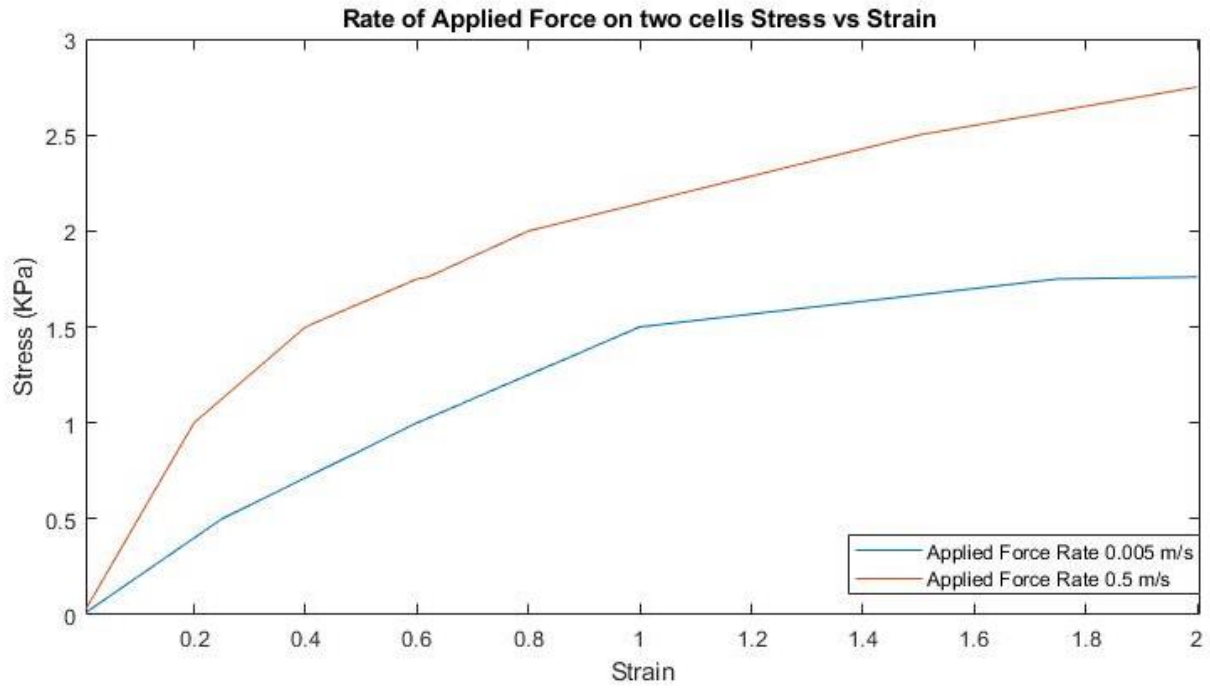

Figure 2.9 *Two cell attachment stress-strain showing the change in the stress-strain curve with rate of strain (Data taken from Esfahani et al., 2020).*

The rate of applied stress or force can make a large difference in the tissue response and the stress-strain curve. Different types of cells also have different stress curves shown in Figure 2.10.

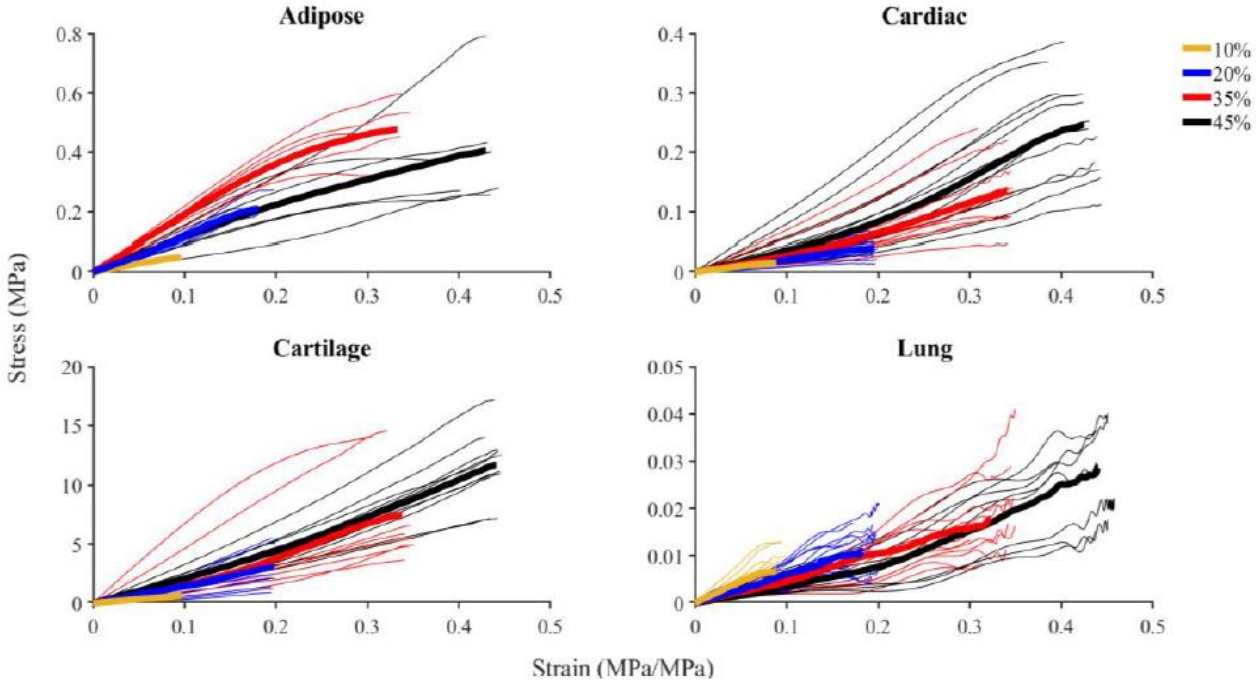

Figure 2.10 *Compression Load Stress – strain graphs for different tissue. Compression Load - 10% (yellow), 20% (blue), 35% (red), 45% (black) compressive strain. Each sample was assigned to a single strain group and was only tested once (Wozniak et al., 2009).*

Tissues that are from the same area such as the trachea and bronchi of the lungs have different Stress-strain curves as seen in Figure 2.11.

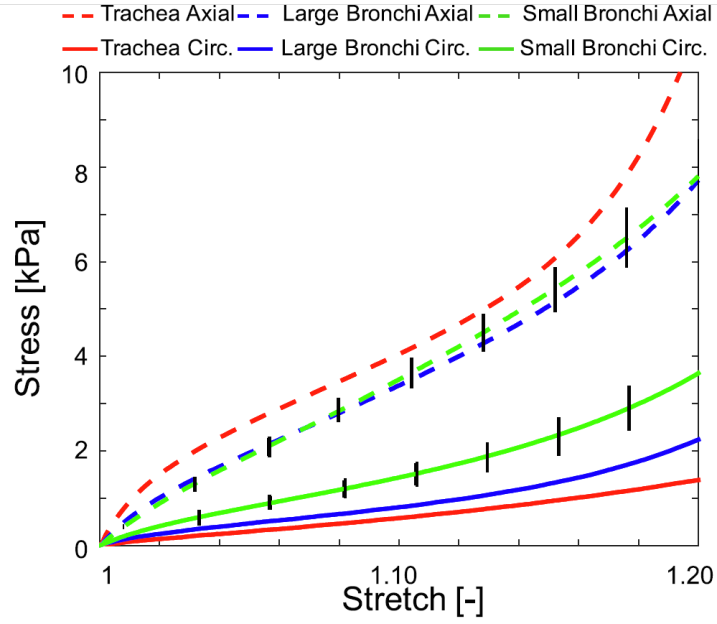

Figure 2.11 *Lung – Porcine sample tissue in tension (Eskandari et al., 2019).*

The number of cells and their orientation also have influence on the Stress-strain curves Figure 2.12.

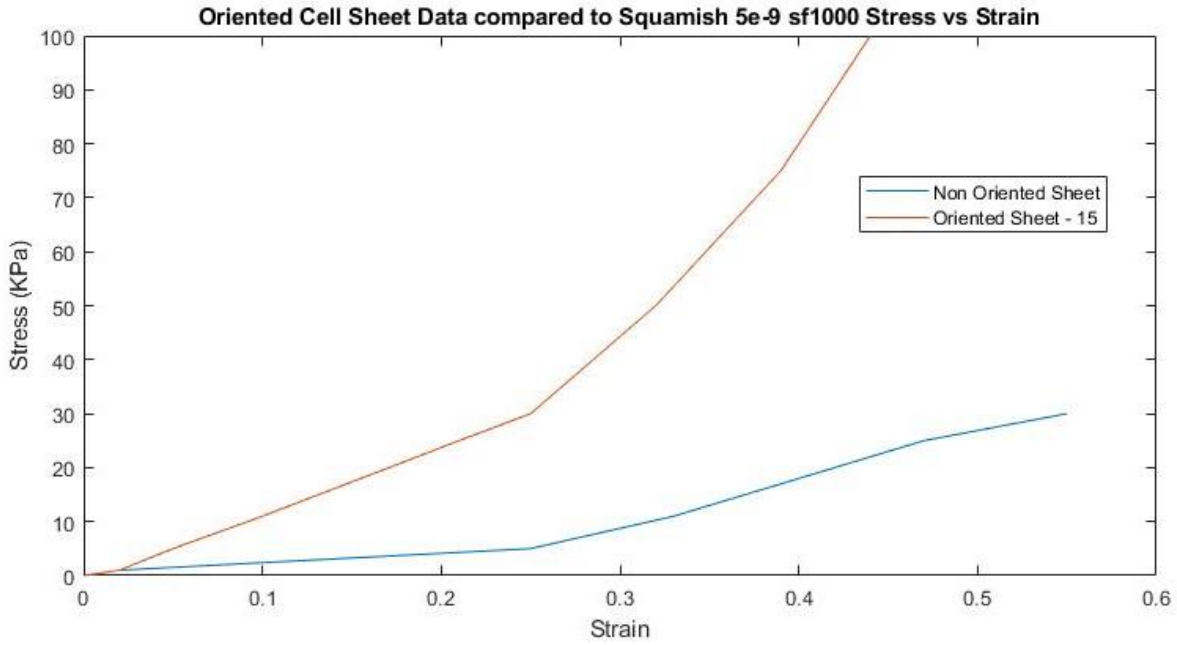

Figure 2.12 *Stress-Strain curve of cell sheets measured with a stretching apparatus. Oriented cell sheets – OCS, Not oriented cell sheets – NOCS, OCS-15 prepared on 15 µm × 15 µm × 5 µm groove patterns Data Taken from (Xu et al., 2022).*

Other graphs in this series are OCS-5 on 5 µm × 5 µm × 5 µm groove patterns, OCS-10 cell sheets prepared on 10 µm × 10 µm × 5 µm grove patterns which are all higher – stiffer than the above curves.

The curves in Figure 2.13 show the influence of the basement membrane on cells also the inset of the figure shows the unevenness of the force-displacement curve as it is not a smooth curve.

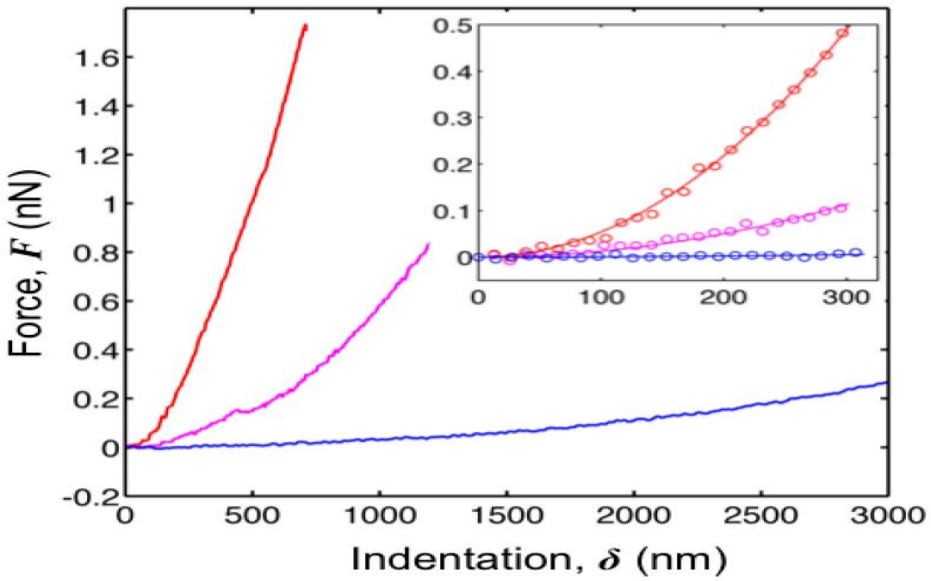

Figure 2.*13* *A set of three representative force curve data acquired for 3T3 fibroblasts cultured on; Red - glass Purple - 17 kPa polyacrylamide gel and Blue - 3 kPa polyacrylamide gel. Cells on the culture dish are 100 times stiffer than cells cultured on polyacrylamide gels. Inset is a close up of the start of the curve (Thomas et al. 2013).*

Basement membranes are estimated between 10 Kpa and 5 MPa (Kozyrina et al., 2020). The fibroblasts grown on a basement membrane would cover the range of the graphs shown in Figure 2.13.

Fibroblasts are epithelial cells and will have a similar structure to the models of cells built in this thesis. They are single cells so do not have the support of the surrounding tissue and will therefore not have the same magnitude of force that goes with the volume of indentation. The yield or fracture point is not noted in the simulations with the models because a yield point was not included in the material properties of the tensegrity compression and tension elements for microtubule and actin bundles. Measurements of the yield points of actin bundles and microtubule bundles has not been thoroughly studied.

2.2 Current methods of modeling tissue properties

2.2.1 Solid Mechanics and Measurement

Three standard formulas are used in defining the solid mechanics of a material formulas (1) to (4). Tissue is mostly composed of water and is therefore an incompressible material. Poison's ratio *v* is a measure of the compressibility of a substance. Poison's ratio ranges between 0 – 0.5 and tissue's range is between 0.45 – 0.5. A Poison's ratio of 0.5 means that the object or substance is incompressible. These values make the measurements of Bulk Modulus and Lame Modulus very large. Therefore the values for E – the

elasticity and for G – the shear modulus are used for tissue (Kennedy and Bamber, 2021). Two other time related measurements are relaxation and creep. Relaxation is the change in stress or force per area produced by a material when a strain is applied to a material and creep is the change in strain- shape that occurs when a constant force is applied to a material.

Young's Modulus – Elasticity $E = \frac{\sigma}{\varepsilon} = \frac{Stress}{strain}$ (1)

Poison's Ratio - Poisson's ratio v is the ratio of lateral to longitudinal strain in uniaxial tensile stress.

$$\text{Bulk Modulus } K = \frac{E}{3(1-2\nu)} \quad (2)$$

$$\text{Shear Modulus } \mu = \frac{E}{2(1+\nu)} \quad (3)$$

$$\text{Lame Modulus } \lambda = \frac{\nu E}{(1+\nu)(1-2\nu)} \quad (4)$$

(Bower, 2010)

2.2.2 Standard Linear solid Model

One method used to model tissue including epithelial tissue are spring-dashpot simulations using springs for elasticity and the dashpots for viscosity modeling. A combination of the spring-dashpot modeling is used with a spring and dashpot in parallel modeling a viscoelastic solid – Voight-Kelvin model and a spring and dashpot in series modeling viscoelastic liquid – Maxwell model also the Maxwell-Wiechert model for some tissues. These models give an approximation of the mechanical behavior of tissue. Relaxation and creep cannot be measured using this model and dynamic analysis is used to find other properties of materials. Other methods of modeling tissue use curve fitting where the measurements of the stress and strain are graphed and an equation is matched to the curve. An example of this is the hyperelastic model called the Ogden method which produces a J like curve (Wikipedia – Ogden hyperelastic model, 2022).

Dynamic analysis is a method used to find the viscoelastic measurements of a material. This method uses sinusoid or pulsed perturbations of the material to find the storage (E') and loss (E") moduli. The storage moduli is the elastic measurement and the loss moduli is the energy dissipated by structural

rearrangements (Guimaraes et al., 2020). Dynamic modulus G (G' + jG") is used to measure the relationship between oscillating stress and strain. Other measures of viscoelastisity are creep and relaxation (Wikipedia, 2023).

2.2.3 Continuum Model

This is a deformable body solid mechanics method that analyses solid mechanics or fluid mechanics usually in three dimensions using infinitesimally small parts of the whole solid to find the forces and strains in the entire solid or fluid. Differential equations are used to describe the object using physics to describe the behavior of the deformable body. Concepts such as mass conservation, momentum conservation, and energy conservation are used to create the differential equations. This method is used in Finite Element Analysis which are usually programmed into mesh structure which closely approximates the behavior of the solids or liquids assuming certain boundary conditions and assumptions about linearity (Wikipedia, 2023).

2.2.4 Cellular Potts Model – Artificial Life

The cellular Potts model is agent based modeling where cells are placed on a grid and their behavior is governed by an energy function. Software specifically made for cells is Cells in Silico (CiS) (Berghoff et al, 2020). This type of modeling does not directly relate to actual cells in a tissue (Barton et al., 2017). CompuCell 3D is an example of the cellular pots model that has been used extensively. Simulation of chemical components as well as cells and tissues have been modeled using this method. The main drawback of this modeling is that there are no exact measurements of forces in the models (Glazier, 2024). Artificial Life is another simulation along the same lines as agent based modeling where life is simulated using computer programming (alife.org).

2.2.5 Vertex Model

The vertex model was created specifically to study cells in tissue using cell shape – perimeter and volume measurements. The two dimensional version is used to study epithelial tissue. The mechanical energy is derived from deviations from preferred cell shape. The apical shapes of epithelial tissues are studied an the perimeter and area of the shapes on the surface are measured. Compared to hexagon shapes the shape index preferred parameter P_0 = P*6(hexagon) and the area A_0 is the preferred area. There is a phase transition in tissue when the target shape index;

Target Shape Index $p_0 = P_0/\sqrt{A_0}$ (5)

when $p_0 > P*6$ or $p_0 > 3.72$ the material becomes soft-fluid (Staddon et al., 2023). When tiled with a regular hexagon lattice the material is ridged. Using this model the shear modulus, bulk modulus Young's modulus and Poisson's ratio can be calculated (Staddon et al., 2023). This model is used for studying active matter.

There is an active vertex model that has been developed by Barton et al. (Barton et al., 2017) for studying the mechanics of confluent epithelial tissues and covers multiple scales with tens of thousands of cells. The model covers the mechanics of active tissue as well as cell growth and apoptosis. Programming for this model is available in the SAMoS software package which is open source. The main problem with this model is that it is difficult to program in 3D.

2.2.6 Active Matter Contribution to Mechanics

Active tissues add to the mechanics through motor molecules fueled by ATP and other energy molecules that cause parts of the cell or the whole cell and tissue to move. In epithelial tissue one of the main contributors is the actin-myosin complex similar to the system that moves muscle (Rodriguez et al., 2013). Living tissue is active matter and produces cell and tissue behavior that is unique to active matter and not seen in dead or passive matter (Rombouts et al., 2023).

2.2.7 Tensegrity Model

Current tissue models reduce the number of unknowns in the stiffness – elasticity matrix so that they are reduced to two unknowns (Doyley, 2011). In a tensegrity model the unknowns can also be reduced to two using linear elastic material for tension only elements and compression only elements. The tensegrity structure gives non-linear responses to force and can produce a J shaped non-linear stress-strain curve. Tensegrity models are valid over a greater range of deformation than other models which are assumed to be linear over small range so that the reference and deformed material have the same coordinates and the force-distance (stress-strain) graph is linear (Kennedy, 2019). This linear approach is used in large deformations to make calculations more efficient and less time consuming.

A tensegrity structure is a modified truss where the straight elements of the structure are attached through pin joints which are free to move in any direction. For a tensegrity the elements are either in tension or compression or both. For the modeling of tissue the elements are either in tension and can take tensile forces or just in compression and can take compressive forces. This allows for the reduction in the number of unknowns to two values the Et – elasticity of the tension elements and Ec – the value of the

compression elements. The boundary conditions for the structure are the attachments to the surface and to the other cell elements in the structure. The prestress of the structure and attachments to the other cells is an important part of the cell attachment boundary condition. The strength of the spring foundation that attaches the structure to the substrate is another boundary condition.

The tensegrity model also known as the Tension Integration Model (Gu et al., 2023) has been used to model cells and was introduced by Ingber (Ingber, 2008). For a tensegrity model structure tension elements and compression elements are used to build a 3D structure in equilibrium. Tension elements are like strings and only take tension stresses. Compression elements are called rods or bars and can take compression but very little tension. Tensegrity structures are built so that the tension elements hold up the structure when prestress is applied to them. Cells are thought to be tensegrity structures (Ermakov, 2018; Ingber 2014; Ingber, 2008). A summary of Ingber's cell tensegrity properties;

1. "The mechanical properties of cells are determined by structured cytoskeleton rather than by unstructured viscous continuum.
2. Prestressed cytoskeleton determines the ability of cells to deform.
3. Microtubules, which function as rods anchored to the extracellular matrix, are affected by the tensional structures of the cytoskeleton; thus, the balance of forces in the whole cell is established" (Ermakov, 2018).

The actin bundles in the cell are considered to be the "strings" and the microtubules are considered to be the "bars" in the tensegrity cell structure. Microtubules are thought to carry higher compressive loads because tension elements are attached to them for bracing like a pole can be braced by steel cables attached to them (Brangwynne et al. 2006).

Some examples of models of tissue made with tensegrity structures include red blood cells (Pandian and Ananthasuresh, 2017). Blood cells exist as single cells so this is a single cell model. A multi-cell model (Zhang et al., 2021) shows how inner tissue cells can be made using tensegrity and then grouped together. Another tissue model of an organoid was made by Fraldi et al. (Fraldi et al., 2021). This model was also of interior cells and includes a study of cancer in cells modeled with tensegrity. Tensegrity modles of cells are also on GitHub (Bharadwaj et al., 2023). This is a site that has coding for Finite Element Model of cells in Matlab .m files. These cells ar individual cells and appear to be interior cells in structure – are rounded and include a nucleus structure. Another model that uses bent strucutes for elements in the tensegrity was done by Fraldi et al., 2019. Microtubules are known to bend inside of cells and the bend elements are based on this fact (Fraldi et al., 2019). The first researcher to build a tensegrity structure of cells was Ingber

(Ingber, 2008; Ingber et al. 2014) who has written many papers on the concept and has made single cell models. These models do not model epithelial tissue which has a specific structure.

2.3 Tensegrity Model of Simple Epithelia

Tensegrity models are structures that are in tension and this is the natural state of cells and they are tensegrity structures (Ingber, 2014; Ermakov, 2018). Tensegrity structures can be modeled using one value of elasticity for the tension elements and one value for the compression elements and boundary conditions of prestress and placement of nodes and substrate values and attachments. This simplifies modeling and makes computations more efficient.

2.3.1 Tensegrity with Truss Finite Element Analysis

Truss models are made with single straight members that can take tension or compression along their axis. Force is applied to each end of the member resulting in compression or tension along the axis of that member. The members are pin jointed allowing them to rotate and transfer forces in the axial direction. Trusses are usually assembled in triangular sections and are their own mesh. Tensegrities can be modeled using trusses. Modeling with Finite Element Method (FEM) can determine the stiffness matrix for 3D tensegrity structures (Al Sabouni-Zawadzka, 2023).

Tensegrity structures stiffen when a load is placed on them and therefore Finite Element Analysis is not the best approach to analysing their structure (Obara and Tomasik, 2023). Finite element analysis uses small displacements to analyse the properties of structures and tensegrities have larger movement and the stiffness of the structure changes when a load is applied. The structure layout and its prestress are dependant on each other. The prestress or stress in a tensegrity is part of its structure (Zhang and Ohsaki, 2015). An extreme example of this are tensegrities that change form and can do so with an incremental change in the forces applied to them if they are near the change of state point. An example of a tensegrity that has this bistable structure is shown in Figure 2.14 below (Hong and Hua Deng, 2023).

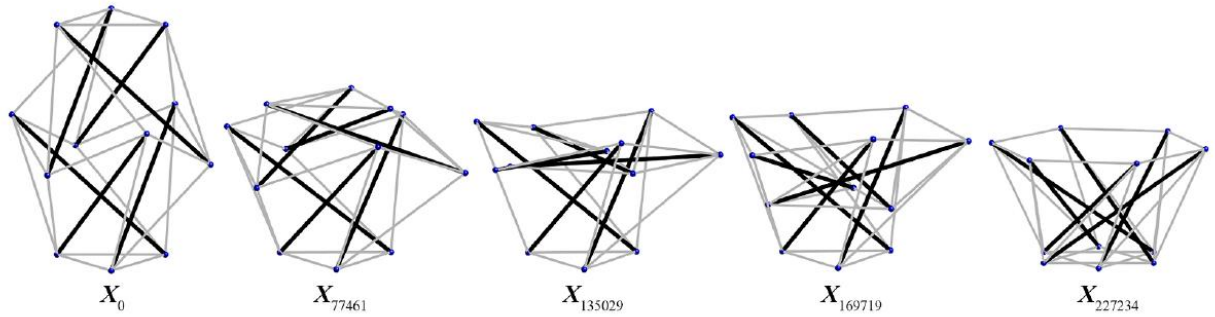

Figure 2.14 *Configurations of a bistable tensegrity showing the transformation between one stable form and the other stable form (Hong and Deng, 2023).*

Tensegrities depending on the properties of their components and boundary conditions will change shape in unconventional ways with the whole structure shifting shape and tension depending on the forces applied to the structure.

Finite Element Modeling of tensegrities using commercial software works if each force is applied to the structure individually and the model is given time to settle or change shape and tension stiffness. The rate of applied force is important as a factor in this modeling.

Tensegrities are a subset of trusses and the tensegrity structure that models confluent tissue will be a tensegrity grid with repeating patterns. The pattern for epithelial cells is one with a top tension ring attached at the corners of hexagon rings with trijunctions that are also tensegrity structures. The hexagons are an idealized surface tiling structure and in living cells the hexagons become distorted due to the forces on the tissue.

The tensegrity structures need to be stable within the grid but not stable on their own. Epithelial cells are confluent so are attached to each other all of the time. They can convert to a moving sheet or into mesenchyme tissue. The mesenchyme tissue is a type of crawling cell that does not rely on its neighbours.

In tensegrities the placement of the compression only bars are important to the stability of the overall tensegrity. When two or more bars touch the tensegrity is indeterminant statically or kinematically see table 2 (Gan 2020). The static condition is denoted by s and the kinematic by k.

kinematically see table 2 (Gan 2020). The static condition is denoted by s and the kinematic by k.

The following are the parameters used in the table below:

"*k*(≥0) is the number of independent zero-energy deformation modes or rigid body mechanisms. A structural system with *k*=0 means the structural system is *kinematically determinate*.

s(≥0) is the number of independent states of self-stress mechanisms. A structural system with *s*=0 means the structural system is *statically determinate*" (Gan, 2020).

Class	Static and kinematic properties		Type of solution
I	s = 0	Statically determinant	Both equilibrium and compatibility equations have unique solutions for any loadings
	k = 0	Kinematically determinate	
II	s = 0	Statically determinant	The equilibrium equation has either a solution for a particular loading or no solution. The compatibility equation has k-dimensional infinity of solutions for any strains
	k > 0	Kinematically indeterminate	
III	s > 0	Statically indeterminate	The equilibrium equation has s-dimensional the infinity of solutions for any loadings. The compatibility equation has a unique solution for compatible strains, but no solution for incompatible strain
	k = 0	Kinematically determinate	
IV	s > 0	Statically indeterminant	Both equilibrium and compatibility equations have s- and k-dimensional infinities of solutions, respectively, for some particular loadings or strains, but otherwise no solution
	k > 0	Kinematically indeterminant	

Table 2 *Classification of the tensegrity structural system (Gan 2020)*

Two ways of finding the equilibrium equations for a tensegrity are equilibrium matrix associated with prestress or axial forces and force density equations using the node coordinates in the structure. The equilibrium matrix is related to the prestresses of the tensegrity and is expressed as the force balance at each node or can be directly derived from the virtual work principle (Zhang and Ohsaki, 2015).

The physical structure of the tensegrity can be represented by a connectivity matrix where two nodes are connected by a specific member. The connections are represented by either a 1 or -1 with all other entries in the row at 0 (Zhang and Ohsaki, 2015). The connectivity matrix allows for linear algebraic representation of the tensegrities and the forces that are placed on them.

Tensegrity structures are complex particularly in 3D and continuum models can be made to find Young's modulus (E) and the shear modulus (G) (Sabouni-Zawadzka, 2023). The variables for the continuum model are the tension to compression elements stiffness ratio and the prestress. The stiffness ratio k which is

different from the k in Classification Table 3. K is the elasticity times the area E*A of the strings over bars needs to be one of the parameters that is varied in the parametric studies.

K value $k = \frac{(EA)string}{(EA)rod}$

Equation (6) (Sabouni-Zawadzka, 2023)

Other studies have looked at short and tall models of the same structure (Fraternali et al., 2015; Sabouni-Zawadzka, 2023).

Epithelial tissue types are squamish – short, cuboidal – medium height, and columnar – tall. These alterations in height also can be used in the model's parametric studies.

Definitions of structures that are related to tensegrities are:

- Truss – pin jointed structure that has no prestress
- Cable-net – only tension members attached to supports
- Tensegrity-dome – has both tension and compression members and is attached to supports
- Tensegrity – has both tension and compression members and is free standing – no supports

Epithelial cells appear to be Tensegrity-domes as they are attached to each other and support each other. When epithelial cells are separated they tend to change cell type and change to mesenchyme cells which are mobile cells. This is know as epithelial to mesenchyme transition (Purta et al., 2023).

Building tensegrities that are stable can be a challenge. Some programs have been specifically written to model tensegrities such as 3D PushMePullyMe (Senatore and Piker, 2015) and MOTES Modeling of Tensegrity Structures for minimum mass or structure control both for statics and dynamics of the structure (Goyal et al., 2019) which uses the Matlab platform. Also software that can accommodate tensegrities such as Grasshopper, Kangaroo and K2E (Roth and McCarthy, 2021) and also Matlab (Gan, 2020; Bharadwaj et al., 2023). Also metamaterial programming that allows analysis of fine structure as well as bulk structure of a material to be analysed – multiscale modeling can be used for example Simcenter3D (www.ata-e.com/software/siemens-plm-software/simcenter-3d/). The Vertex model for epithelial cells describes the behavior of epithelial cell surfaces and this gives an accurate model for the behavior of epithelial tissue. The active vertex model developed by Barton et al. (2017) uses particle based models and might be adapted to tensegrity modeling.

Tensegrities that are stable are often considered to be free standing tensegrities but they often change their configuration suddenly under load. This mainly happens when one of the strings loosens because the structure has changed configuration. Adding attachments to the top and bottom of a bi-triangle structure will make it into more of a tensegrity-dome structure and its stability will be easier to evaluate (Zhang and Ohsaki, 2007). The structure in Figure 2.5 is a T-4 prism and is structurally stable (Oppenheim and Williams, 1997).

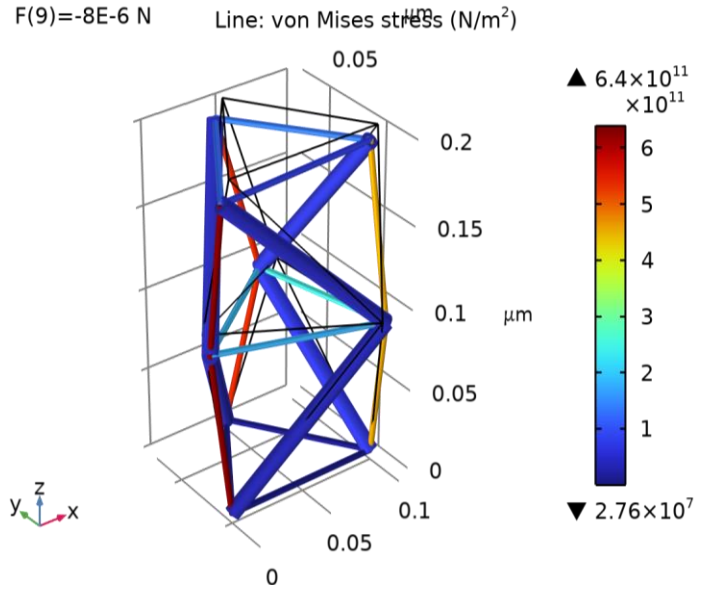

Figure 2.15 *A T4 tensegrity strucuture. Two basic trianglular prisms mirrored on top of each other making a stable structure. The color bar shows the von Mises stress in each member.*

Stable tensegrities can be designed using graph theory and rigidity theory. Topology and geomety can be combined to produce stable structures with predefied shapes and predefiend self-stress states (Aloui et al., 2019).

There are many metamaterial designs and some use tensegrity structures or can be adjusted to use tensegrities. This type of design could be used in future to add to the sides of the tensegrity structure.

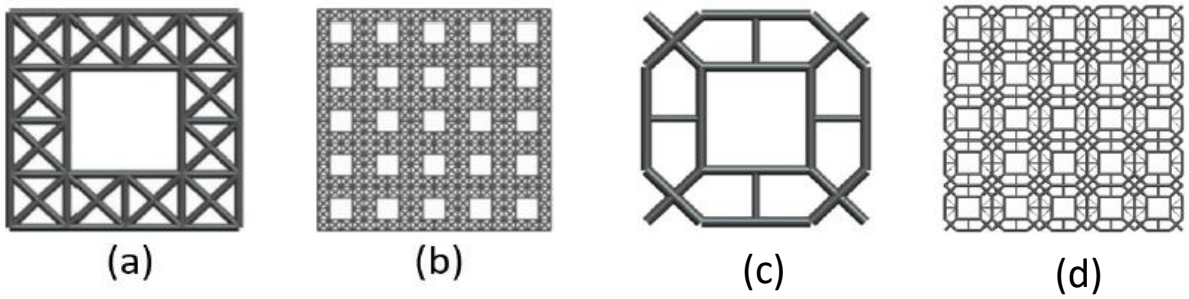

Figure 2.16 *Examples of metamaterials. These structures could be changed into tensegrities and tile the sides of triangles or hexagon prisms to make up a cellular structure. The sides of triangle prisms and hexagons prisms are squares (Jagielloa, 2021).*

Producing a sheet of tensegrity cells connected together could be considered a metamaterial as the cells are micrometers in size and form a larger structure.

3.0 Method

The models were built and tested in COMSOL Multiphysics 6.2 which is a Finite Element Analysis program. Truss stationary studies using the Direct Solver with no itterations was used to test the model. The model also used truss posts to hold up the outer edge of the cells where two cells meet. This creates a trijunction with two cells and then the post for the third position. Originally the posts were distributed around the outside of the model. It was found that the model worked when only three posts at the trijunctions of the posts and cells was used.

The parametric studies will be performed on three styles of triangular tensegrity prisms, hexagone tiled lattice with differing triangular tensegrity prisms as trijunctions. The models were tested in tension and compression measure the stress/strain curve in the form of force/displacement measurments.

The parameters varied in the studies are:

- Prestress
- Modulus of Elasticity for both tension and compression elements
- Ratio k = E*A strings/E*A bars
- Height of the 3D models
- Varying strength of attachment of the models to the substrate (spring constant)

For the trial tensegrities the forms of known tensegrities the T3 and T4 tensegrities were used for the trijunction attachment points. The forms were copied into a hexagon shape with the strings down the

sides and at the top of the tensegrity with bars used as the angled sections. The bars are placed at opposite angles on the top hexagon structure. This lack of rotation will in some instances make the hexagon and triangular form unstable on it's own without support structures but the hexagon structure can stand on its own but does not support any forces. The attachments of each cell to each other and the built in posts are essential to allow the structure to withstand forces. In epithelial tissue each cell is dependant on its attachment with its neighbour and to attachments to surrounding tissue structures so the need for supports for the model is expected.

Tensegrities can be modeled using discrete models and can be converted to continuum mechanics modeling so that Finite Element modeling can be used on more complex models (Sabouni-Zawadzka, 2023). Using Finite Element modeling for tensegrities with the COMSOL Multiphysics package for modeling the shape and physics in terms of ordinary truss modeling with high elasticity for both strings and bars and density close to that of air and Poisson's ratio of 0.4.

3.1 Cell Attachments

Models of epithelial tissue need to include junctions between cells and between cells and the extracellular matrix. This includes tight junctions, adherens junctions; the bijunctions and trijunctions at the actomyosin belt; and the integrins attached from the basal part of the cells to the extracellular matrix are the points within the cell that resist and transmit force. The cells therefore need to be attached with each other and to the substrate with spring attachments. The attachments in cells are protein complexes and are themselves considered to be tensegrity structures. A simple tensegrity attachment structure is one with strings in a rectangle with one compression unit in the diagonal.

Figure 3.1 *2D plain attachments vs a 2D tensegrity structure for attachments. The opposite attachment also forms a simple tensegrity. The blue lines are strings and the black lines are bars.*

The plain attachment doesn't work well and the model does not work when these attachments are used. The 2D tensegrity structure is the base module for the whole tensegrity. The sides of the tensegrity T3 and T4 prisms are made like this and the sides of the hexagon figures in the final models were built like this. The T3 and T4 structures described in Figures 3.3 and 3.4 are used as trijunctions in the final model.

The 2D tensegrity does not have linear movement when equal forces are applied to one side at the corners as shown in Figure 3.2.

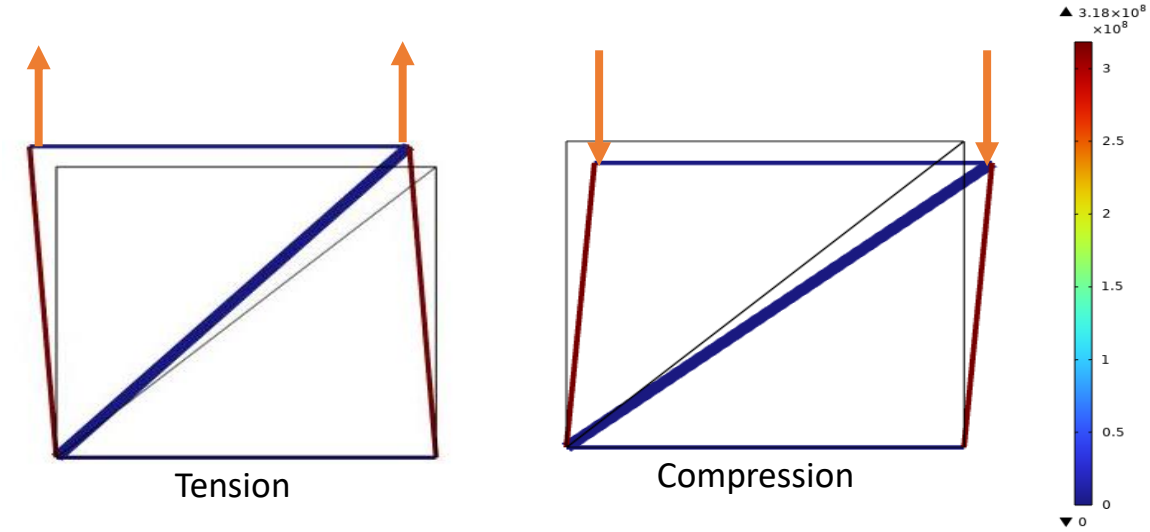

Figure 3.2 *Force on a 2D tensegrity square with a cross bar Force 1 x 10^{-7} N sides are 1.5 um Colored Side Bar von Mises stress (N/m^2) a) Tension force applied at top corners b) Compression force applied at top nodes. The black lines are the original configuration. Color bar blue 0 to red 3.18 x 10^8 von Mises Stress.*

The square with a cross bar does not bend evenly even though the force is the same on both corners at the top of the square. This has consequences for a 3D tensegrity made with this arrangement of elements. They twist as they are compressed or placed in tension. The following figures 13, 14 and 16 are three types of tensegrity structures built as a 3D triangular prism.

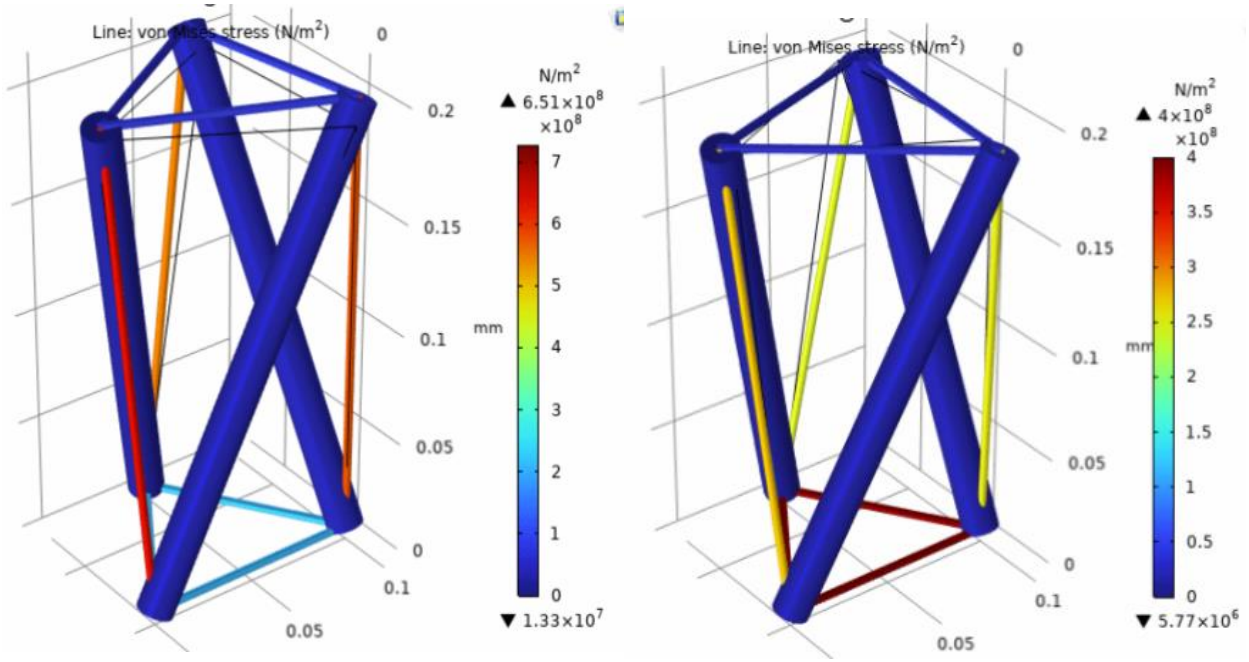

Tension Compression

Figure 3.3 T3 *Tensegrity triangle prism in tension and compression.. This tensegrity is self standing due to a -30^{o} angle of the top triangle compared to the bottom. When it is tensioned or compressed it rotates. The color bars show the von Mises stress of each of the elements. The stress in the tension T3 prism is 6.51 x 10^{8} with the maximum at 7.2 x 10^{8} and the stress in the compression T3 prism is 4x10^{8} with the maximum at 5.98.*

This is a 3D triangle representation of the 2D tensegrity in figures 3.1 and 3.2 . To use the T3 prism as a trijunction structure the structure has to have the 30^{o} twist angle removed making it a three sided basic tensegrity structure and not a true T3 structure.

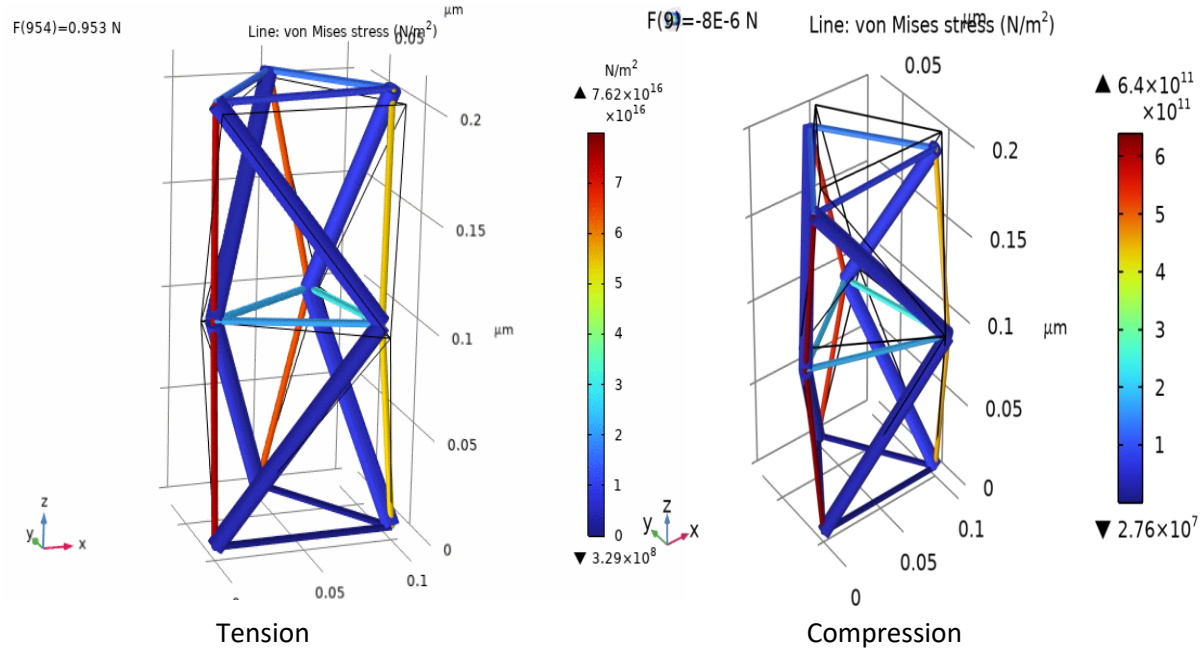

Figure 3.4 *T4 Double tensegrity prism in tension and compression. The structure is two T3 mirrored prisms on top of each other. The color bars show the von Mises stress on the elements of the tensegrity. The maximum stress in tension is 7.62 x 10^{14} N/m^2 and the maximum stress in compression is 6.4 x 10^{11} N/m^2.*

The movement of the Double tensegrity has less rotation as it is stretched and compressed. It has less movement in the z direction and the structure stiffens and stays in the same configuration as force is added after the rotation stops. Because the T4 is a mirrored structure the top and bottom triangles are aligned and can be used as a trijunction in a larger structure. A trijunction structure that moves straight up and down is needed and one that moves at the same rate as the cell structure.

Choosing the basic D- bar configuration on the sides of the triangular prism gives a triangular tensegrity prism Figure 3.5.

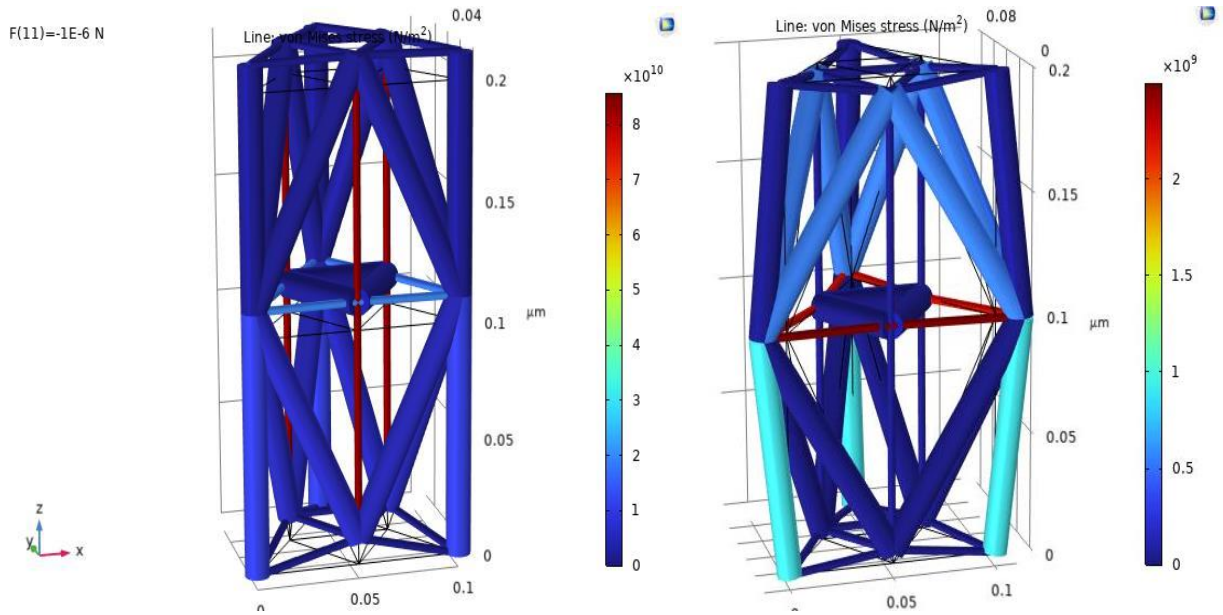

Tension Compression

Figure 3.5 *Diamond - D Side Bar Tensegrity Prism in tension and compression. The tensegrity has bars along the sides of the tensegrity that are split in the middle attached together with the string-elastic components. The maximum von Mises stress in tension is 8.2 x 10^{11} and in compression is 1.2 x 10^{13} N/m^2. In this case the structures have not reached their maximum tolerance for stress.*

The side bar tensegrity prism has a linear motion and does not twist or rotate through an angle in tension or compression. This triangular prism did not work as a trijunction structure with the models.

3.2 Hexagon Build

The hexagon shape was chosen because it tiles a surface and it is the most energy efficient shape (Tang et al., 2022; Barton et al., 2017).

First a hexagon was placed at height or z direction at z=0

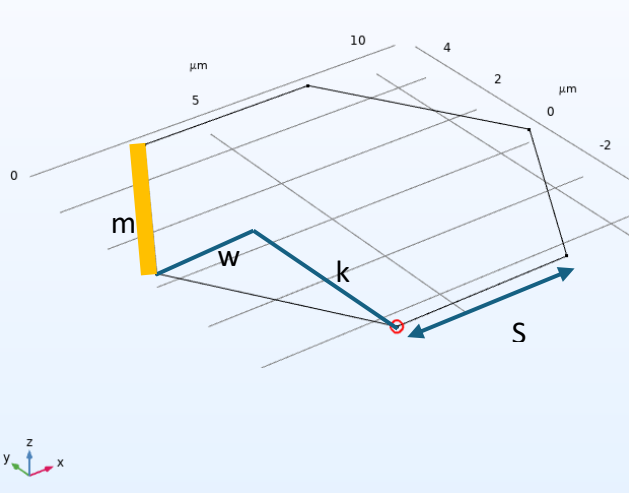

Table of hexagon coordinates

x(μm)	y(μm)	z(μm)
1.4*m	0	0
w+m	k-m	0
s+w-m	k-m	0
s+2*w – 1.4*m	0	0
s+w-m	-k+m	0
w+m	-k+m	0

Figure 3.6 *Hexagon and table of vertices. The 1.4 is the* $\sqrt{2}$*, m is width of cell membrane (yellow), w is polygon width, k is polygon height*

The parameters used to build the model are the span of the hexagon s, the width w and length k of the hexagon and the height of the two hexagons – H and HR. The elasticity of the compression and tension elements and a force need to be listed in the parameters.

Parameters for k value of 4x 10^{-4} medium or cuboidal measurements are:

Name	Expression	Value	Description
s	5[um]	5e-6 m	span
k	5[um]	5e-6 m	polygon height
w	3 [um]	3e-6	polygon width
m	0.1 [um]	1e-7	membrane width
H	3 [um]	3e-6	3d Height
HR	0.5 [um]	1e-8	3D Height of top ring
Et	100 [GPa]	1e11 Pa	Tension element elasticity
Ec	200 [GPa]	2e11 Pa	Compression element elasticity
F	10 [nN]	1e-8	Force

Table 3 – *Example of parameters in COMSOL used to create the tensegrities*

- Bars 0.005 um^2 in cross section area for bar compression elements
- Bars 200 GPa Modulus of Elasticity compression only – the code for COMSOL programing is Ec = (200*(1-0.9999*(truss.en>0))[GPa]) – Insures compression only forces on bars
- Strings 0.001 um^2 in cross section area for string tension elements
- Strings 100 GPa Modulus of Elasticity tension only – the code for COMSOL programming is Et = (100*(1-0.9999*(truss.en<0))[GPa]) – Insures tension only forces on strings

- Truss Post parts 200 GPa Modulus of Elasticity and are the same area as the bars and are tension and compression elements
- Poisson's ratio 0.4
- Density ρ=1.2
- Spring foundation 10 N/m to 10000 N/m and are at all the bottom vertices except the pinned points
- Pinned points are at the edge of each post
- Initial axial stress 0.000001 N/m^2

The posts that are added to the model have the same component values as the Bars. The initial axial stress does not appear to make a difference in the outcome of the experiments but was added due to COMSOL's recommendation that this not be left blank. Poisson's ration of 0.4 was also chosen due to the COMSOL recommendation that the ratio over 0.4 would not give accurate results (Structural Mechanics Module User's Guide, COMSOL, 2022). The K value (Equation 6) calculated for this set of graphs was 0.4×10^{-4}. The formula for the k value is String Modulus of Elasticity x Cross section area of the string/Bar Modulus of Elasticity x Cross section area of the bar. An example of a k value that is out of range for epithelial tissue is the k value = 0.1. The Bars = 500 MPa and the cross section is 0.01 um^2 and the Strings are at 50 GPa and the cross section is 0.005 um^2. This k value might represent ligaments or other stiffer tissue.

The parameters for Actin which make up the strings in this model are listed at 2.6 GPa Modulus of Elasticity. The actin is bundled together and also branches making the string values either higher or lower depending on the makeup of the cross-sections in the bundles and the number of the attachments. The bars also have bundling and attachments to the sides of their structures and are listed as having 1.7 GPa Modulus of Elasticity. An estimate of the bundled and supported microtubules elasticity could range from 1.7 GPa to over 200 GPa depending on how they are supported. Microtubules have a longer persistence length of 5000 µm than microtubules at 10 to 20 µm and so are more likely to be the "bars" in the cell (Stamenovic and Wang, 2011). The 200 GPa is the Modulus of Elasticity for steel (Wikipedia, 2024). To demonstrate the increase in the elasticity under these circumstances take a long small diameter area wood dowel and attach elastics to the sides of it. When the elastics are slack the dowel bends easily, when the elastics are pulled taunt the dowel is stiff. There is a lack of data about the Modulus of Elasticity for in vivo cells and tissues.

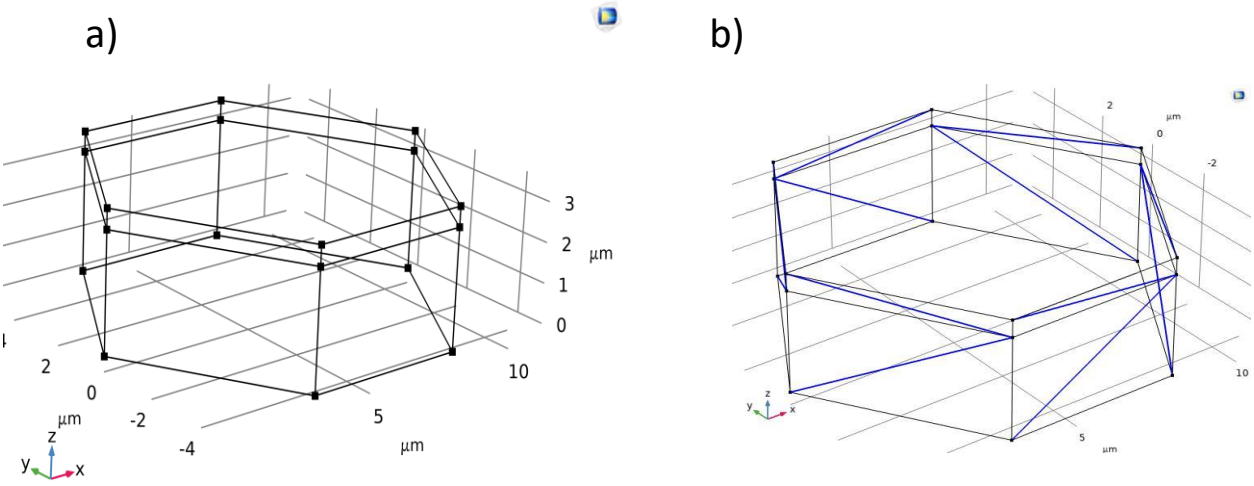

Figure 3.7 *Cell shape build a) A 3D shape was made of stacked hexagons. The top hexagons form a ring to represent the actin ring at the apex of the cell. b) The compression elements were added to the geometry using lines and are shown in blue for this simpler configuration. The tension elements are in black.*

This configuration of compression elements causes the hexagon tensegrity to twist when in tension or compression. Using the side-bar tiling like the triangular prim for the hexagon shape would make it less likely to break when attached to other hexagons of the same type. However, this configuration did not work with the final models.

The single hexagon is a stable structure if the top hexagon is rotated from the bottom hexagon by 120^{o} or -60^{o} (Gan 2020). To make a cell shapes that tile a plane straight hexagons without a twist were chosen. These structures do not stand by themselves but need attachments to their neighbour cells or supports.

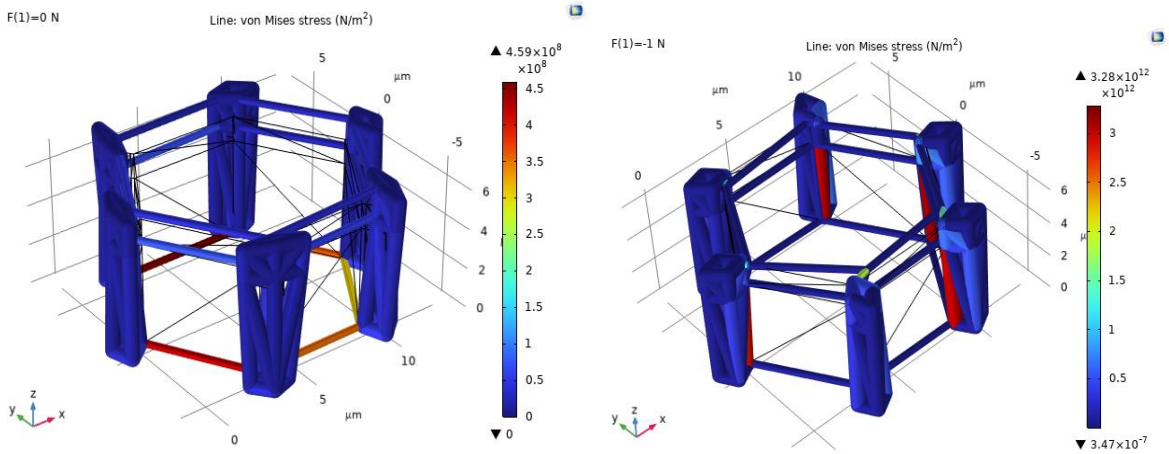

Tension Force applied on the top vertices 1 N

Compression Force applied on the top vertices -1N

Figure 3.8 *Hexagon ring structure. A tensegrity without a twist in angle. The posts hold the structure up. Pre-strain is at 0.01.*

The structure works in the range of -1.0 to 0 N and 0 to 1.0 N but will not work if both positive and negative forces are included in the run (-1.0 to 1.0 N). The maximum stress in this diagram is 3.28 x 10^{12} von Mises stress (N/m^2). The forces were applied at the top vertices of the structure. The tension force had not reached its maximum so the stress the structure can withstand is probable greater that the 5 x 10^8 von Mises stress.

Rectangular truss structures were chosen for supports outside the cell and tissue area. The truss structures are similar to tensegrities being pin jointed structures but the structure parts are all the same area in diameter and are allowed to be in both tension and compression.

3.3 Three Cell Hexagon Model Build

The model is made so that there is a gap m in between hexagon rings to represent the width of the junctions and distance between cells m. Trijunctions are placed in the middle of the structure and at the edges where the posts and two cells form a triangular junction and the triangular prisms T4 for the middle and T3 for the edges are used to form the trijunctions. The size of the trijunctions are determined by the width of the membrane m.

To make a representation of tissue three hexagon cells are copied and attached with trijunctions and other corner junctions shown in Figure 3.9.

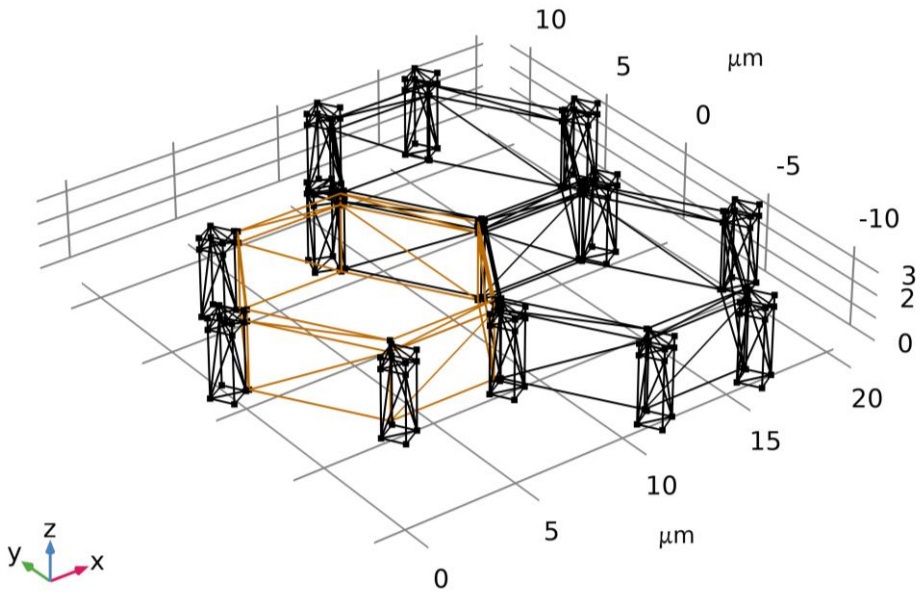

Figure 3.9 *The hexagon cell was copied to two other positions to make a three-cell structure. The first hexagon is outlined in brown-orange. This diagram shows the whole structure with truss posts.*

Connections at the vertices were made by adding lines between the hexagon structures and the posts.

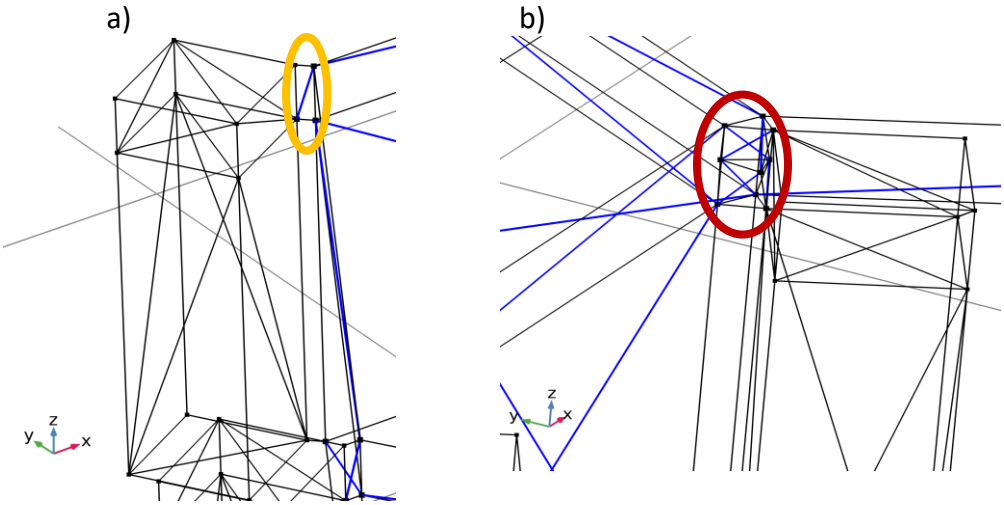

Figure 3.10 *Showing post structure and connections to the posts and other cells a) showing simple tensegrity connection to a post b) showing a trijunction which occurs when two cells and a post meet or when three cells meet. Trijunctions are a main feature holding the structure together. The blue lines are the compression only elements. Only the trijunctions were used in the final configuration.*

Trijunctions naturally occur when there is a membrane like gap between cells. The posts are truss only structures that are like the tensegrity structure but are made of elements that can be in tension or compression.

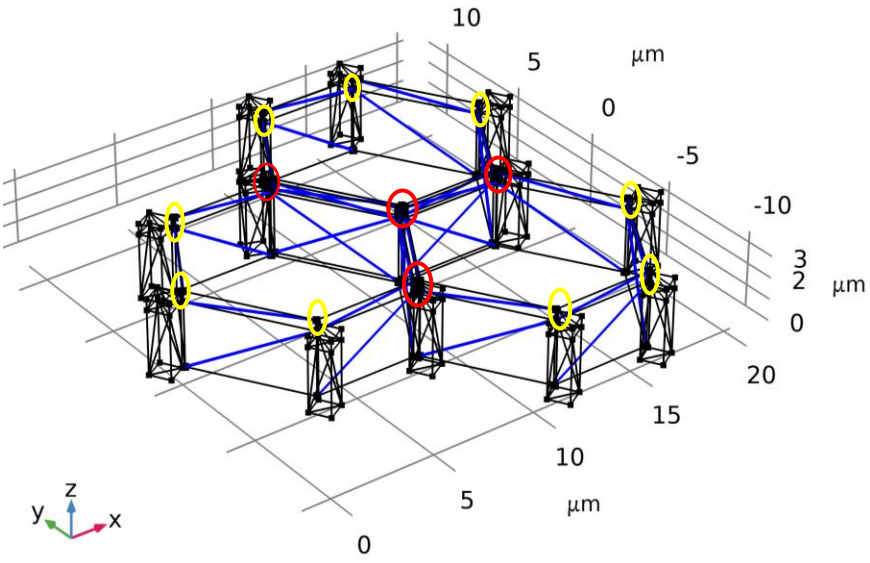

Figure 3.11 *The whole model attachments. Post attachments in yellow and trijunctions in red. The blue lines are the compression only elements.*

The trijunctions are in the middle and at the places where the posts and two cells create a trijunction.

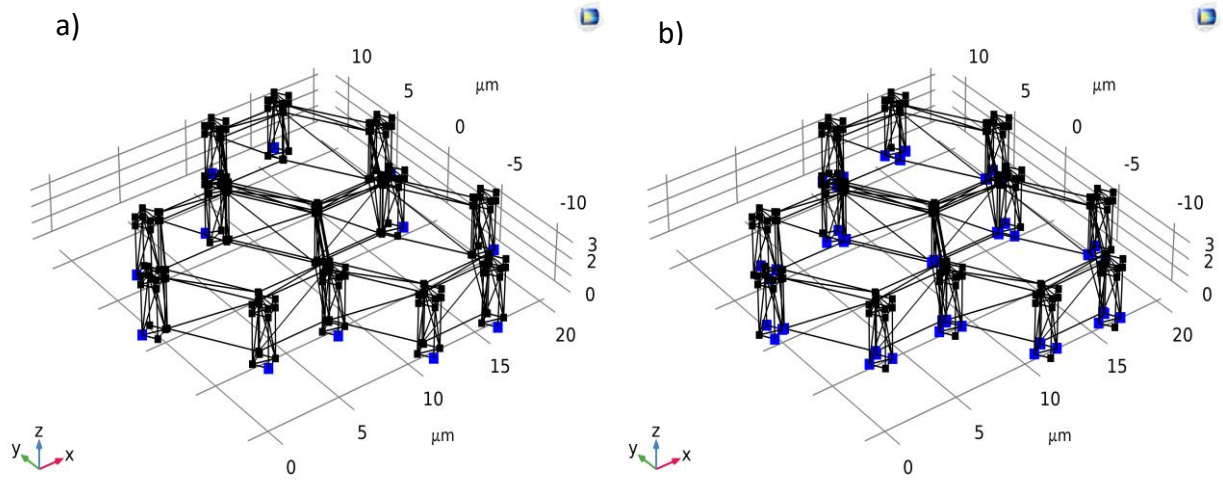

Figure 3.12 *Boundary conditions. Attachments to the substrate a) The pinned elements shown in blue on the outside of the posts. The outside was chosen so that most of the structure was held by the spring foundation. b) The spring foundation points shown in blue. The spring foundation measure is in N/m.*

The boundary conditions are necessary for the structure to successfully stand on its own and withstand forces placed on it.

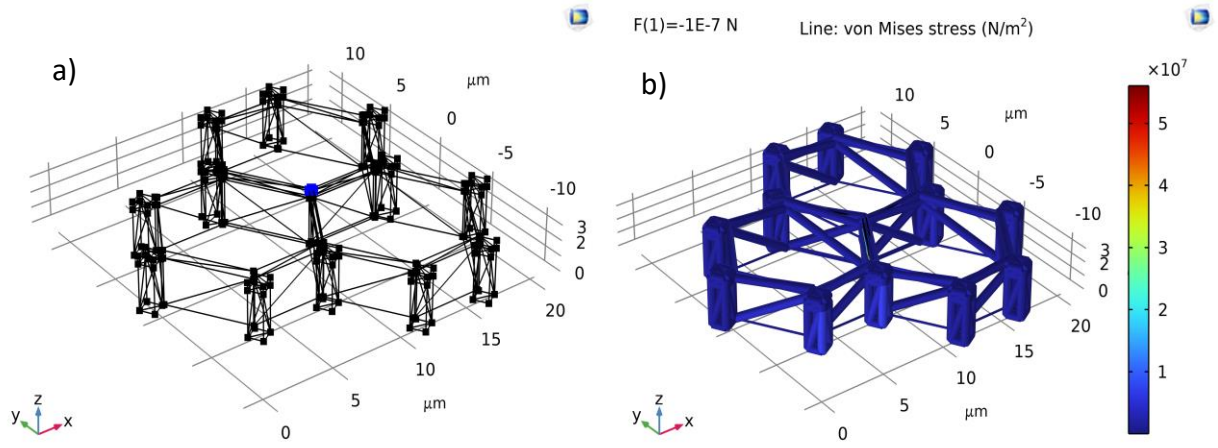

Figure 3.13 *Forces on the model a) Force placed on the three vertices in in the middle at the trijunction in the model. The trijunction is a T4 tensegrity and is open in the middle so the forces are placed at the vertices of the T4 trijunction. b) The resulting stress produced running a stationary study with a force of 3 x -0.000008 N = negative 0.000024 N. The side bar shows the von Mises stress indicating that most of the structure has low stress.*

In the Figures 3.9 to 3.13 multiple posts are shown holding up the hexagons. In the final model all but three of the posts were eliminated.

When a study is set up using automated measurement the model is unstable. The measurements have to be accomplished using a one step process. The Stationary study – step range (-0.0, -0.0000001, -0.00800) start at zero Newtons increment by -0.0000001 N, end at -0.00800 N was tried but did not work. The one step process involves changing the force applied by hand and copying the result. The results were copied into excel and the graphing was done in Matlab.

The three cell structure with a simple T3 triangle used as the trijunctions is not stable. The three cell structure stability is improved by adding the T4 tringle prism to the trijunctions of the hexagon configuration.

The whole structure is shown in Figure 3.14.

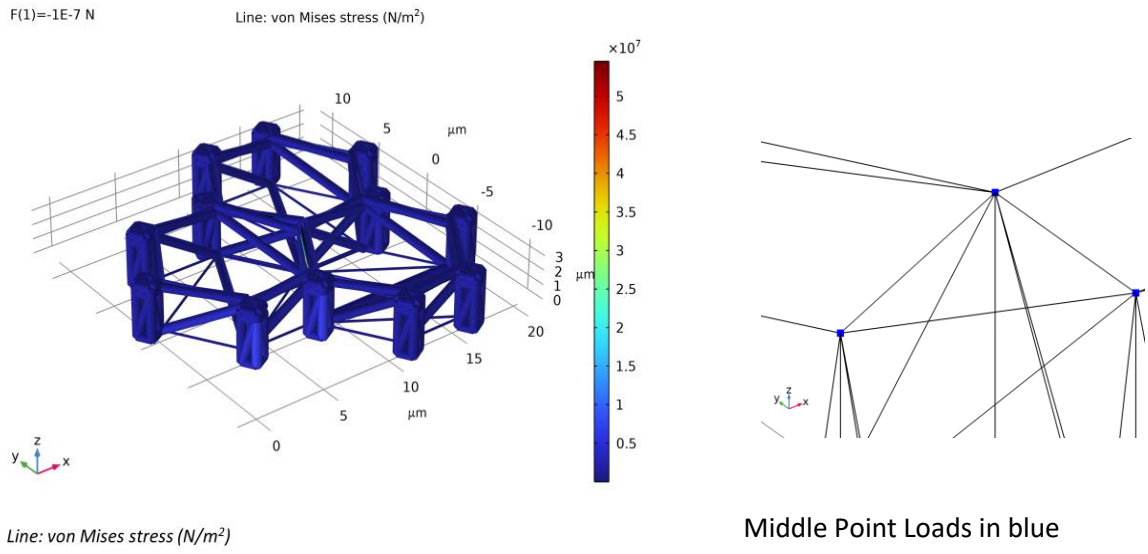

Figure 3.14 *Initial tensegrity three cell model. This structure is close to producing results but is unstable. The force on each of the three triangle corners is 10^{-7} N each. The von Mises stress that can be seen in the diagram has a maximum at around 3.5 N/m^2. Larger forces do not work and generate errors.*

The load was placed on the structure in the middle of the structure at the trijunctions.

3.4 Other Models

Other similar tensegrity structures were tried one with the bars across the hexagon going the same way as the bars on the top hexagon. This structure did not stand as well as the structure where the bars were going the opposite way to each other. The structure with the opposite angled bars is a T4 like tensegrity and works to make a three cell tensegrity that stands on its own with trijunctions attached.

Another model that was tried is a D-Bar structure as shown in Figure 3.15 b). The basic problem with the D-Bar structure is that it tends to splay out or in other words goes out of plane when compressed. It does not have the structural stiffness to support a multicell model and failed with too much stress in the strings. A similar model with an X shaped side Figure 3.15 a) was also tried but it also failed with too much stress in the strings for a 1 nN force. A Theta tensegrity model also failed but most likely was too mobile or unstable for a stationary study.

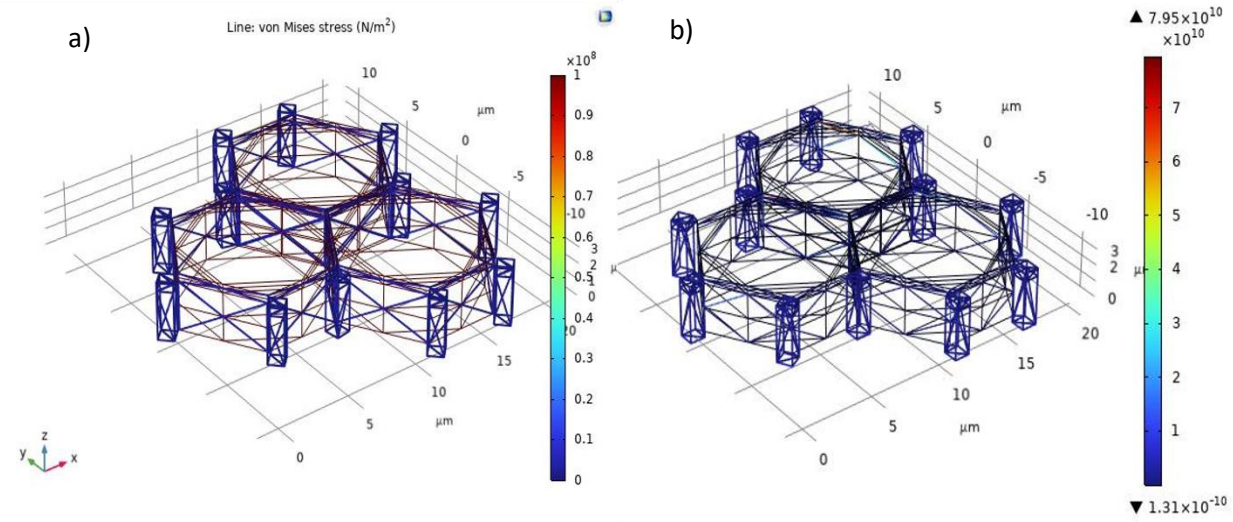

Figure 3.15 *Two alternative models. X-Bar and D-Bar with von Misses stress indicated.*

The models did not work as they were too unstable-flexible for the finite element analysis software to work with. These models should work in an actual build but are probably not as strong as the T4 configuration. The triangular prism models worked well in the finite element models an example of the D-Bar triangular prism is shown in Figure 3.6. A hexagon structure by itself does not stand on its own with this arrangement of strings and bars.

3.5 Experiments on a Stable Three Cell Tensegrity

A stable three cell tensegrity model was developed using hexagon rings with spaces between them for the cell membrane and linkages through trijunctions at the corners of the hexagons. This configuration is similar to that of epithelial cells in tissue. There are only three posts to stabilize the structure.

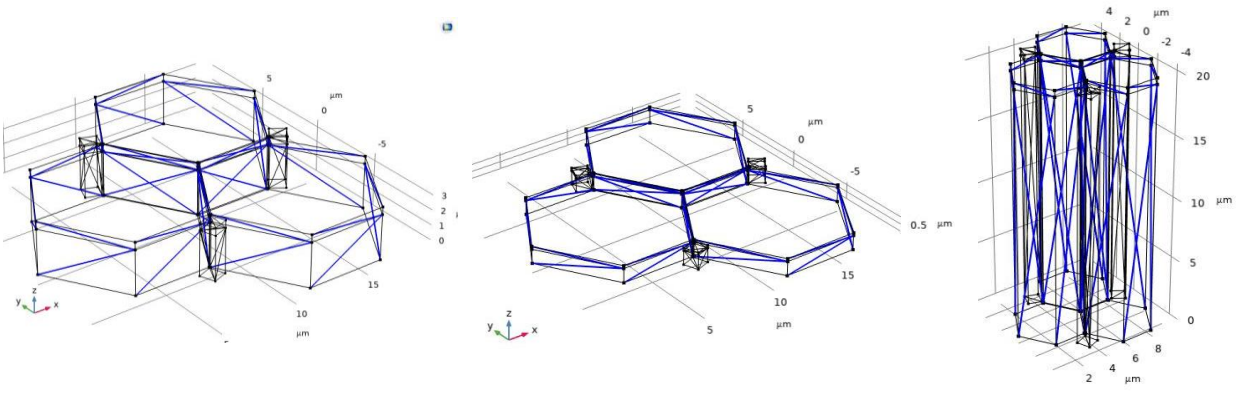

Cuboidal – Medium height

Squamish -

Columnar – tall

Figure 3.16 *Three heights of cell models. These models were used with two varieties of posts for the columnar cells – thin posts which are the same size as the posts in the other two models and wide posts which are double the diameter of the thin posts. The rods are in blue and the strings and posts are in black.*

The squamish model is 1.2 um heigh with the top ring of 0.2 um, the cuboidal model is 3.5 um heigh and the columnar is 20.5 um both with the top ring of 0.5 um.

The other experiments looked at single point and average measurements for the applied forces and a string tensegrity top for the medium height tensegrity. The string and bar elements do not change their elasticity throughout the experiment with rods at the elasticity of 2 GPa and the string elements have an elasticity of 10 MPa. Further experimentation with changes to the elasticity of these components and their cross sectional area could be done. The values were chosen to be close to what exists in cells (Rodriguez et al., 2013; Stamenovic and Wang, 2011) with the changes that cells make to their environments. These changes include changes in the molecules holding he actin bundles together and the tethering of the bundles in the cells.

The structural details show the trijunction in the middle of the structure using the T4 tensegrity and the trijunctions connected to the posts are a simple T3 tensegrity.

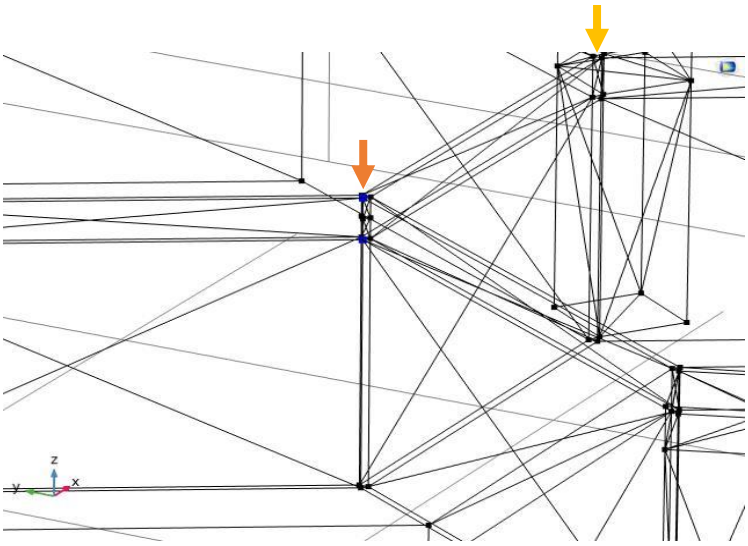

Figure 3.17 *The trijunctions in the models. The orange arrow shows the T4 trijunction and the yellow arrow shows the T3 trijunction that connects to the posts.*

The structure is not stable enough to measure with the finite element analysis without this configuration of trijunctions. The T3s were connected to the posts and the T4 was connected in the middle of the structure.

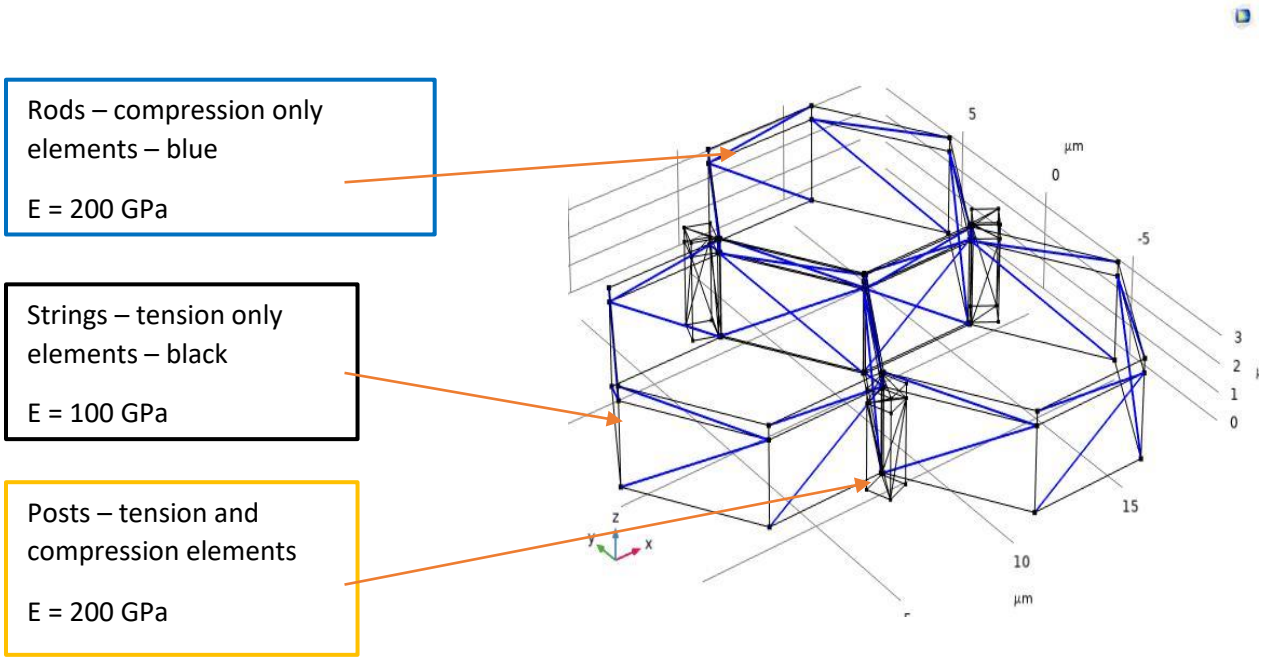

Figure 3.18 *Layout of the Medium or Cuboidal three-cell tissue. The posts have the same E – Elasticity as the Rods at 200 GPa and cross section area of 0.005 µm^2 and the Strings are at E – Elasticity of 100 GPa and cross section area of 0.001 µm^2 for all models (k= 0.0004) except the k = 0.1 model. The k = 0.1 model has Rod elasticity of 50 GPa and cross section area of 0.005 µm with the strings elasticity of 500 MPa and cross section area of 0.01 µm.*

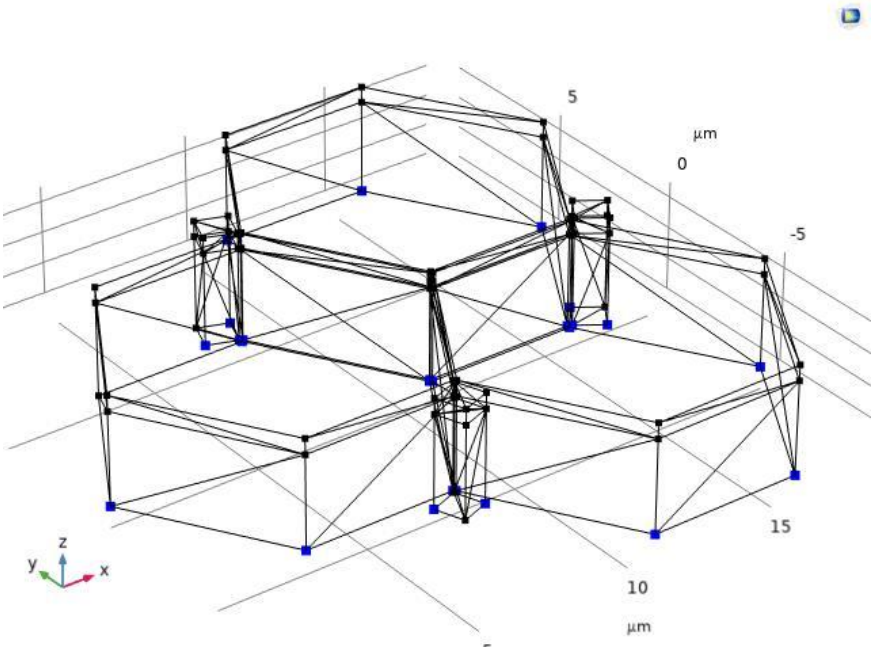

Figure 3.19 *Spring Foundation one of the boundary conditions. The connection to the substrate at the blue points. The points on the outside of the posts are pinned. Simulations were done at spring foundation values of: 10,000 N/m, 1000 N/m, 100 N/m, 10 N/m. The springs are isotropic – the same value in any direction.*

Pre-strains of 0, 0.05, 0.1, 0.2, 0.3 values were measured similar to Fraternaili et al. measurement of a simple T3 tensegrity (Fraternali et al., 2015). The spring foundation which is the substitute for the values of the basement membrane were taken in the same range as that estimated for tissue (Xu et al., 2020) at 10,000 N/m, 1000 N/m, 100 N/m and 10 N/m.

The forces on the structure were placed on the three points on the top of the middle T4 tensegrity. The measurements for the distance traveled due to the forces were measured in the Z direction. This is similar to other tensegrity experiments (Fraternali et al., 2015). The forces used are within measurements taken using AFM on tissue. The force range was between 0 and 200 nN in both tension and compression taken separately this gives a total maximum of 3 x 200 = 600 nN on the middle of the tissue. Some larger measurements were also tried up to 800 nN per point. The measurements for the cuboidal – medium and the squamish models were taken at one point as all points gave the same values. This was not true of the columnar models and both single points and average measurements were taken.

For results stress-strain graphs were produced using the force applied to one point and the displacement of that point or an average of the displacements of the three points with forces applied to them in the middle of the structure.

Cells that were not connected by the trijunctions were tested and found to stand freely without force applied to them but when a small force was added the structure failed. This is similar to what happens in confluent tissue when they loose their attachments they change to mesenchyme tissue or other diseased states (Putra et al., 2023).

The graphs of the Force-Displacement values are in Appendix A.

3.6 Stress-Strain Graphs

The model will use Engineering stress as it will use the constant initial area that is acted on by the forces in the models. Three forces are applied to the top of the middle of the structure as shown in Figure 3.20.

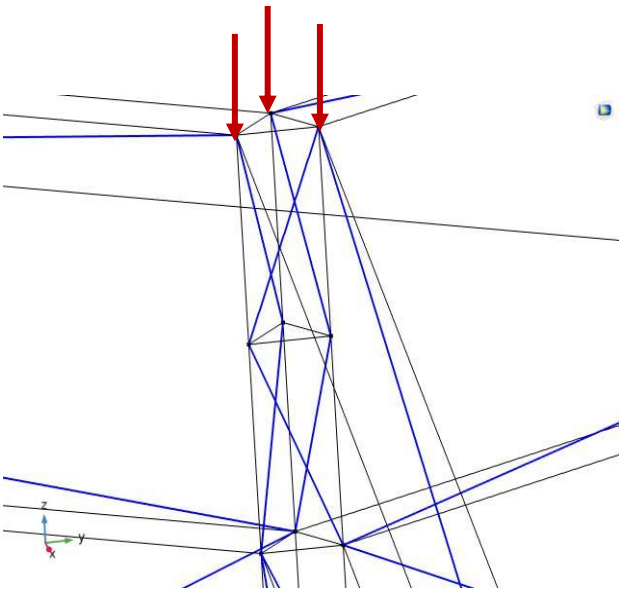

Figure 3.20 *The middle trijunction model. The forces placed on the top of the model. The total force is three times the recorded force and the area is the area of the triangle in the middle.*

To compare the graphs of the model to tissues stress strain curves need to be made of the data. The force applied needs to be the total force which is 3x the recorded force and this needs to be divided by the triangle area to give the stress in Pascals (Pa).

The triangle area is shown in Figure 3. 21.

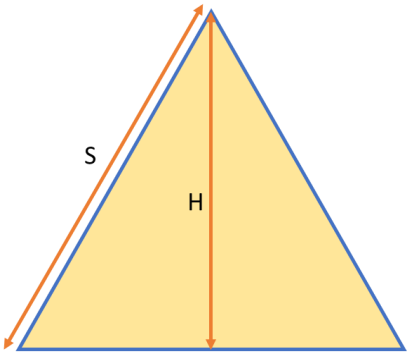

Figure 3.21 *Triangle representing the area of the center of the trijunction. Equilateral triangle. Height = 2m or two times the membrane thickness; Area =* $\frac{1}{2}$ *Height x Side; Side =* $2\sqrt{\frac{2}{3}}$ m^2*; m = 0.1 µm; Area = 1.332 x* 10^{-14}

This area is used to compute the Engineering strain which is in the range of 0 to 80 Kpa or 0 to 0.08 MPa.

For strain calculations the amount that the model moves in the z direction is divided by the original size of the cell. The squamish tissue is 1.2 um heigh, the cuboidal tissue is 3.5 um heigh, and the columnar tissue is 20.5 um heigh. These calculations give engineering stress and engineering strain.

4.0 Results

4.1 Overview

From a controls point of view a separation of the Force – Distance or stress-strain slopes (Elasticity) in the data and graphs allows the structures to change characteristics due to a change in mechanical environment. The mechanics environment change in these experiments are due to changes to either pretrains or basement attachment strength which is the spring foundation in the models. The models are short – squamish, medium – cuboidal, and tall – columnar as well as a cuboidal models with a different k factors.

A broad summary of the results:

- Squamish 3 Cell Model – change in compression prestrain separates the curves and also a change in tension prestrain separates them but not as evenly as the compression curves. The tension curves however do have a change of slope which changes the elasticity. The most even separation is for compression spring foundations of 1000 N/m and 100 N/m and most likely for values between and around these values.

- Cuboidal 3 Cell Model – The curves in compression in the cuboidal model with varying prestrain do not straighten until the larger force – distance portion of the curve. For differing spring foundations the spring foundation of 10 N/m separates from the other spring foundation values. In tension the cuboidal model curves of varying prestrain separate well at all graphs of values spring foundation. In tension varying spring foundation in tension the spring foundation of 10 N/m in a similar way to the compression tests. At 0.3 prestrain the spring foundation of 1000 is out of sequence as in it is higher than the 10,000 spring foundation and the rest of the spring foundations are lower.
- Columnar 3 Cell Model – Columnar model with wide posts in compression separates the curves with large spring foundation of 10,000 N/m and large prestrain of 0.3. In tension the best separation of slopes occurs at spring foundation of 10,000 and large prestrain of 0.3. Columnar with thin posts produce linear graphs that are on top of one another and therefore do not change in elasticity for either prestrain or spring foundation.
- Different k factor in the 3 Cell Model – For a k factor of 0.1 In compression the zero prestrain separates from the rest of the prestrains and has a different slope or elasticity. In tension the prestrain values separate with different slopes as well but the prestrain 0.1 has a large change at spring foundation of 10,000 N/m and prestrain of 0.2 has a large change at a spring foundation of 10 N/m. Changing the k value to smaller k lowers the slopes of the graphs.
- Changing the cell membrane width changes the width of the non-linearity in the Force-Distance and Stress-Strain graphs.
- Removing cell basement attachments in the middle of the model changes the Stress-Strain curve

Note: the original model k factor is 0.0004

4.2 Some Result Details

The following Force-Displacement graphs show the Displacement as the Difference in Displacment so that all of the graphs start at zero. When placing prestrain on the structure the height of the structure changes therefore the height difference is used to compare graphs. All the forces were applied at the trijunction top in the z direction.

4.2.1 Comparing Characteristics of Different Model Heights

The squamish model is 1.2 um heigh, the cuboidal model is 3.5 um heigh and the columnar model is 20.5 um.

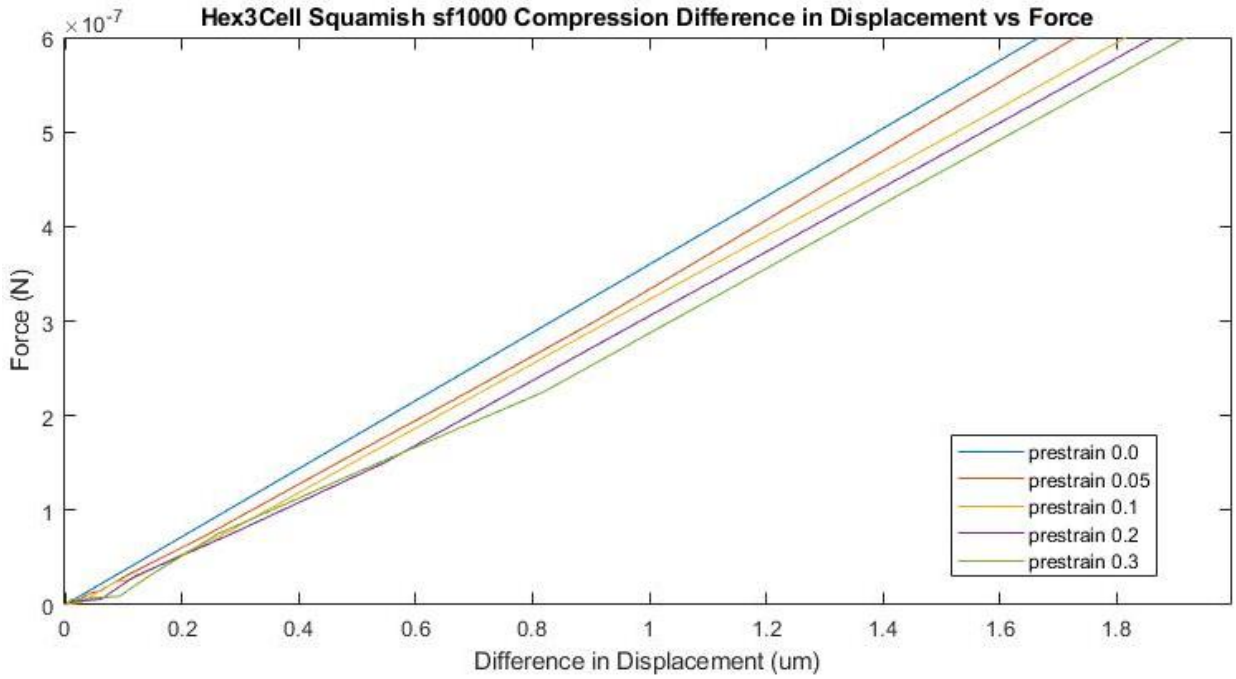

Figure 4.1 *Hex3Cell Squamish model in Compression. Spring foundation of 1000 N/m.*

Figure 4.1 shows a successful squamish cell model in compression Figure 4.1 where the cell has a separation of Force-Displacement curves due to pre-strain. This graph is similar to the squamish sf100 or spring force of 100 N/m graph (appendix A). The structure initially starts with a non-linear curve with the higher pre-strain needing more displacement and force to become linear. Here the higher curve is the zero pre-strain.

Zero pre-strain will acquire strain as the force bears down on it and this will help it hold the force or weight being applied to it.

The nonlinearity of the beginning of the lines could add up to a different elasticity for the tissue if summed over a large number of cells. That would give the graph a curve. The Distance-Displacement graphs are all graphed between the Strain of 0.0 and 1.0 which can also be written as 0% to 100% strain. Most materials have a strain between 0.0 and 0.2 (0% and 20%) and tissue between 0.0 and 0.5 (0% and 50%). Therefore the higher values of Force and Displacement are likely not achievable in real life as the materials will yield and break before reaching a strain of 1.0. The model achieved these higher values because a yield point was not included in the material parameters. Tensegrity models can achieve these high rates of strain whereas other models often only go to a strain of 0.2 such as the Ogden Model (Lohr et al., 2022). For graphing the Force-Distance graphs the standard convention of graphing the compression curves in the positive y axis and graphing the tension forces in the negative y axis was used. Graphing the Stress-strain

curves was kept in the positive y axis in keeping with the literature on the measurement of the different types of tissue.

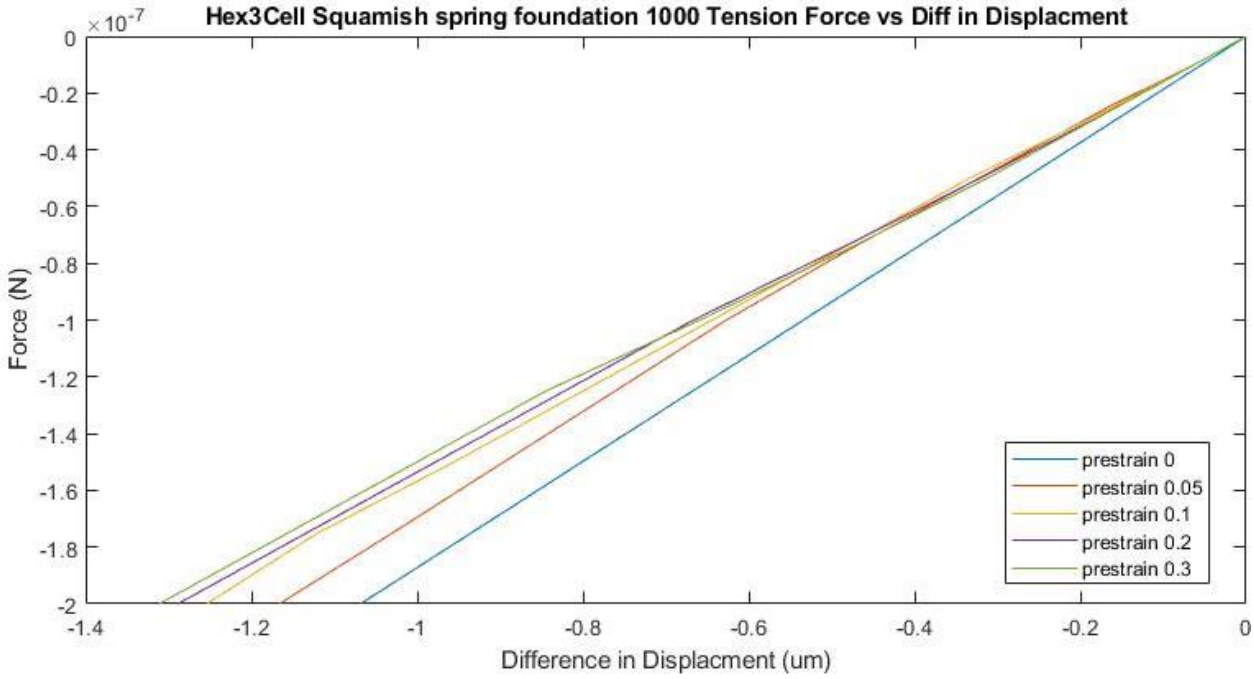

Figure 4.2 *Hex3Cell Squamish model in Tension. Spring foundation of 1000 N/m.*

Figure 4.2 is the squamish cell model in tension showing a separation of lines at varying pre-strains. The separation is not as even as the compression lines with the best separation at pre-strain 0 and 0.05.

The tension pre-strains are more linear than the compression lines and the slopes are different from one another. The compression pre-strain lines are parallel to each other giving them the same elasticity whereas the tension lines have different elasticity. Also the pre-strain zero and then pre-strain 0.05 occur on the bottom of the graph inverting where the lines occur.

Changing the spring foundation does not change the graphs which are linear and on top of one another. More experimentation of spring foundation should be carried out. The attachments are known to be weaker in the middle of a group of cells and cells are attached at many points (Xu et al., 2020, Barreto et al., 2014).

The cuboidal three cell tissue model has different characteristics from the squamish or columnar models.

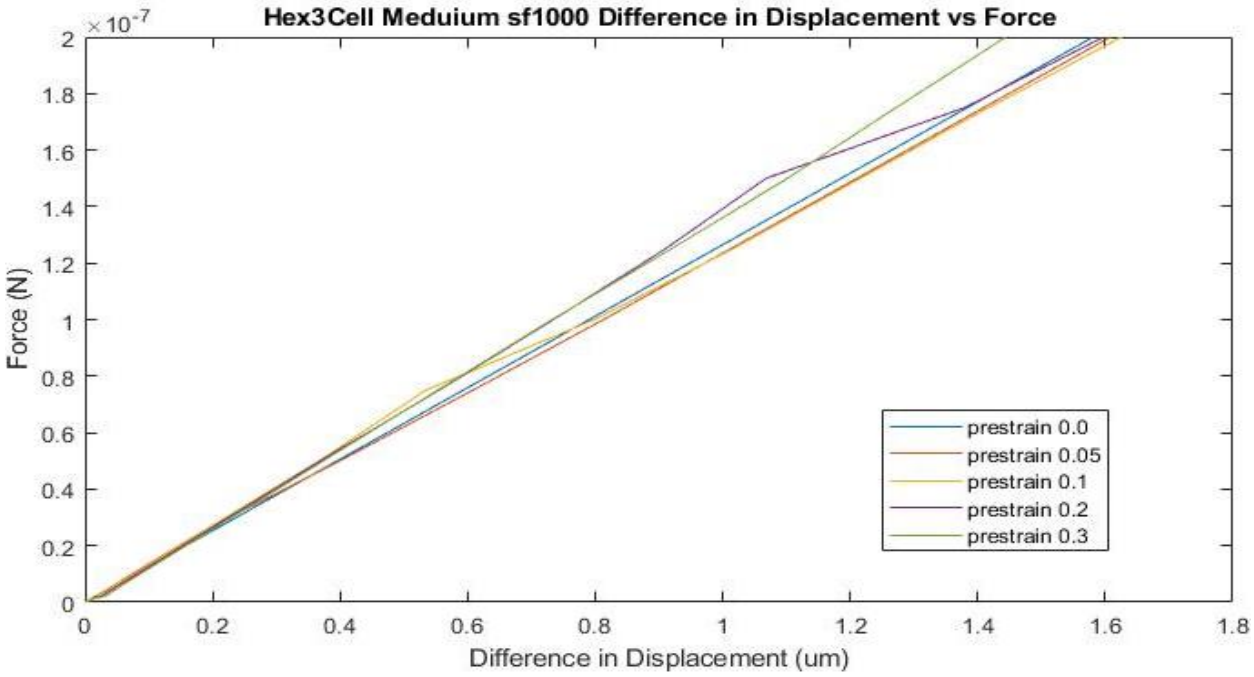

Figure 4.3 *Hex3Cell Cuboidal model in compression. Spring foundation of 1000 N/m.*

The cuboidal cell at spring foundation 1000 N/m shows a lot of non linearity with pre-strains 0, 0.05 and 0.1 being the most linear but they are not separated.

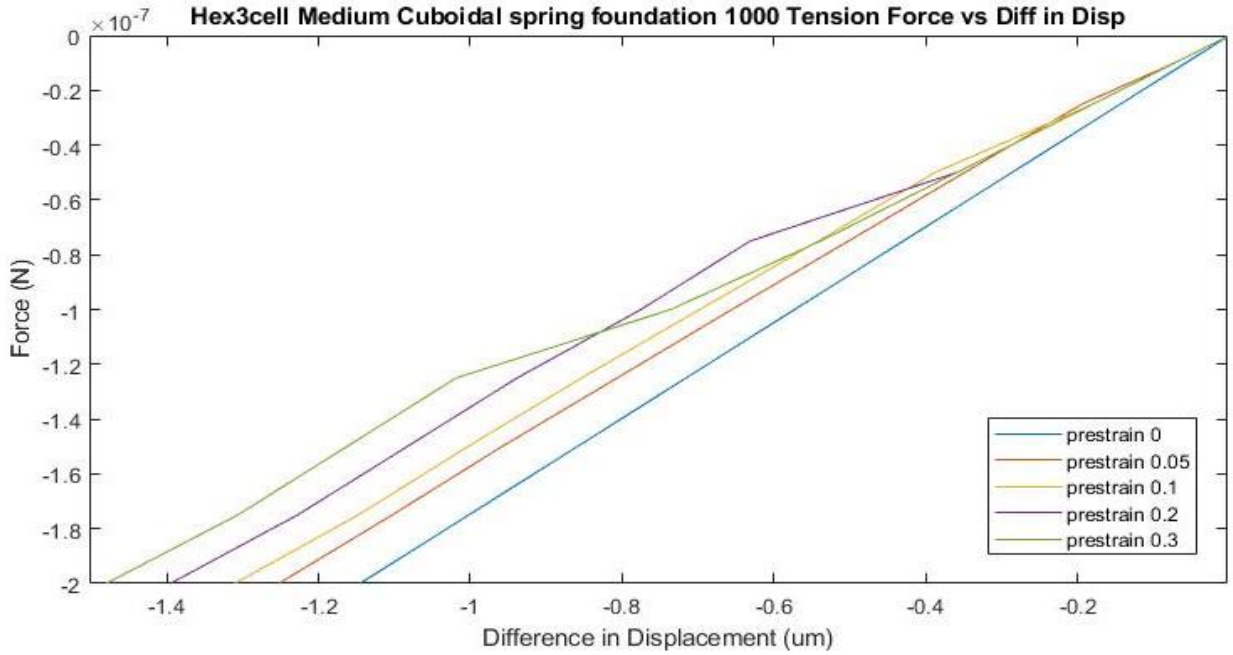

Figure 4.4 *Hex3Cell Cuboidal model in Tension. Spring foundation of 1000 N/m.*

The cuboidal cell model in tension shows a linear parallel separation of elasticity lines. The lines become linear at different points with the pre-strain of 0.2 becoming mostly linear after a displacement of 0.65 um and Force of 0.7 N. Both the pre-strain of 0.2 and 0.3 are slightly non-linear.

Columnar cells with wide posts show the linear parallel separation of elasticity without as much definition as there is in the squamous cells but more than there was in the cuboidal construction. The columnar model was measured by both recording the displacement due to force applied at individual points where the force was applied and using the average measurement of the displacement. The individual points had different displacements from each other but overall produced similar graphs (see appendix A).

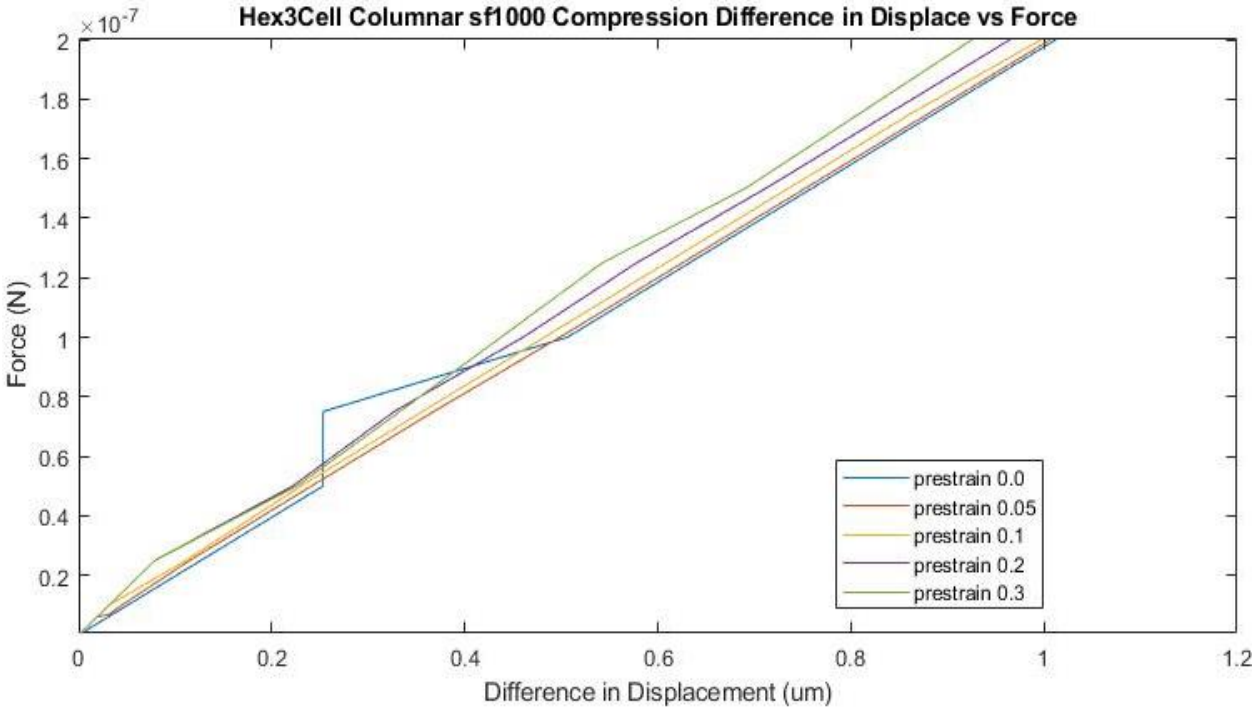

Figure 4.5 *Hex3Cell columnar model wide posts in compression sf 1000 single point graph. Spring foundation (sf) of 1000 N/m.*

The pre-strain of 0.0 has a softening point that tensegrities can develop. The lines straighten by displacement of 0.8 um. Tensegrities often develop points where the strings will not have tension on them due to the shape change due to the forces on the tensegrity. These points are called soft modes and result in sudden changes in the Stress-Strain curves. This is a measurement of a single point on the top triangle.

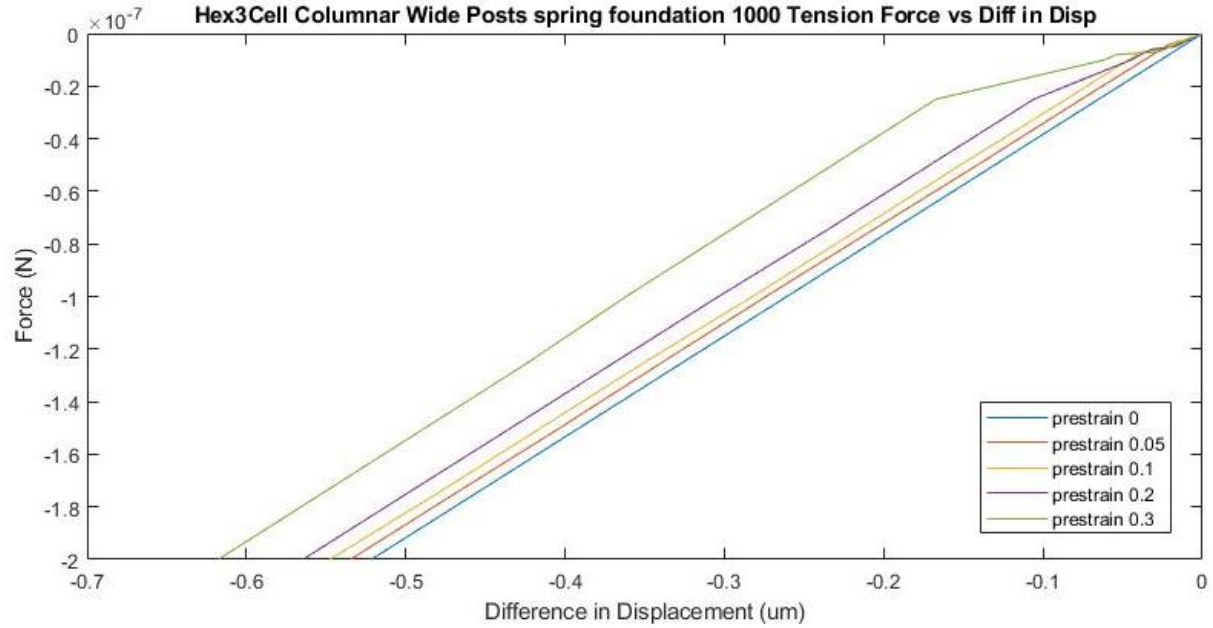

Figure 4.6 Hex3Cell Columnar with wide posts in Tension. Spring foundation of 1000 N/m.

The graph of changing prestrains for the Columnar wide post model shows good separation of curves with the largest change at a prestrain of 0.3.

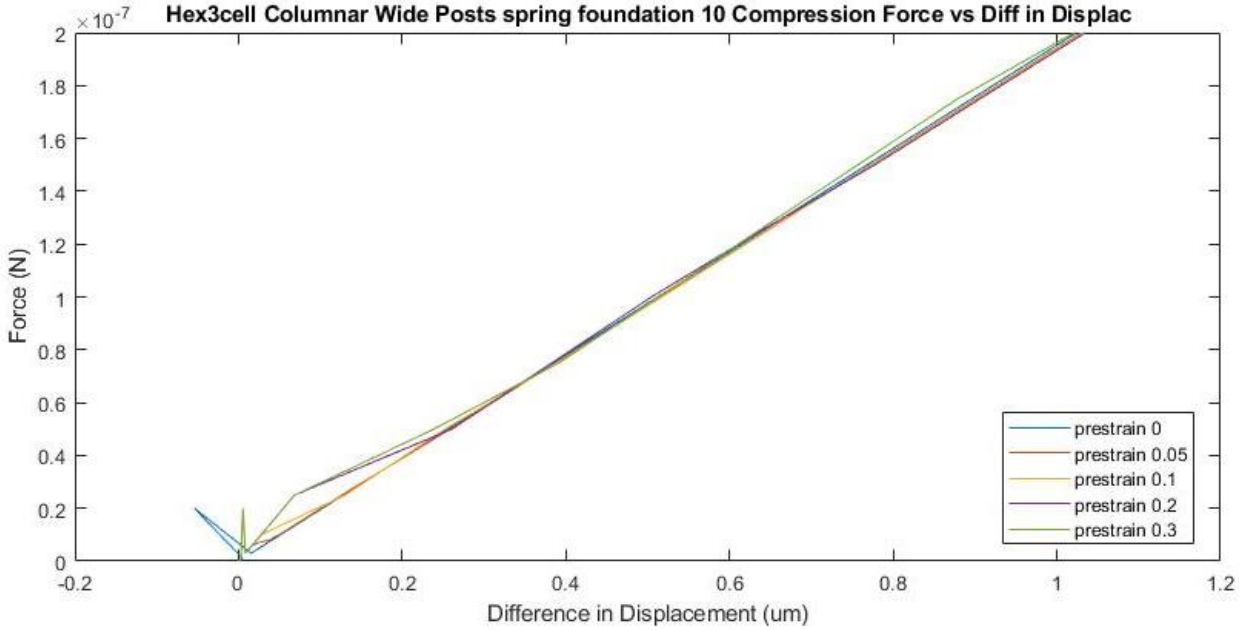

Figure 4.7 *Hex3Cell Columnar model with wide posts in compression sf 10. Spring foundation (sf) 10 N/m.*

This is an example of a mechanical environment that would not work for the hexagon three cell tissue structure. There is very little change in elasticity across pre-strains and starts at small forces in a very nonlinear way. The tension graphs for the spring foundation of 10 N/m also show little change in the elasticity across pre-strains.

The varying spring foundation graphs for this columnar model show the spring foundation of 10 N/m to be separate from the other spring foundation lines which are on top of each other for most of the pre-strains (see Appendix A).

For large pre-strain of 0.3 the columnar cells show separation of linear elasticity at a variety of spring foundations in tension.

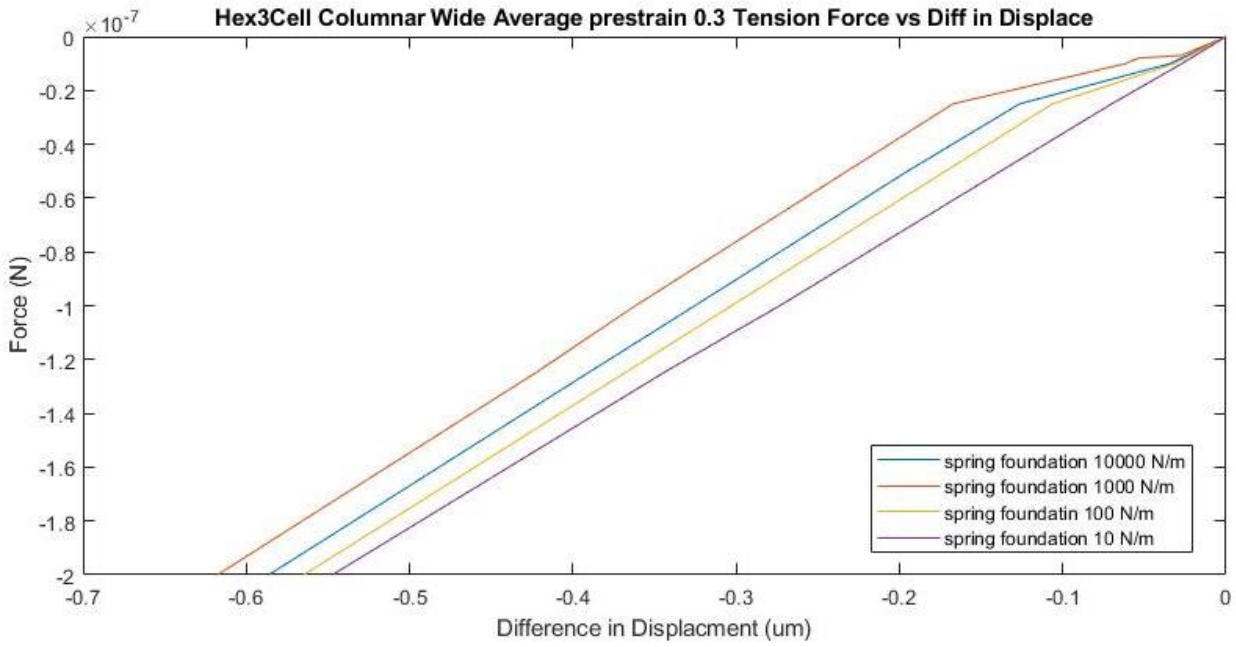

Figure 4.8 Hex3cell *Columnar wide post in tension showing varying spring foundations. The elasticity is the same – has the same slope except for the spring foundation of 10 N/m.*

The spring foundation that needs the most force is 1000 N/m with the spring foundation of 10000 N/m just under that.

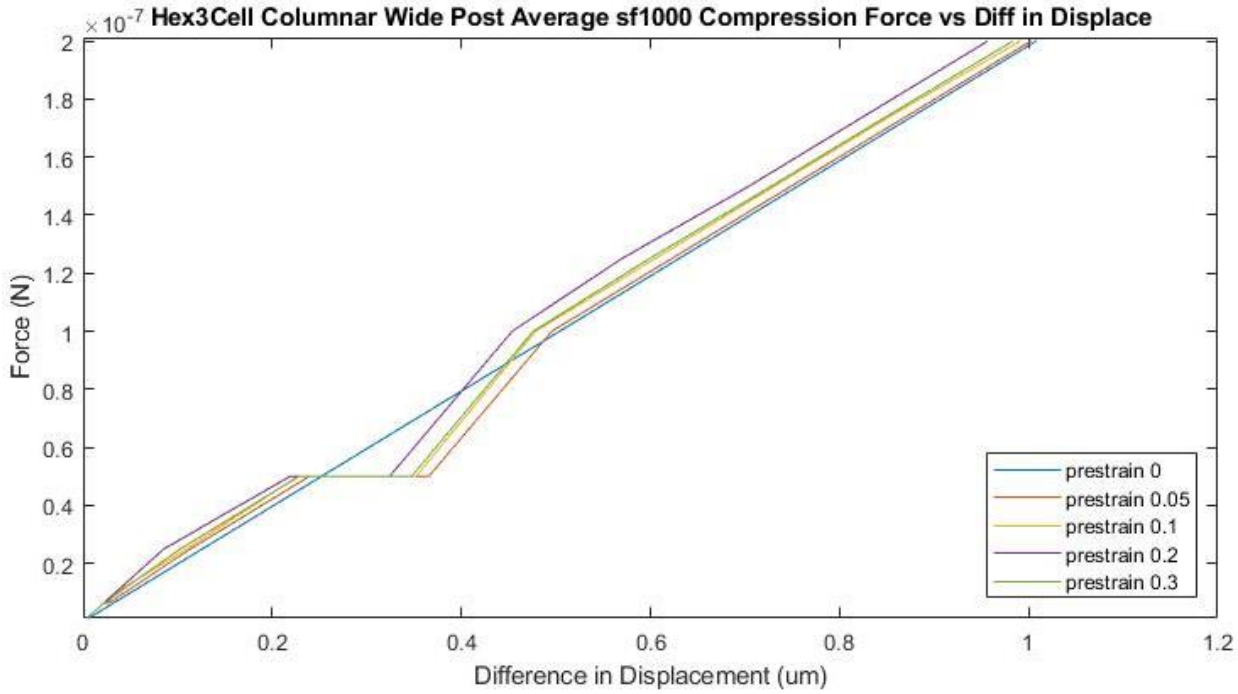

Figure 4.9 Hex3Cell *Columnar model with wide posts in Compression Averaged. Averaged distance moved with applied force. Spring foundation of 1000 N/m.*

An interesting graph was produced for the columnar cells at spring foundation 1000 N/m. At point Displacement 0.4 and Force 40 nN the structure has a tensegrity softening and all of the slopes for the pre-strains except for pre-strain 0 follow each other. The distance moved for each of the top nodes differed for the columnar models. Averaging the distance moved worked well for the model graphing and was used for overall analysis.

4.2.2 Columnar Posts

The columnar three cell tissue model was measured using both narrow posts which are the same size as the posts used in the other models and wide posts which worked better than the narrow post models. The narrow posts show no variation in stress-strain response and were mostly linear with the curves on top of one another both in compression and tension. The narrow posts are the same size as the posts in the squamish and cuboidal models but look thin next to the columnar cells. These posts cause the columnar model to fail – have not separation of graphs due to prestrain.

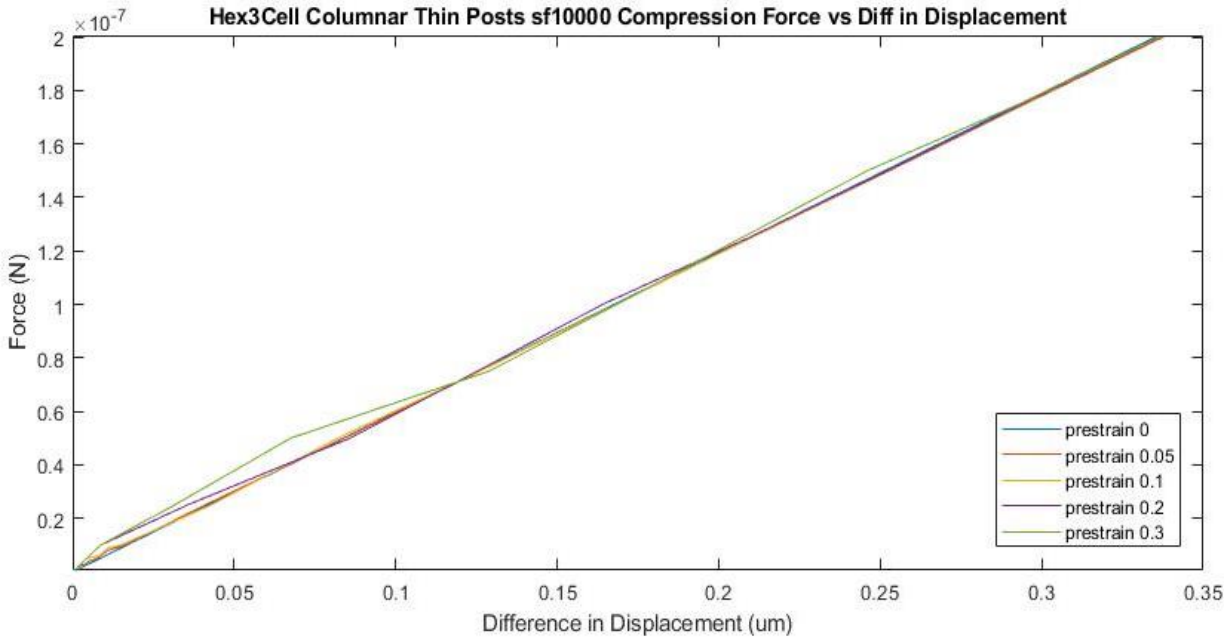

Figure 4.10 *Hex3Cell Columnar model with Thin Posts in compression. Spring foundation 10000 N/m in compression.*

Thin posts in columnar cells do not create separation of graphs for differing prestrains.

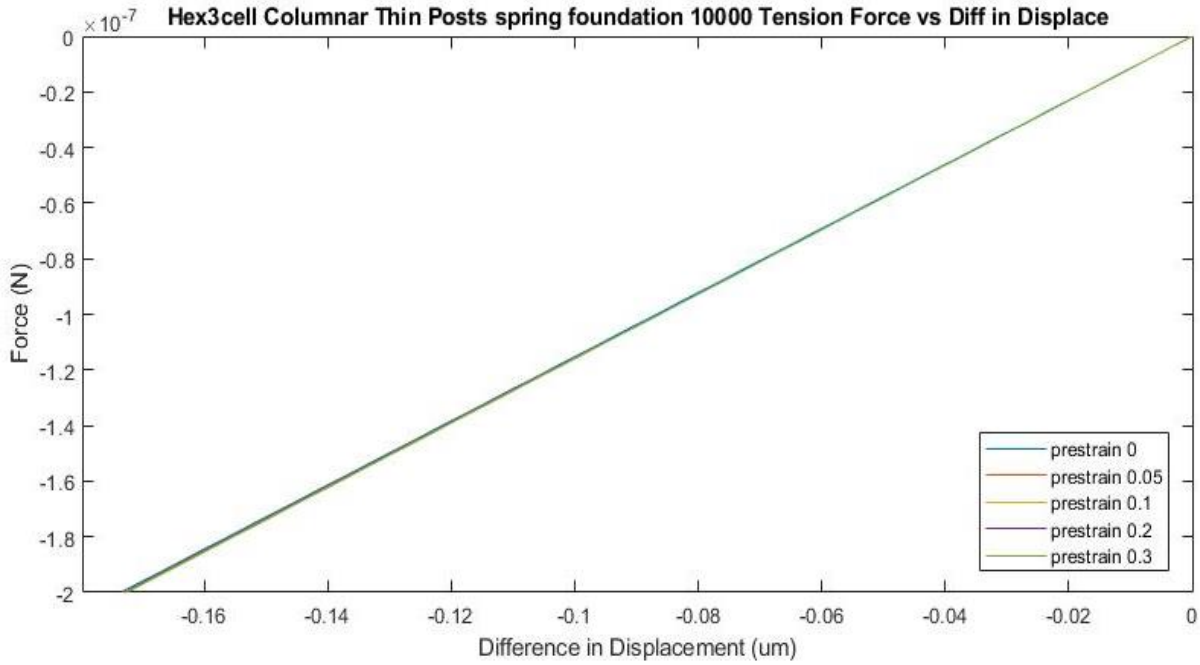

Figure 4.11 *Hex3Cell Columnar model with thin posts in Tension. Spring foundation of 10000 N/m.*

The columnar models with wide posts have a more varied response to applied force.

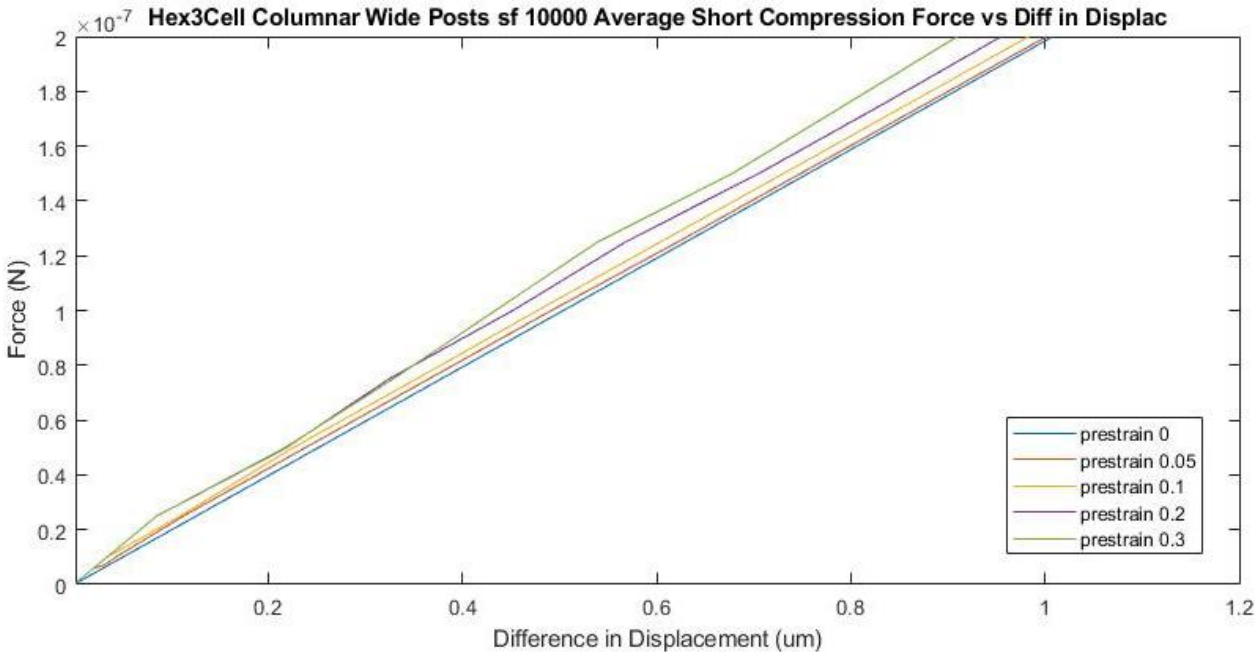

Figure 4.12 *Hex3Cell columnar model with wide posts in Compression. Spring foundation 10,000 N/m*

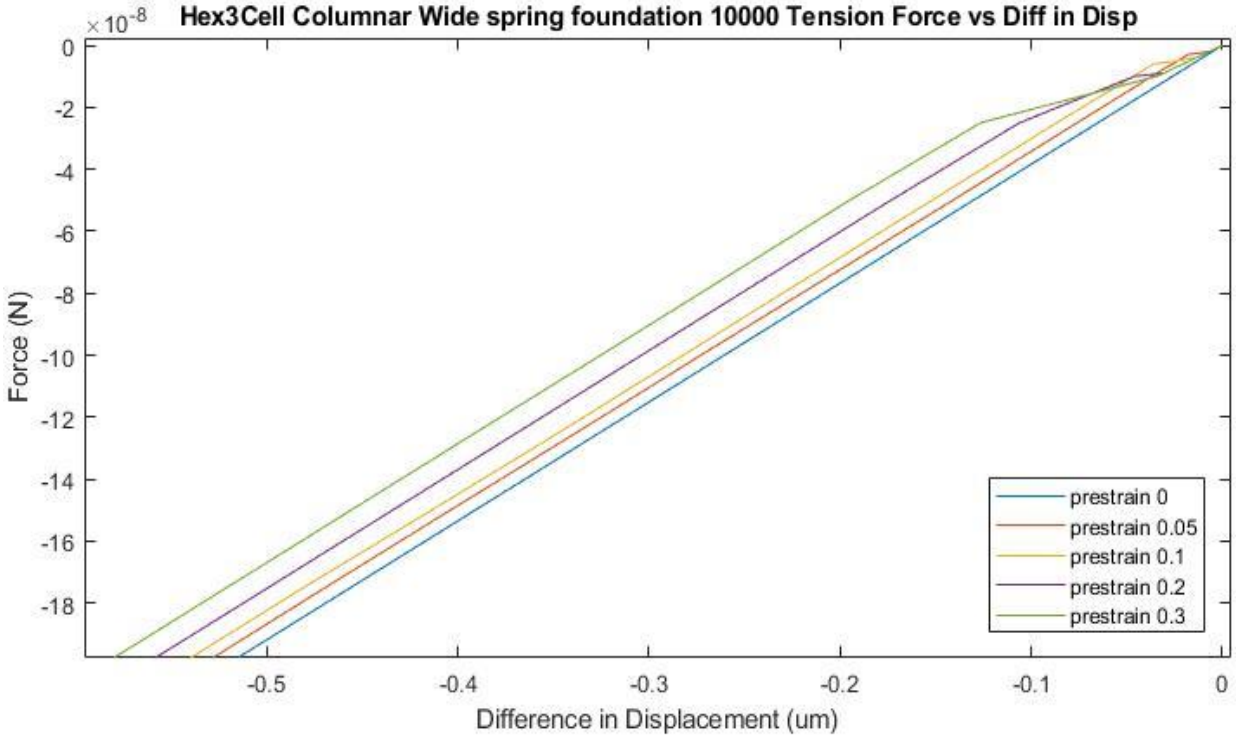

Figure 4.13 *Hex3Cell columnar model with wide posts in Tension. Spring foundation 10,000 N/m*

The separation of the curves for differing prestrain is good for both the compression graphs and the tension graphs for the columnar wide post models.

4.2.3 Changing the k factor

Changing the k factor Makes a large difference in the stress-strain magnitude of the tissue.

$$k = \frac{(EA)string}{(EA)rod}$$

Equation (6) (Sabouni-Zawadzka, 2023)

The k factors used were k = 0.0004, k = 5 x 10^{-9}, 8 x 10^{-9}, and k=0.1.

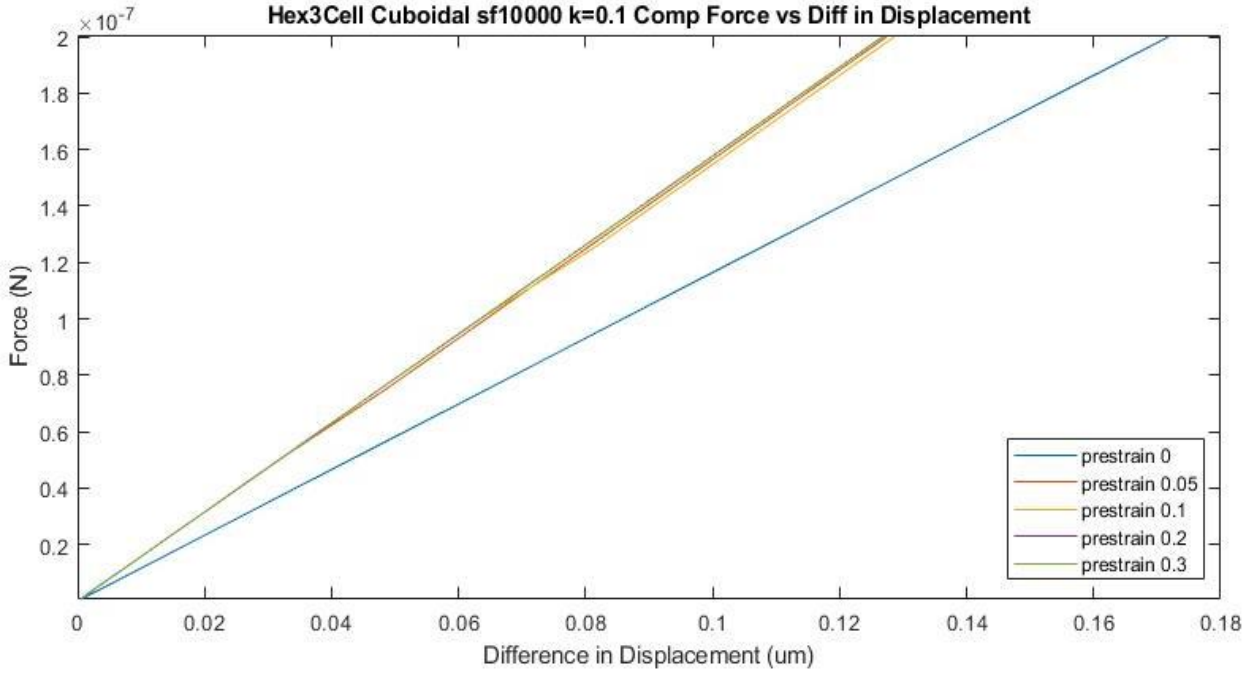

Figure 4.14 *Hex3Cell Cuboidal model in compression, k = 0.1. Spring foundation 10,000 N/m.*

There is not a good separation of graph lines except for the prestrain of zero and the displacement is ten times smaller that in the k = 0.0004 graphs.

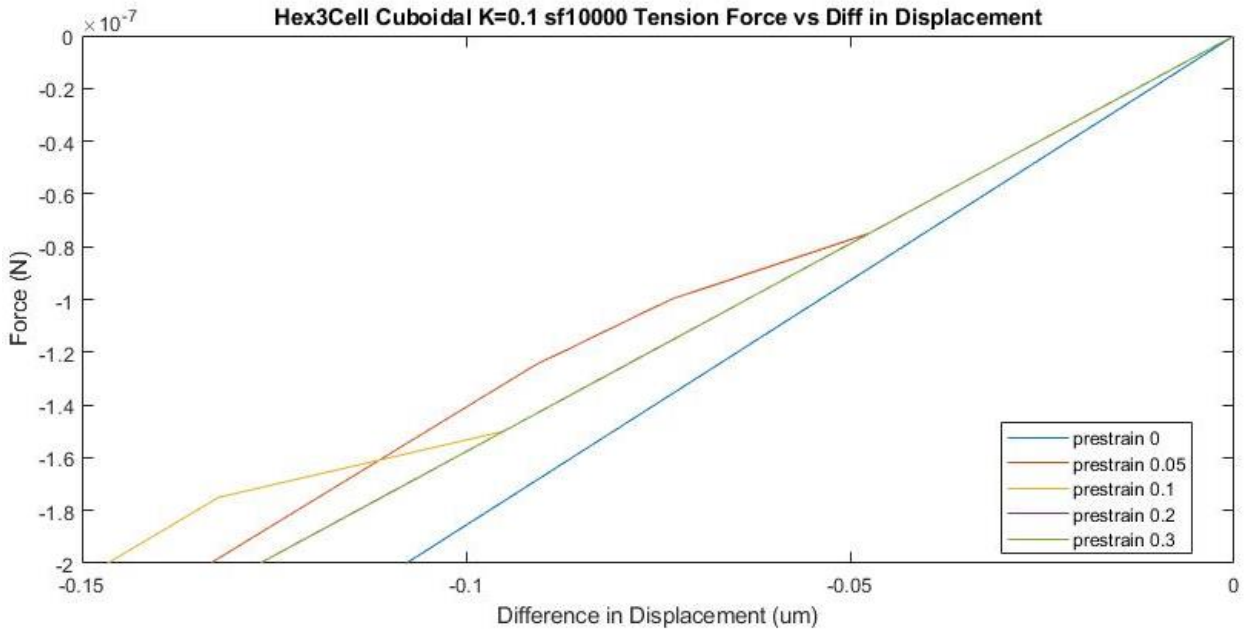

Figure 4.15 *Hex3Cell Cuboidal model in Tension k = 0.1. Spring foundation 10,000 N/m in Tension.*

The compression graph for k=0.1 shows a large separation of the restrained graphs and the zero prestrain in compression and also a difference in tension. The graphs are a factor of three smaller in displacement movement per force applied.

4.2.4 Modifying the distance between cells m

The distance between cells changes the amount of displacement of the nonlinearity in the Force – Displacement and the Stress-Strain curves.

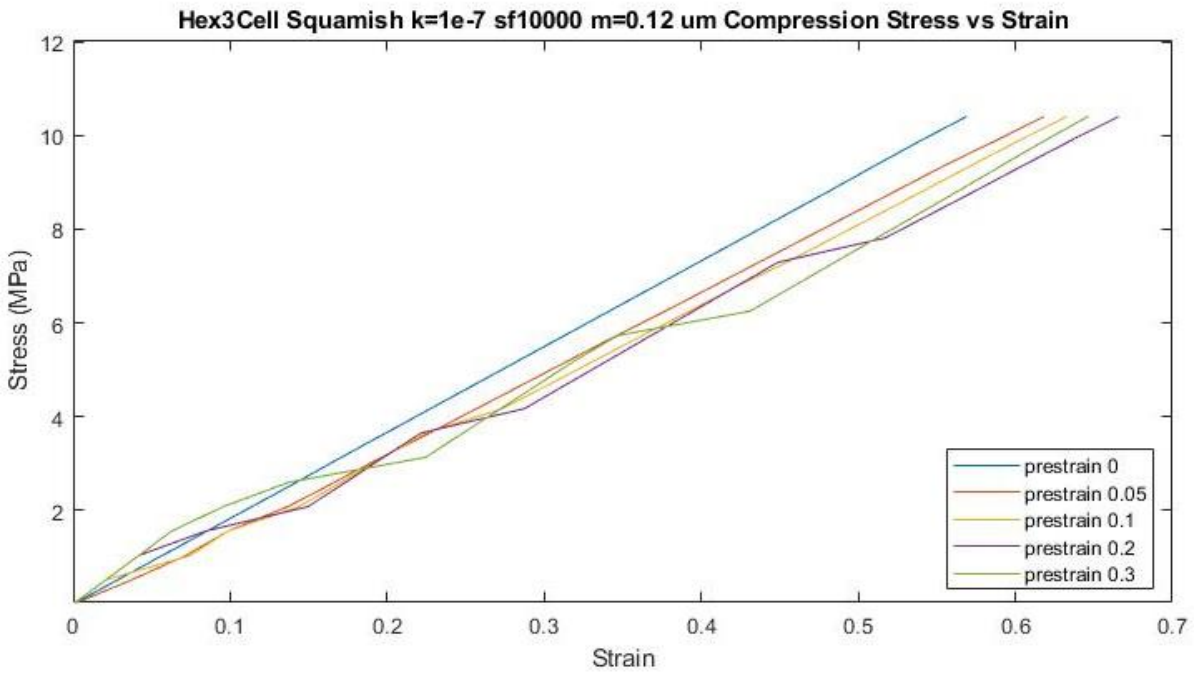

Figure 4.16 *Hex3Cell squamish model in compression m = 0.12 um*. k = 10^{-7}, a *cell membrane distance of 0.12 um is at the average range in a cell.*

The distance m is close to actual measurements in cells (Vanslembrouck et al., 2022). There is nonlinearity in the curves until about 0.5 strain except for zero prestrain.

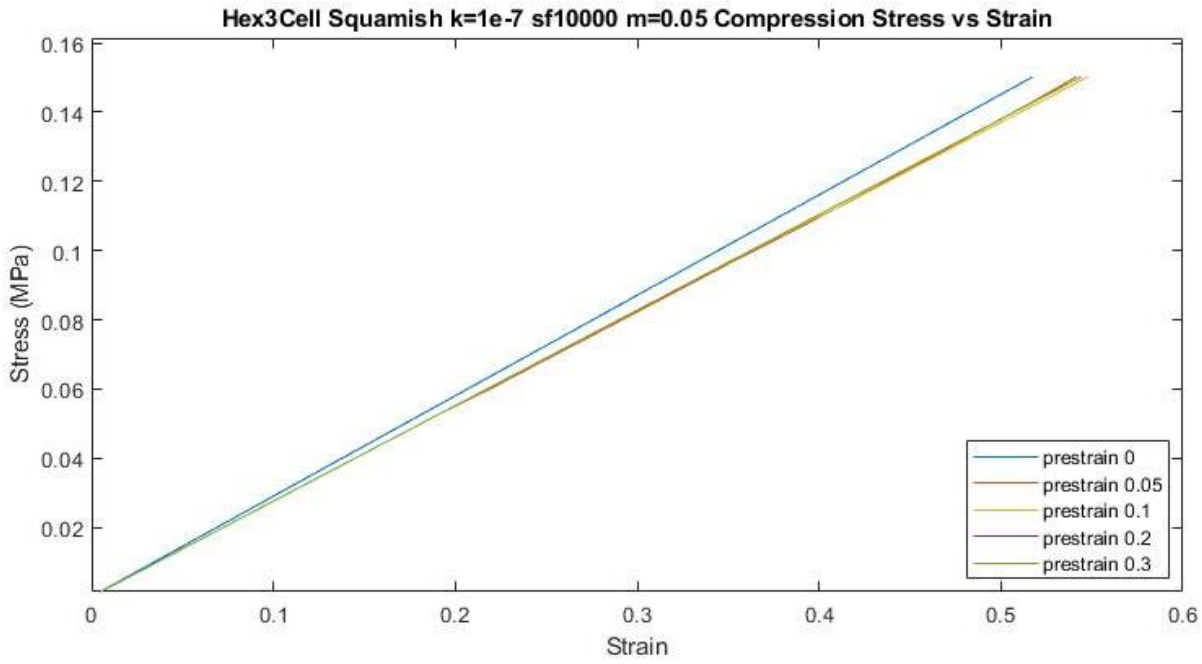

Figure 4.17 Hex3Cell squamish model in compression m=0.05. k = 10^{-7}. T*he smallest cell membrane distance at 0.5 um.*

These curves are more linear with prestrain of 0 separated out from the other prestrains which are on top of one another.

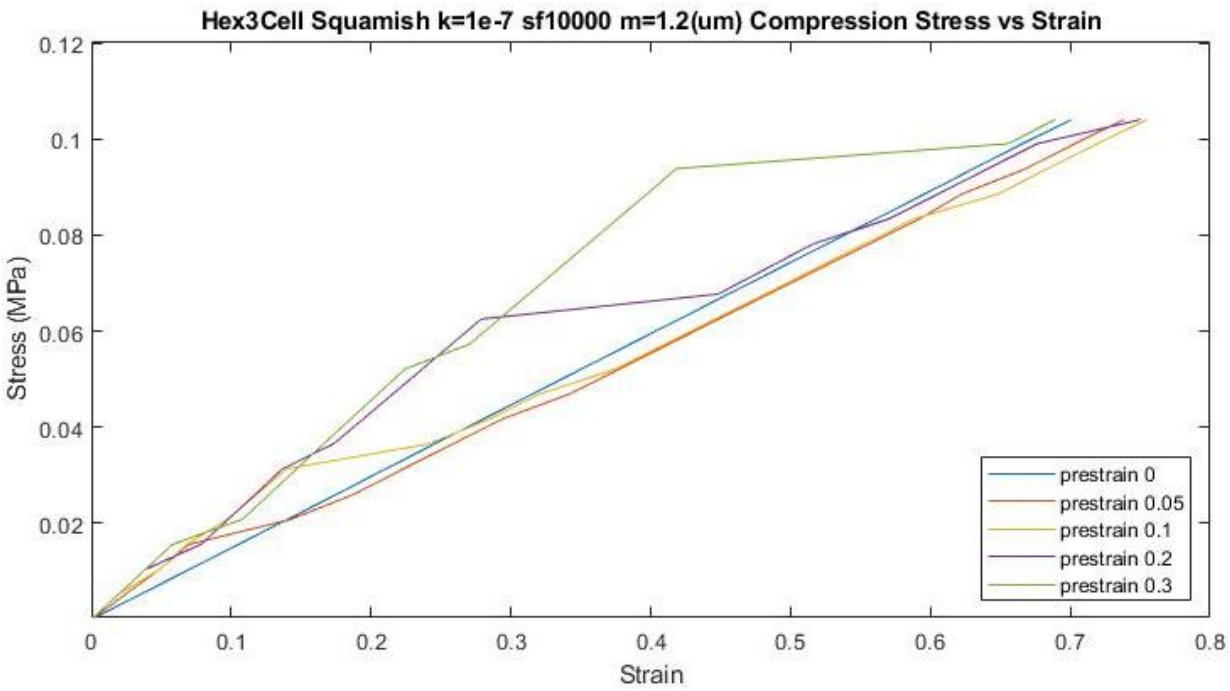

Figure 4.18 *Hex3cell squamish in compression m=1.2 um. Extreme spacing between cells and a large swing in the nonlinearity.*

There are occasions when cells are detached or loosely attached in tissue but these cells don't have the same structure as the mature epithelial tissue (Putra et al., 2023).

4.2.5 Changing Top and Bottom of the Structures

Changing the top and bottom of the three cell structure can also change the stress/strain reaction of the model. Adding a tension only structure to the top of the cuboidal model shows that this didn't change the Force-Displacement curve by much.

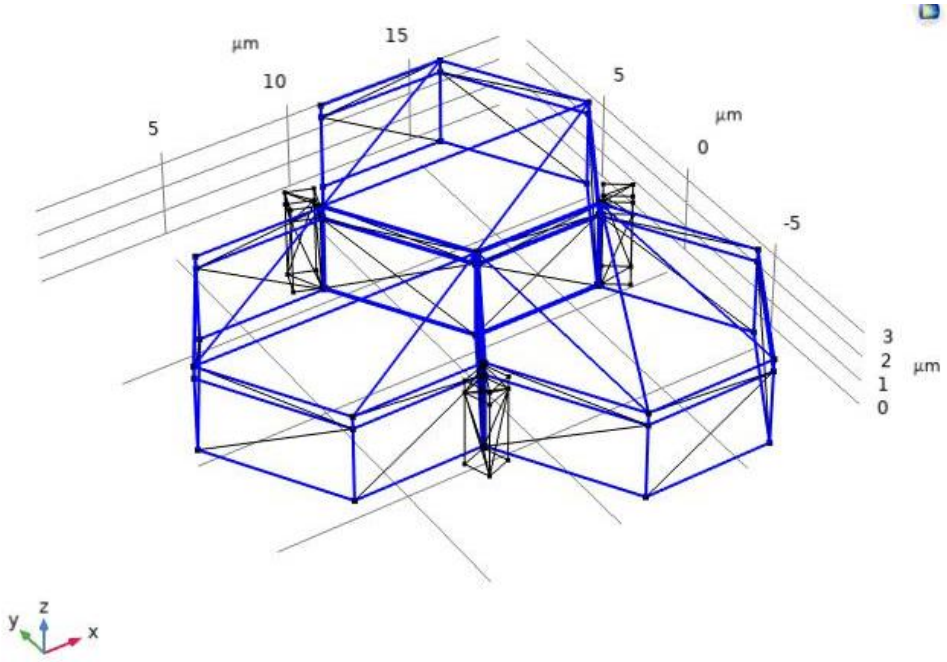

Figure 4.19 *Top of the cuboidal model with extra stings added. The strings are shown in blue and the black lines are the rods or compression elements except for the posts.*

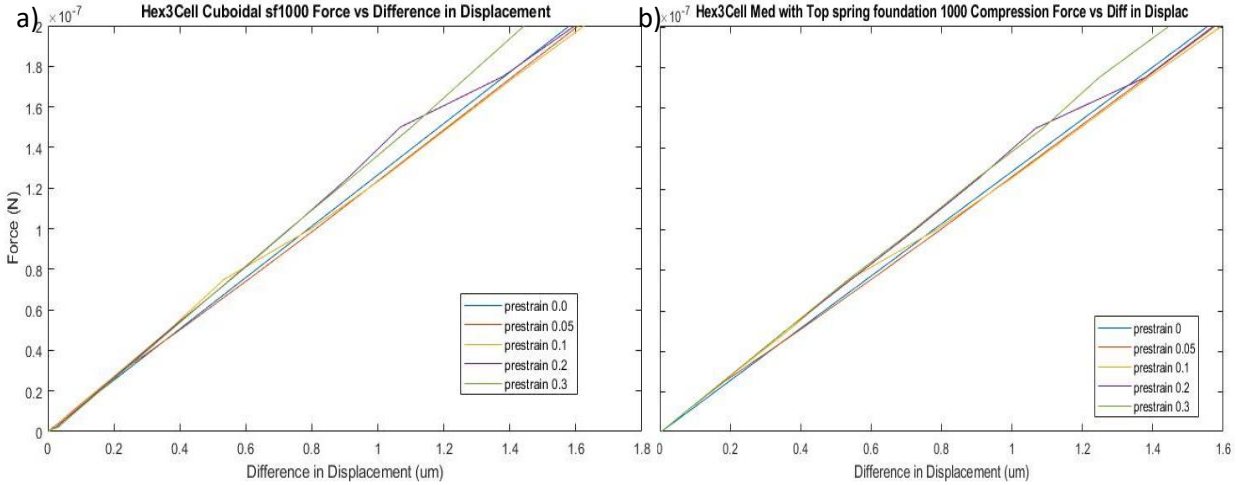

Figure 4.20 ***Comparison of compression curves a) without a top***

Adding a tensegrity top to the cuboidal model to see if top structures have an effect on the force – displacement curve.

Adding a top narrows the nonlinearity of the 0.2 prestrain curve.

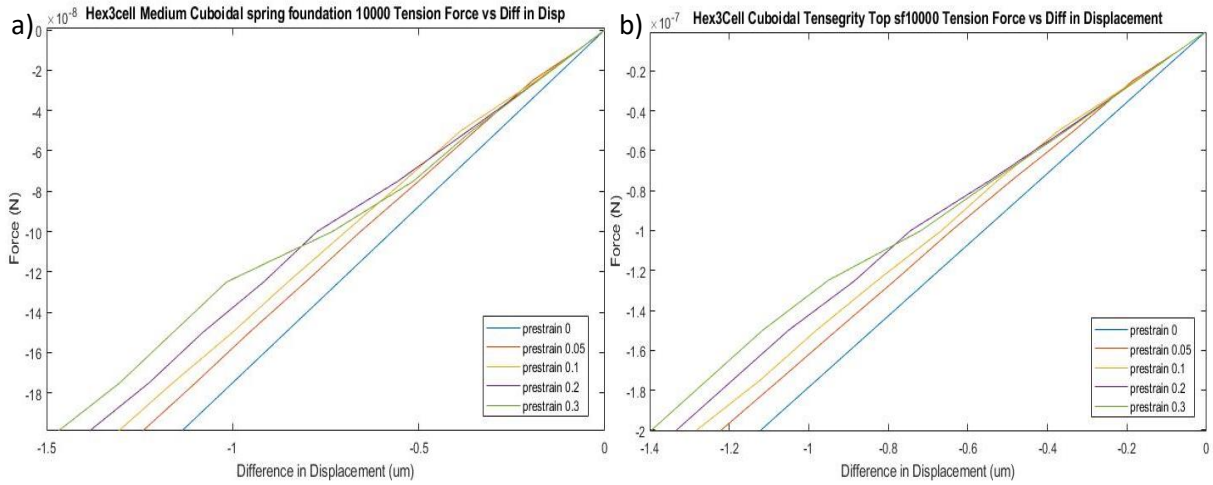

Figure 4.21 *Comparison of Hex3Cell Cuboidal tension curves with and without top a) without a top and b) with a top. Spring foundation 10000 N/m.*

Adding a top structure modifies the Force-Distance curve slightly. The 0.3 prestrain is closer to the other curves and the nonlinearity changes slightly.

It is speculated that the actin in the apical region of cells could affect the mechanical behavior of cells. More experimentation could be done on this model to see what makes a difference in this type of structure. There are also microtubules in the apical region often in abundance as seen in Figure 1.2 so tensegrity configurations with actomyosin-microtubule structures are possible in the cellular environment. The actomyosin-microtubule mesh could form a tensegrity structure therefore a cuboidal tensegrity top model as shown in Figure 4.19.

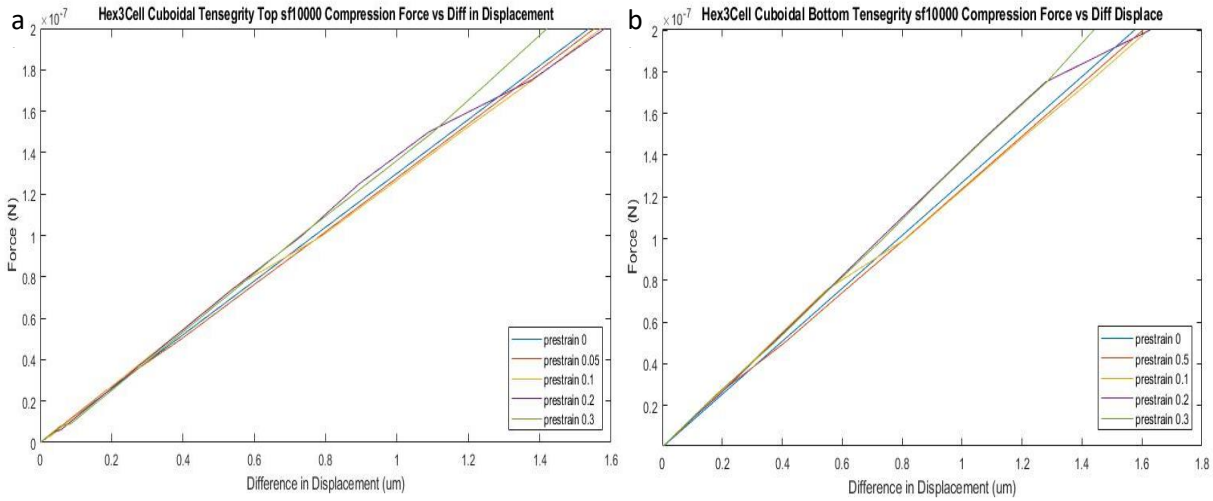

Figure 4.22 *Hex3Cell Cuboidal curves in Compression with and without tensegrity bottom. a) without added tensegrity bottom b) with tensegrity bottom. Spring foundation 10,000 N/m.*

A basal tensegrity is added to the bottom of the cuboidal model to see if that changed it's stress-strain nonlinearity response in compression. The addition of the tensegrity bottom did change the prestrain 0.2 curve and slightly altered the other curves in compression.

The basal part of cells are attached to the basement membrane in patterns (Xu et al., 2020) and this type of patterning or lack of patterning with varying spring foundations could also be investigated.

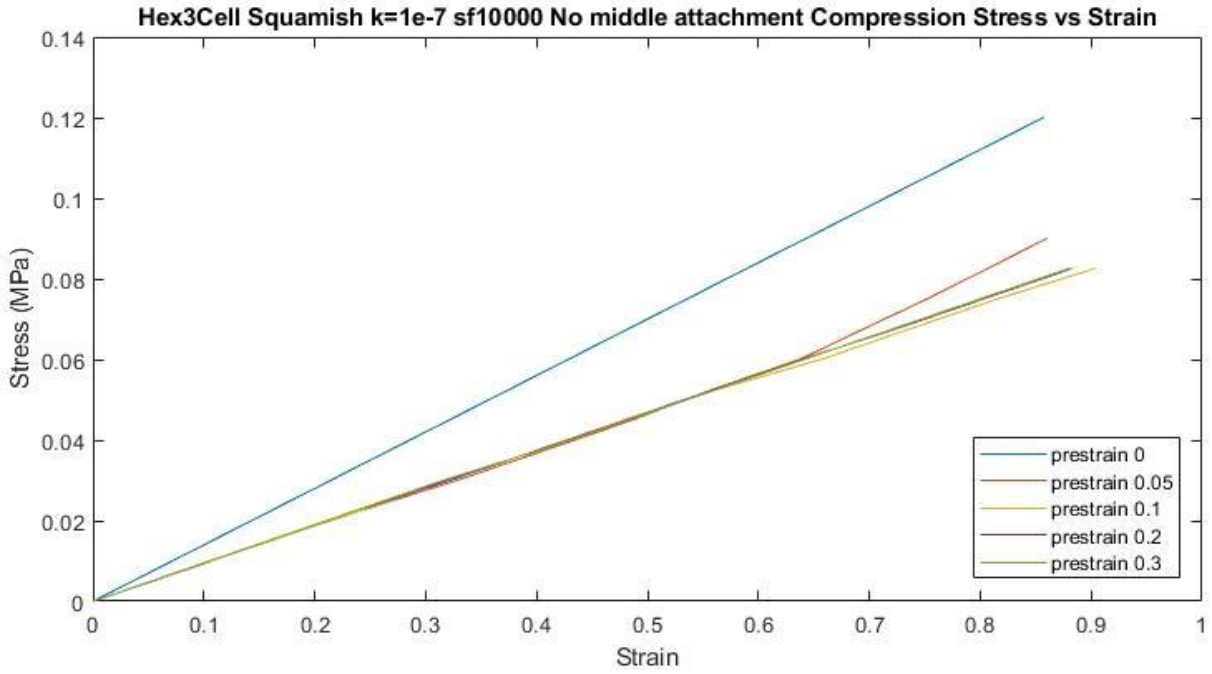

Figure 4.23 *Experiment with detached middle spring foundation. Hex3cell Squamish model in Compression, spring foundation 10,000 N/m with stress-strain curves.*

The Hex3Cell Squamish compression prestrain curves become more linear and the prestrain 0 is separated from the other prestrain curves increasing the elasticity of the zero prestrain curve. This experiment could represent a diseased state. Further investigation into changing the spring foundation points rather than a basal tensegrity would show how the basement membrane attachments change the mechanics in tissues.

This graph stops at a strain of 0.9 or 90% due to a discontinuation of recorded data. The actual strain that is probably achievable in an actual tissue or model is around 0.5 or 50% strain.

5.0 Validation

The initial model and set of graphs are done at a k value of k = 4 x 10^{-4} and this is high for single cell or tissue that has single cell characteristics. The values of k that worked to match tissue samples are k of 8 x 10^{-9} and 5 x 10^{-9}. Shown in Figures 5.1 and 5.3 are Stress-Strain curves of experiments in tension and compression on two different tissues. In Figure 5.1 the tension data is graphed as a stress-strain curve and is in the same range as the data for the model of squamish tissue on a stiff substrate of 10,000 N/m. The figure shows how the model stress-strain curve aligns with the data from single cell sheets.

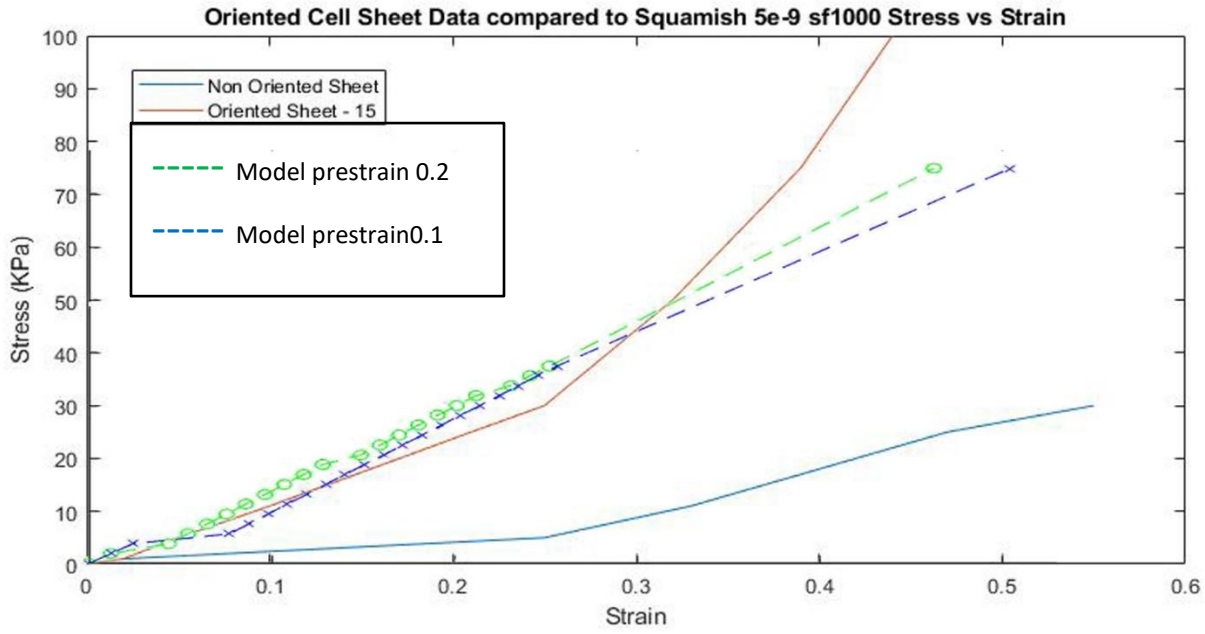

Figure 5.1 *Stress-Strain Tension curves of single layer of live cells and the Hex3Cell Model k= 5x 10^{-9} . Tension curves with dashed lines. The squamish model prestrain of 0.1 in green and prestrain 0.2 in blue dashed lines. The NOCs are Not Oriented Cell sheets, OCS Oriented Cell sheets with 5, 10, 15 µm grove patterns (Data from Xu et al., 2022) modified. The type of cell used for this study was rat cardiomyocytes.*

An image of the live cells in their various orientations is shown in Figure 5.2.

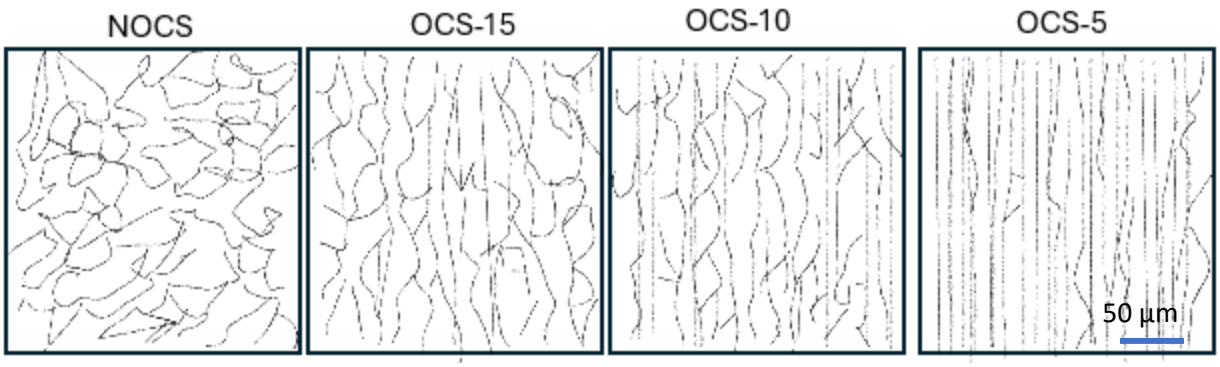

Figure 5.2 *Textures of the cell sheets from the florescence images of the live cells on the cell sheets (Xu et al., 2022).*

The model lines up with the OCS-15 cell sheet but has a slightly different slope partially due to its linearity. The model is not oriented but only contains three cells plus posts. The posts are not a tensegrity and may have influenced the linearity of the slope. A closer look at the Model curves in Figure 5.3 shows that there is some nonlinearity in the model curves.

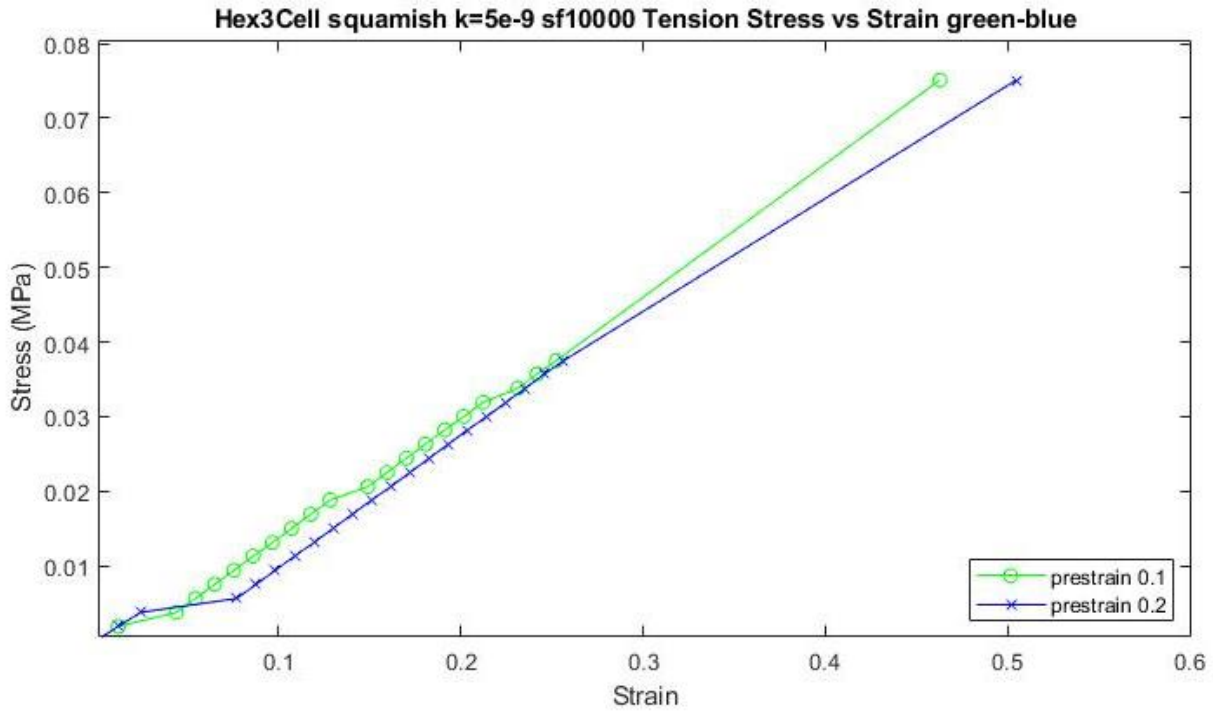

Figure 5.3 *Stress-strain curves for squamish cell in Tension k= 5x 10^{-9} and spring foundation of 10,000 N/m. Shows nonlinearity at the start of the curve.*

Another Stress-strain curve is shown in the Xu et al., 2022 paper with stretch at 90° to the grove orientation and the Model stress-strain Curve also show a similar match to the live cell sheet curves.

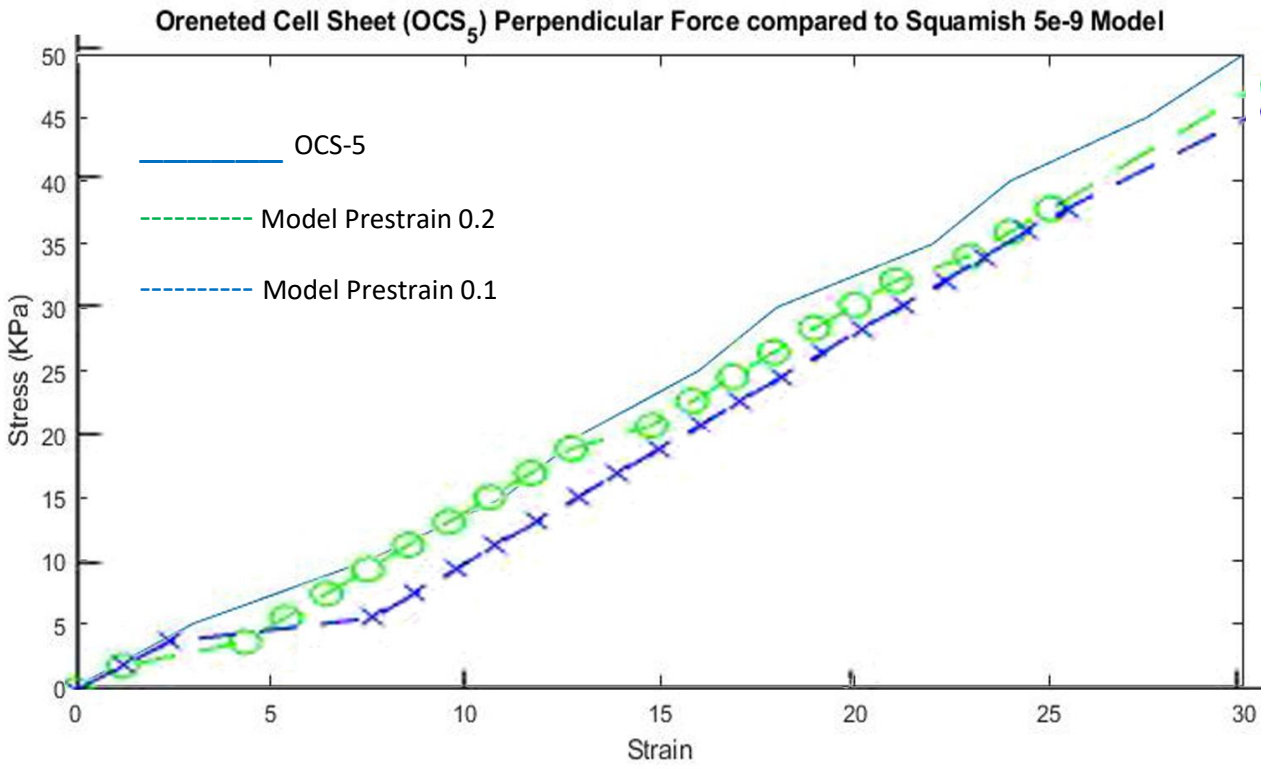

Figure 5.4 *Stress-Strain curves of live cell sheets and squamish Hex3Cell model. Stress-Strain Tension curves of single layer of live cells stretched perpendicular to the orientation of the cells and the Hex3Cell Model k= 5x 10^{-9} . Tension model curves shown with dashed lines. Model prestrain of 0.1 in green and prestrain 0.2 in blue dashed lines. The cells originally were cardiomyocytes. The NOCs are Not Oriented Cell sheets, OCS Oriented Cell sheets with 5, 10, 15 µm grove patterns (Xu et al., 2022) modified.*

The Hex3Cell model is squamish with k= 5x 10^{-9} prestrain of 0.1 shown in green has a close match the OCS-5 stress-strain graph.

Compression curves for excised lung tissue have been measured by Wozniak, 2009 and the Model curve at 8x10^{-9} was matched to it in compression up to 0.2 strain as seen in Figure 5.4.

The stress-Strain curves for the tensegrity model are more linear than the cell sheet curves. This could be due to the fact that the cell sheets have a large number of cells and the model consists of only three cells. In a tissue cell sheet there are likely differences between cells in their attachments to each other and to the basement membrane which in the live cell experiment is a collagen substrate. Substrates have influence on the mechanics of tissue and the stress-strain curve and elasticity of the substrate was not measured in this experiment. The collagen was observed via staining and found that there was a relaxation of the collagen when stretched. The three cell model substrate are the spring foundation and are linear springs. Live cells can change their behavior and in this case it was observed that the F-actin bundles

(strings in the tensegrity model) increased in size to resist the tension forces (Xu et al., 2022). The three cell tensegrity model does not simulate the increase in actin bundle size as a result of increasing tension and this makes a difference in the stress-strain curve.

The live cells and the model show that overall the mechanics is due to the cell cytoskeleton, the attachment between cells and the attachment to the basement membrane (Xu et al., 2022).

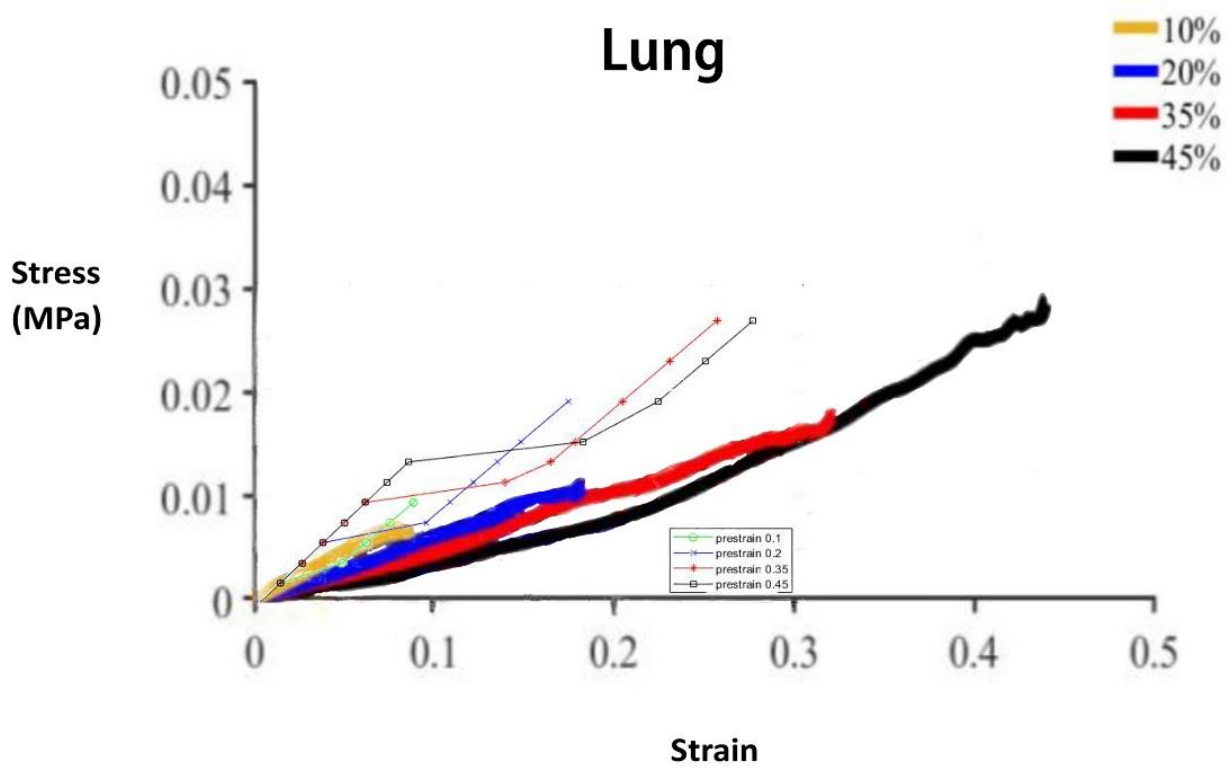

Figure 5.5 *Compression Stress-Strain curves of the lung and compression Stress-Strain curves of the model at k= 8 x 10^{-9}. Spring foundation of 10000 N/m. The 10% prestrain curve of the lung tissue is shown in yellow and the model curve for 10% prestrain is shown in green. The prestrain curves for the lung tissue and model are blue 20% prestrain, red 35% prestrain, black 45% prestrain (Wozniak, 2009). Modified from the Lung in Figure 2.10 and Wozniak, 2009.*

The model and tissue are represented by engineering stress and strain where the original area of the tissue and length (height) are used to evaluate the stress and strain of the tissue.

The graphs are in a reverse order to what normally occurs. The lower slope in the graphs have the higher prestrain. This separation also happens sometimes in the tensegrity model as illustrated in Figure 5.4.

The lung tissue data shows a non-linear stress-strain curves that follows a straight line. The lack of J curve in these tissues may be because there is a lot of elastin in the tissue which acts as the “strings” in the tissue. Lung parenchyma is about 30% elastin and elastin has an elastic modulus of 0.6 to 3.5 MPa. For the k in the range of 10^{-9} the string elasticity was chosen to be 0.5 MPa (Trebacz and Barzycka, 2023). With a smaller elasticity the whole structure will act less like a tensegrity and more like a squishy ball or squish (Levin, 2022 in conversation).

Another observation of the data for tissue shows that the models with k = 4 x 10^{-4} the matching skin tissue.

A set of graphs showing human epithelial tissue comes from Dwivedi et al., 2022 shown in Figure 5.5. Other data from fresh autopsy of pig skin is seen in Figure 5.3 (Dwivedi et al., 2022).

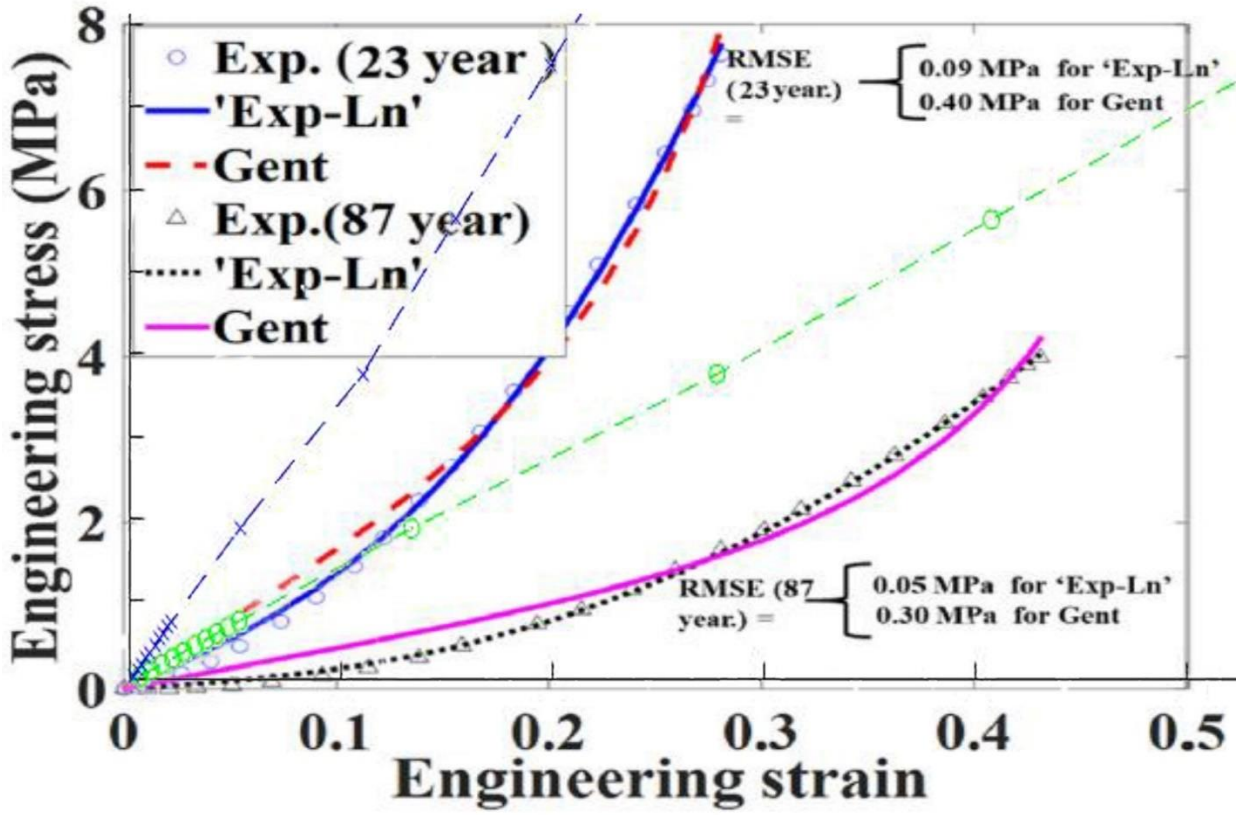

Figure 5.6 *Human skin compared to squamish and cuboidal model k= 0.0004. Human skin from freshly autopsied younger and older skin from two individuals in tension (Dwivedi et al., 2022). Compared to squamish (green) and cuboidal (blue) models at prestrain 0.1 spring foundation 1000 and 10000 respectively.*

Since the skin is freshly autopsied it should give a similar magnitude to in vivo tissue.

The data for squamish cells from the model shown in graph from in Figure 5.5 show similar values in between the older skin sample and the younger skin sample shown in Figure 5.5. The cuboidal cells have a slightly higher modus of elasticity than the younger skin.

The data from the tensegrity models is more linear than the skin graphs and other models and this is probably due to the influence of the posts in the model and the fact that there are only three cells in the model.

The differences in the curves may be to differences in loading rate between the model and the tissue measurement. The loading rate is how fast the force is applied. This parameter was not tested for and could be done at a later date.

6.0 Discussion

Building a minimalist tensegrity model for tissue using the measurements and structure of epithelial tissue has returned results that model tissue. The individual hexagon structures work together with trijunctions and spring foundation attachments to give an overall result. The entire structure depends on the triangular prism attachments and base spring attachments. Without these attachments the model will not support any force.

A triple hexagon using the simple tensegrity build and the T3 and T4 prisms used for trijunction cell attachments produced the model for tissue. The T4 was used as the middle trijunction attachment in the structure and the T3 prisms were used in the outer trijunction attachments to the posts. The posts are not a tensegrity object but are a truss. The posts were necessary for the structure to work and are a stand in for the rest of the cells in the tissue. The model is labelled Hex3Cell and was produced in short, medium and tall forms to mimic squamish, cuboidal and columnar epithelial tissue. The parameters of pre-strain and substrate spring foundation attachments were used as variables. Changes in the value of k or ratio of string elasticity and area over the bar elasticity and area were investigated.

The posts may have influence on the model mechanics and maybe causing more linearity in the mechanical output than a tensegrity would. The models as a whole have nonlinear parts but are more linear than the examples of tissue. In columnar cells the thin posts were a failure as the graphs for all prestrain and spring foundation were linear with the same slope and graphed on top of one another. The wide post columnar model worked well.

To change the k value the elasticity of the strings were changed from 100 GPa to 50 MPa. The 100 GPa represents actomyosin in tension and the 50 MPa represents elastin the mixture of cell cytoskeleton components. The data for the exact values of actomyosin bundles and elastin structures does not appear to be in the literature so the values used were approximations.

The amount of elastin in the cell which lowers the k value will also have an overall effect on the mechanics. Stiffer elasticity of strings makes a tensegrity. If the strings are stiff the structure will change its entire shape when a force is applied. If the strings are soft elastic the force will just change the area where the force is applied and the force will not transmit to the rest of the model. This has been observed in simple tensegrity models and is a known factor in designing tensegrities (Levin, 2022).

Separation of curves in the models with differing prestrain was a parameter that shows the success of the model. The models were tested with forces from 0 to 200 nN and the results were in um. The range of forces depended on the k value with lower k values with lower forces of 0 to 2 nN. From a controls point of view this makes sense as a tissue can change it's mechanical behavior by varying the tightening of the cytoskeleton which in effect changes the prestrain. The effect of the spring foundation is more subtle changing the Force distance curves separation, slope and places where the non-linearity occurs. All the graphs show nonlinear behavior at lower applied forces and more linear behavior at higher forces.

A short investigation into the Spring Foundation where the middle attachment at the base of the squamish model. The response showed a collapse of the response into similar slope and lines In the experiment for different prestrains. It is known that the bottom attachments to the basement membrane make a large difference in the behavior of cells. It appears that the placement of attachments and the values of the attachments are important and should be investigated further.

Changing the cell membrane width m changes the width of the non-linearity in the Force-Distance and Stress-Strain graphs. The value of 0.5 um for the cell membrane gives a linear curve with poor separation of prestrain values.

Another interesting observation is that there are sometime reverse order graphs where the higher prestrain lowers the Force-Distance or Stress-Strain curve slope or elasticity. This is the case for the graphing of the lung in Figure 5.4. Normally the higher the prestrain the higher the curve of the elasticity on the graph.

The model Force-Distance curves translate into the Stress-Strain curves with linear multiplication and division for all models. The models in general show separation of the curves and nonlinearity sections at

lower forces or stresses. The squamish model had good separation of curves in both tension and compression. When matched with actual tissue samples they showed a large range of strain in tension that matched the tissue and sufficiently large strain of 0.2 for compression curves. The tension curves showed changes in slope which is a change in the elasticity of the model as well. The cuboidal curves did not become linear until higher values Force and Distance. There was good separation of curves in both tension and compression for the cuboidal model. The columnar model with wide post support showed the best separation of curves at higher spring foundation of 10,000 N/m (graphs for this summary are shown in Appendix A).

Solving tensegrity structures using Finite Element Analysis is challenging because structures in tension tend to change in overall shape when a force is applied. This often is read as a structural failure by the software. Careful application of the Finite Element Method to a more stable tensegrity structure with the forces added individually gives results. The three cell tissue model developed in this thesis only works with specific trijunction with T3 triangular prisms attached to the stabilising posts and the T4 triangular prism attached to the three hexagon cells in the middle of the structure. Any other configuration does not work.

The top structure of cells is thought to influence the mechanics of tissue. Placing a tensegrity structure on the top of the cuboidal cell did not significantly change the Force-Distance curves of the model. More work should be done on this model to see if different structures on the of the top of the cell changes the mechanical behavior of the cell.

Other variables that were not investigated are the rate of applied force and the application of bijunction tensegrity structure were not modeled at this time. The model analysis for rate of applied force did not work with the current finite element analysis The k factors change the slope of the stress-strain curves and are dependent on the elasticity and area of the compression and the tension elements. Changing the k factor in the model allows for flexibility in finding matching stress-strain curves for relevant tissue samples.

7.0 Conclusion

The tensegrity model has successfully modeled tissue in both tension and compression but is more linear than the tissue curves. The overall observations are that the three cell tissue model mechanics is influenced by the cytoskeleton values, the cell-cell connections, and the cell to basement membrane attachments. This occurs in measurement of tissue and other models. The Hexagon 3 cell (Hex3Cell) model can handle large stress and strain. Models normally handle up to 0.2 or 20% strain while tissues often yield

above 0.5 or 50% strain. The tensegrity model does handle stresses above 50% and therefore can handle tissue modeling.

Adding structures to the top of the model does not change its mechanical response significantly. Adding a tensegrity structure to the bottom of the model also has minimal effect on the mechanical response but removing a point of attachment on the base of the structure has a large effect causing the linear curves for the prestrains to be linear and not separated. Changing the value of the spring attachments on each cell in the tissue to see the effects this would have is a future experiment.

The Hexagon three cell tissue model is a very simplified model and is made of linear elements. To get curves that are J shaped the model needs to be more complicated. One possible way to do this is to increase the complexity of each hexagon cell or to increase the number of cells.

For future work into this type of modeling many types of modifications to the structure of the model can be made. One such as change is to modify the elasticity of the strings and bars of only one cell. . A seven cell model should be made as a more accurate representation of tissue as well and the number of cells increased and the shape of the cells to different hexagon like tillings could be investigated.

Other changes in the makeup of the parts of the model could be investigated. Adding metamaterial type tilling on the sides of the triangle prism for trijunctions and adding tilling on the side of the hexagon structure sides gives a wide range of structures. This will allow for further experimentation with the model. Also using this model in programs specifically made for tensegrity structures would give a more complete understanding of the model.

Other mechanical tests for future work include:

- Height/width ratios of cells
- Number of cells in the model (7 cell model)
- Bottom attachment placement and value
- Top of model structures
- Adding structures like the nucleus
- Adding other attachments to the sides of the cells
- Rate of applied force
- Creep and Relaxation
- Frequency measurements

- Change in the elasticity or area of only one cell (simulating damage or cancer)
- Adjusted Finite Element program that can work with structures that change overall conformation when a force is applied to the model.

Tissues have different mechanical characteristics than single cells. Epithelial tissues are built by attaching cells to a basement membrane and then to each other using trijunctions at the corner attachments where three cells meet. In modeling epithelial tissue the structure of the cells and their stage needs to be taken into account. For the purposes of modeling a single layer mature cell sheet was chosen for the model. The three cell hexagon tensegrity works to model tissue in both tension and compression and can be adjusted to other measurements of tissue.

References

1. alife.org - International Society for Artificial Life (ISAL), *Artificial Life* (published by MIT Press) accessed Jan. 2024

2. Arnaud Ambrosini, Mélanie Gracia, Amsha Proag, Mégane Rayer, BrunoMonier, Magali Suzanne. 2017. Apoptotic forces in tissue morphogenesis. Mechanisms of Development 144 33–42
3. Anna Al Sabouni-Zawadzka. 2023. High Performance Tensegrity-Inspired Metamateriala and Structures. CRC Press. ISBN: 978-I-003-34320-2 (ebk)

4. Josep-Maria Armengol-Collado, Livio Nicola Carenza, Julia Eckert, Dimitrios Krommydas, and Luca Giomi. 2023. Epithelia are multiscale active liquid crystals. Nature Physics. https://doi.org/10.1038/s41567-023-02179-0

5. Lior Atia and Jeffrey J. Fredberg. 2023. A life off the beaten track in biomechanics: Imperfect elasticity, cytoskeletal glassiness, and epithelial unjamming. Biophysics Review 4, 041304

6. Maria S. Balda and Karl Matter. 2003. Epithelial cell adhesion and the regulation of gene expression. TRENDS in Cell Biology. 13 (6)

7. Sara Barreto, Cecile M. Perrault, Damien Lacroix. 2014. Structural finite element analysis to explain cell mechanics variability. Journal of the mechanical behavior of biomedical materials 38, 219 – 231

8. Daniel L. Barton, Silke Henkes, Cornelis J. Weijer, Rastko Sknepnek. 2017. Active Vertex Model for cell-resolution description of epithelial tissue mechanics. PLoS Comput Biol 13(6): e1005569

9. Marco Berghoff, Jakob Rosenbauer, Felix Hoffmann and Alexander Schug. 2020. Cells in Silico – introducing a high-performance framework for large-scale tissue modeling.

10. Chandan Bharadwaj, B.V., Abiram, K., Harish, K., Vivek, S., Chandrashekara, C.V. (2023). Dynamic Analysis of MCF-7 Using Tensegrity Model. In: Gupta, V.K., Amarnath, C., Tandon, P., Ansari, M.Z. (eds) Recent Advances in Machines and Mechanisms. Lecture Notes in Mechanical Engineering. Springer, Singapore. https://doi.org/10.1007/978-981-19-3716-3_16

11. Peter Bieling, Tai-De Li, Julian Weichsel, Ryan McGorty, Pamela Jreij, Bo Huang, Daniel A. Fletcher, and R. Dyche Mullins. 2016. Force Feedback Controls Motor Activity and Mechanical Properties of Self-Assembling Branched Actin Networks. Cell 164, 115–127

12. Allan F. Bower. 2010. Applied Mechanics of Solids. CRC Press. Taylor and Francis Group. ISBN: 978-1-4398-0247-2

13. A. R. B. Boyd, S. Moore, J. E. Sader, P. V. S. Lee. 2017. Modelling apical columnar epithelium mechanics from circumferential contractile fibres. Biomech Model Mechanobiol. 16:1555–1568 DOI 10.1007/s10237-017-0905-7

14. Clifford P. Brangwynne, Frederick C. Mackintosh, Sanjay Kuumar, Nicholas A. Geisse, Jennifer Talbot, L. Mahadevin, Kevin K. Parker, Donald E. Ingber, David A Weitz. 2006. Microtubules can bear enhanced compressive loads in living cells because of lateral reinforcement. Journal of Cell Biology. 173 (5), 733-741 June

15. Silvia Budday, Timothy C. Ovaert, Gerhard A. Holzapfel, Paul Steinmann, Ellen Kuhl. 2020. Fifty Shades of Brain: A Review on the Mechanical Testing and Modeling of Brain Tissue *Archives of Computational Methods in Engineering* 27:1187–1230

16. Patrice D Cani. 2018. Human gut microbiome: hopes, threats and promises. 0:1–10. doi:10.1136/gutjnl-2018-316723

17. Alexander X. Cartagena-Rivera , Christina M. Van Itallie, James M. Anderson & Richard S. Chadwick. 2017. Apical surface supracellular mechanical properties in polarized epithelium using noninvasive acoustic force spectroscopy. Nature Communications 8, 1030 https://github.com/Chandan-Bharadwaj/Tensegrity-FEM-Models-of-Cells

18. Muhao Chen, Jun Chen, Manoranjan Majji, Robert E. Skelton. 2021. Tensegrity system dynamics in fluids. Nonlinear Dynamics https://hal.archives-ouvertes.fr/hal-03287826 (ISSN : 0924-090X, EISSN : 1573-269X)

19. Silvia Chifflet and Julio A. Hernandez. 2012. The Plasma Membrane Potential and the Organization of the Actin Cytoskeleton of Epithelial Cells. International Journal of Cell Biology, doi:10.1155/2012/121424

20. COMSOL. 2022. Structural Mechanics Module User's Guide. COMSOL 6.1 and 6.2

21. Ernesto Cortes, Dariusz Lachowski , Benjamin Robinson, Muge Sarper, Jaakko S Teppo, et al. 2019. Tamoxifen mechanically reprograms the tumor microenvironment via HIF-1A and reduces cancer cell survival. EMBO reports 20: e46557

22. Mark F. Coughlin and Dimitrijie Stamenovic. 2003. A prestressed Cable Network Model of the Adherent Cell Cytoskeleton. Biophysical Journal, 18, February, 1328-1336

23. Claire A. Dessalles, Claire Leclech, Alessia Castagnino and Abdul I. Barakat. 2021. Integration of substrate- and flow-derived stresses in endothelial cell mechanobiology. Nature. Communications Biology 4:764 https://doi.org/10.1038/s42003-021-02285-w |www.nature.com/commsbio

24. MM Doyley. 2012. Model-based elastography: a survey of approaches to the inverse elasticity problem. Physics in Medicine and Biology. 57, R35-R73

25. Christopher C. DuFort, Matthew J. Paszek, and Valerie M. Weaver. 2011. Balancing forces: architectural control of Mechanotransduction; Nat Rev Mol Cell Biol. May ; 12(5): 308–319. doi:10.1038/nrm3112

26. Krashn Kr. Dwivedi, Piyush Lakhani, Sachin Kumar, Navin Kumar. 2022. A hyperelastic model to capture the mechanical behaviour and histological aspects of the soft tissues. Journal of the Mechanical Behavior of Biomedical Materials 126, 105013

27. Yu M. Efremov, A.A. Dokrunova, D.V. Bagrov, K.S. Kudryashova, O.S. Sokolova, K.V. Shaitan. 2013. The effects of confluency on cell mechanical properties. Journal of Biomechanics 46, 1081 - 1087
28. H. Ebata, K. Umeda, K. Nishizawa, W. Nagao, S. Inokuchi, Y. Sugino, T. Miyamoto, D. Mizuno. 2023. Activity-dependent glassy cell mechanics I: Mechanical properties measured with active microrheology. Biophysical Journal

29. Adam J. Engler, Shamik Sen, H. Lee Sweeney, Dennis E. Discher. 2006. Matrix Elasticity Directs Stem Cell Lineage Specification. Cell. 126 (4) 677-689

30. A.S. Ermakov. 2018. The Theory of Tensegrity and Spatial Organization of Living Matter. Russian Journal of Developmental Biology. 49(2), 87-100

31. Amir Monemian Esfahani, Jordan Rosenbohm, Bahareh Tajvidi Safa, Nickolay V. Lavrik, Grayson Minnick, Quan Zhou, Fang Kong, Xiaowei Jin, Eunju Kim, Ying Liu, Yongfeng Lua, Jung Yul Lim, James K. Wahl III, Ming Dao, Changjin Huang, and Ruiguo Yang. 2020. Characterization of the strain-rate–dependent mechanical response of single cell–cell junctions. PNAS 2021 Vol. 118 No. 7 e2019347118

32. Mona Eskandari, Tara M. Nordgren, Grace D. O'Connell. 2019. Mechanics of pulmonary airways: Linking structure to function through constitutive modeling, biochemistry, and histology. Acta Biomaterialia 97, 513

33. Maria G. Fernandes, Lucılia P. da Silva, and Alexandra P. Marques. 2019. Skin Mechanobiology and Biomechanics: From Homeostasis to Wound Healing. Chapter 17, Advances in Biomechanics and Tissue Regeneration II. https://doi.org/10.1016/B978-0-12-816390-0.00017-0

34. M. Fraldi, S. Palumbo, A.R. Carotenuto, A. Cutolo, L. Deseri, N. Pugno. 2019. Buckling soft Tensegrities: Fickle Elasticity And Configurational Switching In Living Cells. arXiv:1904.04610v1 [physics.bio-ph] 9 Apr 2019

35. Massimiliano Fraldi, Arsenio Cutolo, Angelo Rosario Carotenuto, Stefania Palumbo, Nicola Pugno. 2021. A lesson from earthquake engineering for selectively damaging cancer cell structures. Journal of the mechanical behavior of biomedical materials 119 (2021) 104533

36. Fernando Fraternali, Gerardo Carpentieri, Ada Amendola. 2015. On the mechanical modeling of the extreme softening/ stiffening response of axially loaded tensegrity prisms. Journal of the Mechanics and Physics of Solids 74, 136–157

37. Rong Fu , Xiaowan Jiang, Gang Li, Yi Zhu and Huimin Zhang. 2022. Junctional complexes in epithelial cells: sentinels for extracellular insults and intracellular homeostasis. The FEBS Journal. 289, 7314–7333

38. Buntara Sthenly Gan. 2020. Computational Modeling of Tensegrity Structures Art, Nature, Mechanical and Biological Systems. Springer. ISBN 978-3-030-17836-9 (eBook), page 44, https://doi.org/10.1007/978-3-030-17836-9

39. Pablo D. Garcia, Carlos R. Guerrero and Ricardo Garcia. 2020. Nanorheology of living cells measured by AFM based force–distance curves. Nanoscale, 2020, 12, 9133–9143

40. Wojciech Gilewski, and Anna Al Sabouni-Zawadzka. 2021. Towards Recognition of Scale Effects in a Soid Model of Lattices with Tensegrity-Inspired Microstructure. Solids 2, 50-59

41. Nikolce Gjorevski and Celeste M. Nelson. 2012. Mapping of Mechanical Strains and Stresses around Quiescent Engineered Three-Dimensional Epithelial Tissues. Biophysical Journal 103(1) 152-162

42. James A. Glazier. 2024. In conversation – CompuCell3D course August 2024. Biocomplexity Institute, Intelligent Systems Engineering, Indiana University, Bloomington, IN 47405

43. Raman Goyal , Muhao Chen , Manoranjan Majji , and Robert E. Skelton. 2019. MOTES: Modeling of Tensegrity Structures. Journal of Open Source Software, 4(42), 1613. https://doi.org/10.21105/joss.01613 1, https://github.com/ramaniitrgoyal92/Modeling_of_Tensegrity_Structures_MOTES

44. Yanyu Gu, Chuang Zhang, Yiwei Zhang, Wejun Tan, Xiaobin Yu. Tianbiao Zhang, Lianqing Liu, Ying Zhao, and Lina Hao. 2023 A Review of the Development and Challenges of Cell Mechanical Models. IEEE Transactions on Nanobioscience 22(3) July

45. Carlos F. Guimaraes, Luca Gasperini, Alexandra P. Marques, and Rui L. Reis. 2020. The stuffiness of living tissues and its implications for tissue engineering. Nature Reviews, Materials, 5, 351-370, May

46. Ajay B. Harish, Vijay Nandurdikar, Shubbam Deshpande, and Steophanie Andress. 2023. Mathematics of stable tensegrity structures. Journal of Theoretical, Computational and Applied Mechanics. 26

47. Andrew R. Harris, Loic Peter, Julien Bellis, Buzz Baum, Alexandre J. Kabla, and Guillaume T. Charras. 2012. Characterizing the mechanics of cultured cell monolayers. PNAS. October 9. 109 (41) 16449–16454. www.pnas.org/cgi/doi/10.1073/pnas.1213301109

48. Tomohito Higashi and Ann L. Miller. 2017. Tricellular junctions: how to build junctions at the TRICkiest points of epithelial cells. Molecular Biology of the Cell. 28, 2023-2034

49. Hao Hong and Hua Deng. 2023. A general theory for analyzing morphing bistable tensegrities based on quasi-static assumption. International Journal of Solids and Structures 265-266, 112127

50. Mikiko Inaki, Jingyang Liu and Kenji Matsuno. 2016. Cell Chirality: its origin and roles in left-right asymmetric development. Phil. Trans. R. Soc. B 371: 20150403

51. D.E. Ingber, N. Wang and D. Stamenovic. 2014. Tensegrity, cellular biophysics and the mechanics of living systems. Rep. Prog. Phys. 77(4), 046603

52. Donald E. Ingber. 2008. Tensegrity-based mechanosensing from macro to micro. Prog. Biophys. Mol. Biol. 97(2-3), 163-179

53. Malina K. Iwanski, Eugene A. Katrukha, and Lukas C. Kapitein. 2024. Lattice Light-Sheet Motor-PAINT: A Method to Map the Orientations of Microtubules in Complex Three-Dimensional Arrays. Single Molecule Analysis: Methods and Protocols (Chapter 8), Methods in Molecular Biology, 2694, https://doi.org/10.1007/978-1-0716-3377-9_8

54. Elias Jagielloa, Pablo Andrés Muñoz-Rojas. 2021. An Extended Multiscale Finite Element Method (EMsFEM) Analysis of Periodic Truss Metamaterials (PTMM) Designed by Asymptotic Homogenization. Latin American Journal of Solids and Structures, 18(2), e347

55. Yohalie Kalukul, Andrew D. Stephens, Jan Lammerding, and Sylvain Gabriele. 2022. Mechanics and functional consequences of nuclear deformations. Nature Review. Molecular Cell Biology 23, 583 – 602 September

56. Sara Kaliman, Maxime Hubert, Carina Wollnik, Lovro Nuić, Damir Vurnek, Simone Gehrer, Jakov Lovrić , Diana Dudziak, Florian Rehfeldt, and Ana-Sunčana Smith. 2021. Mechanical Regulation of Epithelial Tissue Homeostasis. Physical Review X11, 031029

57. Elena Kassianidou, Sanjay Kumar. 2015. A biomechanical perspective on stress fiber structure and function. Biochimica et Biophysica Acta (BBA) – Molecular Cell Research. 1853(11) Part B, 3065-3074

58. Ronald Kaunas, Shinji Deguchi. 2011. Multiple Roles for Myosin II in Tensional Homeostasis Under Mechanical Loading. Cellular and Molecular Bioengineering, 4(2), 182- 191

59. Andrew S. Kennard, Mugdha Sathe, Ellen C. Labuz, Christopher K. Prinz, Julie A. Theriot. 2023. Post-injury hydraulic fracturing drives fissure formation in the zebrafish basal epidermal cell layer. Current Biology 33, 2616–2631, July

60. Brendan F. Kennedy and Jeffrey C. Bamber. 2021. Introduction to Optical Coherence Elastography, in Optical Coherence Elastography: Imaging Tissue Mechanics on the Micro-Scale. AIP Publishing

61. M.I. Kokkinos, P. Murthi, R. Wafai, E.W. Thompson, D.F. Newgreen. 2010. Cadherins in the human placenta- epithelial-mesenchymal transition (EMT) and placental development. Placenta 31: 747-755

62. A. N. Kozyrina, T. Piskova and J. Di Russo. 2020. Mechanobiology of Epithelia From the Perspective of Extracellular Matrix Heterogeneity.Front. Bioeng. Biotechnol. 8:596599.doi: 10.3389/fbioe.2020.596599

63. Sandra B. Lemke and Celeste M. Nelson. 2021. Dynamic changes in epithelial cell packing during tissue morphogenesis. Current Biology 31, R1098–R1110

64. Lohr MJ, Sugerman GP, Kakaletsis S, Lejeune E, Rausch MK. 2022. An introduction to the Ogden model in biomechanics: benefits, implementation tools and limitations. *Phil. Trans. R. Soc. A* 380: 20210365. https://doi.org/10.1098/rsta.2021.0365

65. Jeus M. Lopez-Gay, Hayden Nunley, Meyl Spencer, Florecia di Pietro, Boris Guirao, Floris Bosveld, Olga Markova, Isabell Gaugue, Stephane Pelletier, David K. Lubensky, Yohanns Bellaiche. 2020. Science. 370, 213 October

66. Charlotte Lorenz, Johanna Forsting, Robert W. Style, Stefan Klumpp, Sara Koster. 2023. Keratin filament mechanics and energy dissipation are determined by metal-like plasticity. Matter 6, 1-15

67. Stephen Leven. 2022. Conversations (email) with Stephen Levin - Ezekiel Biomechanics Group

68. Ariadna Marin-Llaurado, Sohan Kale, Adam Ouzeri, Tom Golde, Raimon Sunyer, Alejandro Torres-Sanchez, Ernest Latorre, Manuel Gomez-Gonzalez, Pere Roca-Cusachs, Marino Arroyo, Xavier Trepat. 2023. Mapping mechanical stress in curved epithelia of designed size and shape. Nature Communications. 14:4014

69. M. Modano, I. Mascolo, F. Fraternali and Z. Bieniek (2018) Numerical and Analytical Approaches to the Self-Equilibrium Problem of Class =1 Tensegrity Metamaterials. Front. Mater. 5:5. doi: 10.3389/fmats.2018.00005

70. Timothy Morris, Eva Sue, Caleb Geniesse, William M Brieher, and Vivian W Tang. 2021. Synaptopodin is required for stress fiber and contractomere assembly at the epithelial junction. bioRxiv preprint doi: https://doi.org/10.1101/2020.12.30.424702 Sept. 30

71. A.N. Naser, Guiler, W., Lu, Q., & Chen, Y.-H. 2022. Nanoarchitecture and molecular interactions of epithelial cell junction proteins revealed by super-resolution microscopy. Ann NY Acad Sci., 1516, 175–187. https://doi.org/10.1111/nyas.14855

72. Qin Ni, Kaustubh Wagh, Aashli Pathni, Haoran Ni, Vishavdeep Vashisht, Arpita Upadhyaya, Garegin A Papoian. 2022. A tug of war between filament treadmilling and myosin induced contractility generates actin rings. Ni *et al*. eLife 2022;11:e82658

73. Ekaterina Novitskaya, Po-Yu Chen, Elham Hamed, Jun Li, Vlado A. Lubarda, Iwona Jasiuk, Joanna McKittrick. 2011. Recent advances on the measurement and calculation of the elastic moduli of cortical and trabecular bone: a review. Theoret. Appl. Mech., Vol. 38, No. 3, pp. 209–297, Belgrade

74. Paulina Obara and Justyna Tomasik. 2023. Dynamic Stability of Tensegrity Structures – Part I: The Time-Independent External Load. Materials. 16, 580

75. Oppenheim, I., and Williams, W. 1997: Mechanics of tensegrity prisms. Proceedings of the 14th international symposium on automation & robotics in construction

76. Navaneeth K . R. Pandian and G. K. Ananthasuresh. 2017. Synthesis of tensegrity structures of desired shape using constrained minimization. Struct Multidisc Optim. 56:1233–1245 DOI 10.1007/s00158-017-1716-2

77. Michelle Peckham, Adele Knibbs, Steve Paxton. 2003. Histology Guide © Faculty of Biological Sciences, University of Leeds

78. Adrian F. Pegoraro, Paul Janmey and David A. Weitz. 2017. Mechanical Properties of the Cytoskeleton and Cells. Cold Spring Harbor Perspect. Biol. 9:a022038

79. Marco Pensalfini, Tom Golde, Xavier Trepat, and Marino Arroyo. 2023. Nonaffine Mechanics of Entangled Networks Inspired by Intermediate Filaments. Physical Review Letters. 131, 058101

80. Samuel R. Polio, Aritra Nath Kundu, Carey E. Dougan, Nathan P. Birch, Ezra Aurian-Blajeni, Jessica D. Schiffman, Alfred J. Crosby, Shelly R. Peyton. 2018. Cross-platform mechanical characterization of lung tissue. PLoS ONE 13(10): e0204765. https://doi. org/10.1371/journal.pone.0204765

81. Alberto Puliafito, Luca Primo, and Antonio Celani. 2017. Cell-size distribution in epithelial tissue formation and homeostasis. J. R. Soc. Interface 14: 20170032. http://dx.doi.org/10.1098/rsif.2017.0032

82. Vina D. L. Putra, Kristopher A. Kilian, and Melissa L. Knothe Tate. 2023. Biomechanical, biophysical and biochemical modulators of cytoskeletal remodeling and emergent stem cell lineage commitment. Nature Communications Biology, 6:75 https://doi.org/10.1038/s42003-022-04320-w www.nature.com/commsbio

83. ML Rodriguez, PJ McGarry, NJ Sniadecki. 2013. Review on cell mechanics: experimental and modeling approaches. Applied Mechanics Reviews. 65,060801-3, November

84. Jan Rombouts, Jenna Elliott, and Anna Erzberger. 2023. Forceful patterning: theoretical principles of mechanochemical pattern formation. EMBO Reports e57739|2023

85. Svetlana N. Rubtsova , Irina Y. Zhitnyak and Natalya A. Gloushankova. 2021. Phenotypic Plasticity of Cancer Cells Based on Remodeling of the Actin Cytoskeleton and Adhesive Structures. Int. J. Mol. Sci. 22,1821

86. Anna Sabouni-Zawadzka. 2023. High Performance Tensegrity-Inspired Metamaterials and Structures. CRC Press ISBN:978-1-003-34320-2 (ebk)

87. Preeti Sahu, Janice Kang, Gonco Erdemci-Tandogan and M. Lisa Manning. 2019. Nonlinear analysis of the fluid-solid transition in a model for ordered biological tissues. arXiv:1905.12714c1 [cond-at.soft] May 29

88. Filipoe A. Santos. 2023. Toward a Novel Energy-Dissipation Metamaterial with Tensegrity Architecture. Adv. Matter. 2300639

89. Aashrith Saraswathibhatla, Dhiraj Indana and Ovijit Chaudhuri. 2023. Cell–extracellular matrix mechanotransduction in 3D. Nature reviews, Molecular Cell Biology 24, July

90. Mirit Sharabi. 2022. Structural Mechanisms in Soft Fibrous Tissues: A Review. Front. Mater. 8:793647. doi: 10.3389/fmats.2021.793647

91. Anna Schepers. 2022. Intermediate Filament Mechanics Across Scales From Single Filaments to Single Interactions and Networks in Cells. Gottingen Series in Biophysics. University of Gottingen

92. Mark Shipman, James Blyth and Louise Cramer. 2020. Cytoskeleton Image. Laboratory for Molecular Cell Biology, University College London, UK Cytoskeleton – the movers and shapers in the cell | British Society for Cell Biology (bscb.org)

93. Cornelia Schwayer and David B. Bruckner. 2023. Connecting theory and experiment in cell and tissue mechanics. Journal of Cell Science 136, jcs261515. doi:10.1242/jcs.261515

94. Gennaro Senatore and Daniel Piker. 2015. Interactive real-time physics An intuitive approach to form-finding and structural analysis for design and education. Computer-Aided Design 61, 32–41

95. Joo Yong Sim, Jens Moeller, Kevin C. Hart , Diego Ramallo , Viola Vogeld , Alex R. Dunn , W. James Nelson, and Beth L. Pruitt. 2015. Spatial distribution of cell–cell and cell–ECM adhesions regulates force balance while maintaining E-cadherin molecular tension in cell pairs. Molecular Biology of the Cell. 2456-2465

96. Rod Smallwood. 2009. Computational modeling of epithelial tissues. WIREs Systems Biology ad Medicine 1, 191-201 September/October, DOI:10.1002/wsbm.018

97. Michael F. Staddon, Arthur Hernandez, Mark J. Bowick, Michael Moshe, and Cristina Marchetti. 2023. The role of non-affine deformations in the elastic behavior of the cellular vertex model. Soft Matter. 19, 3080-3091

98. Dimitrije Stamenovic and Ning Wang. 2011. Stress Transmission within the Cell. Comprehensive Physiology. Volume 1, January

99. Kaoru Sugimura, Pierre-François Lenne, and François Graner. 2016. Measuring forces and stresses in situ in living tissues. Published by The Company of Biologists Ltd. Development 143, 186-196 doi:10.1242/dev.119776

100. Bela Suki, Demitrije Stamenovic, and Rolf Hubmayr. 2011. Lung Parenchyma Mechanics. Compr Physiol. 1(3), 1317-1351

101. Wenhui Tang, Amit Das, Adrian F. Pegoraro, Yu Long Han, Jessie Huang, David A. Roberts, Haiqian Yang , Jeffrey J. Fredberg, Darrell N. Kotton, Dapeng Bi and Ming Guo. 2022. Collective curvature sensing and fluidity in three-dimensional multicellular systems. Nature Physics, 18, 1371-1378

102. Gawain Thomas, Nancy A. Burnham, Terri Anne Camesano, Qi Wen. 2013. Measuring the Mechanical Properties of Living Cells Using Atomic Force Microscopy. *J. Vis. Exp.* (76), e50497, doi:10.3791/50497).

103. Sijie Tong, Navreeta K. Singh, Rastko Sknepnek, and Andrej Kosmrij. 2022. Linear viscoelastic properties of the vertex model for epithelial tissues. PLoS Comput Biol. 18(5): e1010135

104. Hanna Trebacz and Angelika Barzycka. 2023, Mechanical Properties and Functions of Elastin: An Overview. Biomolecules 13, 574

105. Mustafa Ünal, Ozan Akkuş, and Randall E. Marcus. 2016. Fundamentals of Musculoskeletal Biomechanics. Springer International Publishing Switzerland 2016, 15, F. Korkusuz (ed.), *Musculoskeletal Research and Basic Science*, DOI: 10.1007/978-3-319-20777-3_2

106. Timothy E. Vanderleest, Celia M Smits, Yi Xie, Cayla E Jewett, J Todd Blankenship, Dinah Loerke. 2018. Vertex sliding drives intercalation by radial coupling of adhesion and actomyosin networks during Drosophila germband extension. eLife 2018;7:e34586. DOI: https://doi.org/10.7554/eLife.34586

107. Bieke Vanslembrouck, Jian-hua Chen, Carolyn Larabell, and Jolanda van Hengel3. 2022. Microscopic Visualization of Cell-Cell Adhesion Complexes at Micro and Nanoscale. Frontiers in Cell and Developmental Biology. 10, Article 819534

108. Devin Matthew Wozniak. 2009. Viscoelastic Properties of Thoraco-Abdominal Tissue Under Dynamic Compressive Loading. Thesis, Marquette University, https://epublications.marquette.edu/theses_open

109. Wikipedia, Cell Junction, 2023
110. Wikipedia – Ogden hyperelastic model, 2022
111. Wikipedia – Viscoelastisity, 2023

112. www.ata-e.com/software/siemens-plm-software/simcenter-3d/ also https://www.youtube.com/watch?v=bqmwUdq1GoA

113. Han Xu , Stephanie Donegan, Jordan M. Dreher, Alicia J. Stark, Elizabeth P. Canovi , Dimitrije Stamenovi , Michael L. Smith. 2020. Focal adhesion displacement magnitude is a unifying feature of tensional homeostasis. Acta Biomaterialia 113, 372–379

114. Wei Xu, Shuangshuang Chen, Mengting Yao and Qinghua Lu. 2022. Mechanical behavior of biomimetic oriented cell sheets from a perspective of living materials. Biomater. Sci.10, 3099–3109

115. Haokang Zhang, Jie Fan, Joshua M. A. Maclin, Leo Q. Wan. 2023. The Actin Crosslinker Fascin Regulates Cell Chirality. Adv. Biology. 7, 2200240

116. J.Y. Zhang, M. Ohsaki. 2017. Stability conditions for tensegrity structures. International Journal of Solids and Structures. 44, 3875-3886

117. Jing Yao Zhang and Makoto Ohsaki. 2015. Tensegrity Structures Form, Stability, and Symmetry. Mathematics for Industry, Volume 6, Springer, ISBN 978-4-431-54813-3

118. Li-Yuan Zhang , Jin-Hong Jiang , Kai Wei, Xu Yin, Guang-Kui Xu, Jingyao Zhang. 2021. Self-equilibrium and super-stability of rhombic truncated regular tetrahedral and cubic tensegrities using symmetry-adapted force-density matrix method. International Journal of Solids and Structures 233, 111215

Appendix A - Tensegrity Structure of Epithelial Tissue Modeling and Simulation

Stress Strain Curves for the three cell tensegrity model produced using COMSOL Multiphysics 6.1

The stress strain curves created using force and difference in displacement of movement. Starting with the curves created due to varying pre-strain and then varying spring foundations. The pre-strains covered are 0, 0.05, 0.1, 0.2, and 0.3. These strains are commonly used in tensegrity structure studies (Fraternali, 2015). The spring foundations represent the basement membrane. They are 10,000, 1000, 100, and 10 N/m isometric spring strength. The forces used are 0, 0.1 – 1.0, 2.50, 5.0, 7.5, 10.0, 12.5, 15.0, 17.5, 20.0 nN. These values were chosen to match the forces placed on cells to measure their elasticity. The range also shows the variation in the graphs at the start of applied force and is not enough of a variation in applied force rate to change the results of the measurements. The rod elements have an elasticity of 2 GPa and the string elements have an elasticity of 10 MPa.

Cuboidal or Medium height model

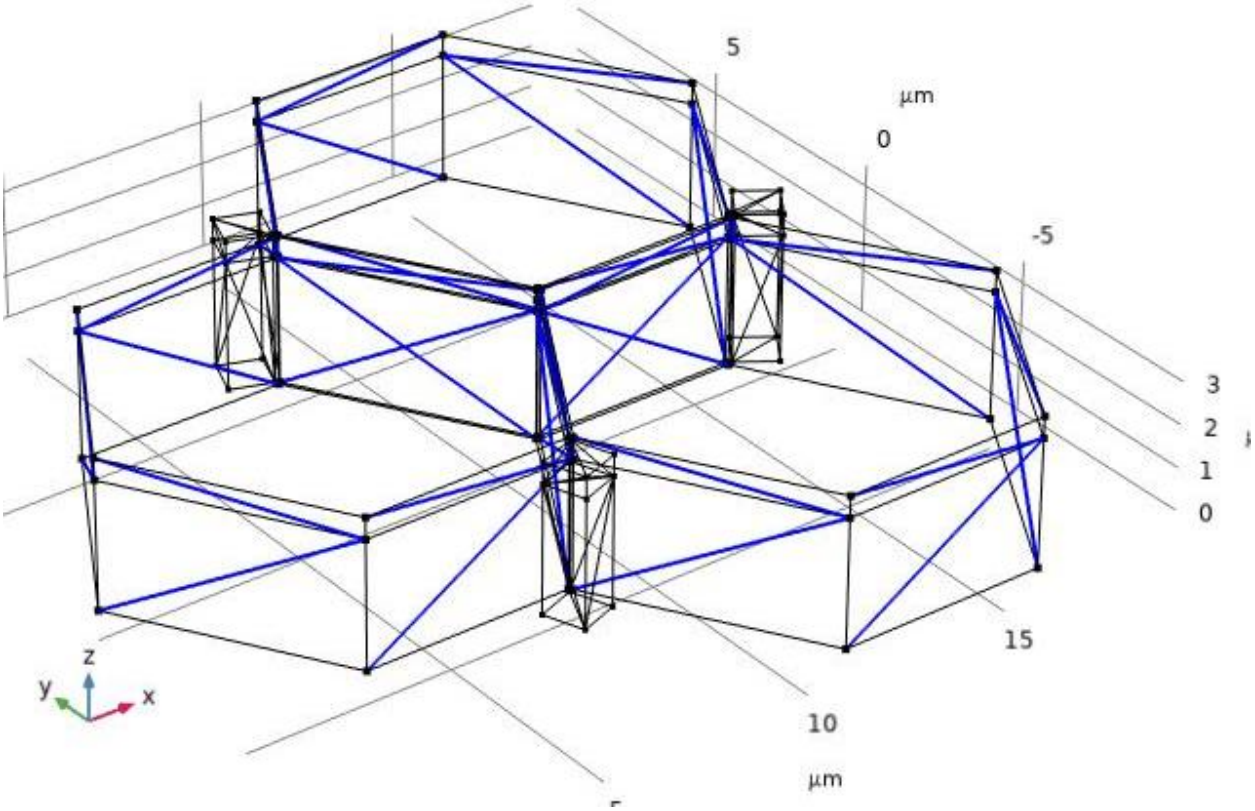

Hex3Cell Model medium or cuboidal height of 3.5 um.

The blue lines are the compression elements of the tensegrity and the black lines are the tension elements with the exception of the black square posts that are both tension and compression elements.

Compression Varying prestress

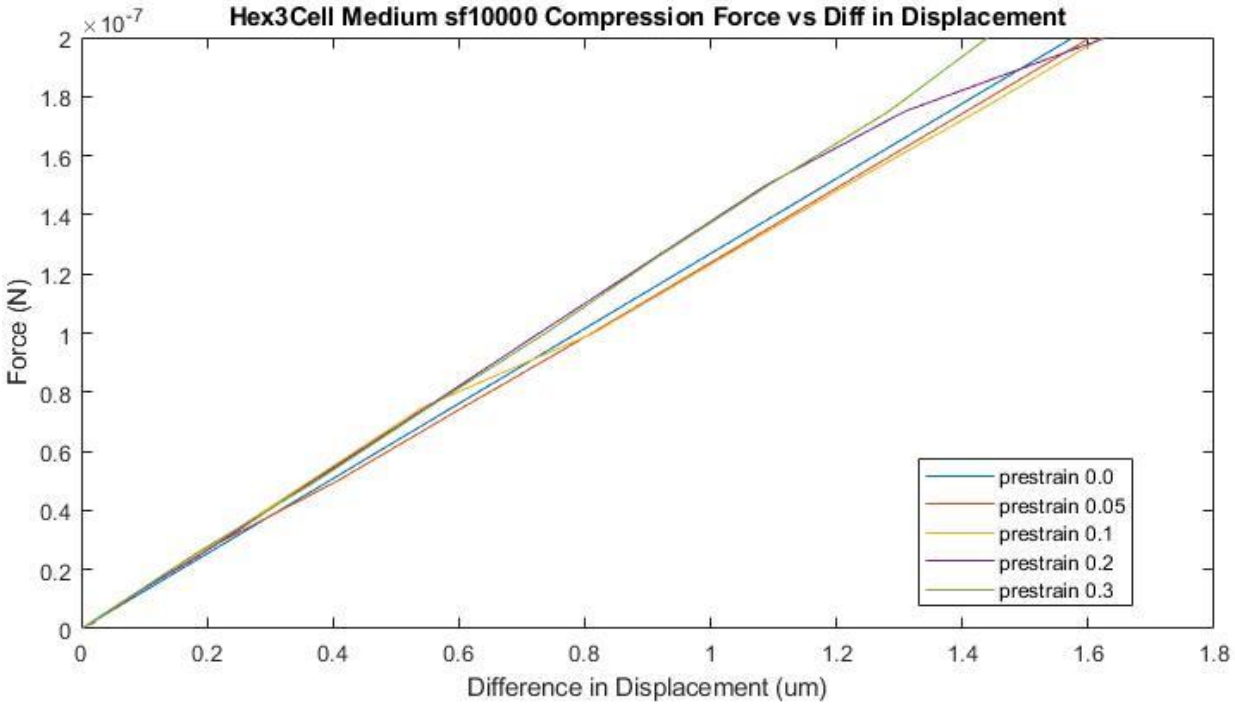

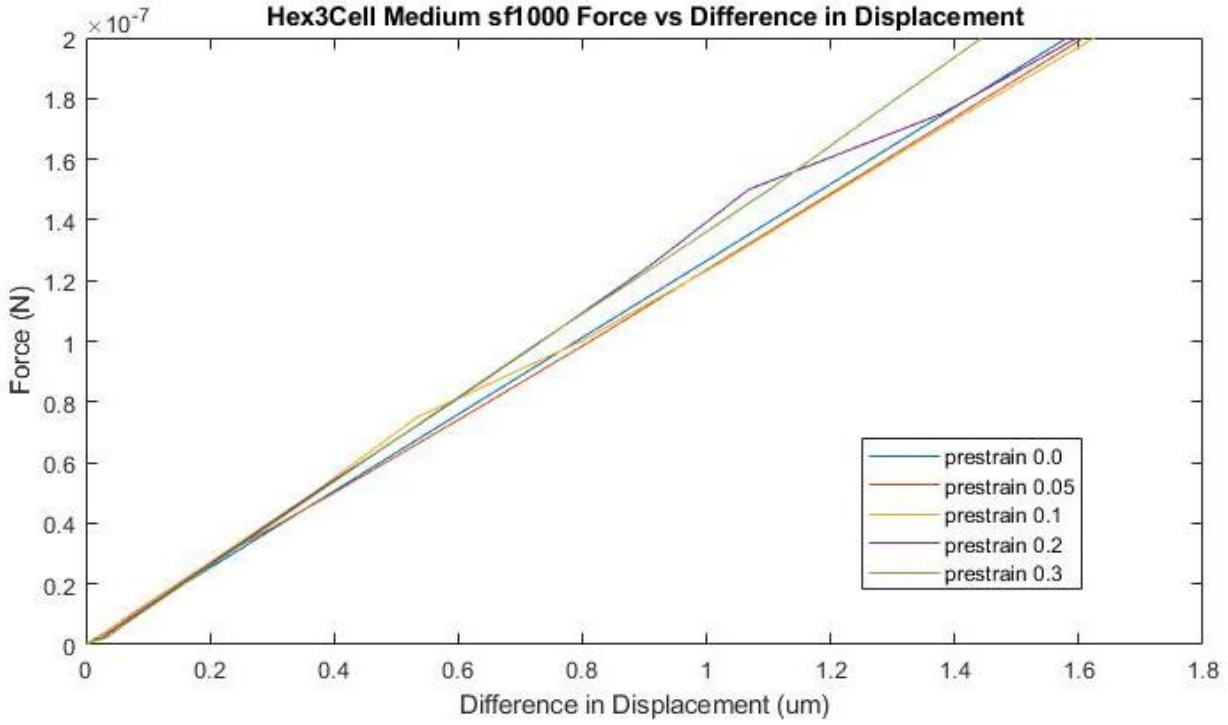
Hex3Cell Medium sf1000 Force vs Difference in Displacement
×10^-7
Force (N)
Difference in Displacement (um)
prestrain 0.0
prestrain 0.05
prestrain 0.1
prestrain 0.2
prestrain 0.3

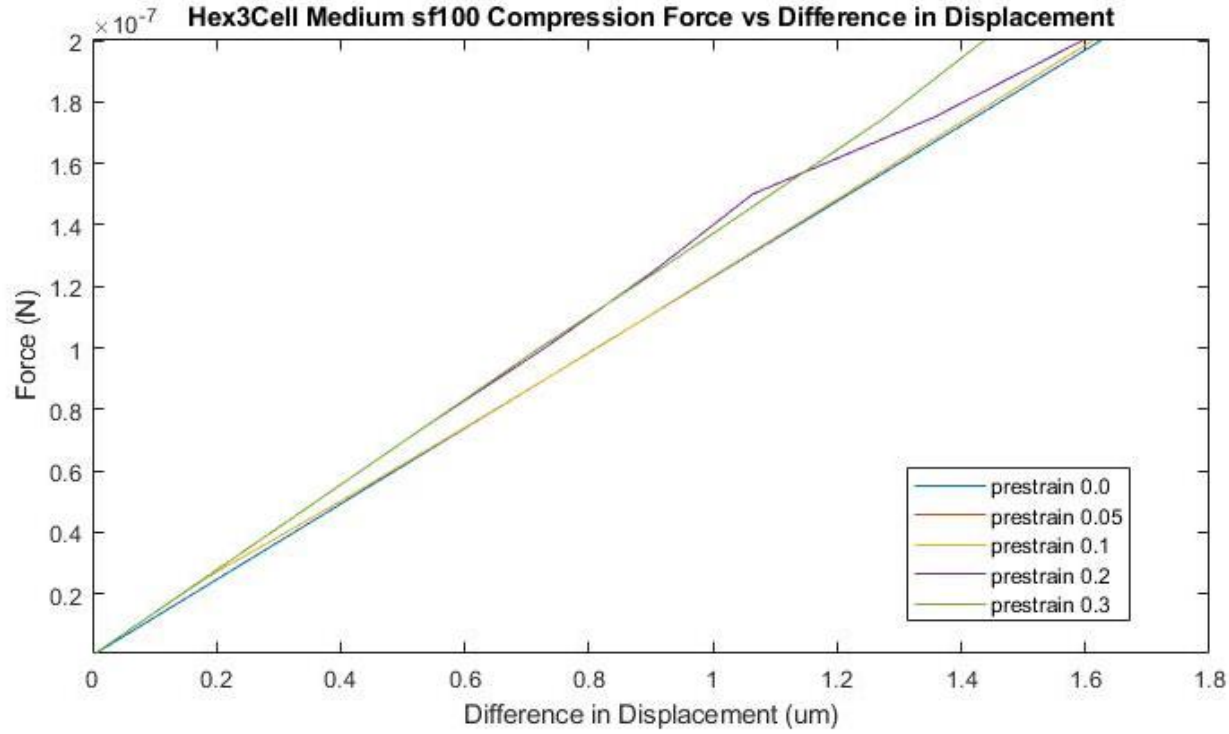
Hex3Cell Medium sf100 Compression Force vs Difference in Displacement
×10^-7
Force (N)
Difference in Displacement (um)
prestrain 0.0
prestrain 0.05
prestrain 0.1
prestrain 0.2
prestrain 0.3

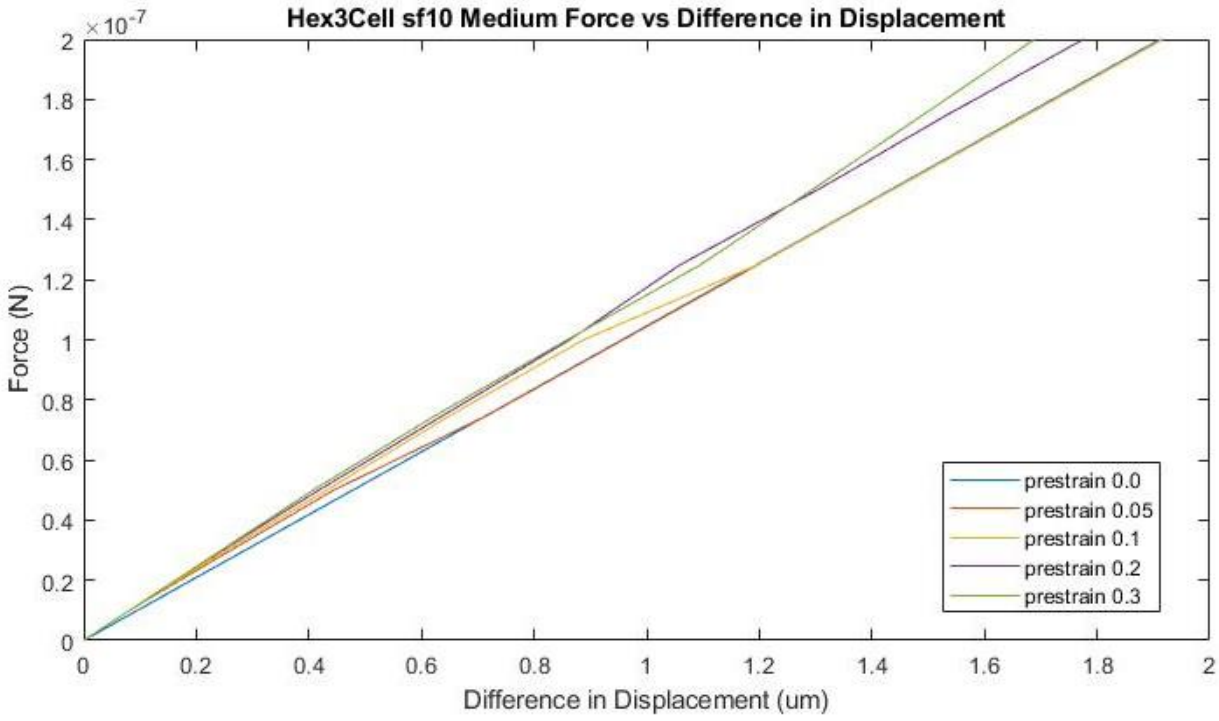

Varying Spring Foundation

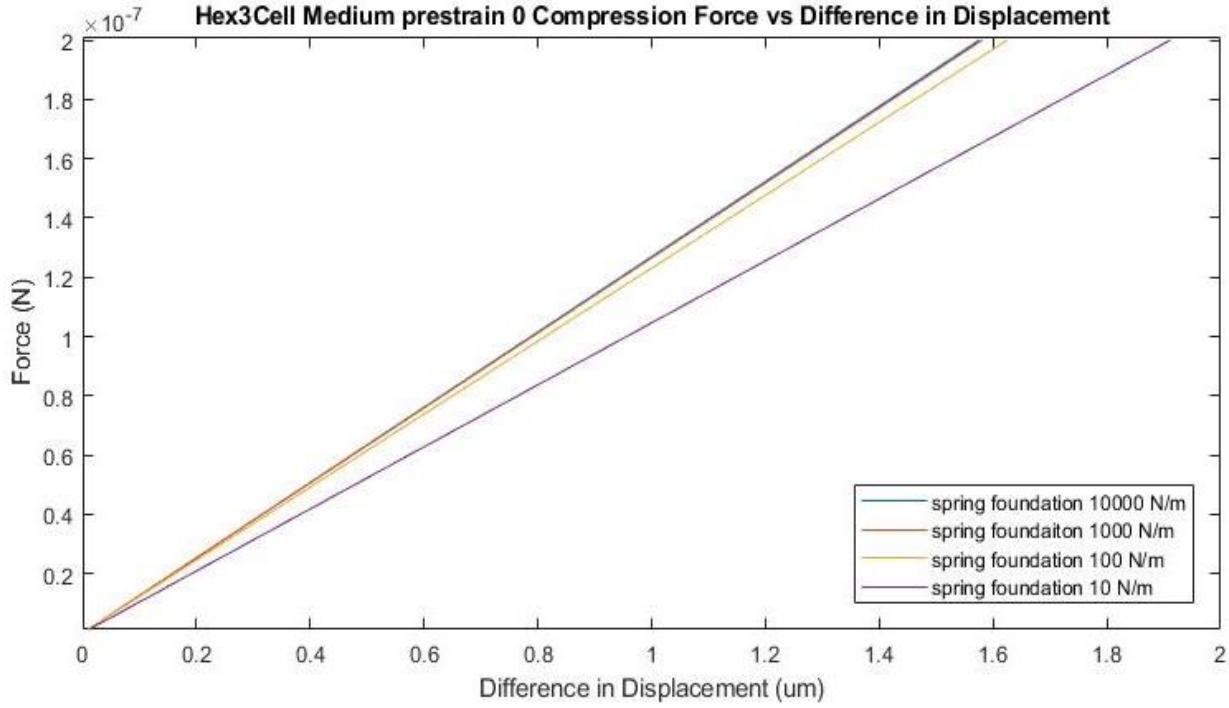
Hex3Cell Medium prestrain 0 Compression Force vs Difference in Displacement
×10^-7
Force (N)
Difference in Displacement (um)
spring foundation 10000 N/m
spring foundaiton 1000 N/m
spring foundation 100 N/m
spring foundation 10 N/m

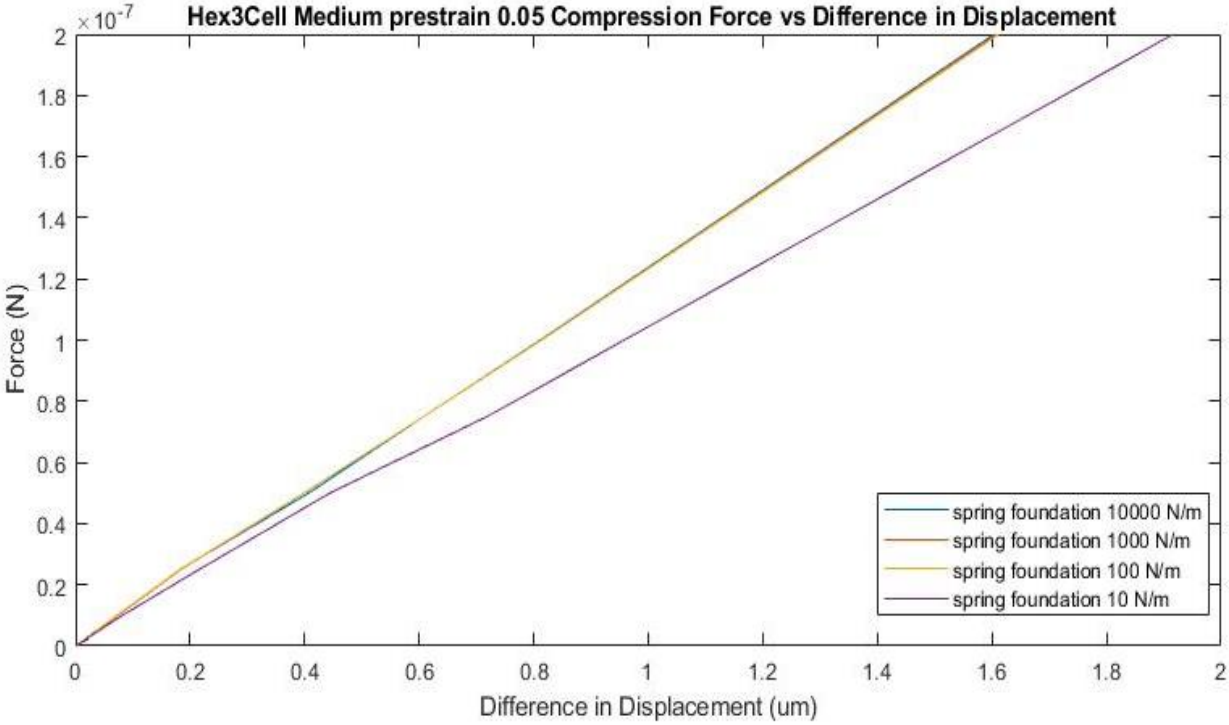
Hex3Cell Medium prestrain 0.05 Compression Force vs Difference in Displacement
×10^-7
Force (N)
Difference in Displacement (um)
spring foundation 10000 N/m
spring foundation 1000 N/m
spring foundation 100 N/m
spring foundation 10 N/m

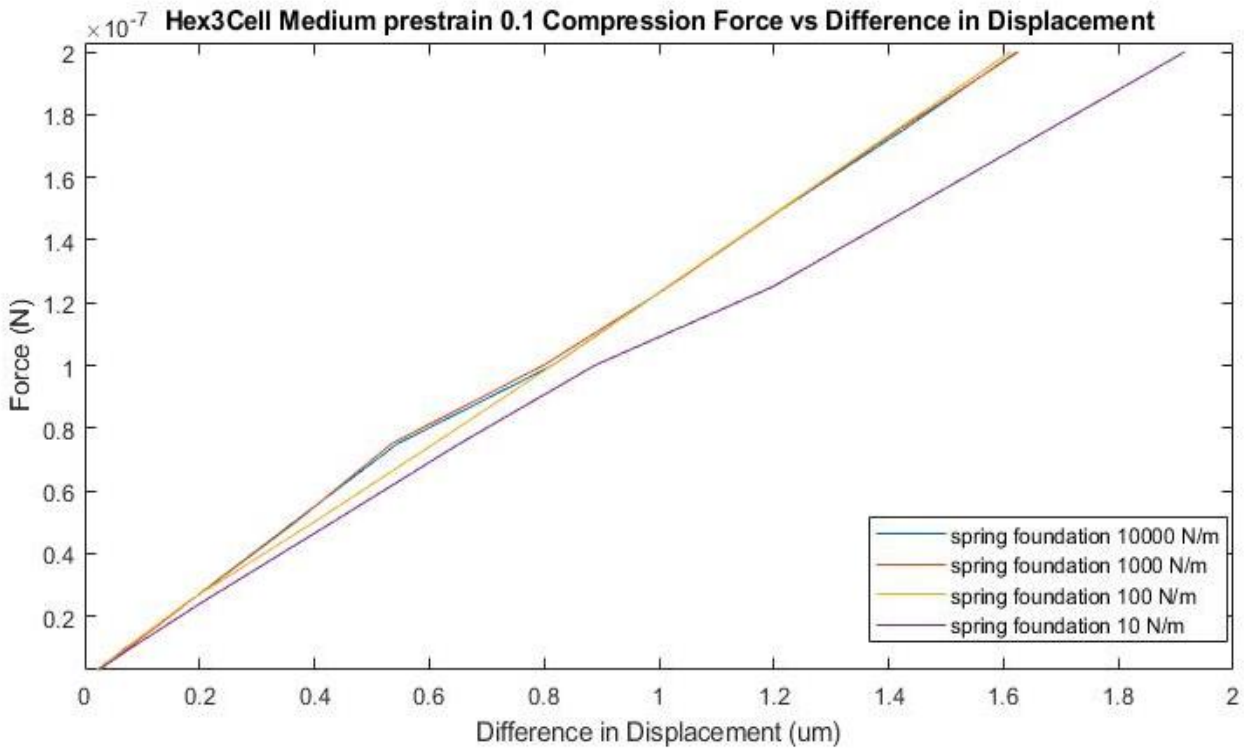
Hex3Cell Medium prestrain 0.1 Compression Force vs Difference in Displacement
×10^-7
Force (N)
Difference in Displacement (um)
spring foundation 10000 N/m
spring foundation 1000 N/m
spring foundation 100 N/m
spring foundation 10 N/m

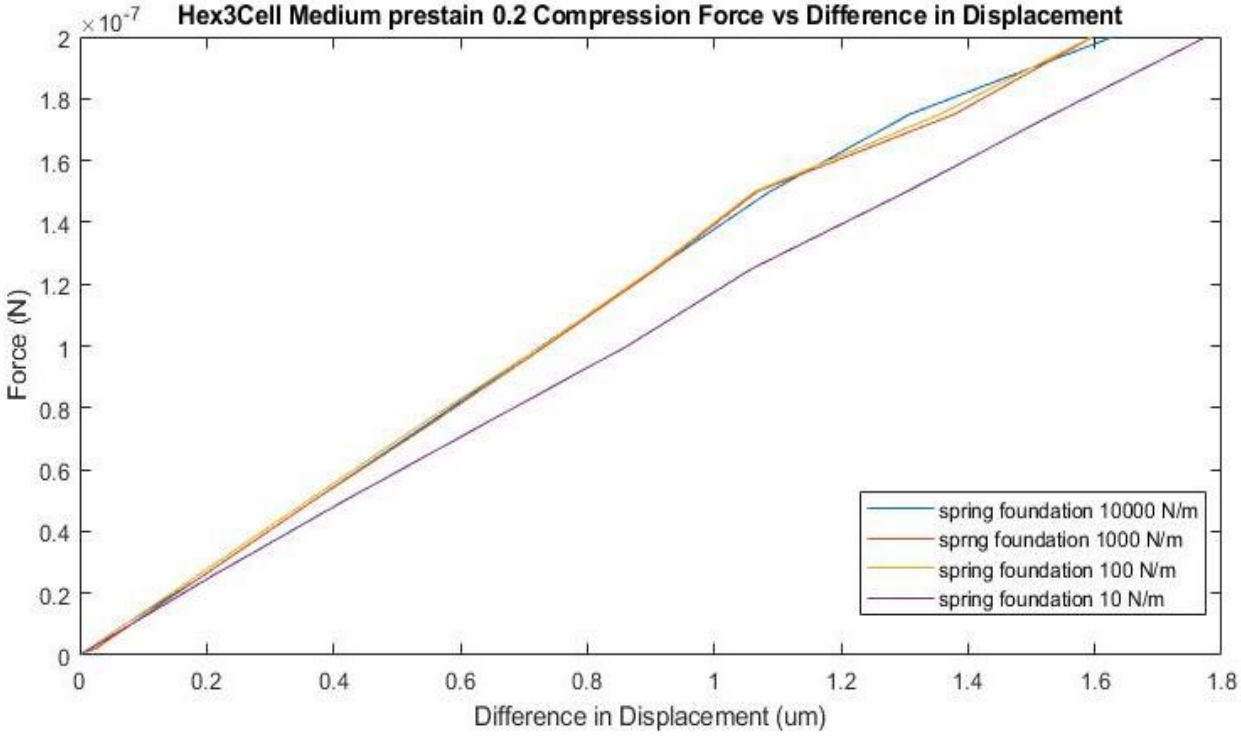
Hex3Cell Medium prestain 0.2 Compression Force vs Difference in Displacement
×10^-7
Force (N)
Difference in Displacement (um)
spring foundation 10000 N/m
sprng foundation 1000 N/m
spring foundation 100 N/m
spring foundation 10 N/m

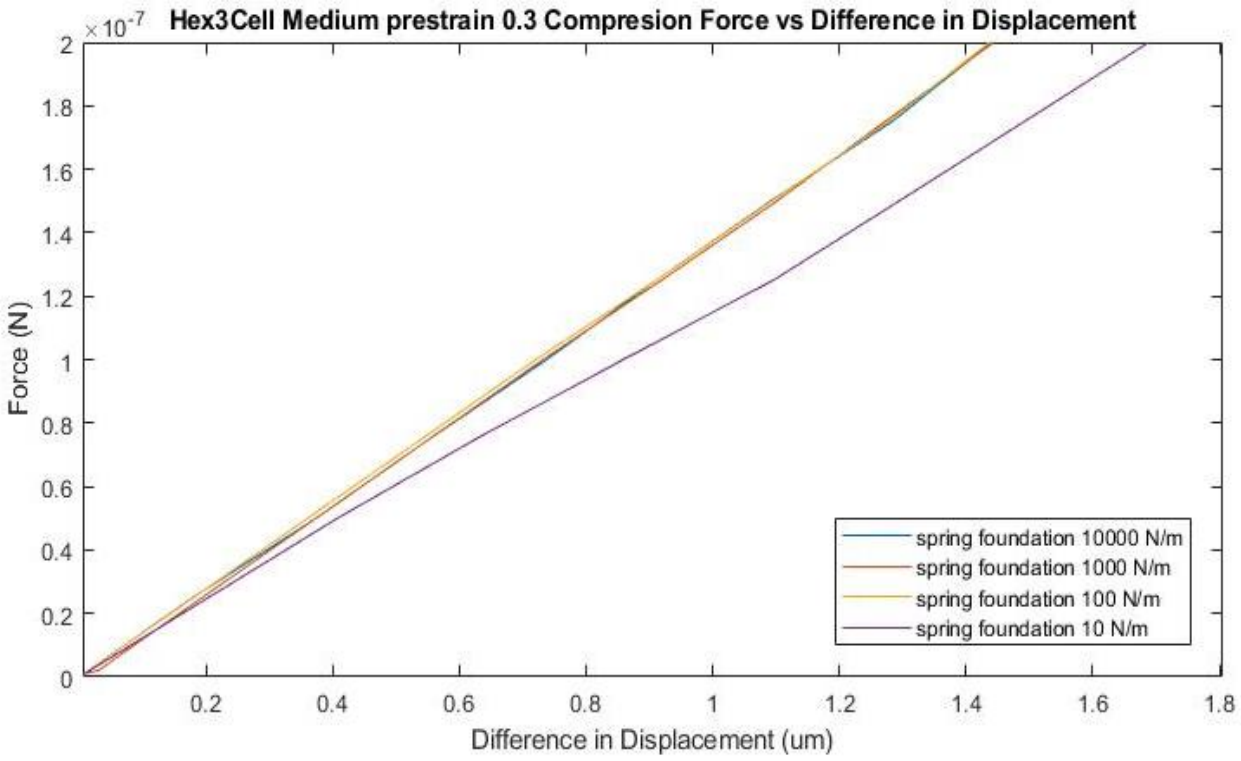

Tension Graphs for Medium Cuboidal

Varying pre-strain

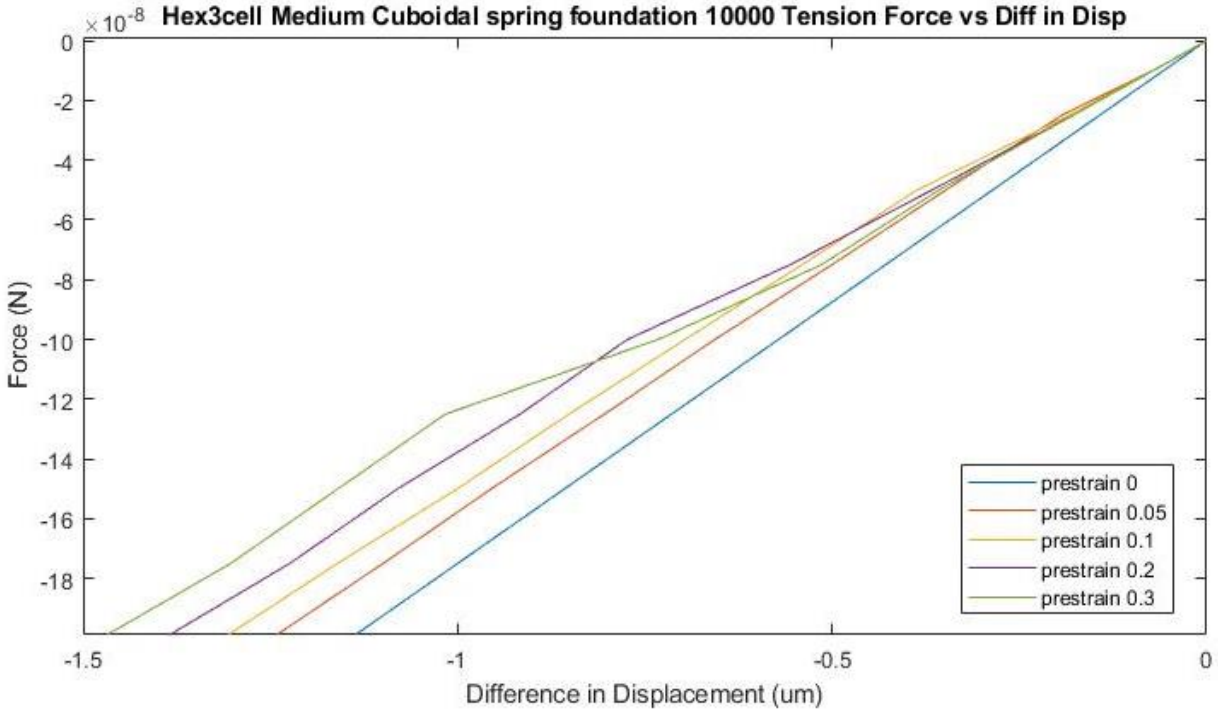

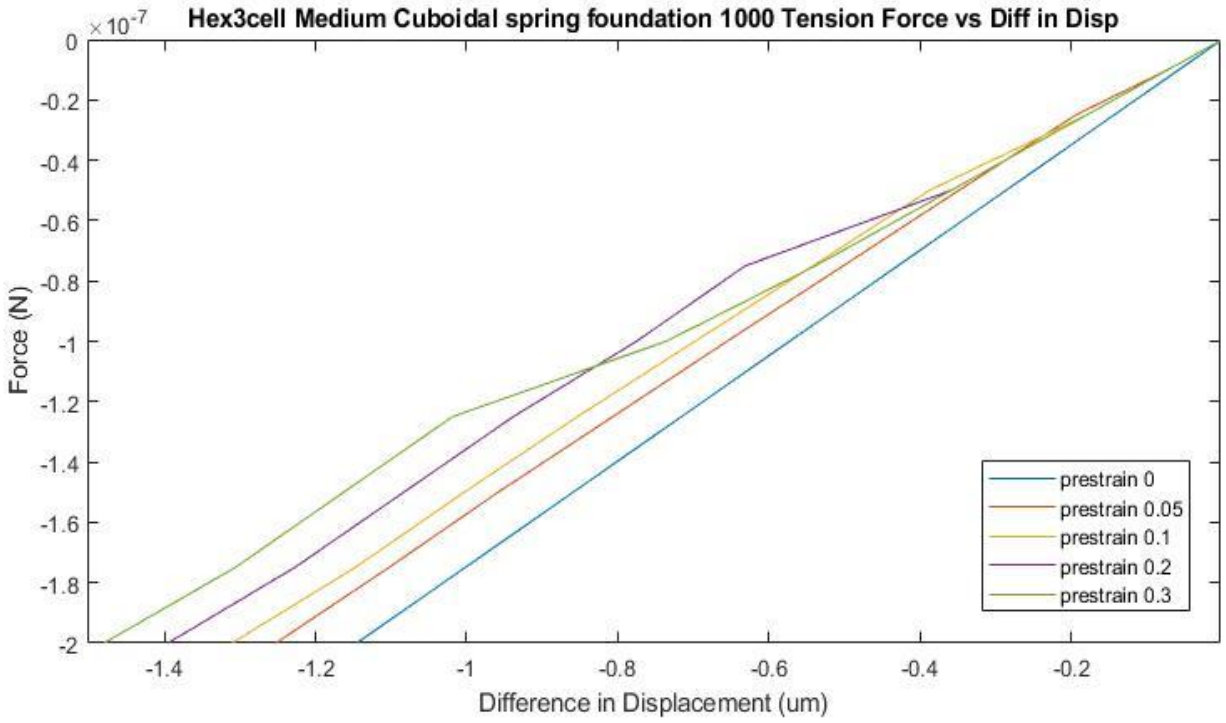
Hex3cell Medium Cuboidal spring foundation 1000 Tension Force vs Diff in Disp
×10^-7
Force (N)
Difference in Displacement (um)
prestrain 0
prestrain 0.05
prestrain 0.1
prestrain 0.2
prestrain 0.3

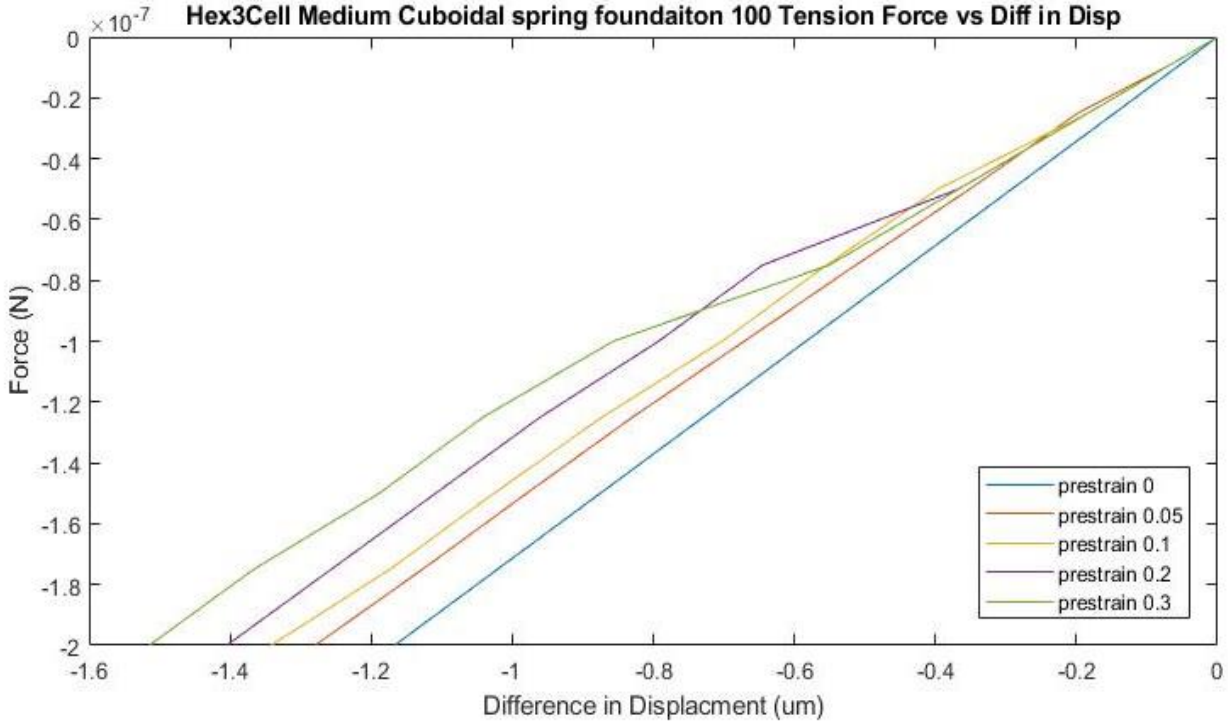
Hex3Cell Medium Cuboidal spring foundaiton 100 Tension Force vs Diff in Disp
×10^-7
Force (N)
Difference in Displacment (um)
prestrain 0
prestrain 0.05
prestrain 0.1
prestrain 0.2
prestrain 0.3

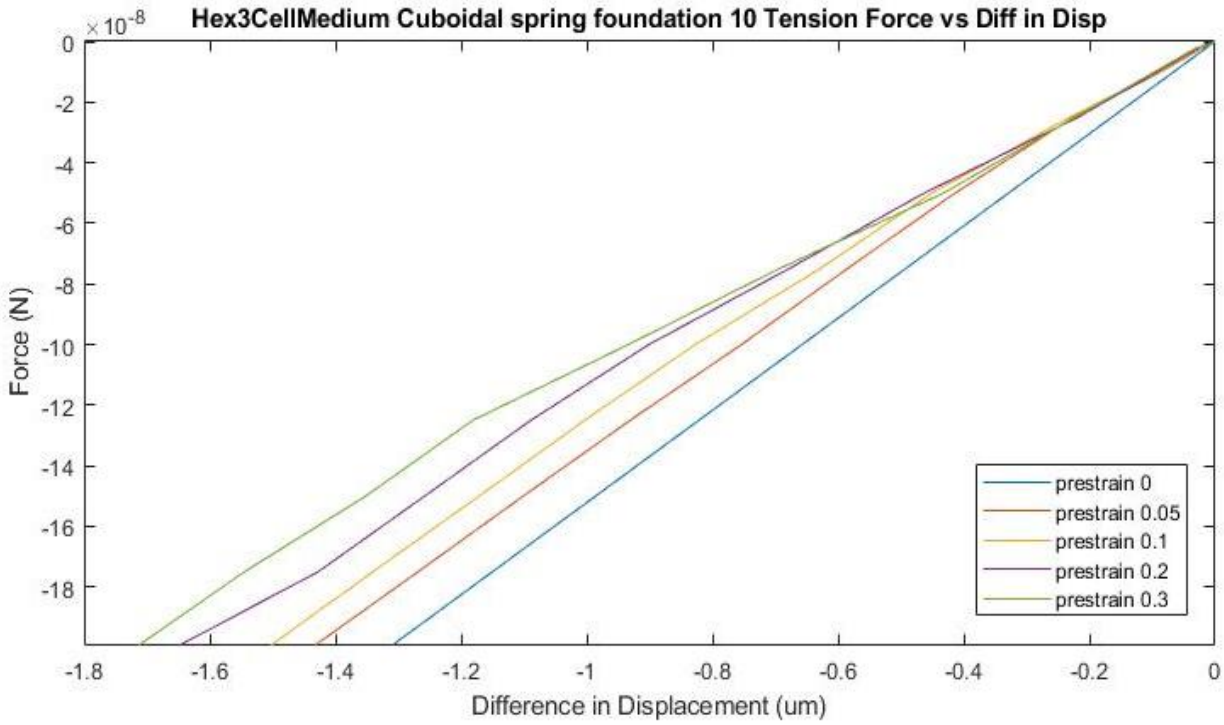

Varying Spring Foundation

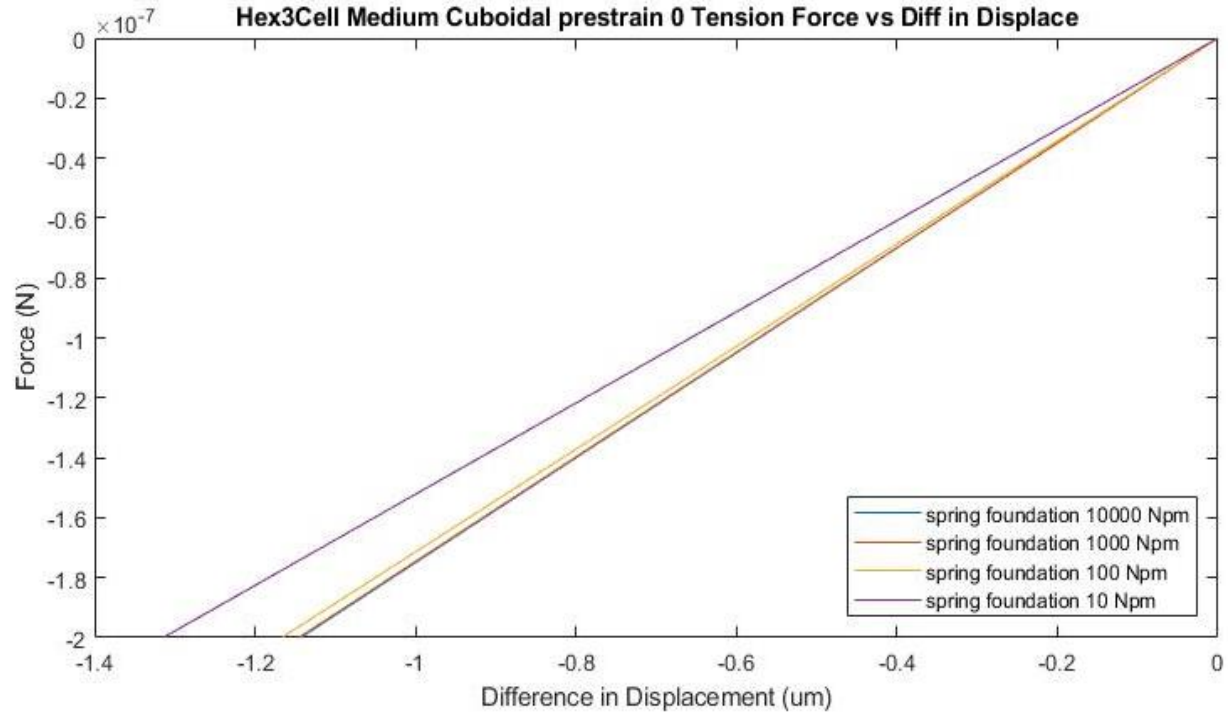

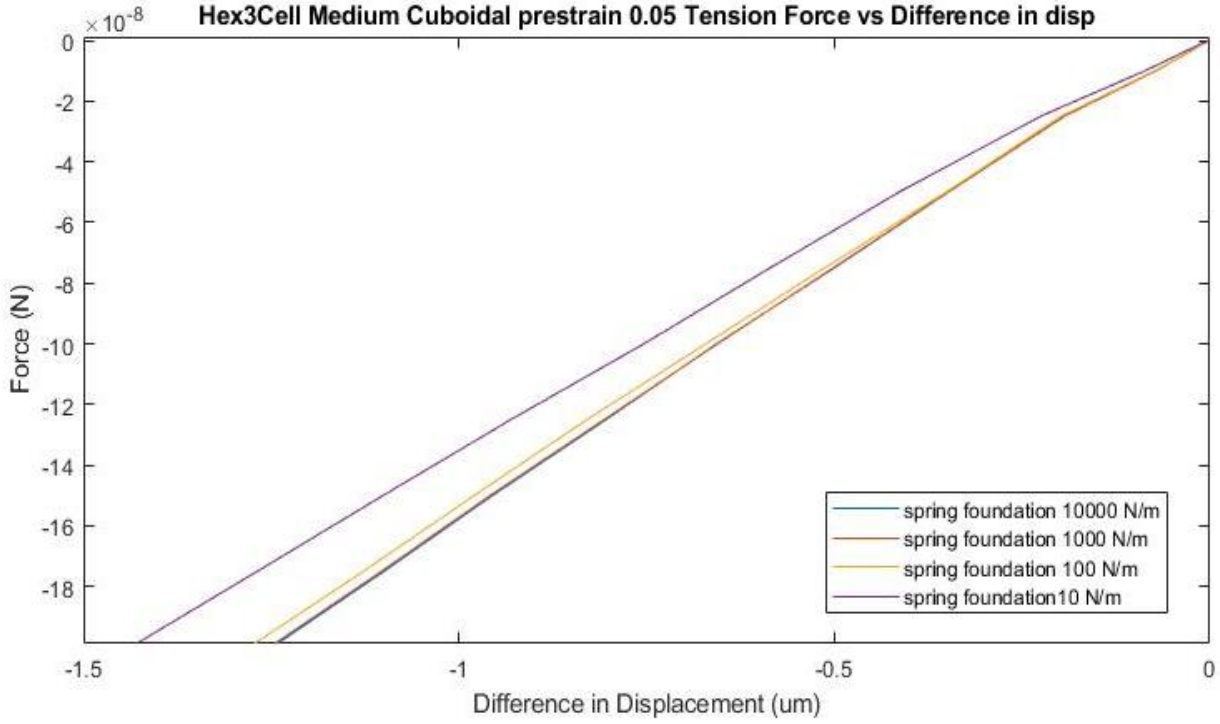
Hex3Cell Medium Cuboidal prestrain 0.05 Tension Force vs Difference in disp
×10^-8
0
-2
-4
-6
-8
-10
-12
-14
-16
-18
Force (N)
-1.5
-1
-0.5
0
Difference in Displacement (um)
spring foundation 10000 N/m
spring foundation 1000 N/m
spring foundation 100 N/m
spring foundation10 N/m

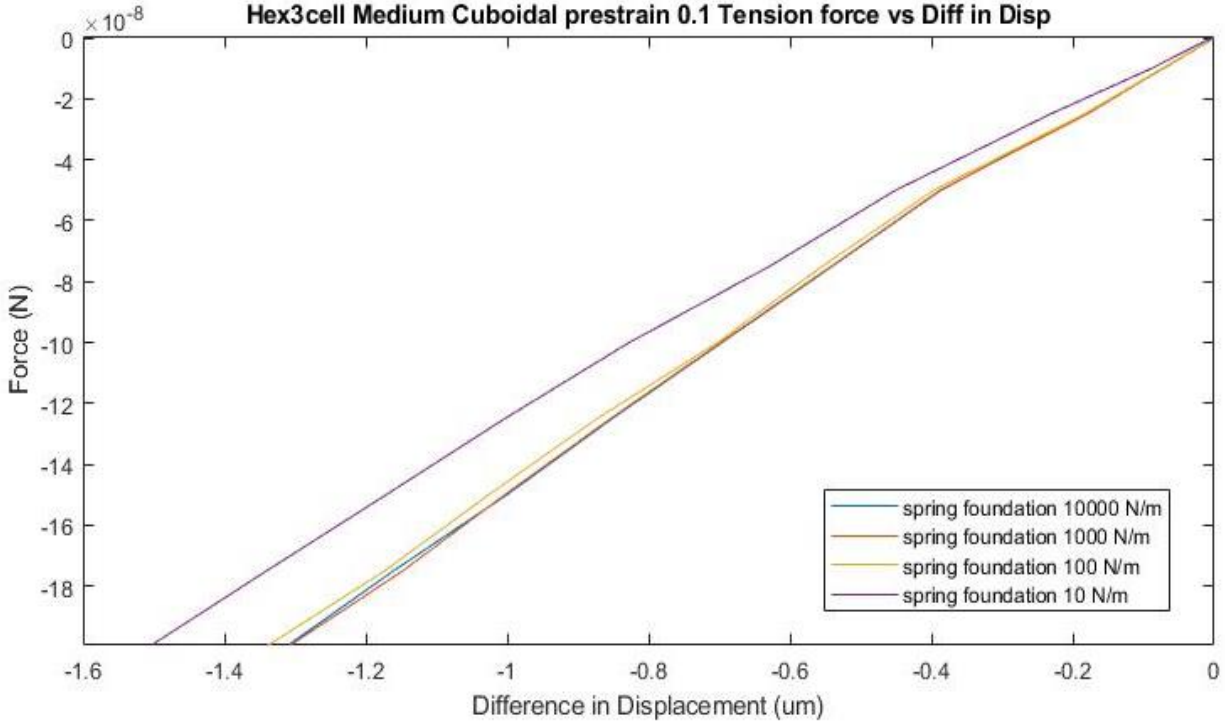
Hex3cell Medium Cuboidal prestrain 0.1 Tension force vs Diff in Disp
×10^-8
0
-2
-4
-6
-8
-10
-12
-14
-16
-18
Force (N)
-1.6
-1.4
-1.2
-1
-0.8
-0.6
-0.4
-0.2
0
Difference in Displacement (um)
spring foundation 10000 N/m
spring foundation 1000 N/m
spring foundation 100 N/m
spring foundation 10 N/m

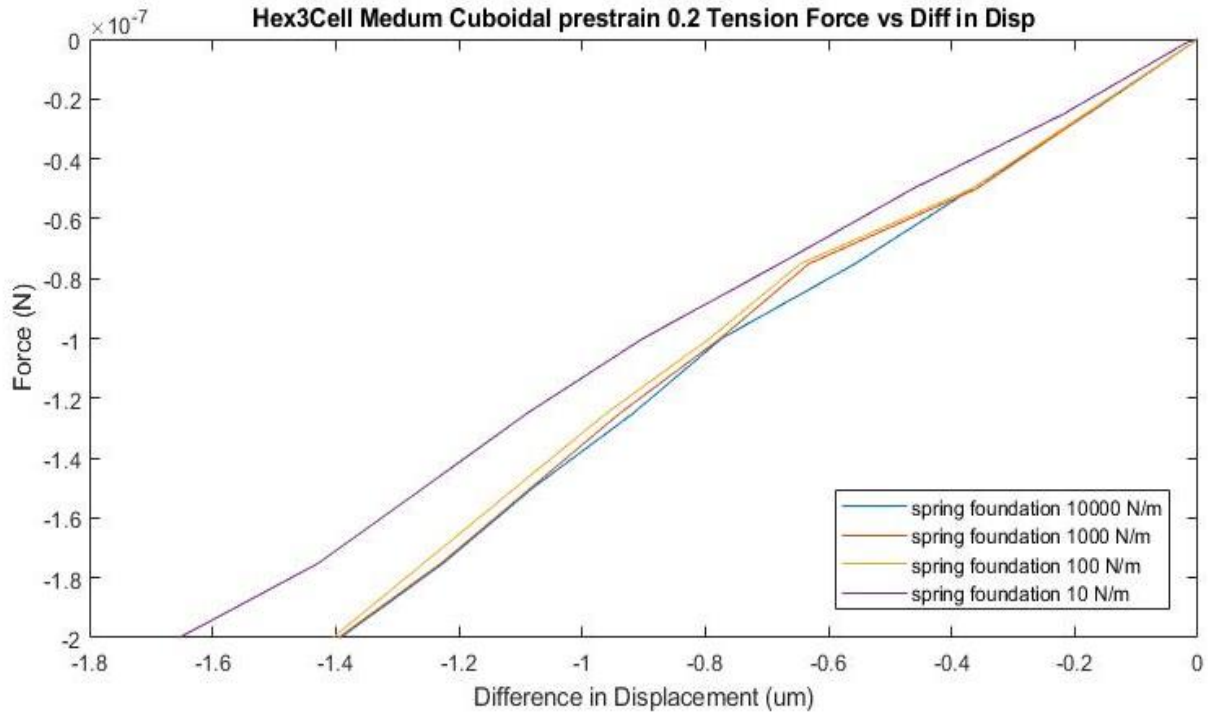
Hex3Cell Medum Cuboidal prestrain 0.2 Tension Force vs Diff in Disp
×10^-7
Force (N)
Difference in Displacement (um)
spring foundation 10000 N/m
spring foundation 1000 N/m
spring foundation 100 N/m
spring foundation 10 N/m

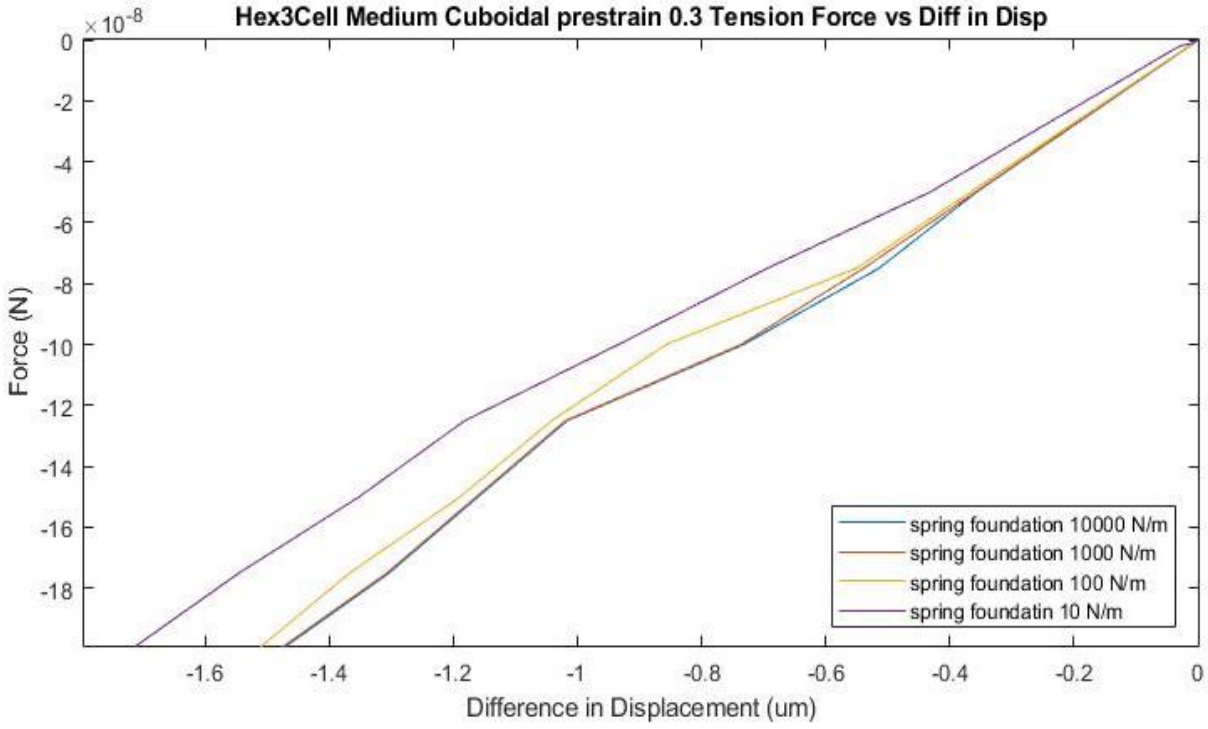
Hex3Cell Medium Cuboidal prestrain 0.3 Tension Force vs Diff in Disp
×10^-8
Force (N)
Difference in Displacement (um)
spring foundation 10000 N/m
spring foundation 1000 N/m
spring foundation 100 N/m
spring foundatin 10 N/m

Squamish or short model

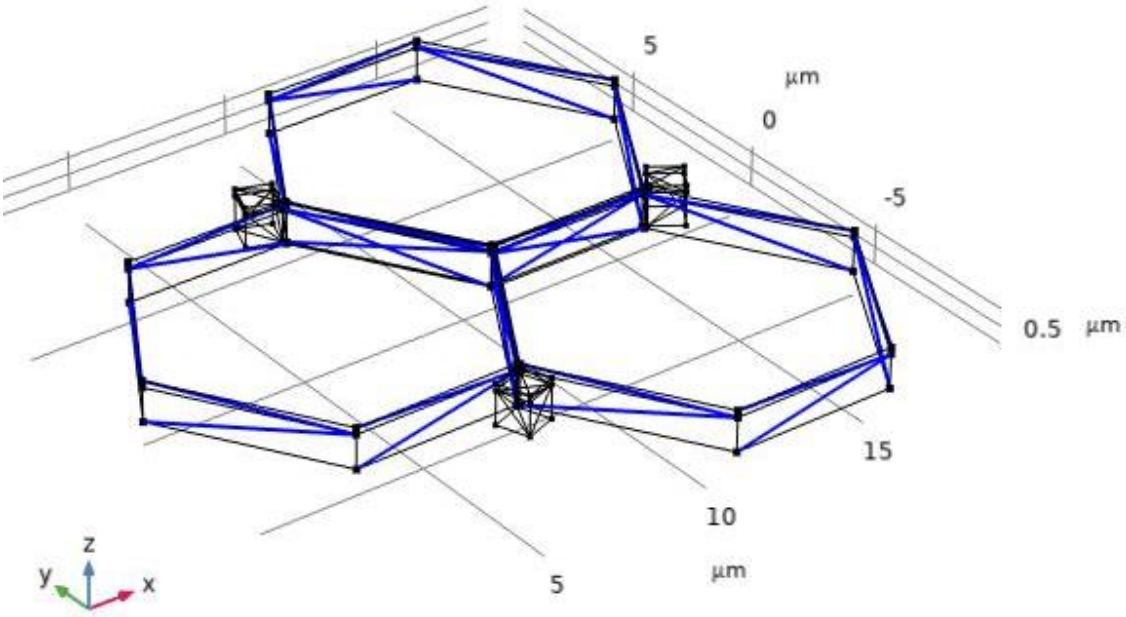

The blue lines are the compression elements of the tensegrity and the black lines are the tension elements with the exception of the black square posts that are both tension and compression elements.

Varying Pre-strain

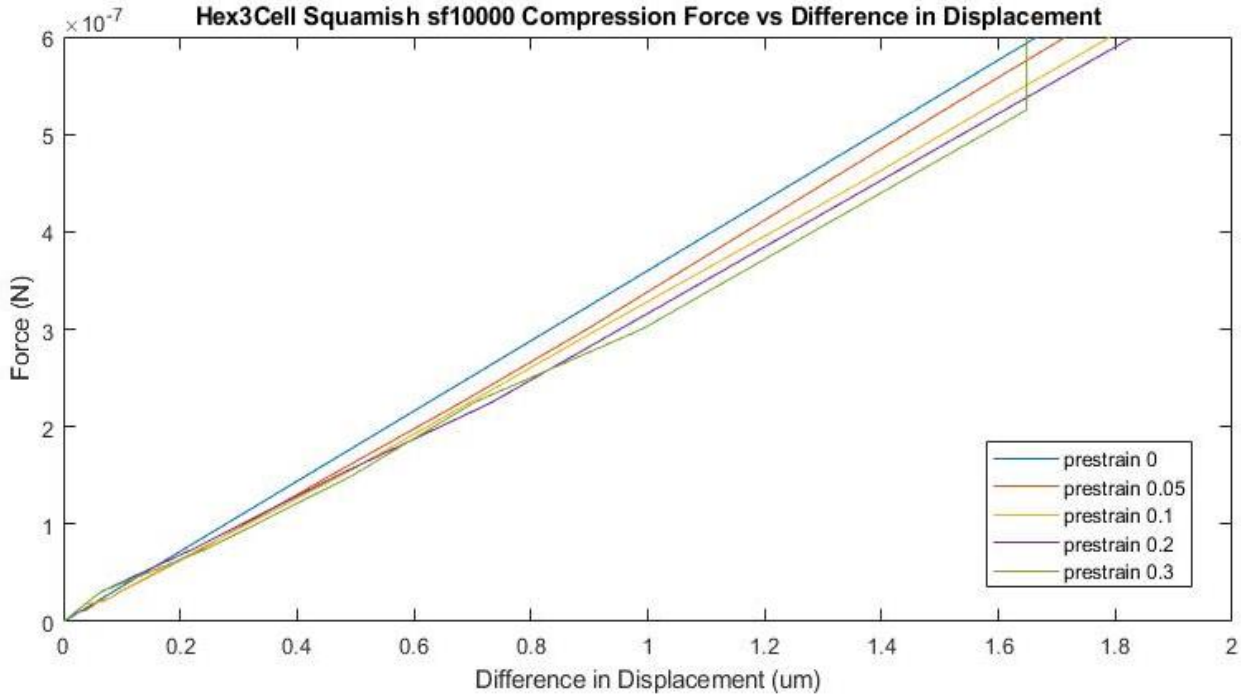

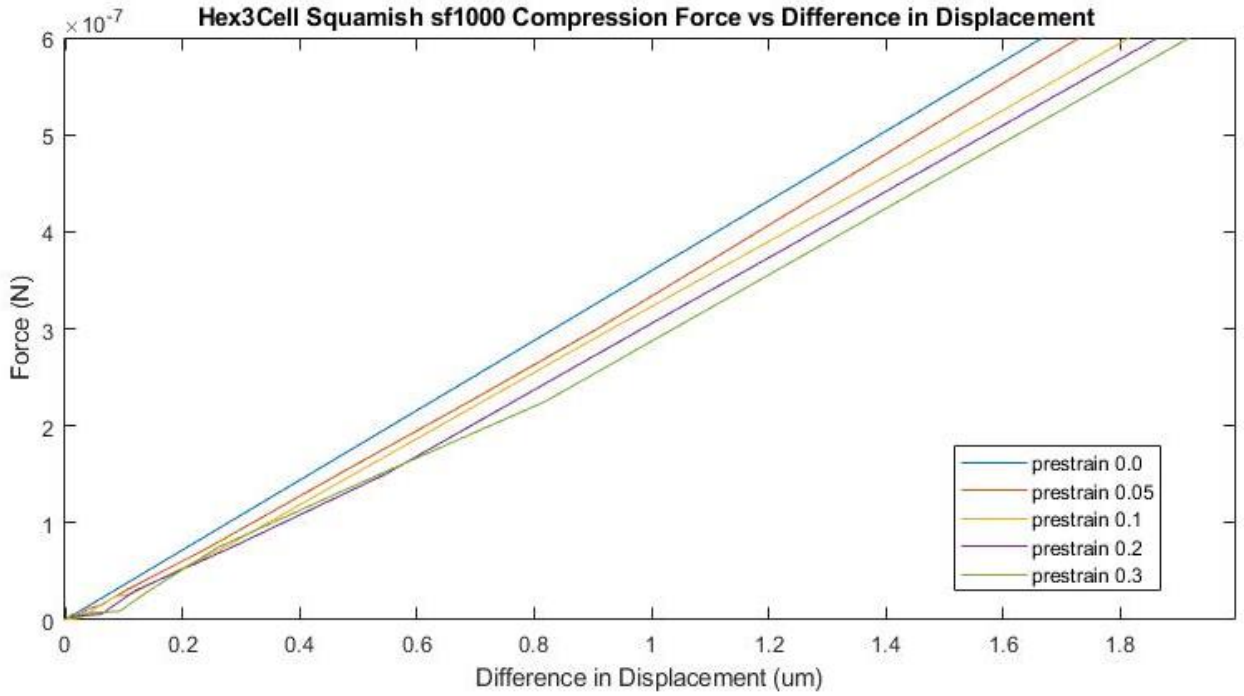
Hex3Cell Squamish sf1000 Compression Force vs Difference in Displacement
×10^-7
Force (N)
Difference in Displacement (um)
prestrain 0.0
prestrain 0.05
prestrain 0.1
prestrain 0.2
prestrain 0.3

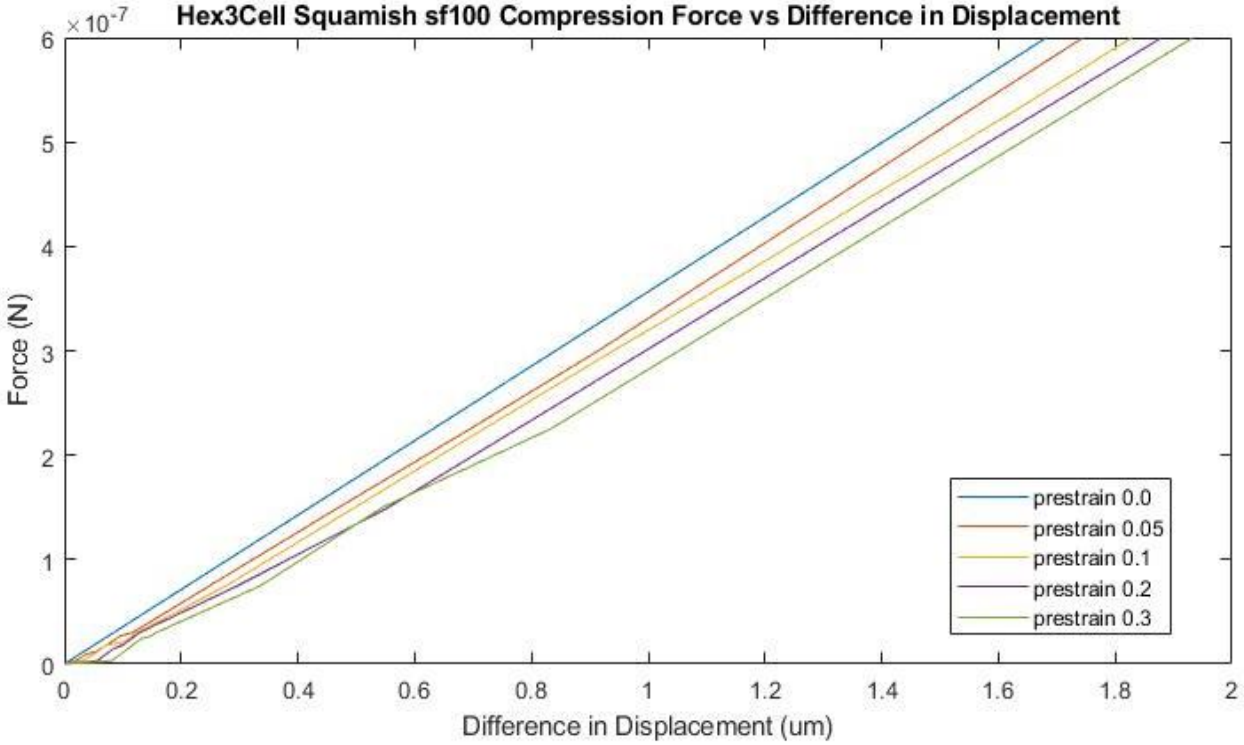
Hex3Cell Squamish sf100 Compression Force vs Difference in Displacement
×10^-7
Force (N)
Difference in Displacement (um)
prestrain 0.0
prestrain 0.05
prestrain 0.1
prestrain 0.2
prestrain 0.3

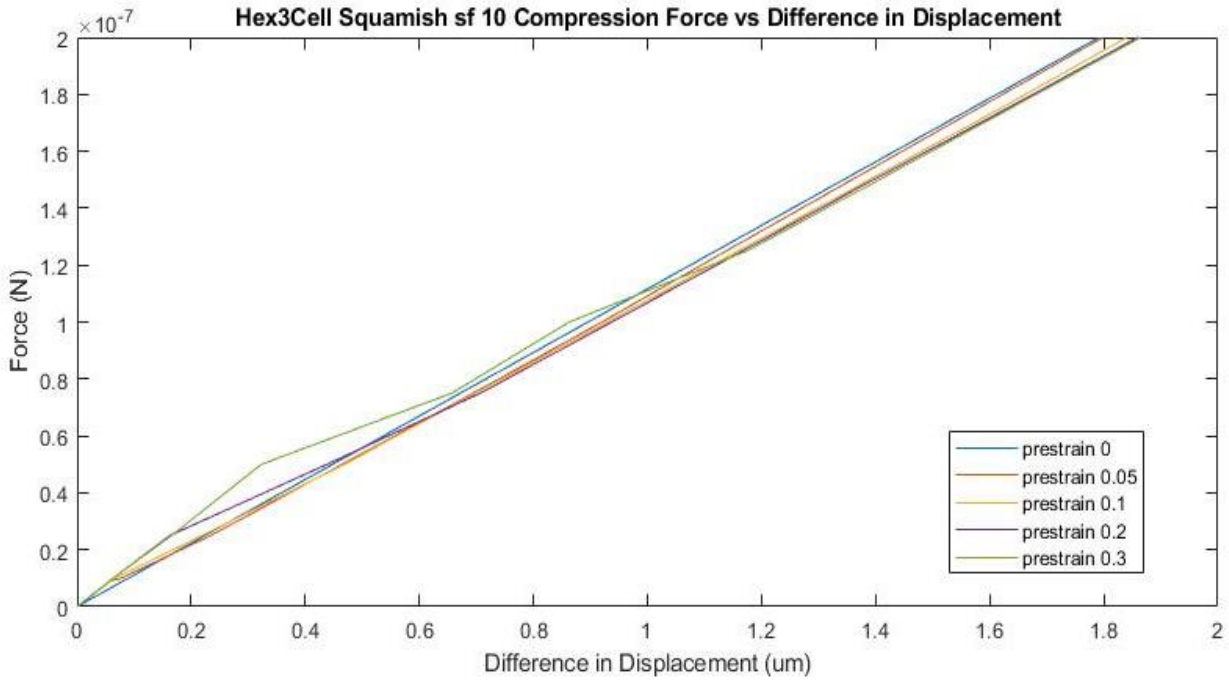

Varying Spring Foundation

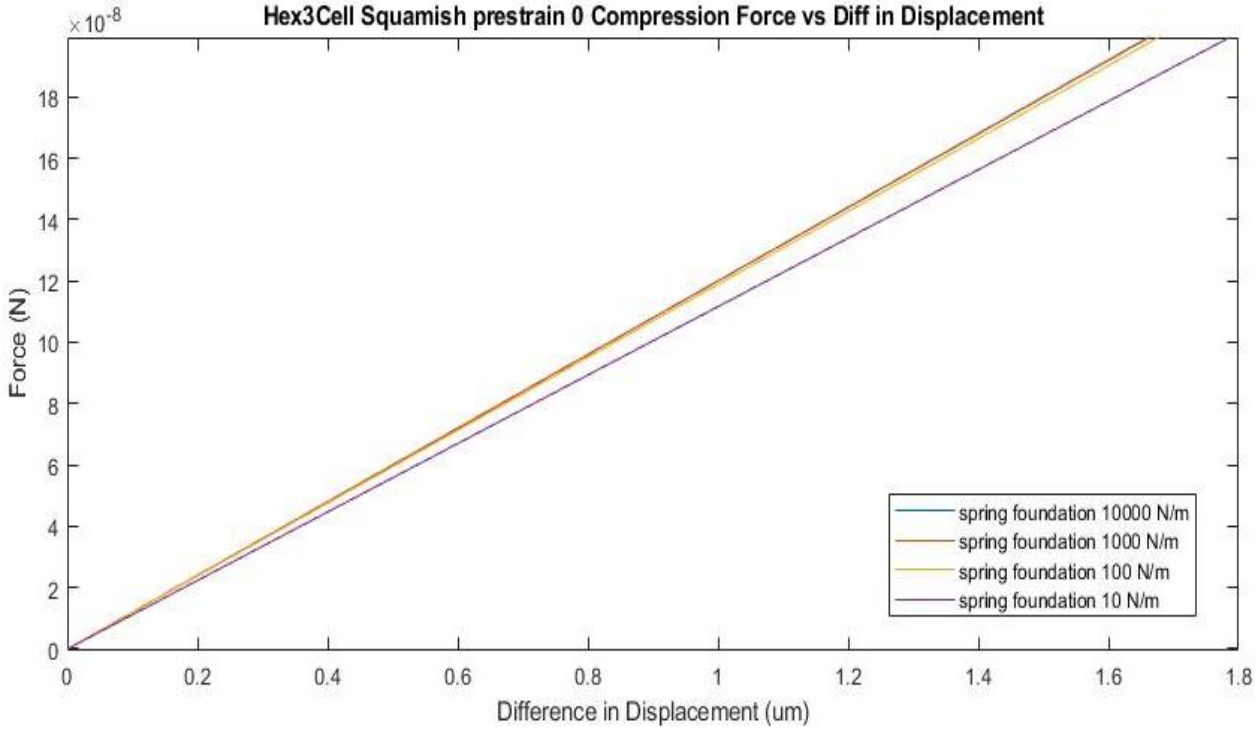

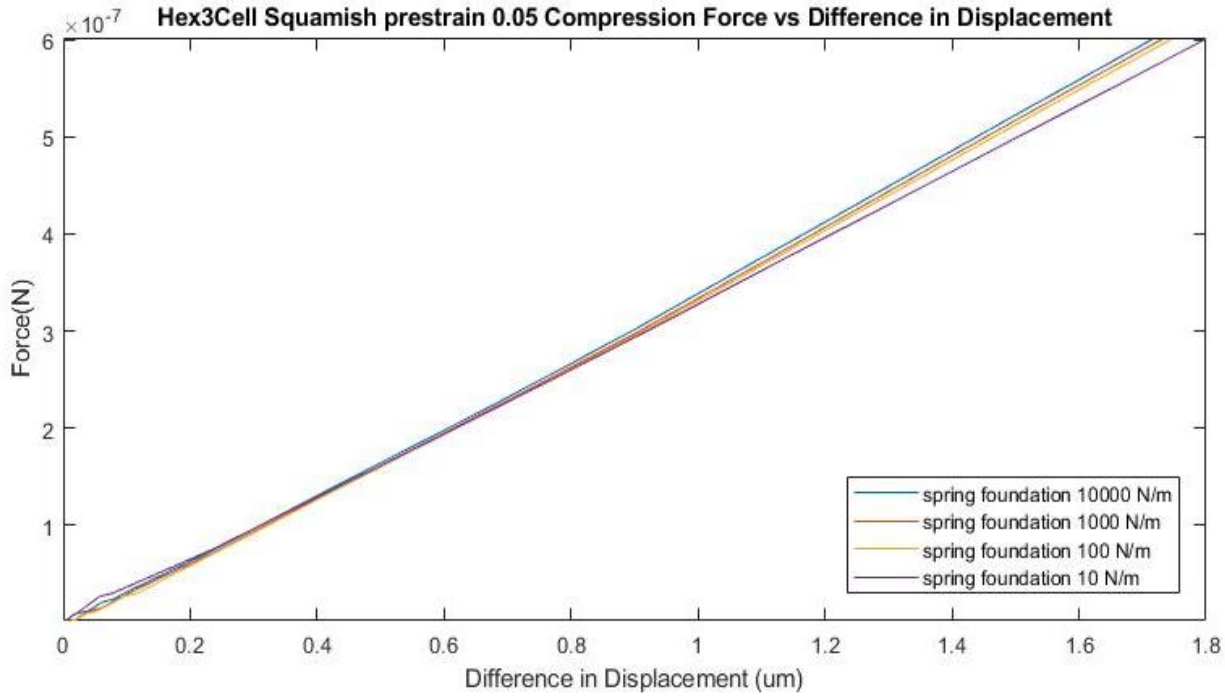
Hex3Cell Squamish prestrain 0.05 Compression Force vs Difference in Displacement
×10^-7
Force(N)
Difference in Displacement (um)
spring foundation 10000 N/m
spring foundation 1000 N/m
spring foundation 100 N/m
spring foundation 10 N/m

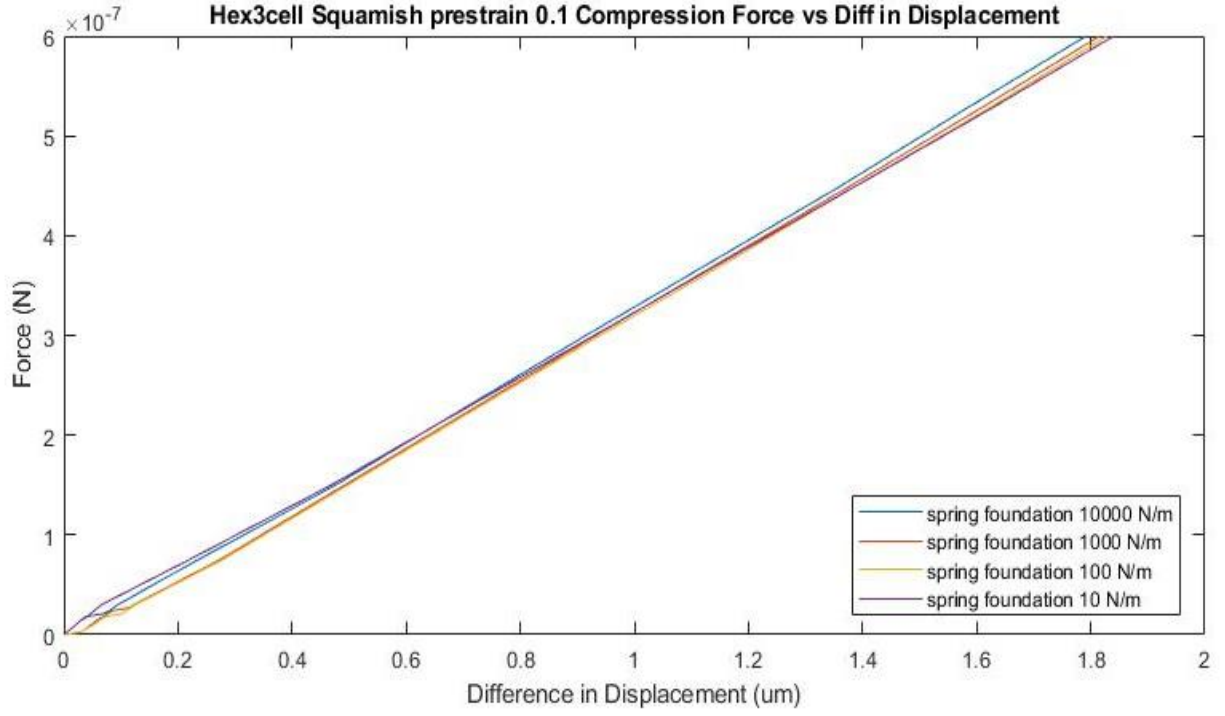
Hex3cell Squamish prestrain 0.1 Compression Force vs Diff in Displacement
×10^-7
Force (N)
Difference in Displacement (um)
spring foundation 10000 N/m
spring foundation 1000 N/m
spring foundation 100 N/m
spring foundation 10 N/m

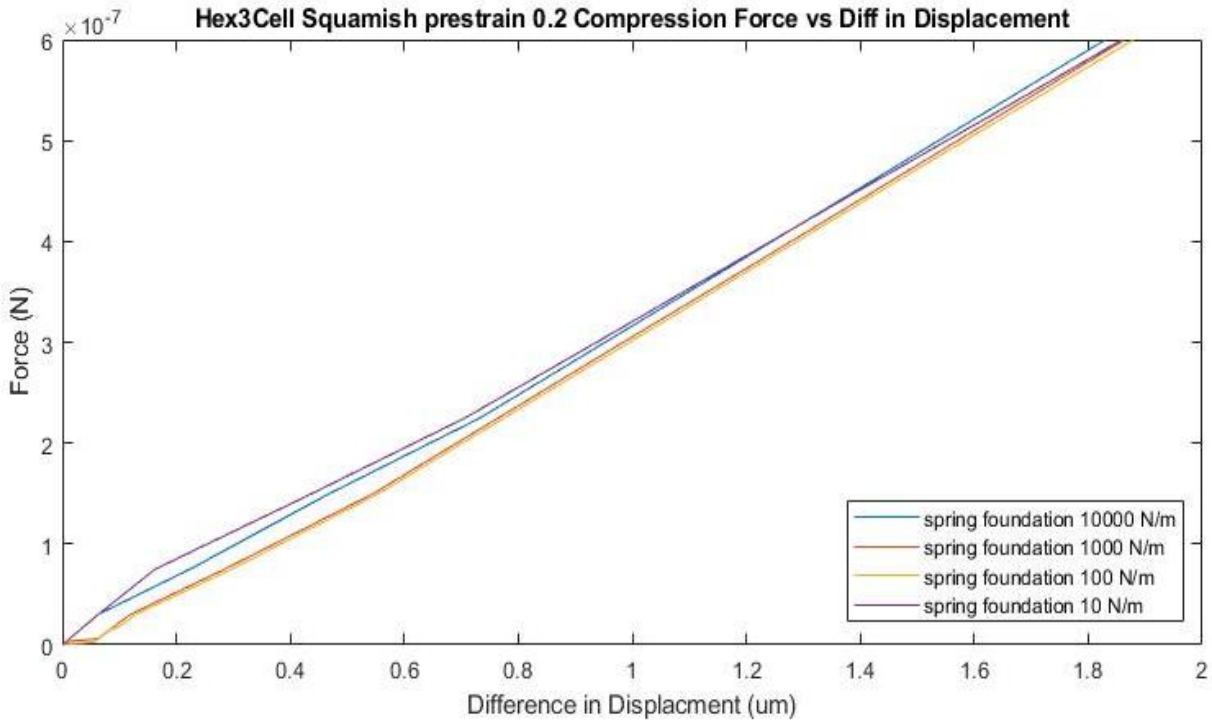
Hex3Cell Squamish prestrain 0.2 Compression Force vs Diff in Displacement
×10^-7
Force (N)
Difference in Displacment (um)
spring foundation 10000 N/m
spring foundation 1000 N/m
spring foundation 100 N/m
spring foundation 10 N/m

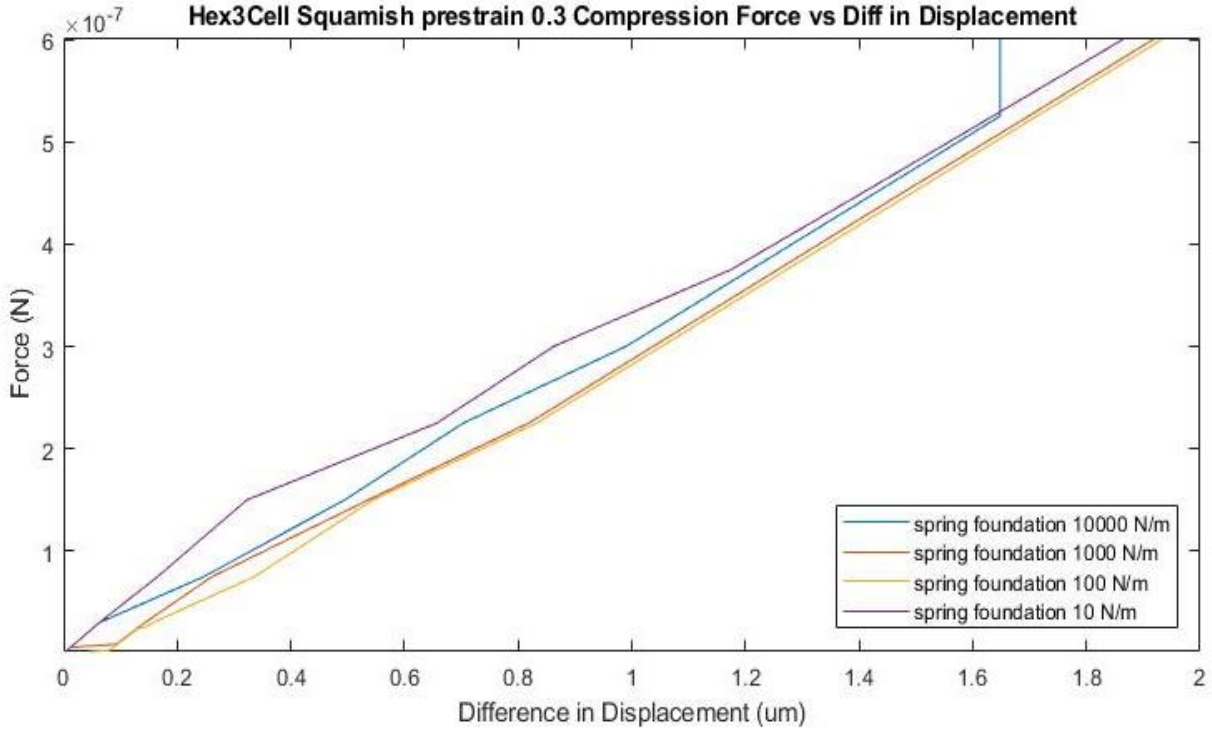
Hex3Cell Squamish prestrain 0.3 Compression Force vs Diff in Displacement
×10^-7
Force (N)
Difference in Displacement (um)
spring foundation 10000 N/m
spring foundation 1000 N/m
spring foundation 100 N/m
spring foundation 10 N/m

Tension graphs for squamish three cell hexagon

Varying pre-strain

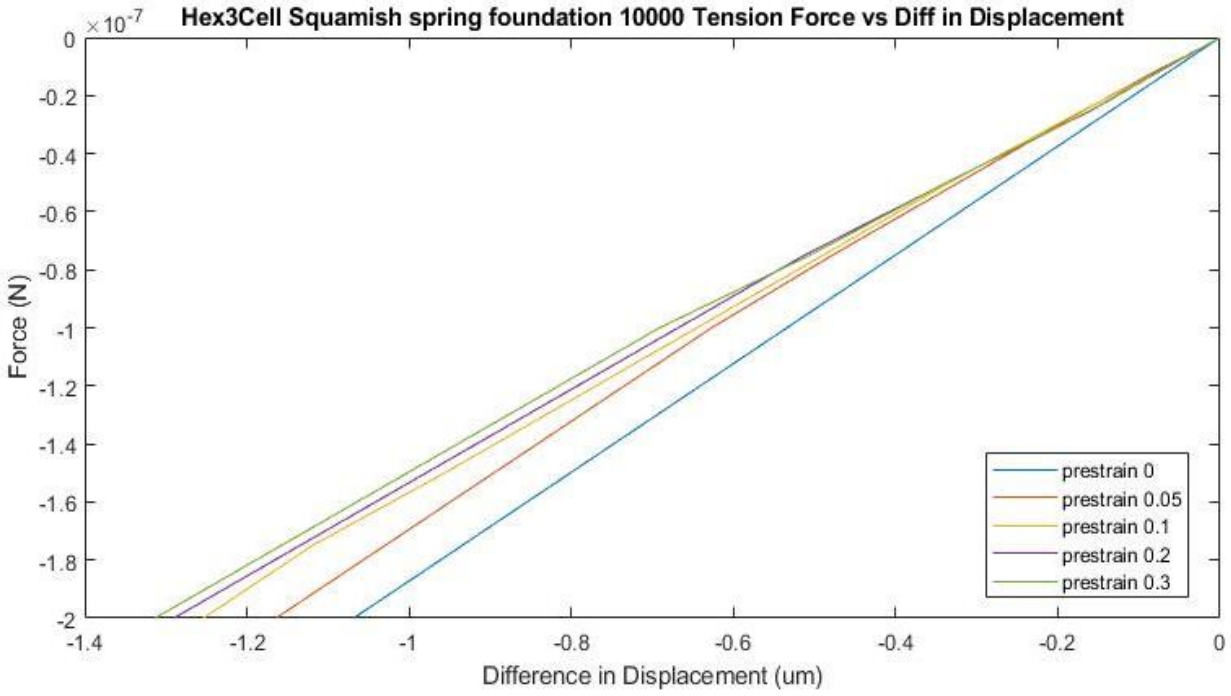

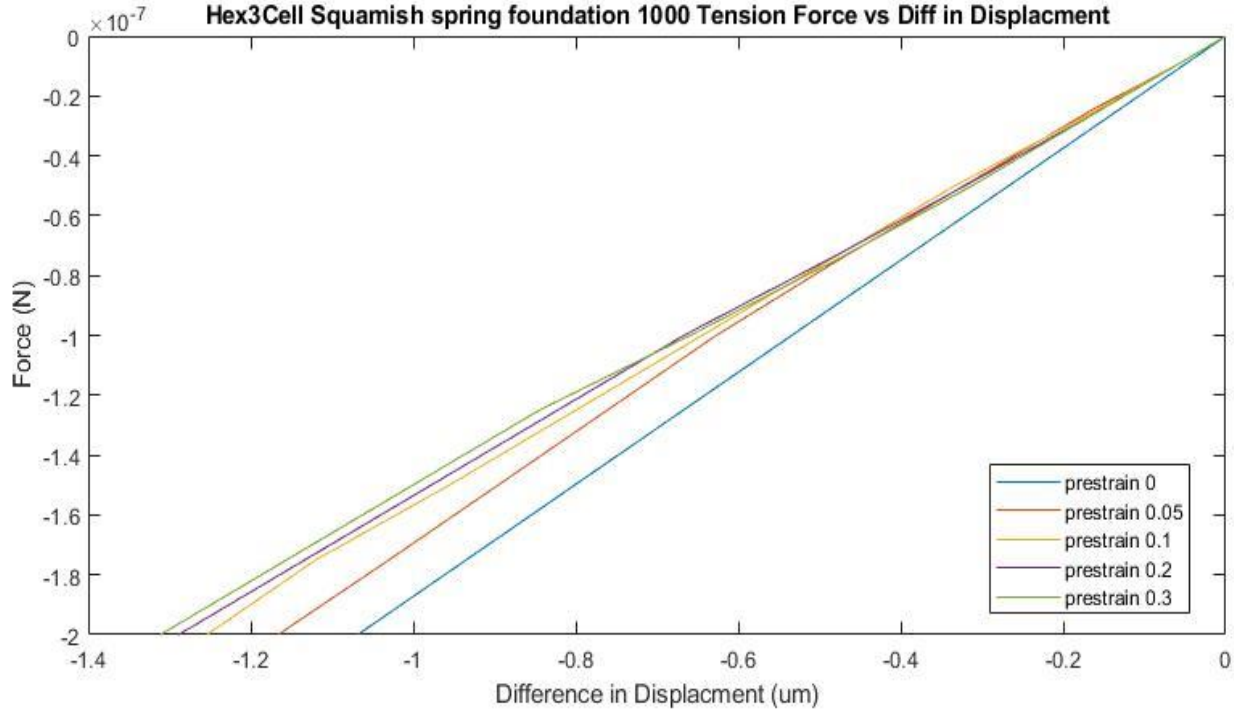

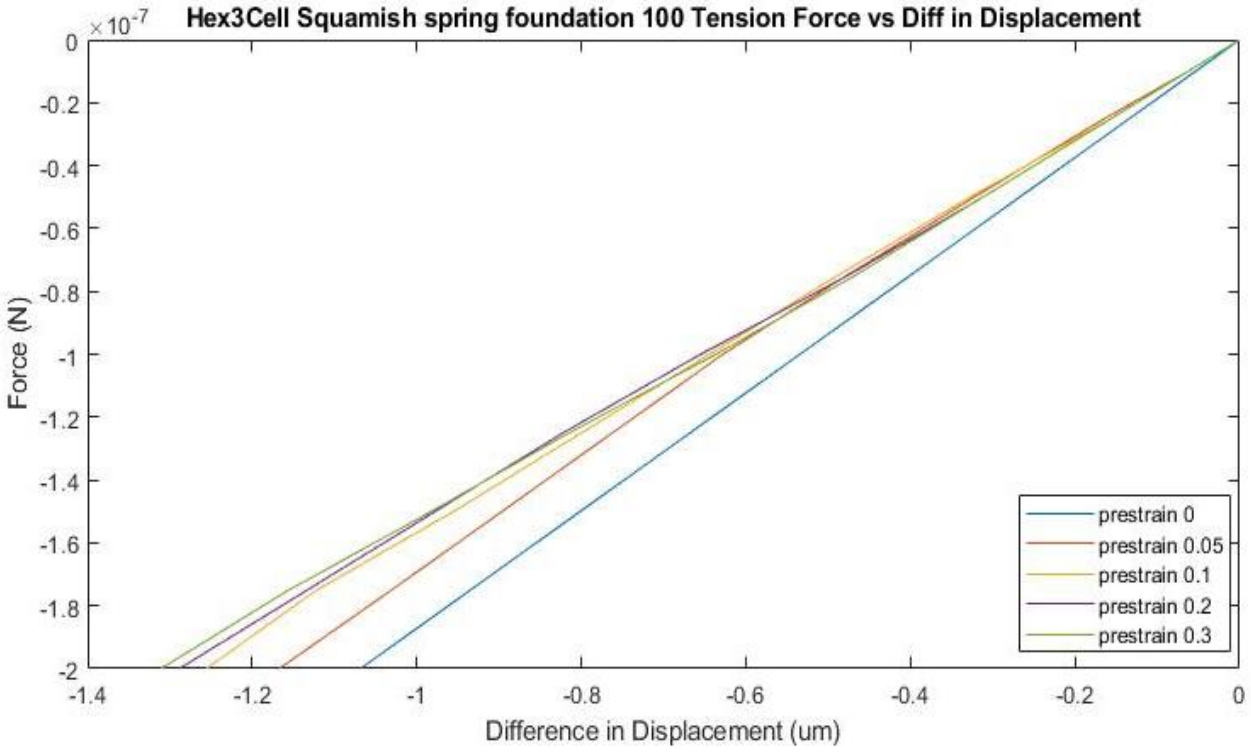
Hex3Cell Squamish spring foundation 100 Tension Force vs Diff in Displacement
×10^-7
0
-0.2
-0.4
-0.6
-0.8
-1
-1.2
-1.4
-1.6
-1.8
-2
Force (N)
-1.4
-1.2
-1
-0.8
-0.6
-0.4
-0.2
0
Difference in Displacement (um)
prestrain 0
prestrain 0.05
prestrain 0.1
prestrain 0.2
prestrain 0.3

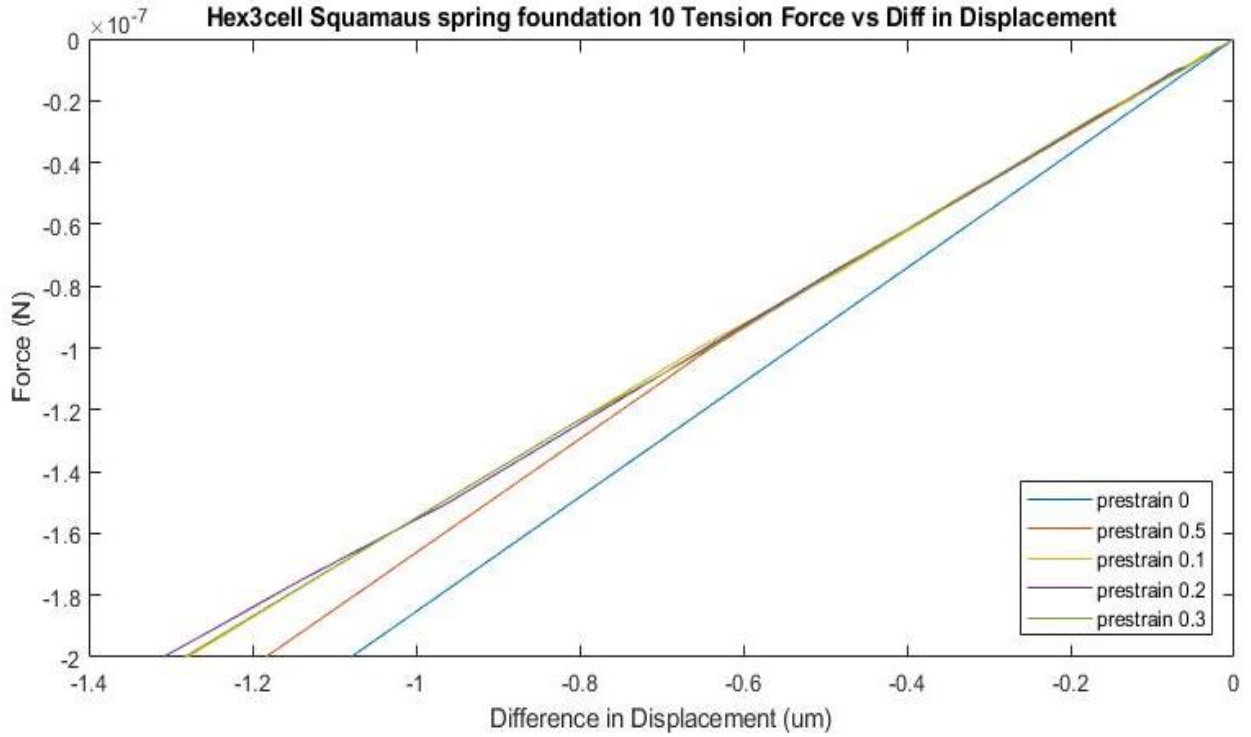
Hex3cell Squamaus spring foundation 10 Tension Force vs Diff in Displacement
×10^-7
0
-0.2
-0.4
-0.6
-0.8
-1
-1.2
-1.4
-1.6
-1.8
-2
Force (N)
-1.4
-1.2
-1
-0.8
-0.6
-0.4
-0.2
0
Difference in Displacement (um)
prestrain 0
prestrain 0.5
prestrain 0.1
prestrain 0.2
prestrain 0.3

Varying spring foundation Tension

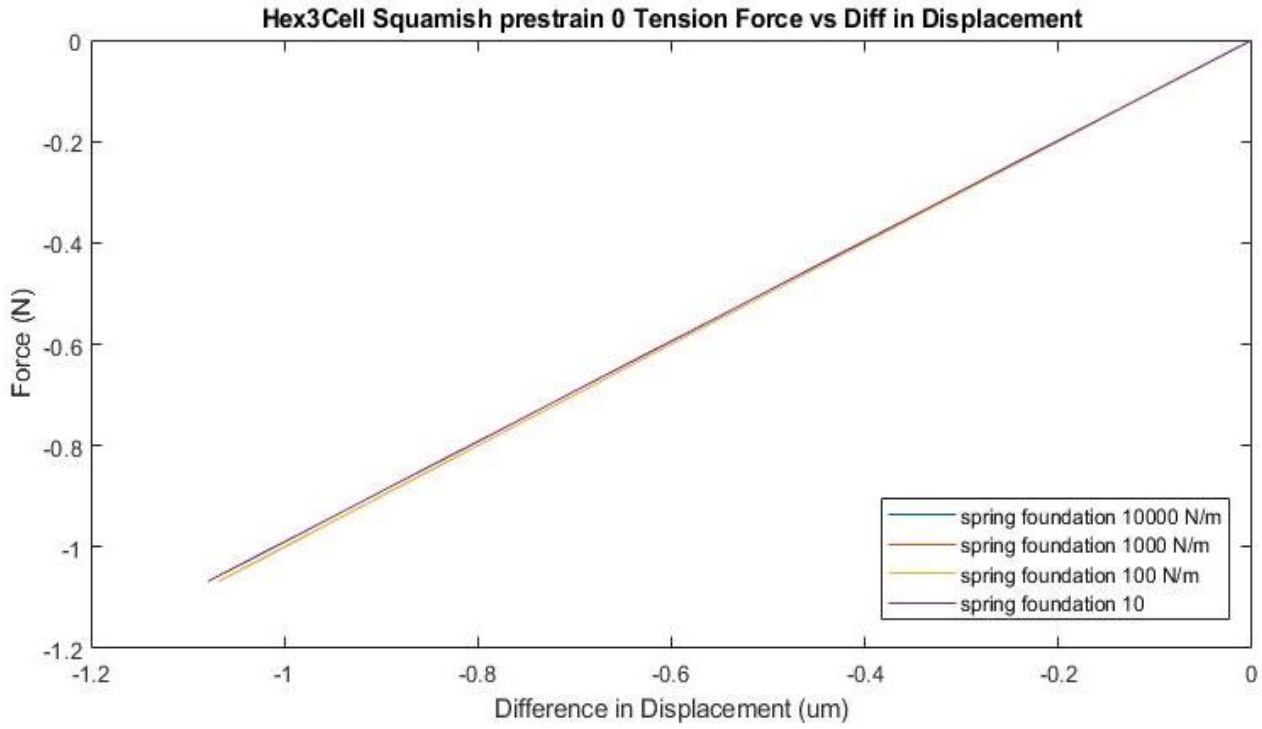

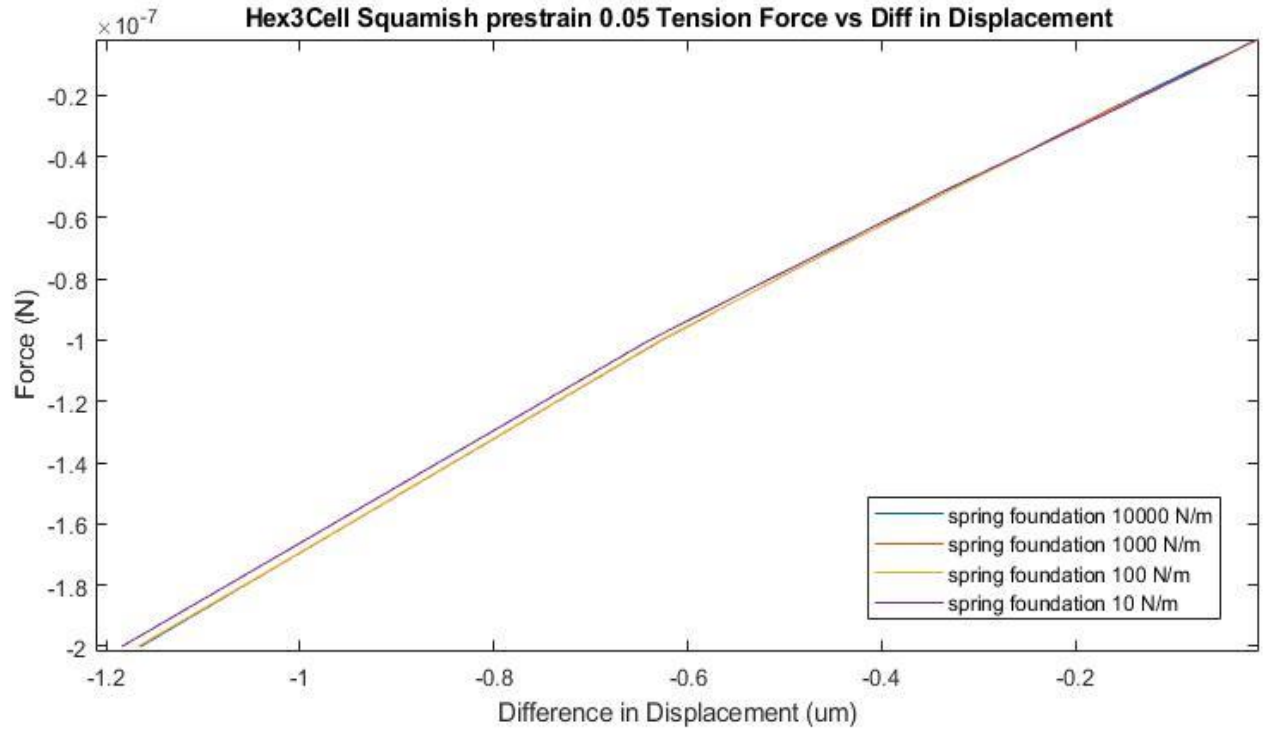

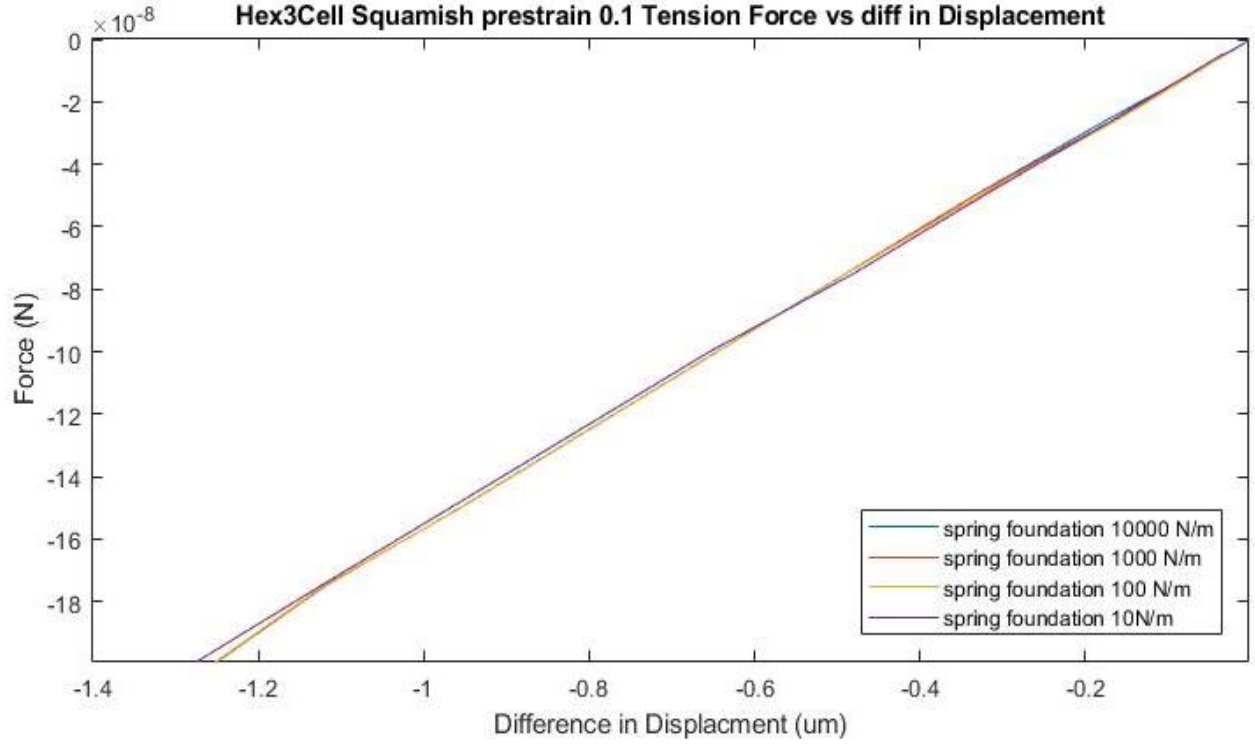
Hex3Cell Squamish prestrain 0.1 Tension Force vs diff in Displacement
×10^-8
0
-2
-4
-6
-8
-10
-12
-14
-16
-18
Force (N)
-1.4
-1.2
-1
-0.8
-0.6
-0.4
-0.2
Difference in Displacment (um)
spring foundation 10000 N/m
spring foundation 1000 N/m
spring foundation 100 N/m
spring foundation 10N/m

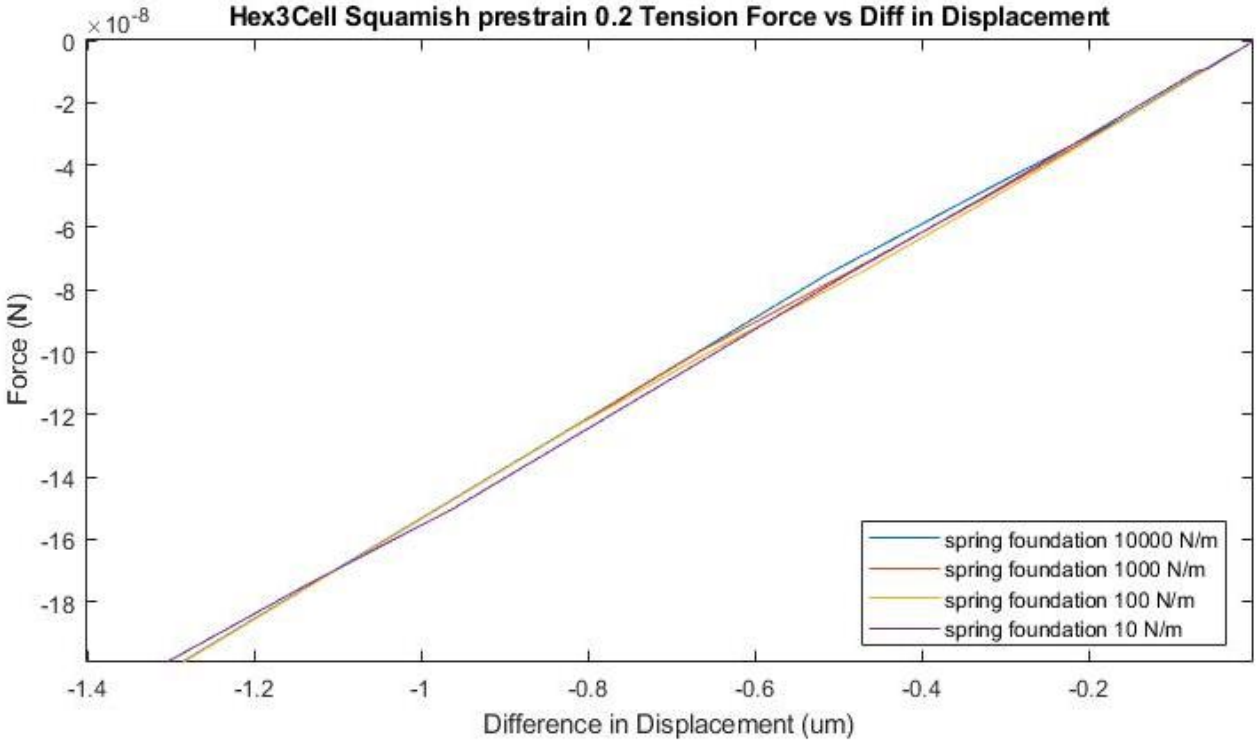
Hex3Cell Squamish prestrain 0.2 Tension Force vs Diff in Displacement
×10^-8
0
-2
-4
-6
-8
-10
-12
-14
-16
-18
Force (N)
-1.4
-1.2
-1
-0.8
-0.6
-0.4
-0.2
Difference in Displacement (um)
spring foundation 10000 N/m
spring foundation 1000 N/m
spring foundation 100 N/m
spring foundation 10 N/m

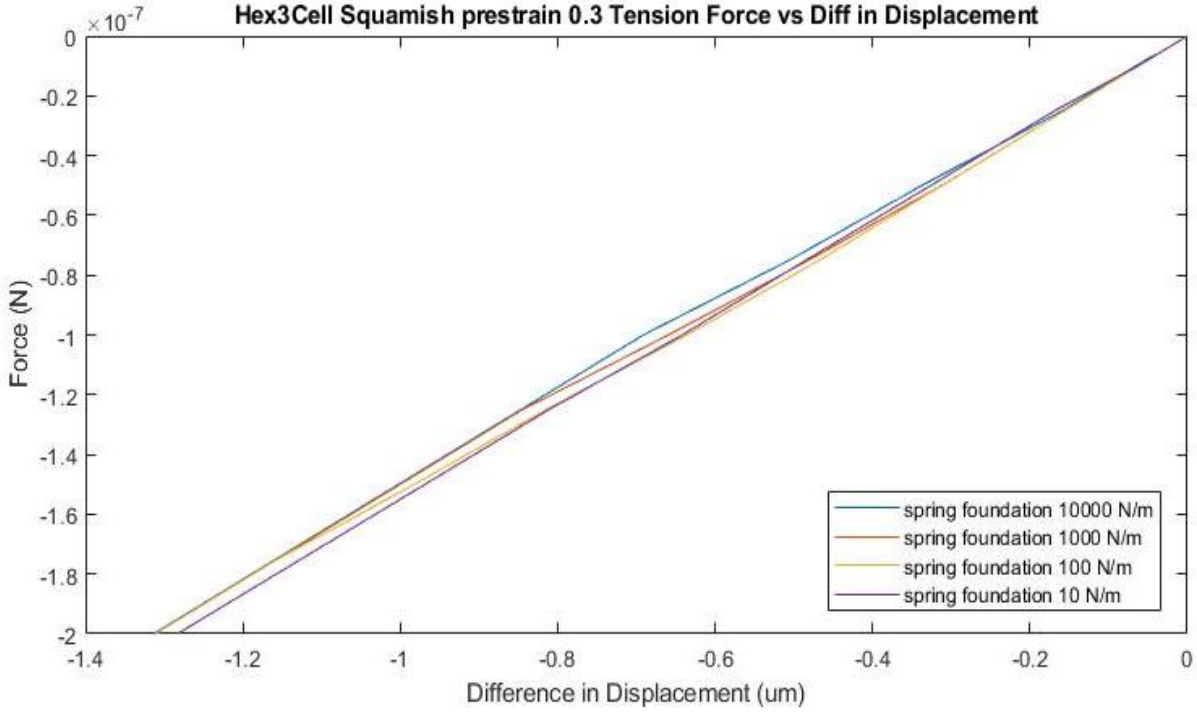
Hex3Cell Squamish prestrain 0.3 Tension Force vs Diff in Displacement
×10^-7
0
-0.2
-0.4
-0.6
-0.8
-1
-1.2
-1.4
-1.6
-1.8
-2
Force (N)
-1.4
-1.2
-1
-0.8
-0.6
-0.4
-0.2
0
Difference in Displacement (um)
spring foundation 10000 N/m
spring foundation 1000 N/m
spring foundation 100 N/m
spring foundation 10 N/m

Columnar or tall with narrow posts

Averaging between the three top points

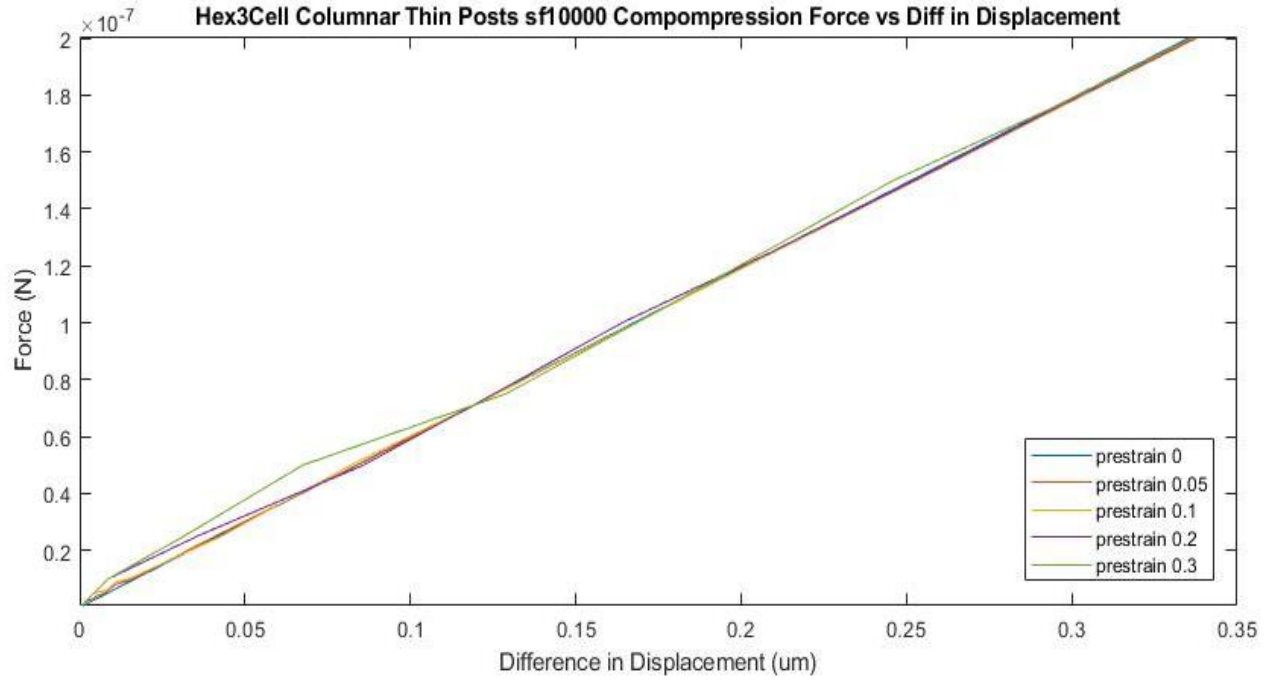

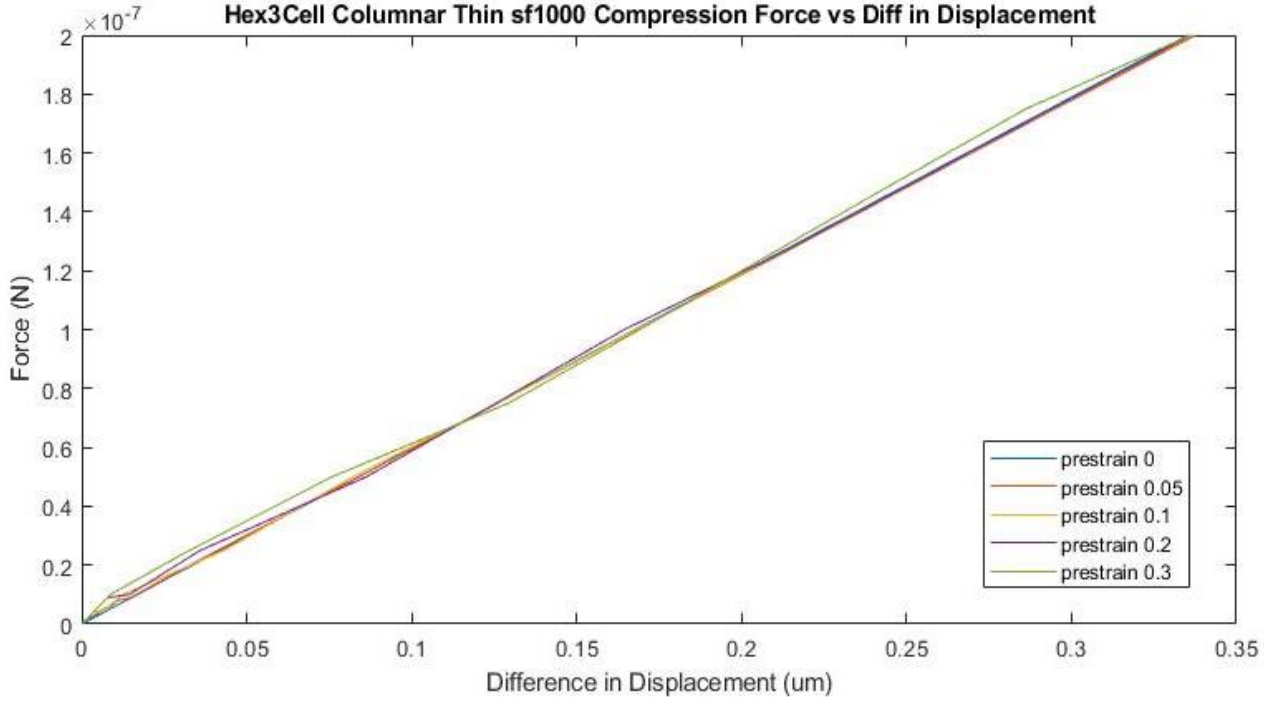

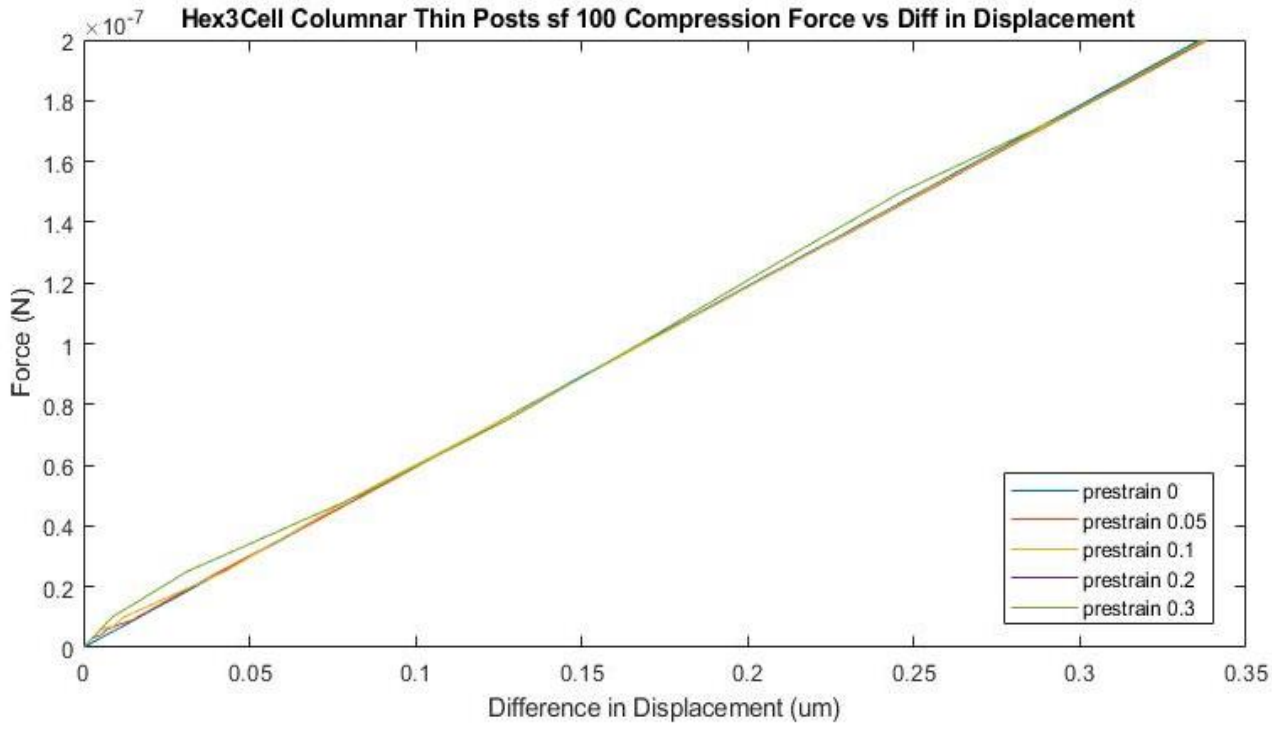
Hex3Cell Columnar Thin Posts sf 100 Compression Force vs Diff in Displacement
×10^-7
Force (N)
Difference in Displacement (um)
prestrain 0
prestrain 0.05
prestrain 0.1
prestrain 0.2
prestrain 0.3

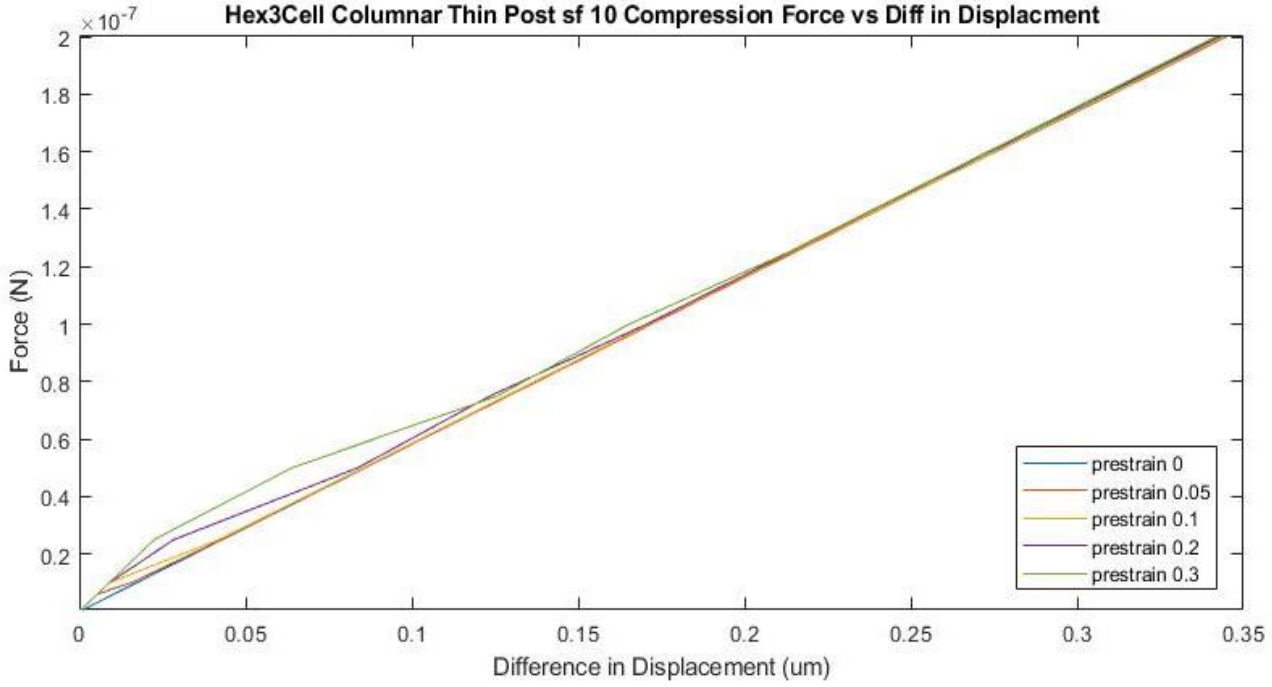
Hex3Cell Columnar Thin Post sf 10 Compression Force vs Diff in Displacment
×10^-7
Force (N)
Difference in Displacement (um)
prestrain 0
prestrain 0.05
prestrain 0.1
prestrain 0.2
prestrain 0.3

Tension Graphs Varying Pretrain

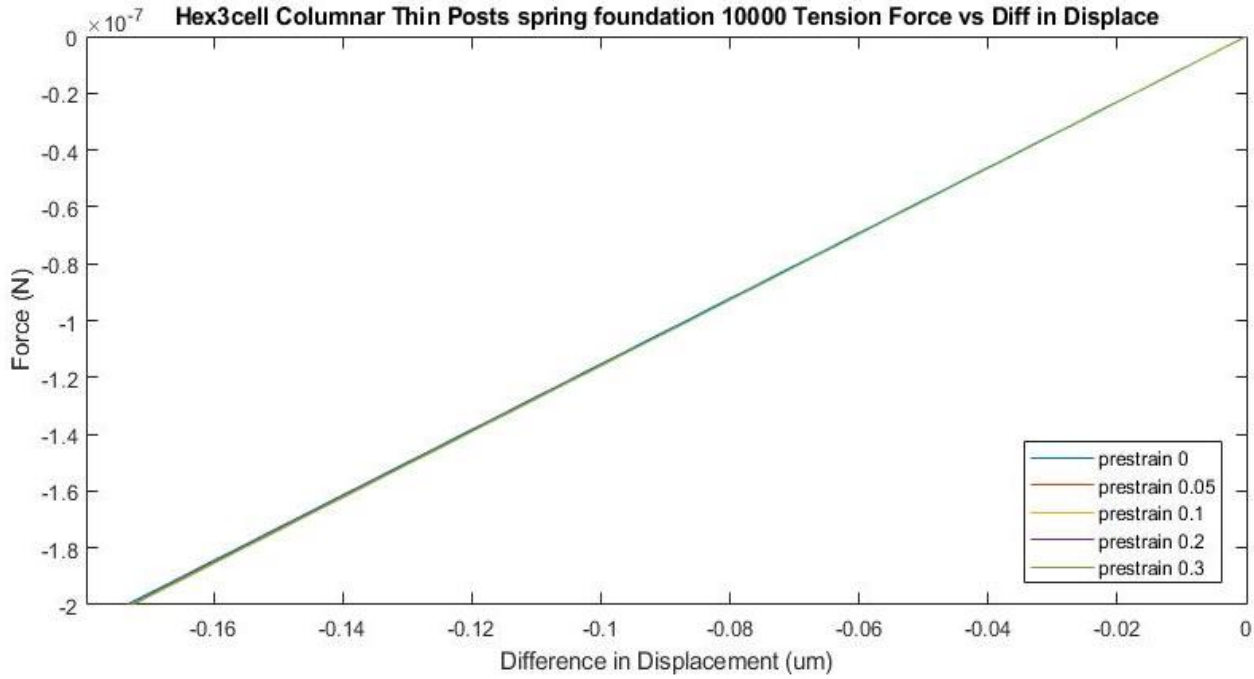

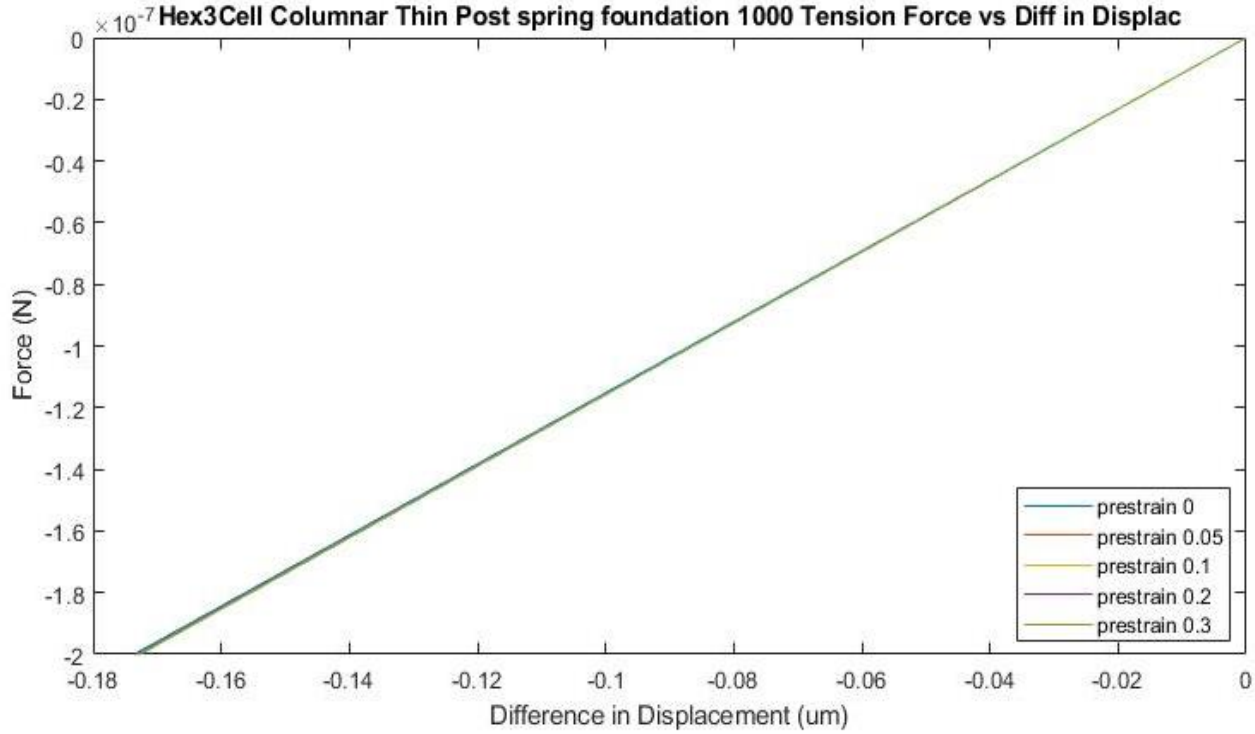

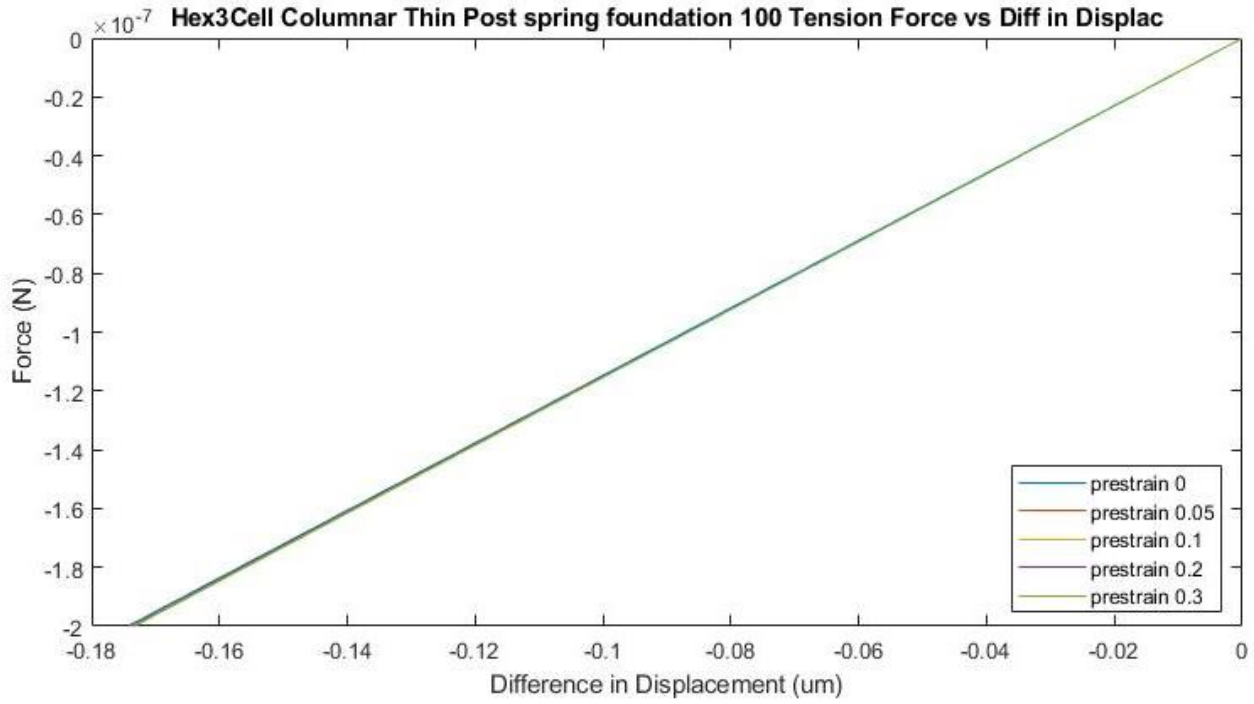
Hex3Cell Columnar Thin Post spring foundation 100 Tension Force vs Diff in Displac
×10^-7
Force (N)
Difference in Displacement (um)
prestrain 0
prestrain 0.05
prestrain 0.1
prestrain 0.2
prestrain 0.3

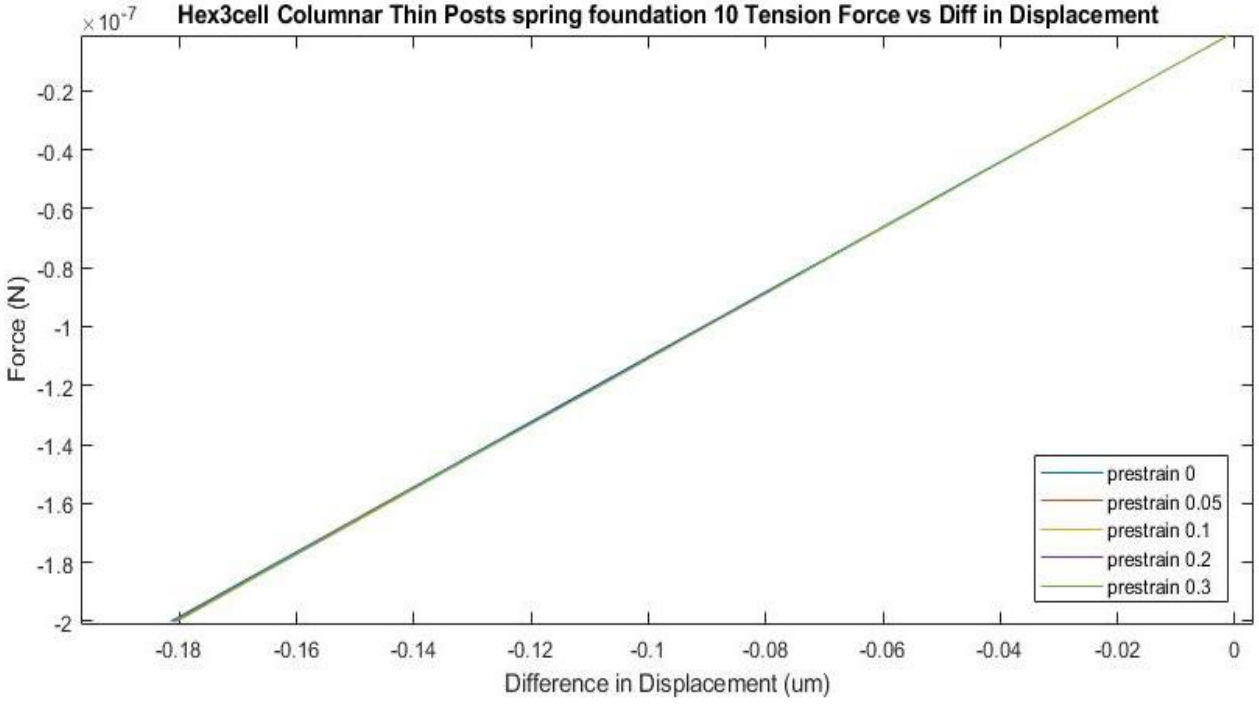
Hex3cell Columnar Thin Posts spring foundation 10 Tension Force vs Diff in Displacement
×10^-7
Force (N)
Difference in Displacement (um)
prestrain 0
prestrain 0.05
prestrain 0.1
prestrain 0.2
prestrain 0.3

Varying Spring Foundation

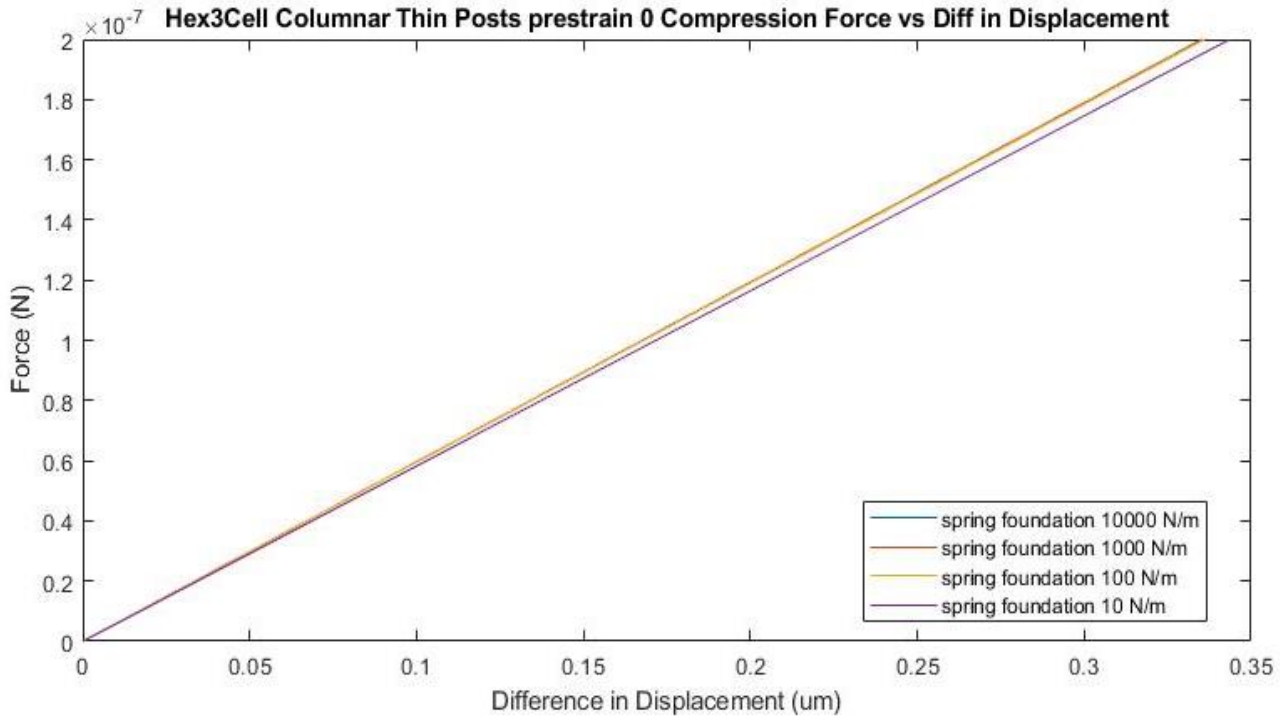

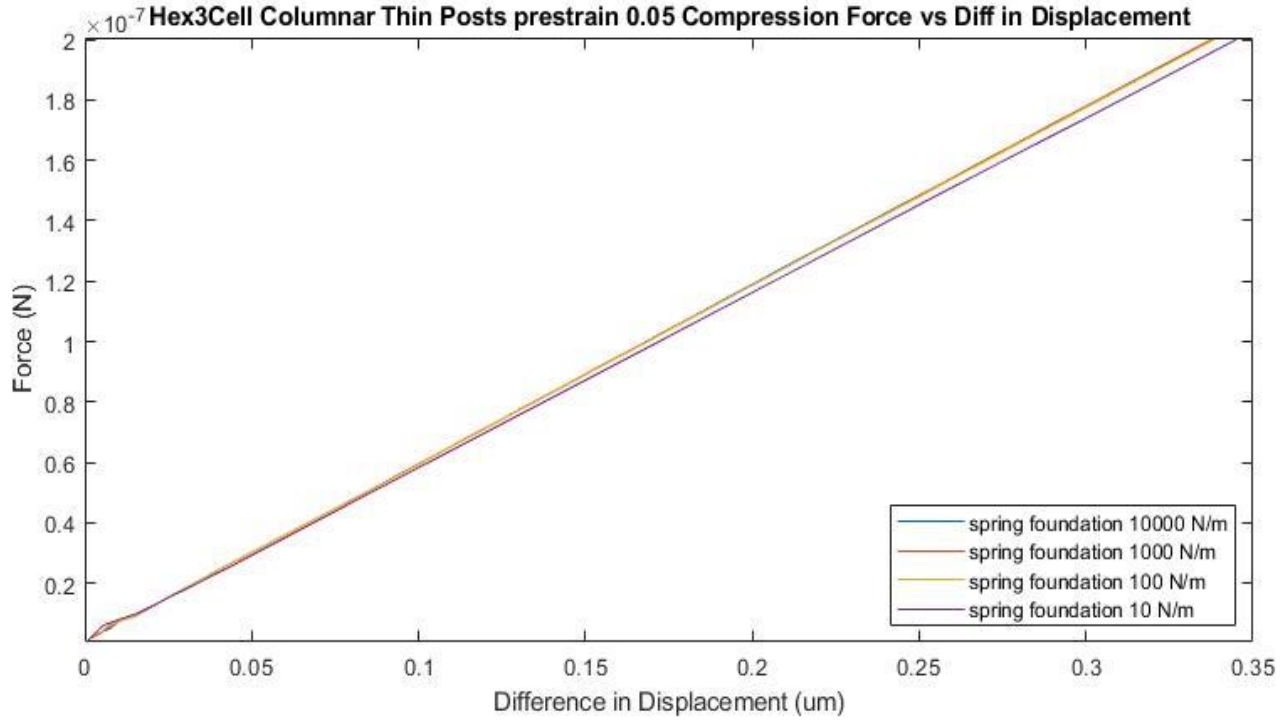

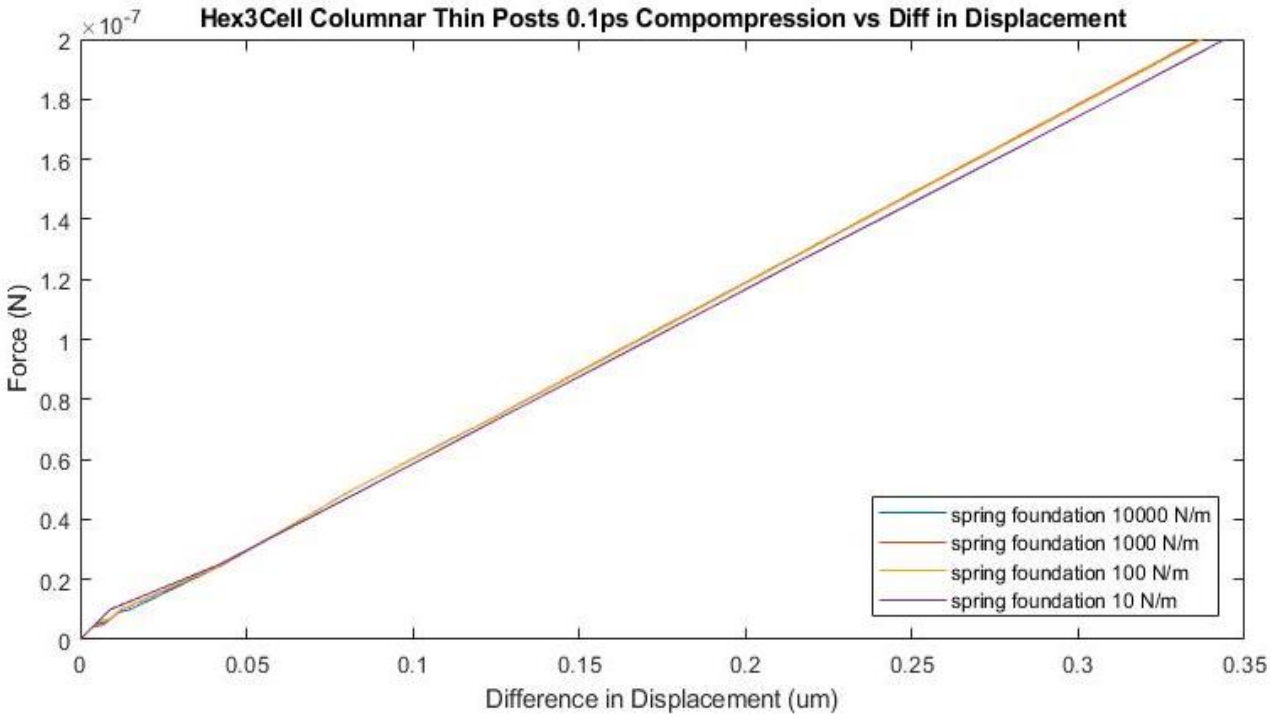
Hex3Cell Columnar Thin Posts 0.1ps Compompression vs Diff in Displacement
×10^-7
Force (N)
Difference in Displacement (um)
spring foundation 10000 N/m
spring foundation 1000 N/m
spring foundation 100 N/m
spring foundation 10 N/m

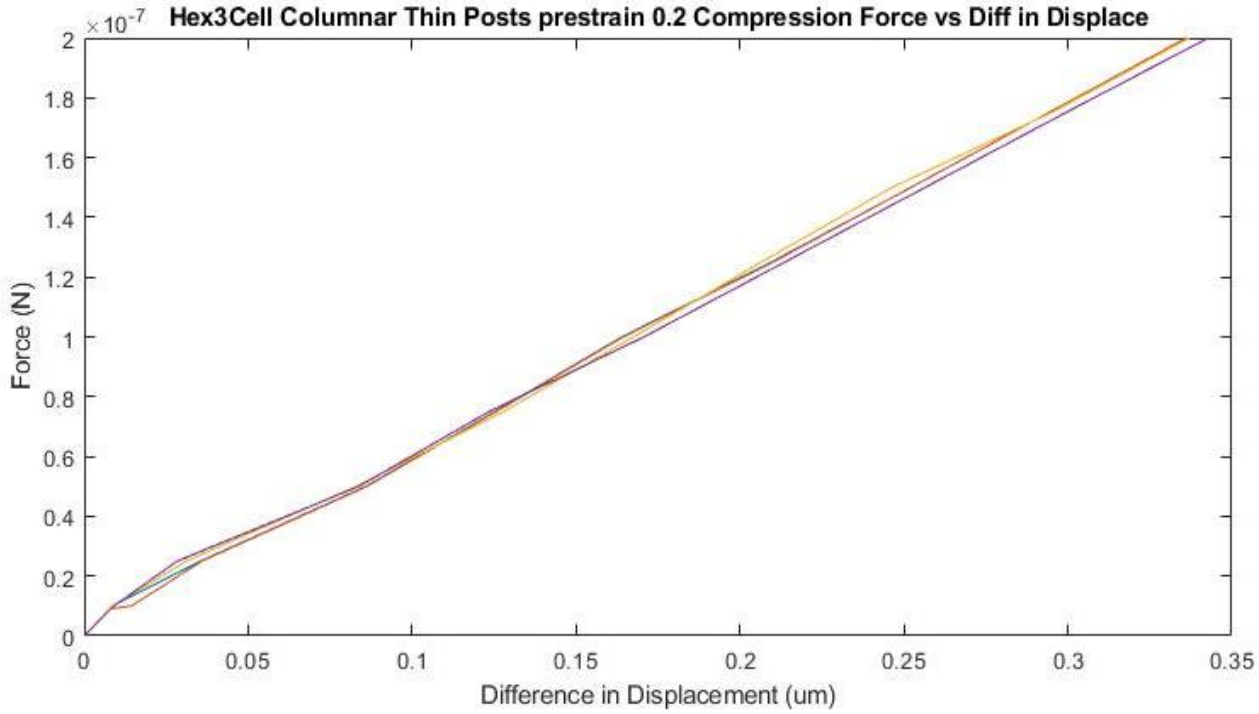
Hex3Cell Columnar Thin Posts prestrain 0.2 Compression Force vs Diff in Displace
×10^-7
Force (N)
Difference in Displacement (um)

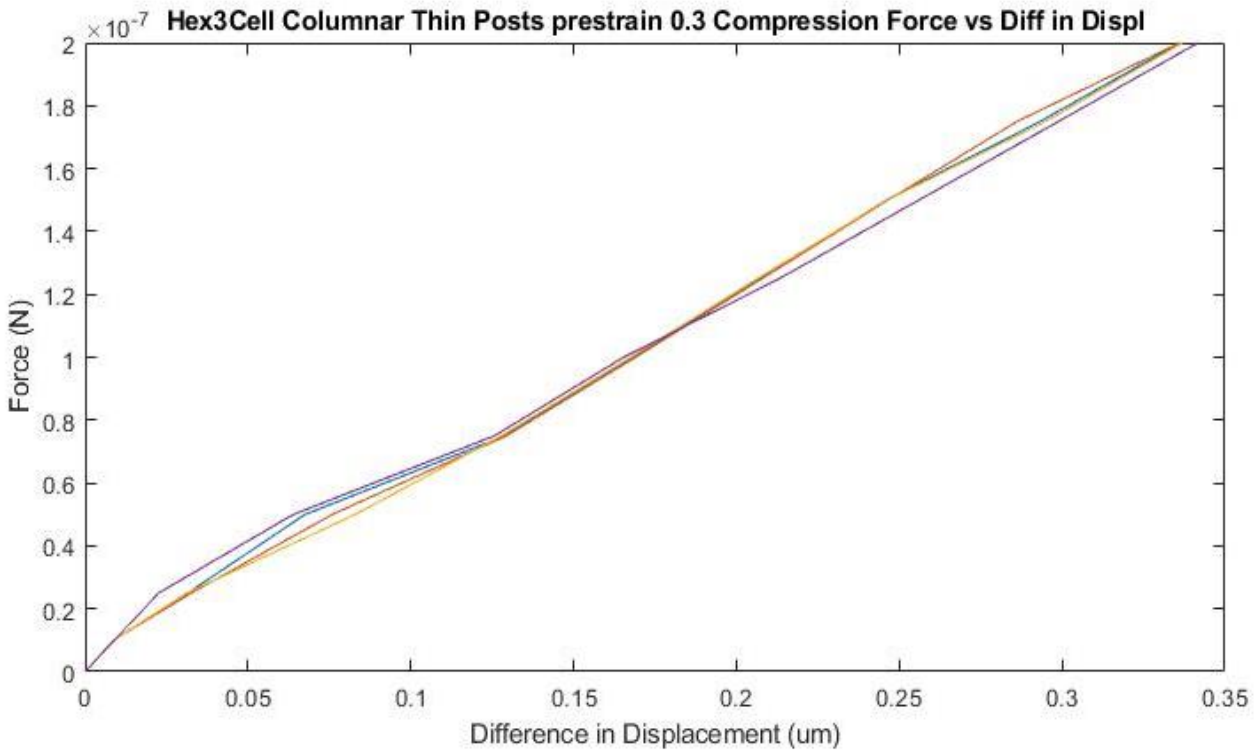

Tension graphs are all linear and very similar to each other as seen by the previous tension graphs

Columnar wide posts

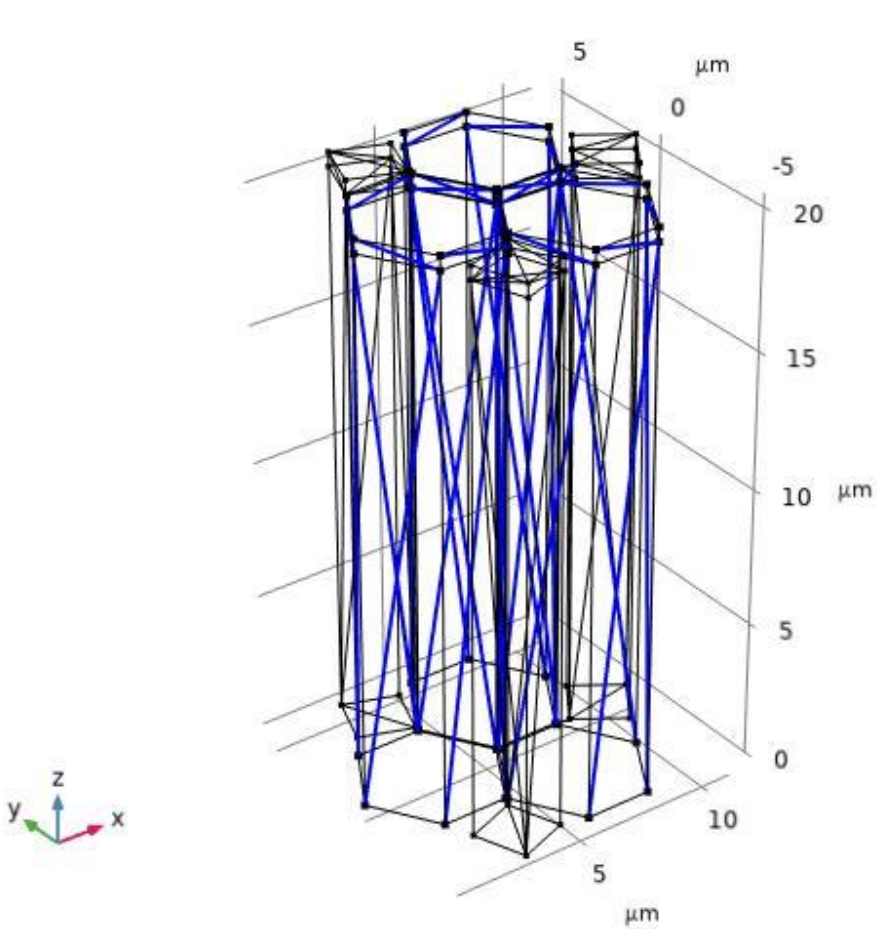

Image of the Hex3Cell columnar model with wide posts.

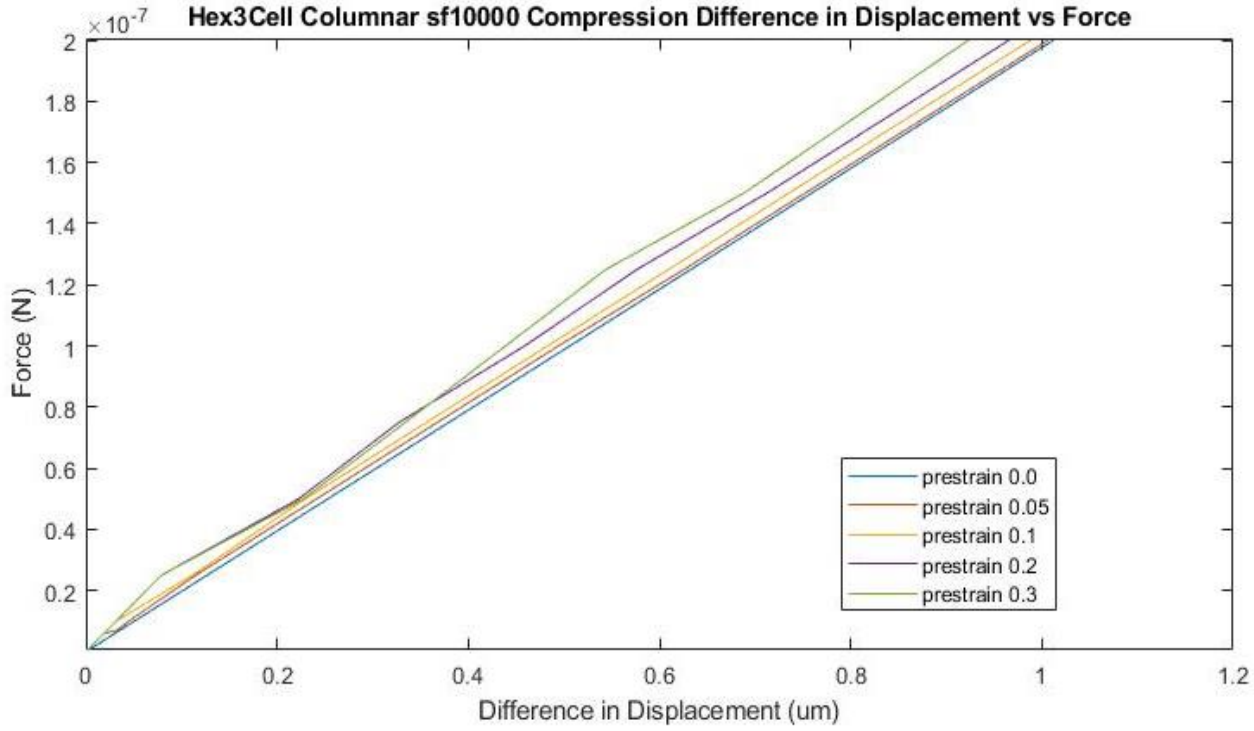
Hex3Cell Columnar sf10000 Compression Difference in Displacement vs Force
×10^-7
Force (N)
Difference in Displacement (um)
prestrain 0.0
prestrain 0.05
prestrain 0.1
prestrain 0.2
prestrain 0.3

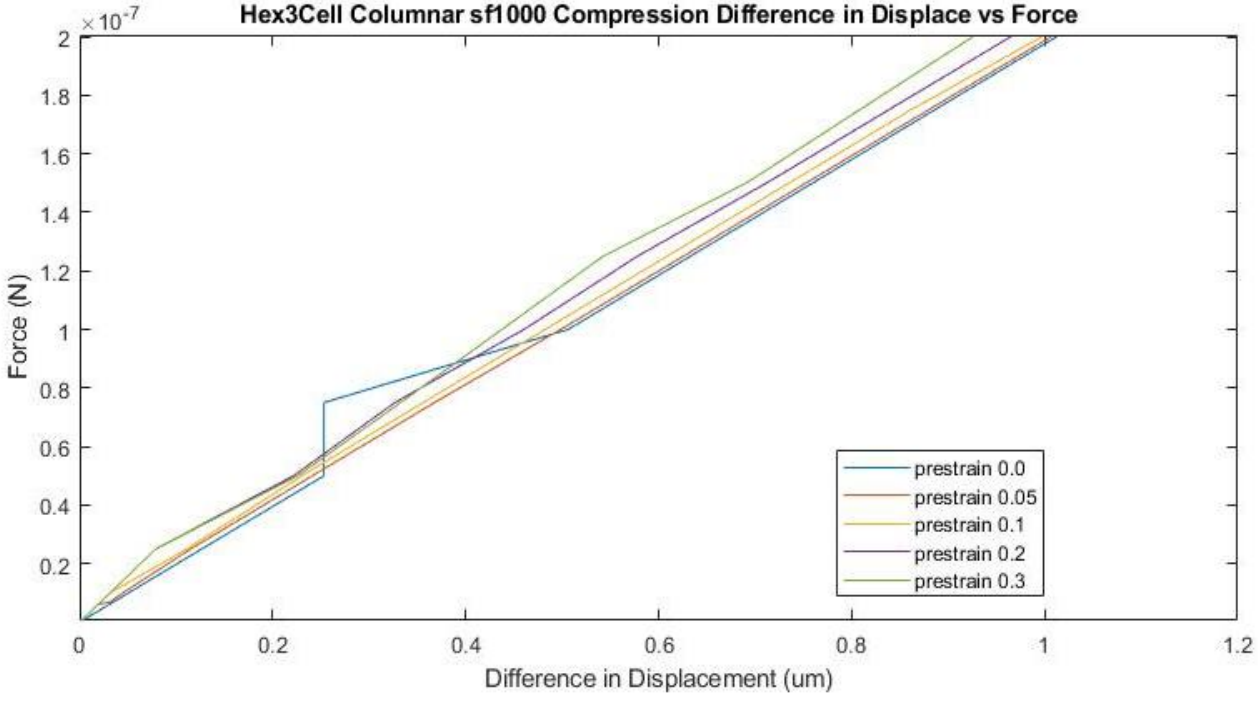
Hex3Cell Columnar sf1000 Compression Difference in Displace vs Force
×10^-7
Force (N)
Difference in Displacement (um)
prestrain 0.0
prestrain 0.05
prestrain 0.1
prestrain 0.2
prestrain 0.3

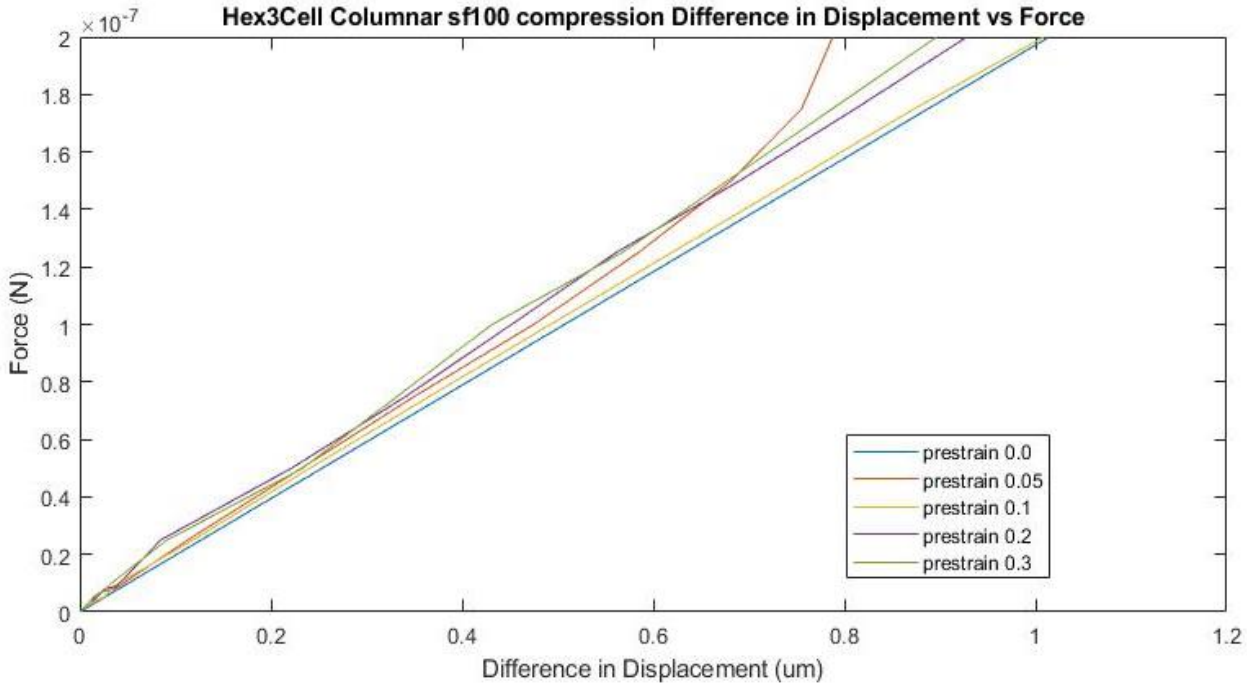
Hex3Cell Columnar sf100 compression Difference in Displacement vs Force
×10^-7
Force (N)
Difference in Displacement (um)
prestrain 0.0
prestrain 0.05
prestrain 0.1
prestrain 0.2
prestrain 0.3

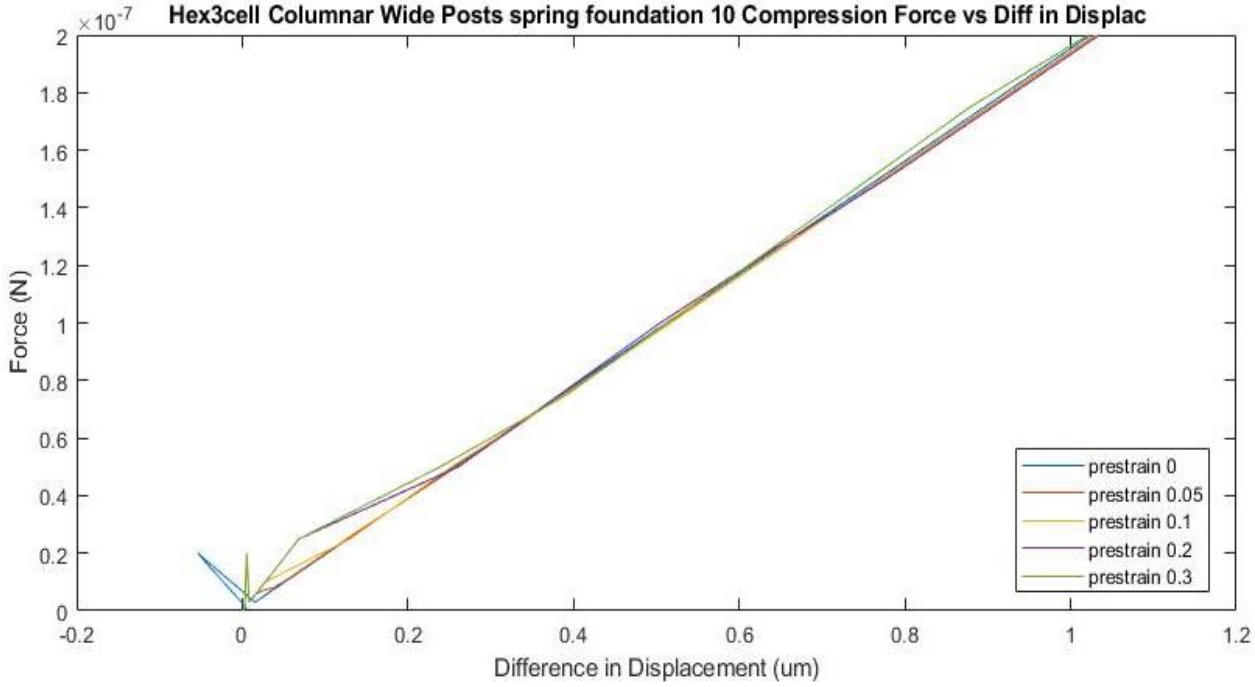
Hex3cell Columnar Wide Posts spring foundation 10 Compression Force vs Diff in Displac
×10^-7
Force (N)
Difference in Displacement (um)
prestrain 0
prestrain 0.05
prestrain 0.1
prestrain 0.2
prestrain 0.3

Varying spring foundation

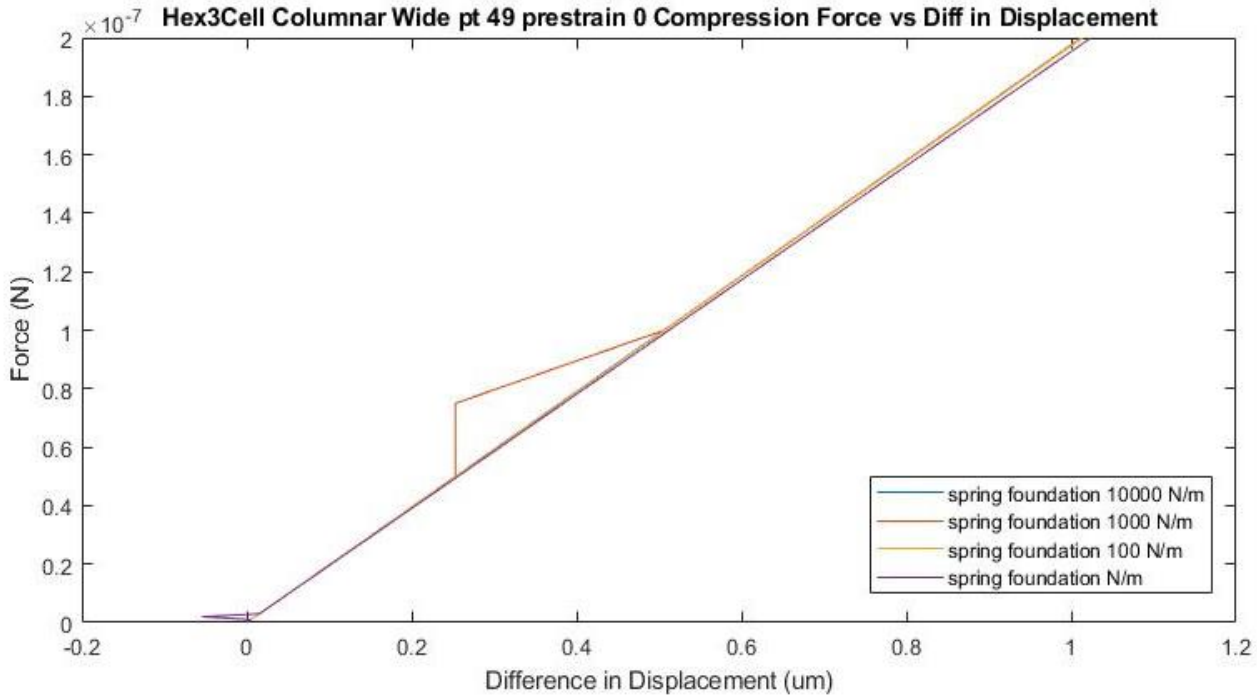

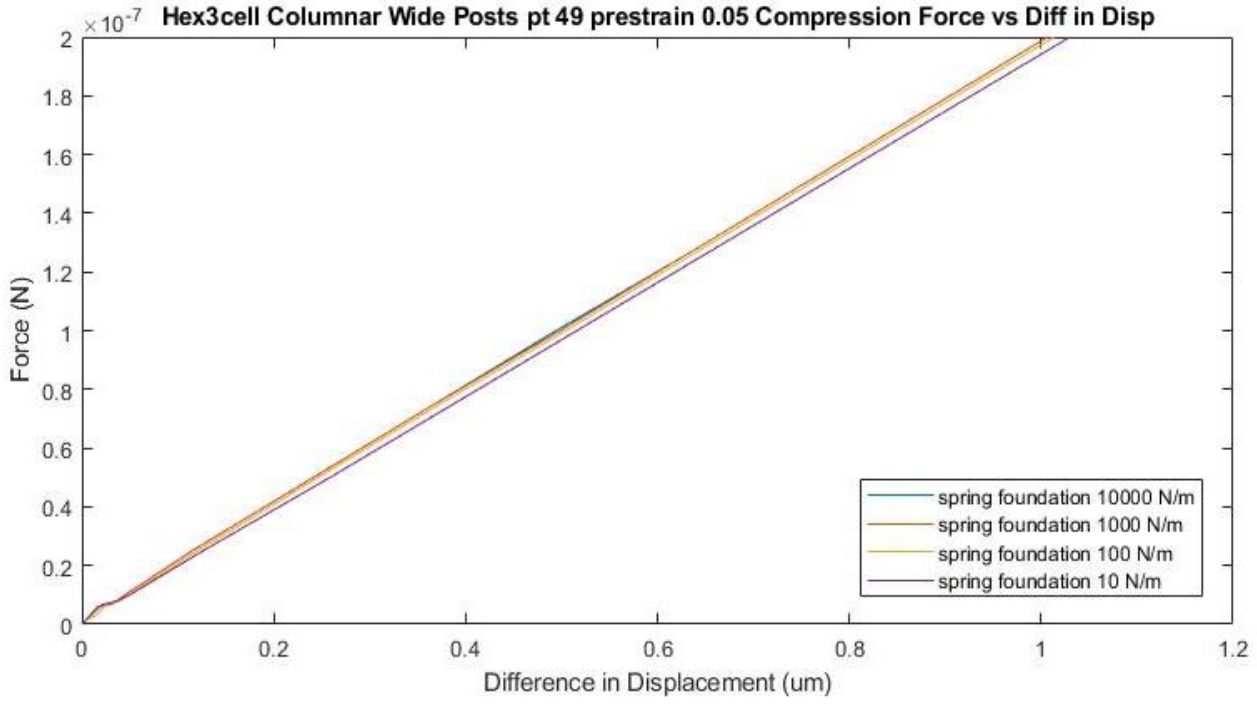

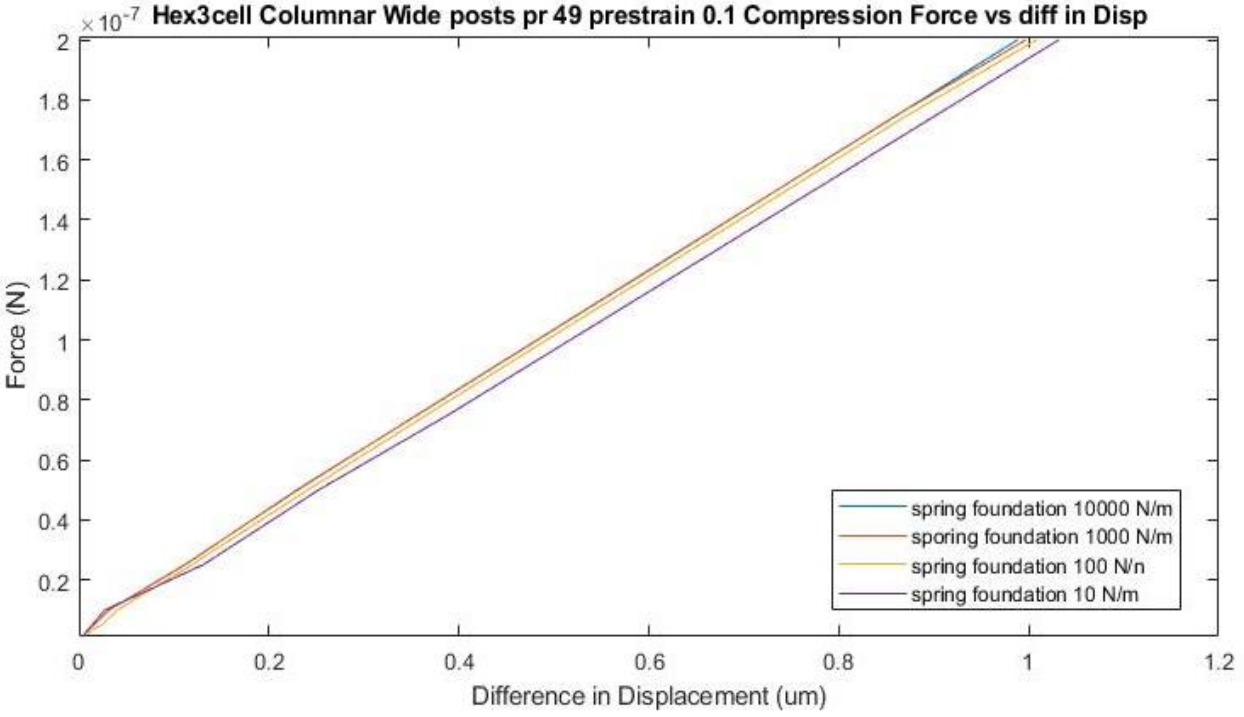
Hex3cell Columnar Wide posts pr 49 prestrain 0.1 Compression Force vs diff in Disp
×10^-7
Force (N)
Difference in Displacement (um)
spring foundation 10000 N/m
sporing foundation 1000 N/m
spring foundation 100 N/n
spring foundation 10 N/m

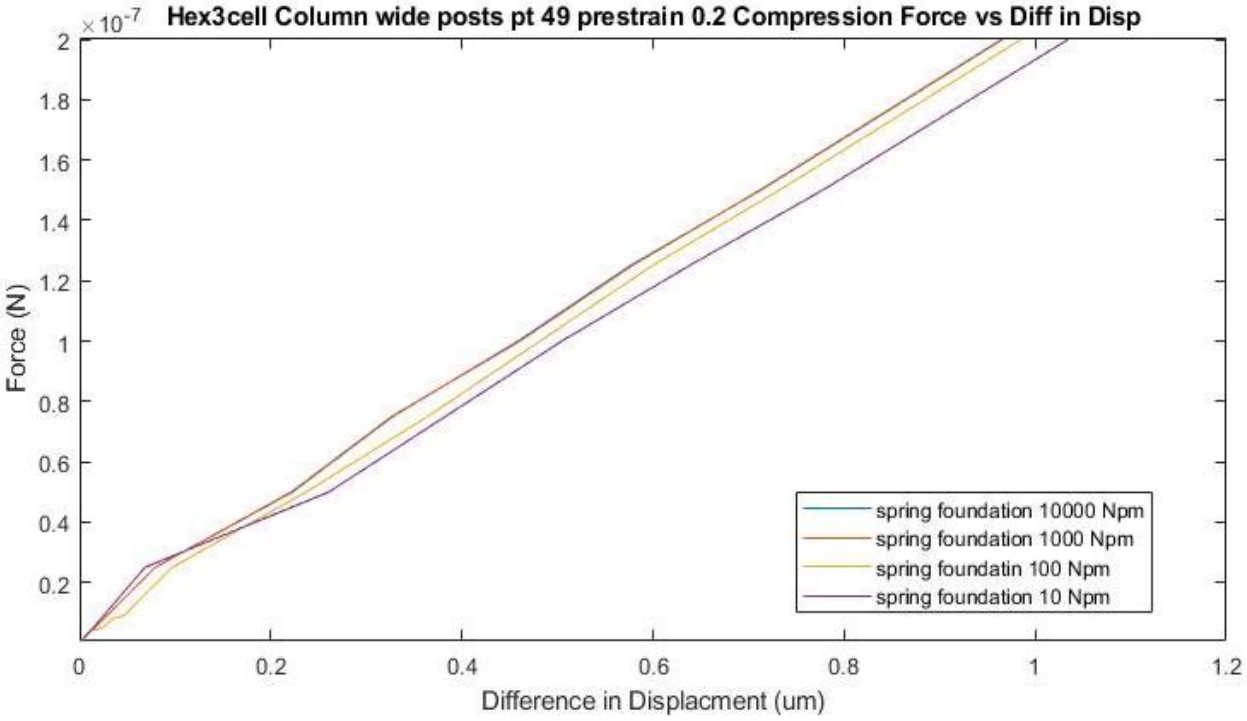
Hex3cell Column wide posts pt 49 prestrain 0.2 Compression Force vs Diff in Disp
×10^-7
Force (N)
Difference in Displacment (um)
spring foundation 10000 Npm
spring foundation 1000 Npm
spring foundatin 100 Npm
spring foundation 10 Npm

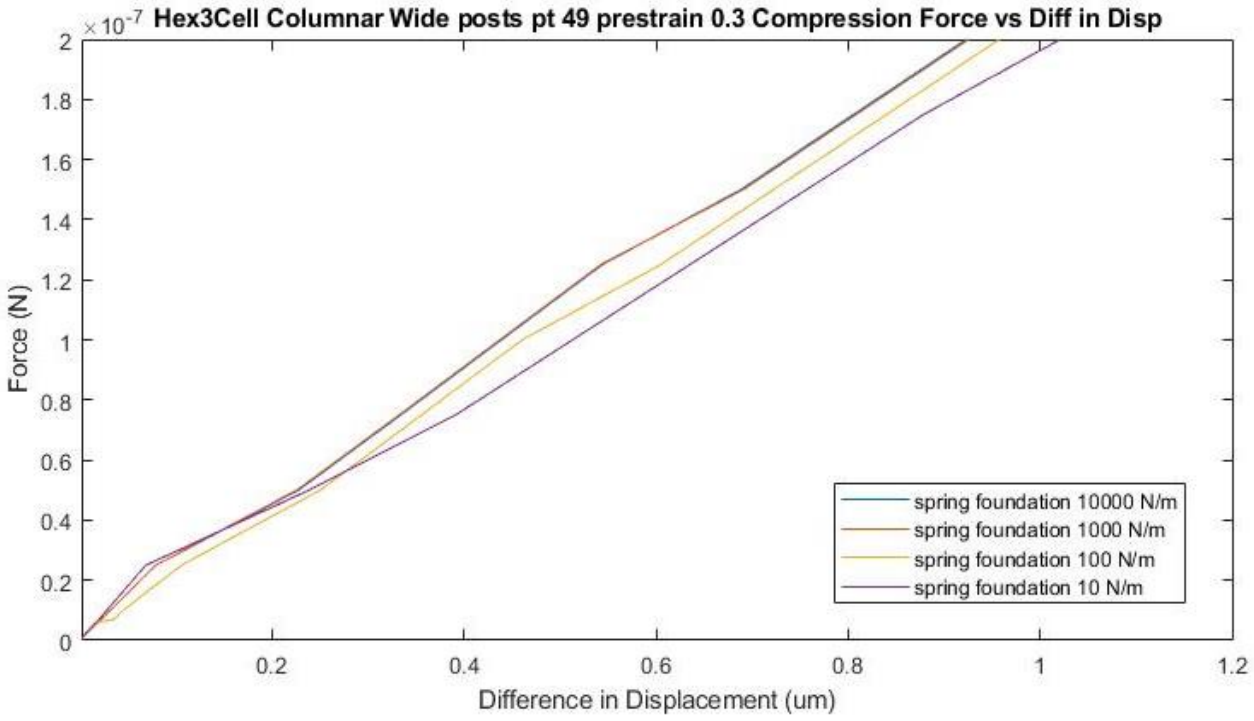

Tension graphs

Are similar to the Columnar Wide posts average graphs

Columnar wide posts Average force between three middle points

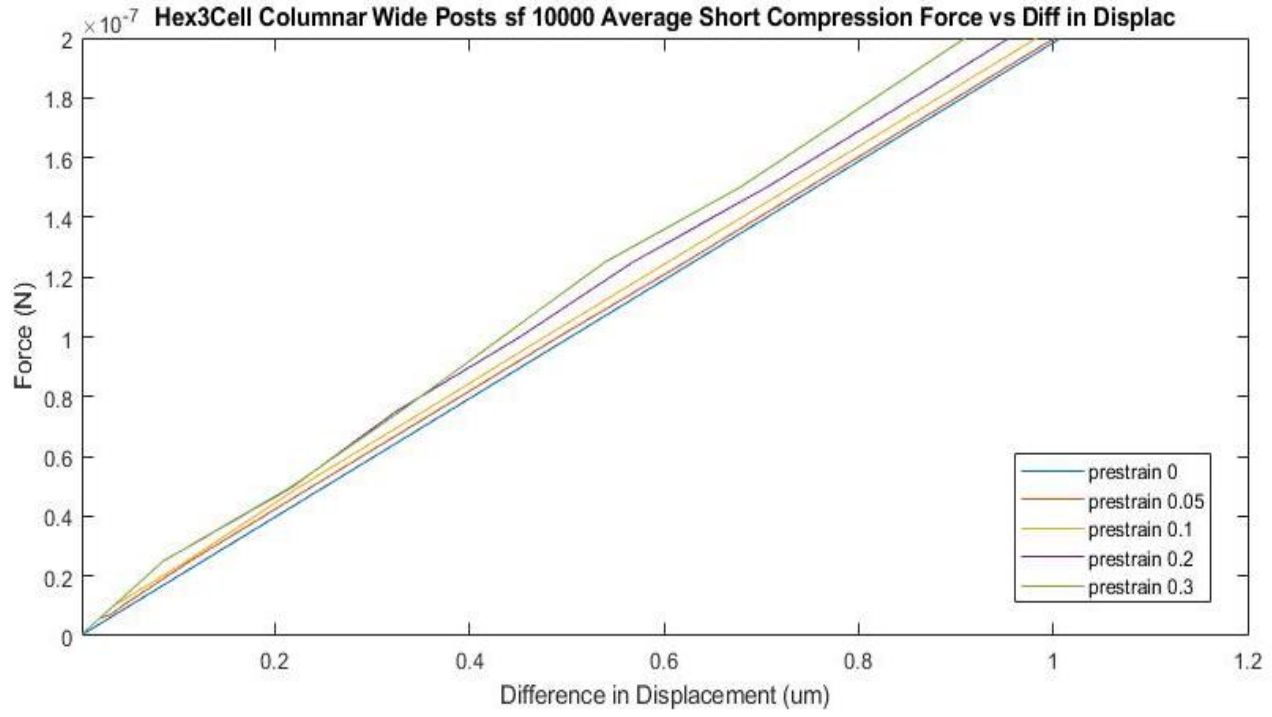

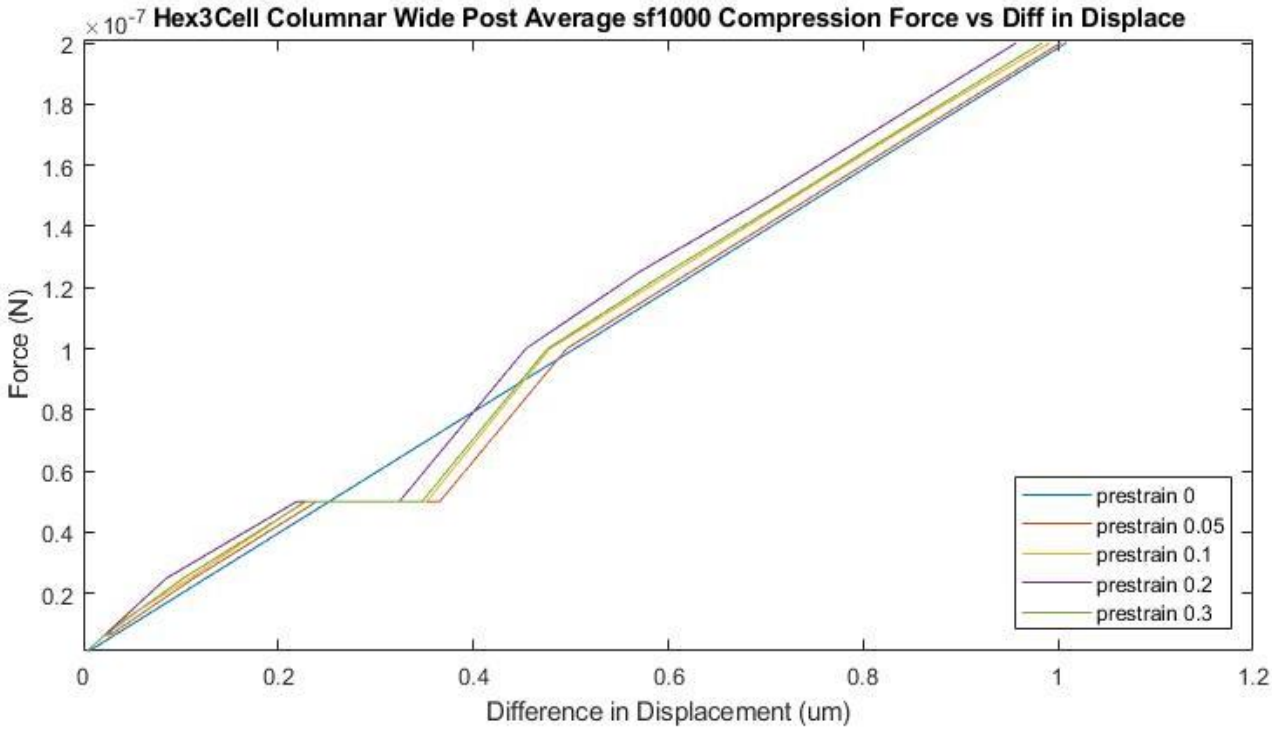

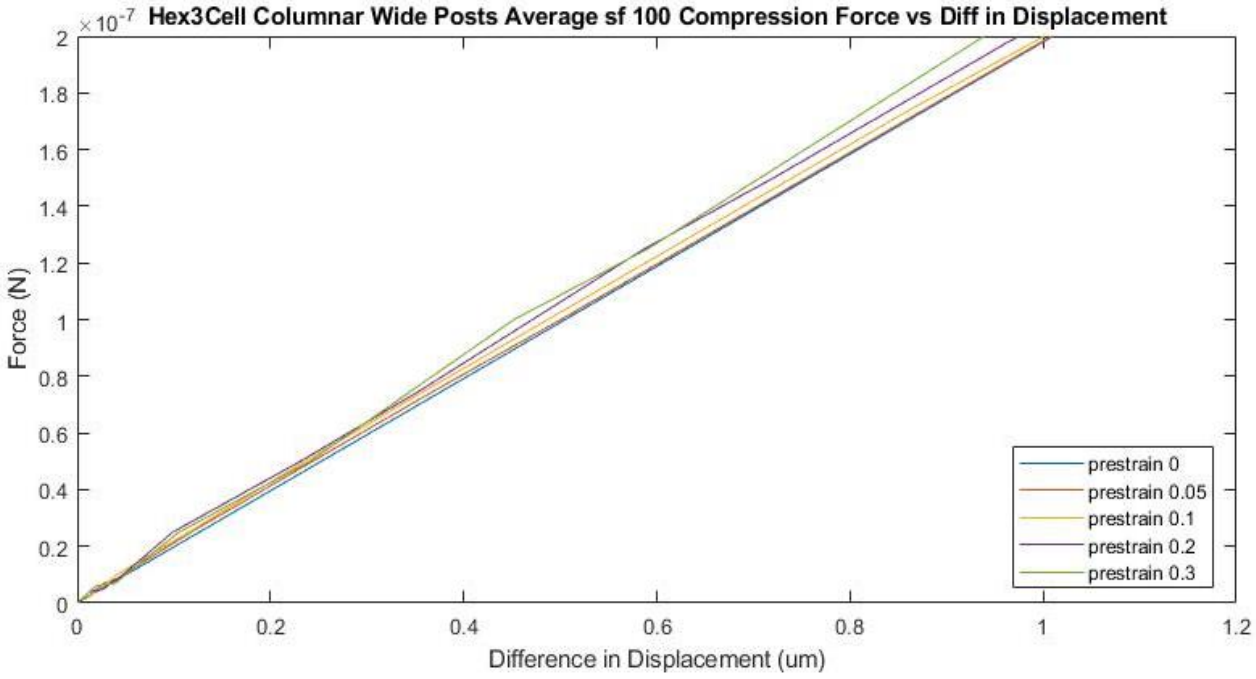
Hex3Cell Columnar Wide Posts Average sf 100 Compression Force vs Diff in Displacement
×10^-7
Force (N)
Difference in Displacement (um)
prestrain 0
prestrain 0.05
prestrain 0.1
prestrain 0.2
prestrain 0.3

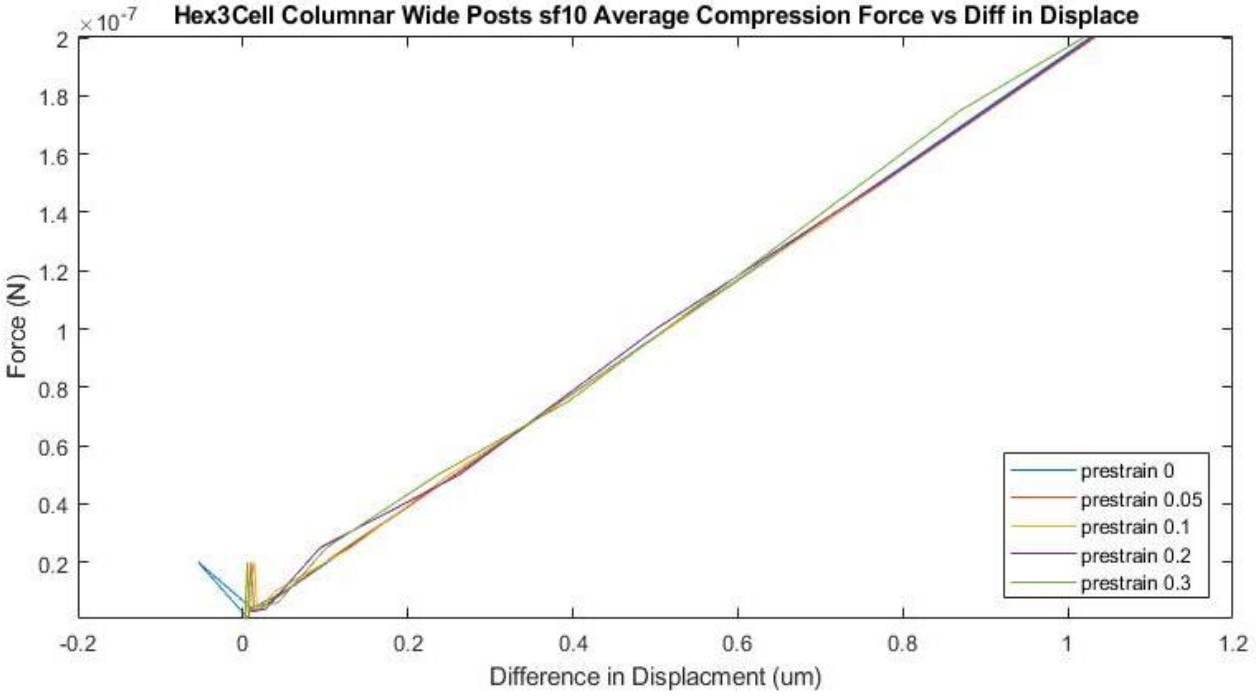
Hex3Cell Columnar Wide Posts sf10 Average Compression Force vs Diff in Displace
×10^-7
Force (N)
Difference in Displacment (um)
prestrain 0
prestrain 0.05
prestrain 0.1
prestrain 0.2
prestrain 0.3

Varying Spring Foundation

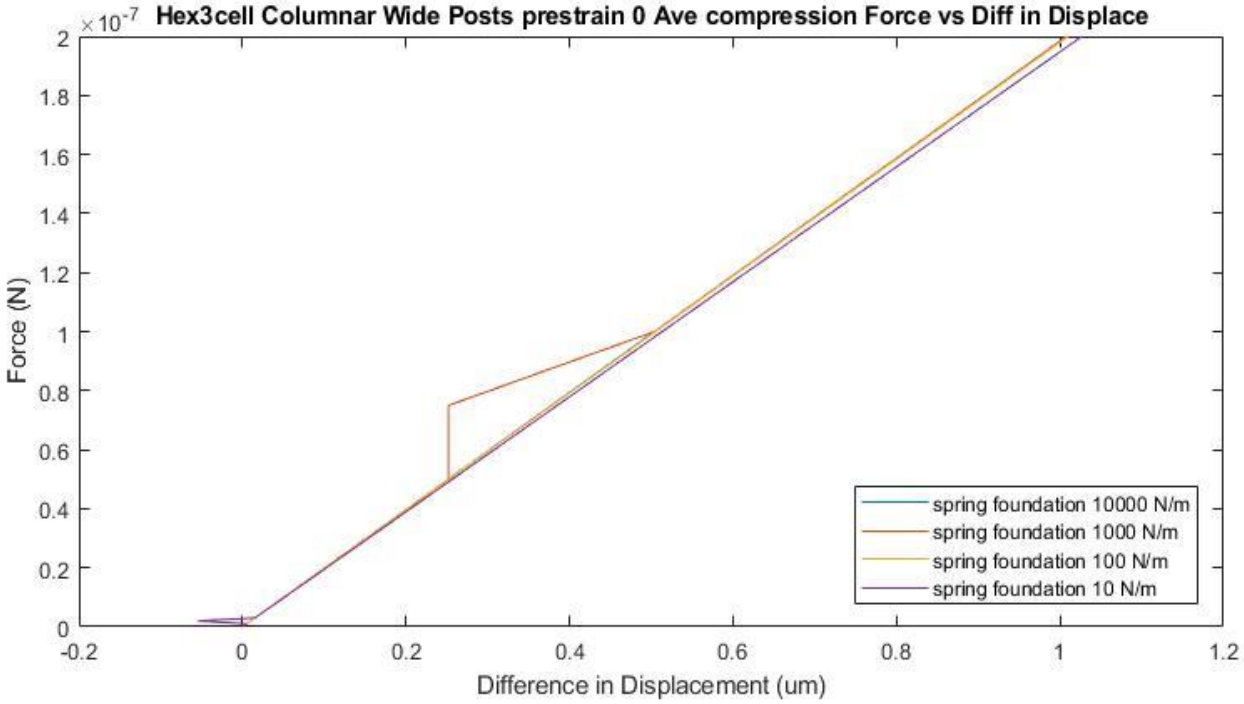

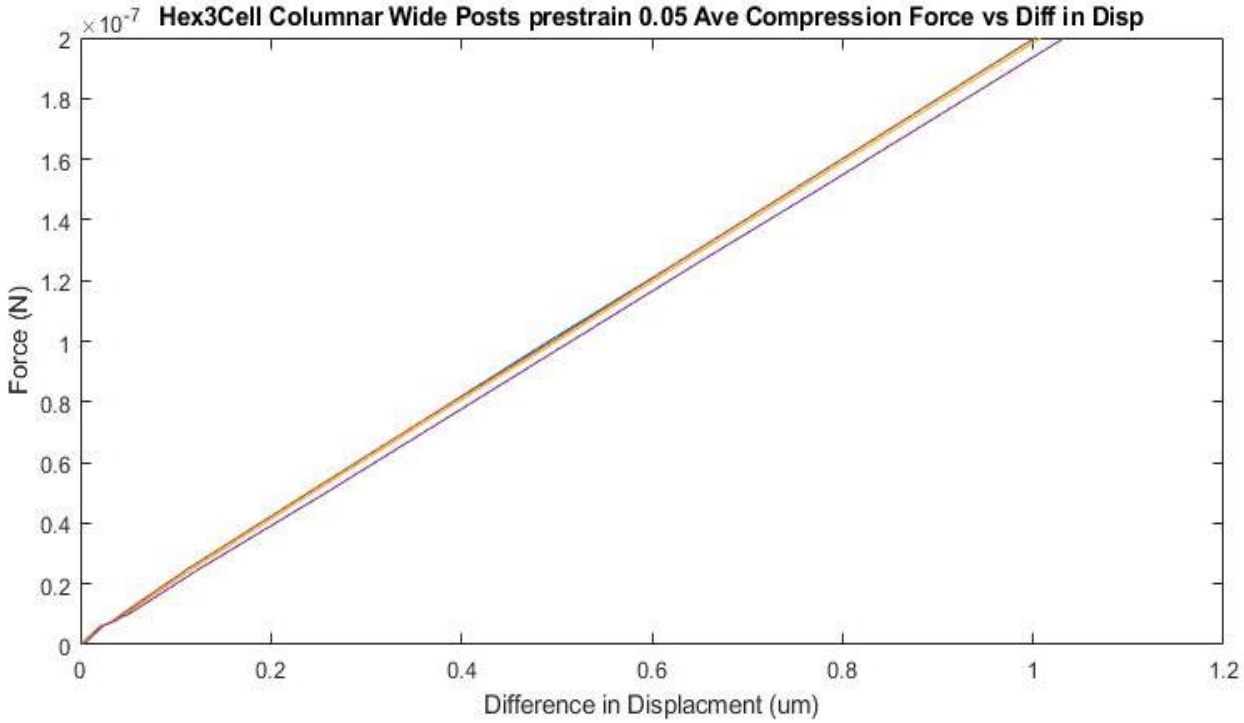

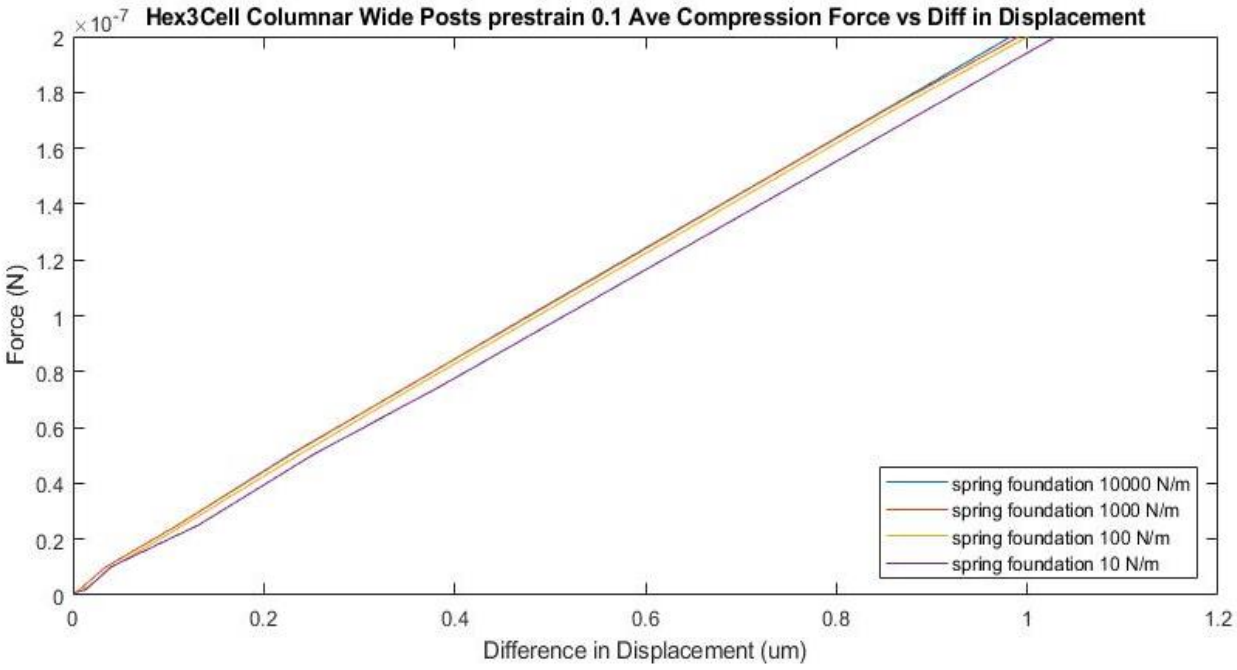
Hex3Cell Columnar Wide Posts prestrain 0.1 Ave Compression Force vs Diff in Displacement
×10^-7
Force (N)
Difference in Displacement (um)
spring foundation 10000 N/m
spring foundation 1000 N/m
spring foundation 100 N/m
spring foundation 10 N/m

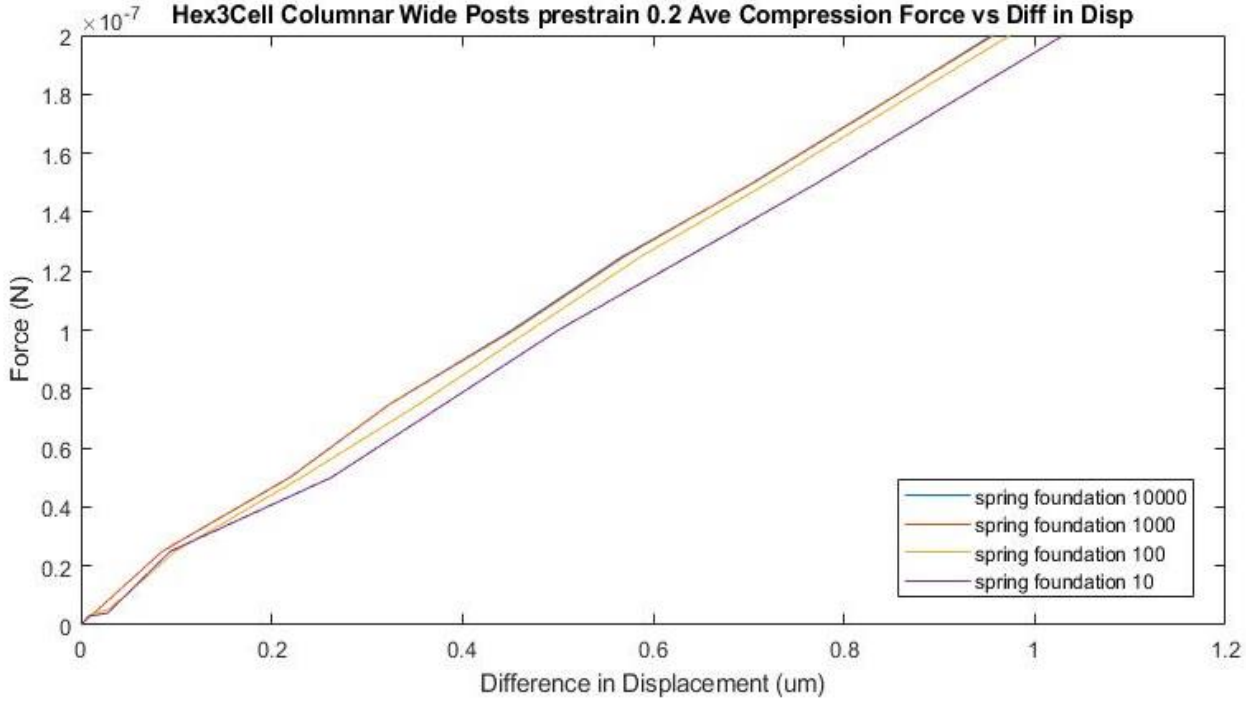
Hex3Cell Columnar Wide Posts prestrain 0.2 Ave Compression Force vs Diff in Disp
×10^-7
Force (N)
Difference in Displacement (um)
spring foundation 10000
spring foundation 1000
spring foundation 100
spring foundation 10

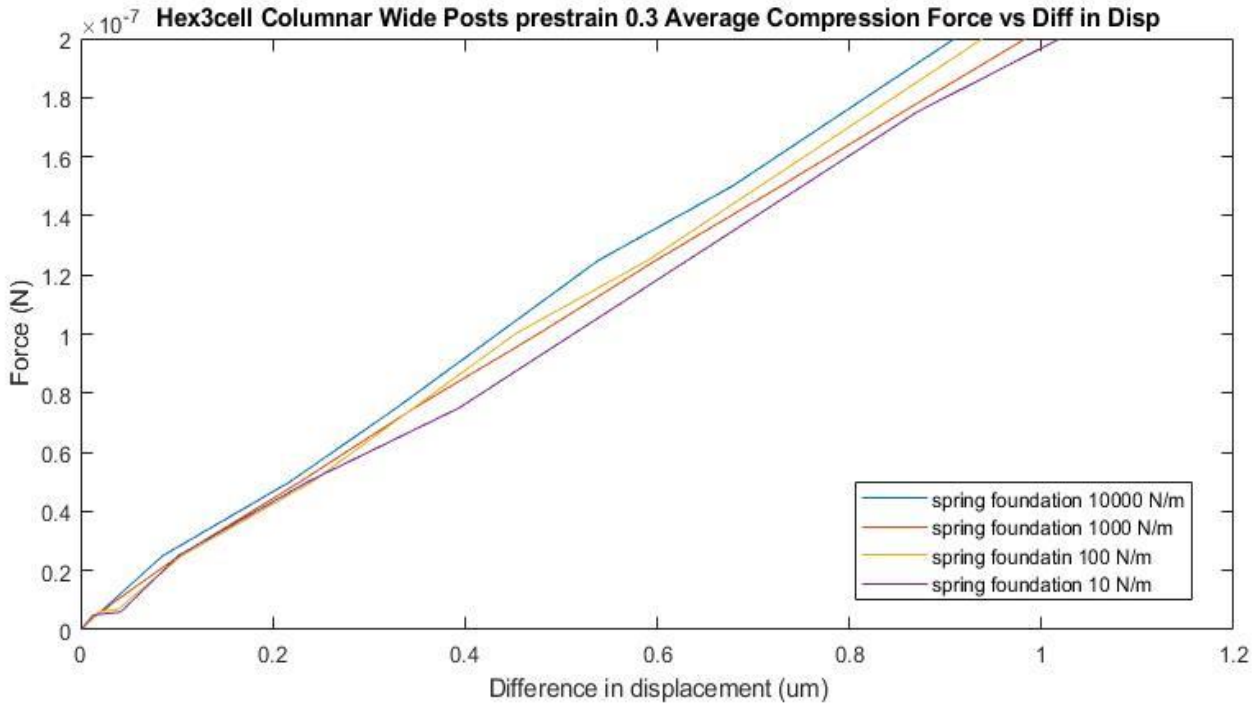

Columnar Wide Posts Average over three points Tension Graphs

Tension Wide Post Columnar Varying prestrain

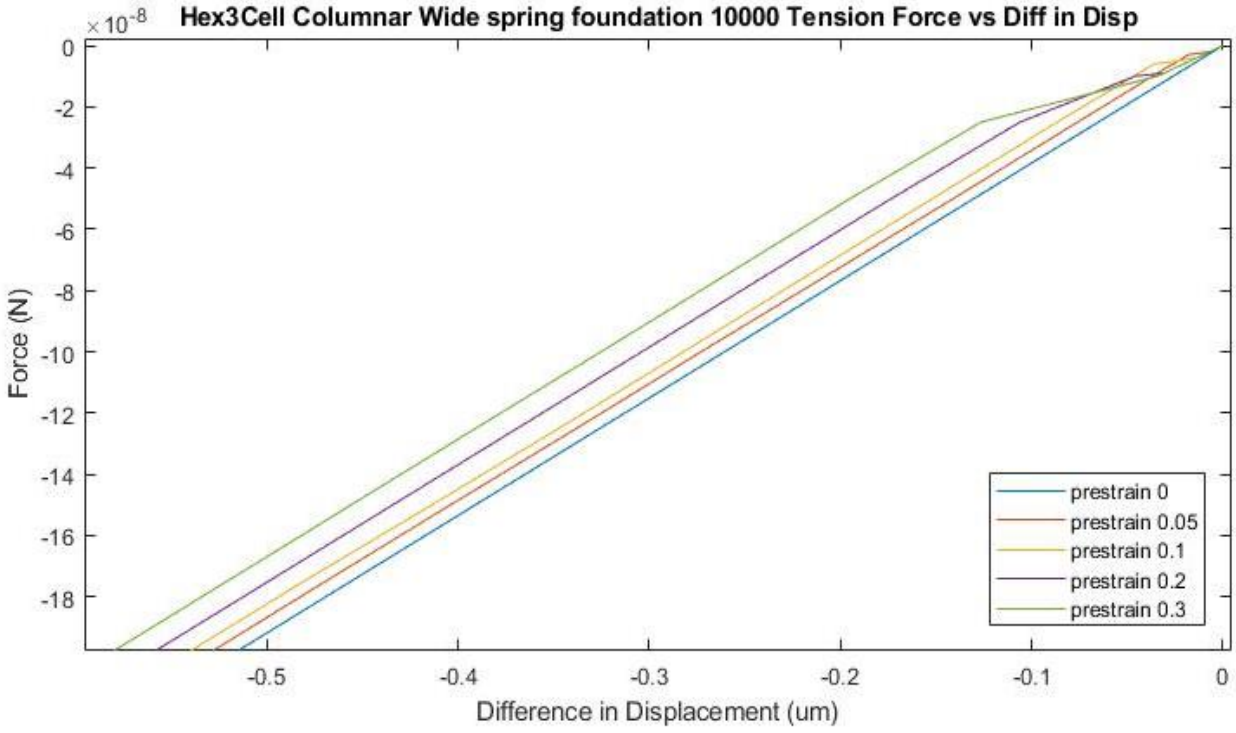

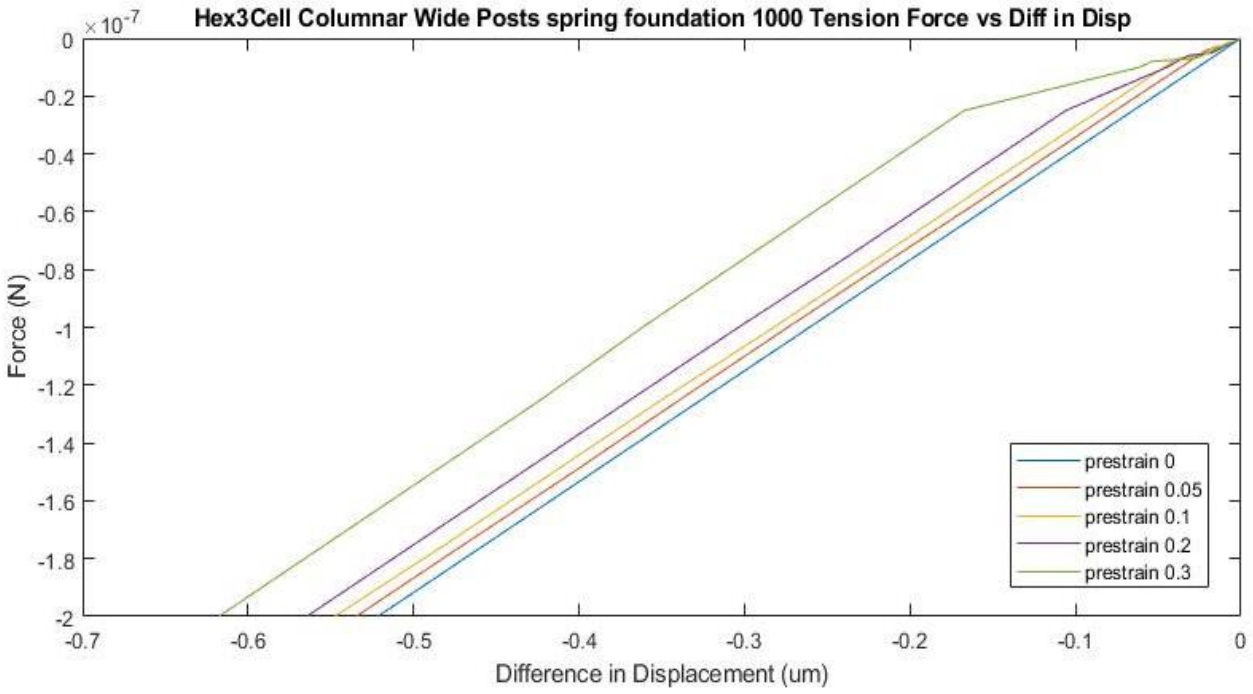
Hex3Cell Columnar Wide Posts spring foundation 1000 Tension Force vs Diff in Disp
×10^-7
0
-0.2
-0.4
-0.6
-0.8
-1
-1.2
-1.4
-1.6
-1.8
-2
Force (N)
-0.7
-0.6
-0.5
-0.4
-0.3
-0.2
-0.1
0
Difference in Displacement (um)
prestrain 0
prestrain 0.05
prestrain 0.1
prestrain 0.2
prestrain 0.3

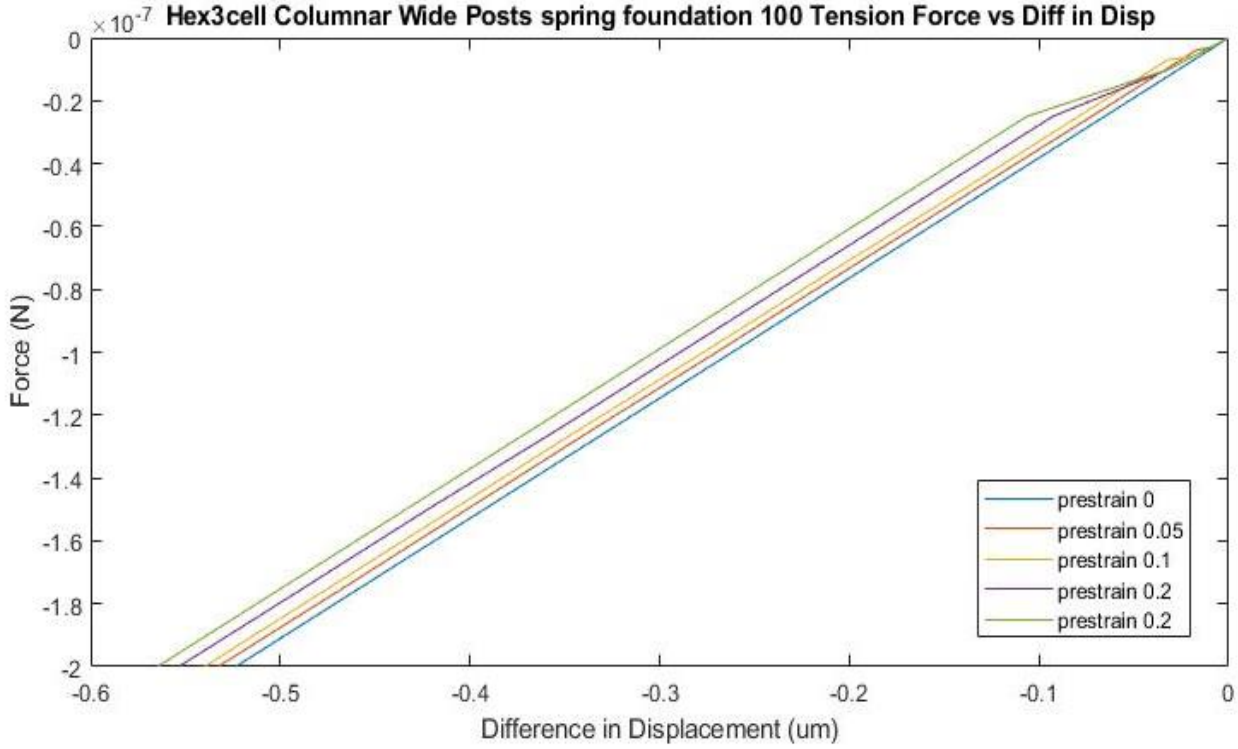
Hex3cell Columnar Wide Posts spring foundation 100 Tension Force vs Diff in Disp
×10^-7
0
-0.2
-0.4
-0.6
-0.8
-1
-1.2
-1.4
-1.6
-1.8
-2
Force (N)
-0.6
-0.5
-0.4
-0.3
-0.2
-0.1
0
Difference in Displacement (um)
prestrain 0
prestrain 0.05
prestrain 0.1
prestrain 0.2
prestrain 0.2

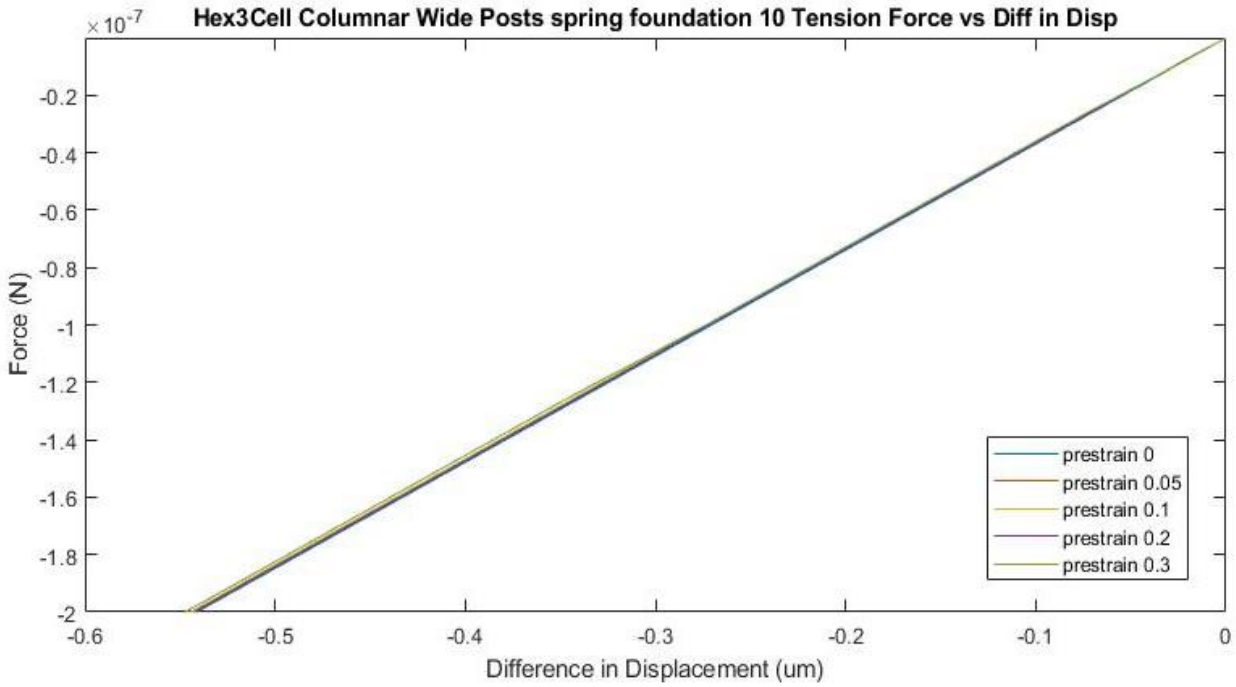

Varying Spring Foundation

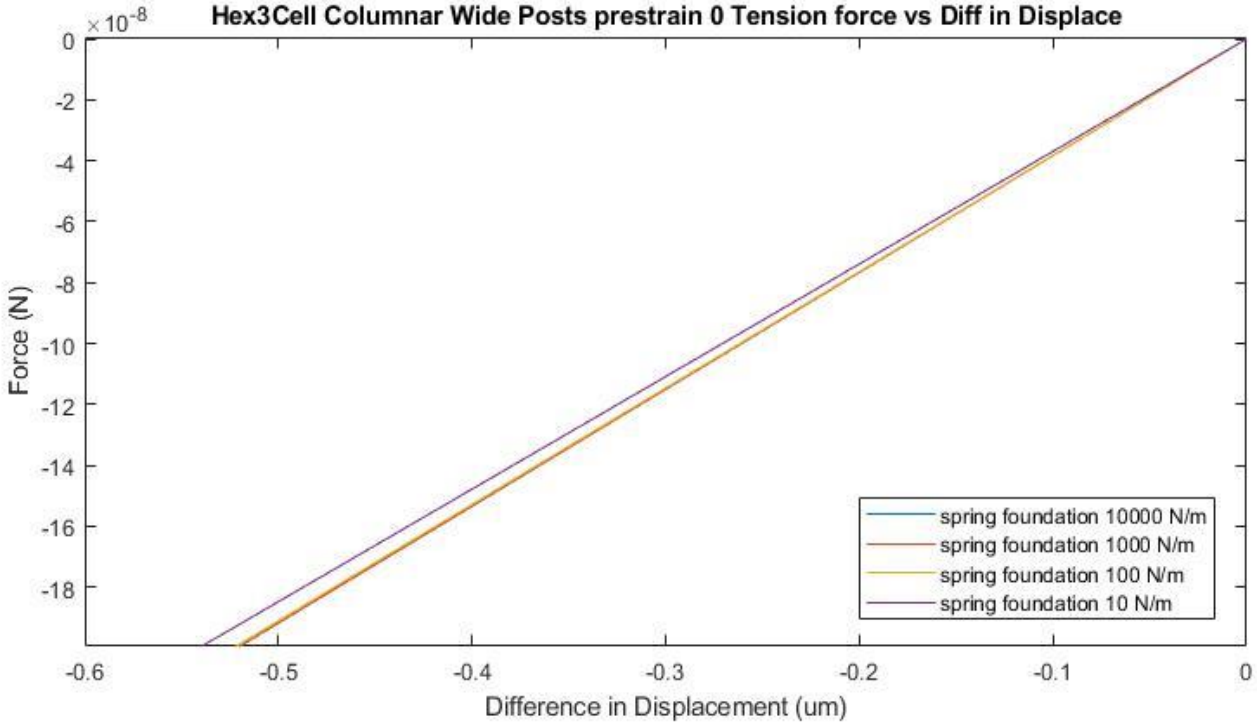

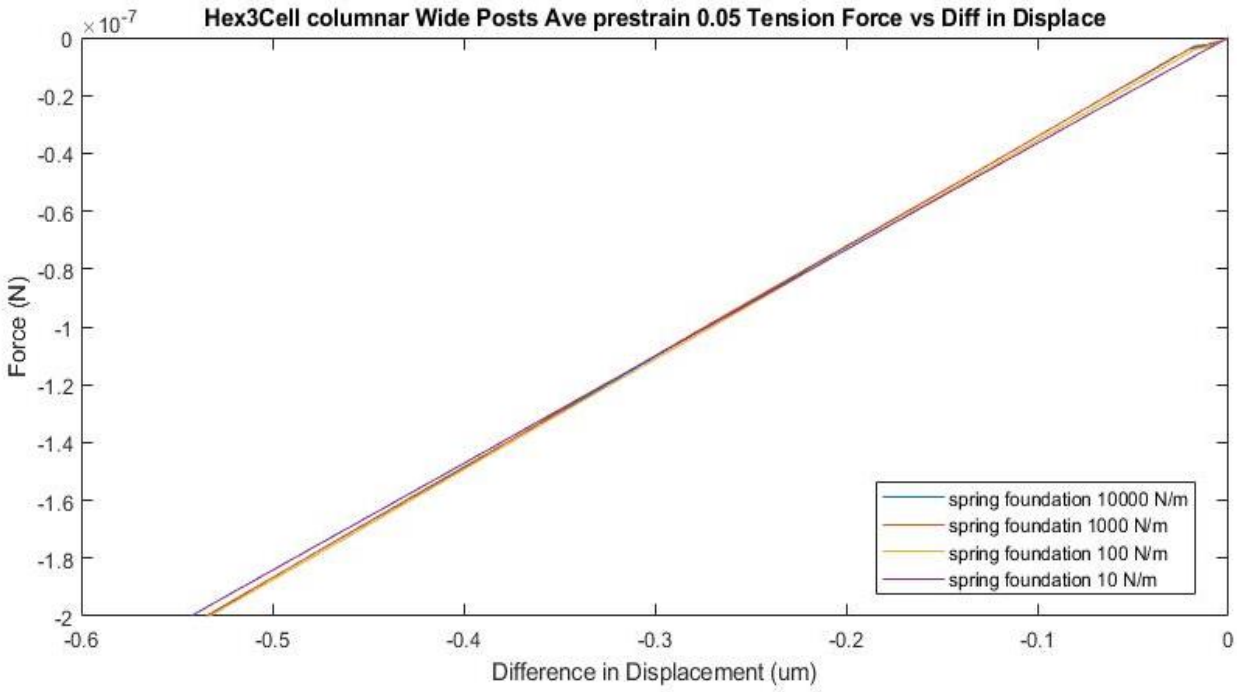
Hex3Cell columnar Wide Posts Ave prestrain 0.05 Tension Force vs Diff in Displace
×10^-7
0
-0.2
-0.4
-0.6
-0.8
-1
-1.2
-1.4
-1.6
-1.8
-2
Force (N)
-0.6
-0.5
-0.4
-0.3
-0.2
-0.1
0
Difference in Displacement (um)
spring foundation 10000 N/m
spring foundatin 1000 N/m
spring foundation 100 N/m
spring foundation 10 N/m

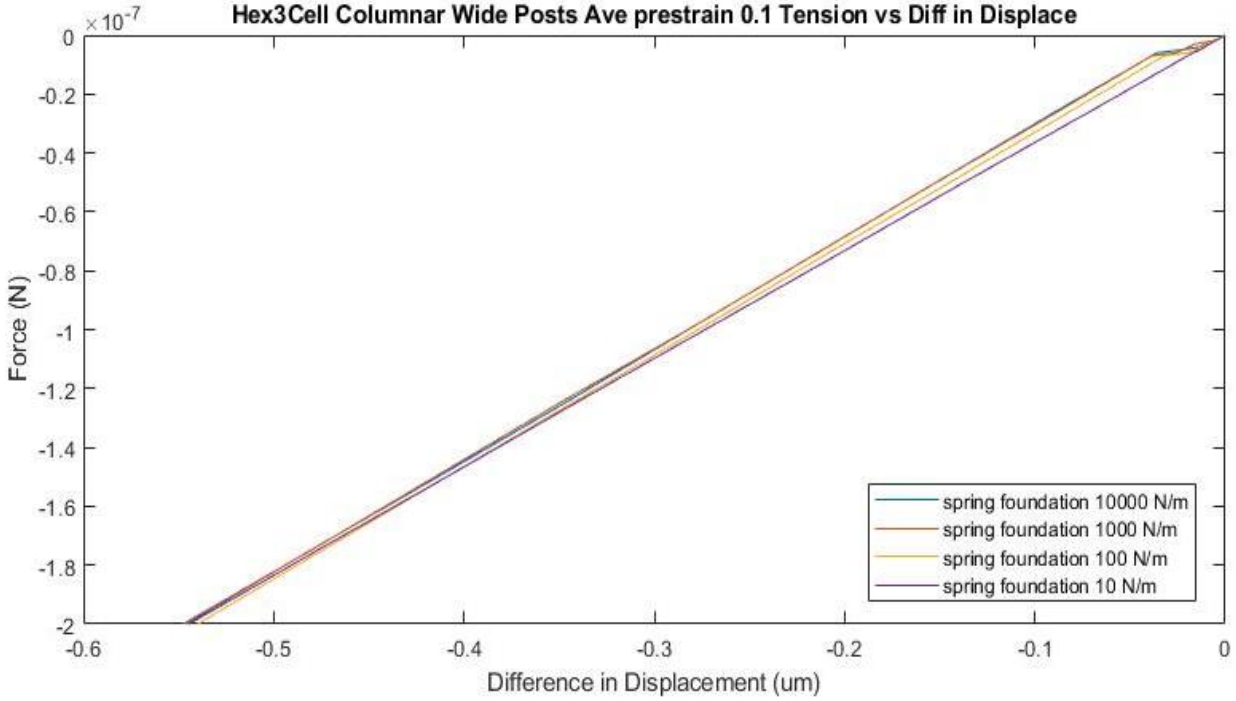
Hex3Cell Columnar Wide Posts Ave prestrain 0.1 Tension vs Diff in Displace
×10^-7
0
-0.2
-0.4
-0.6
-0.8
-1
-1.2
-1.4
-1.6
-1.8
-2
Force (N)
-0.6
-0.5
-0.4
-0.3
-0.2
-0.1
0
Difference in Displacement (um)
spring foundation 10000 N/m
spring foundation 1000 N/m
spring foundation 100 N/m
spring foundation 10 N/m

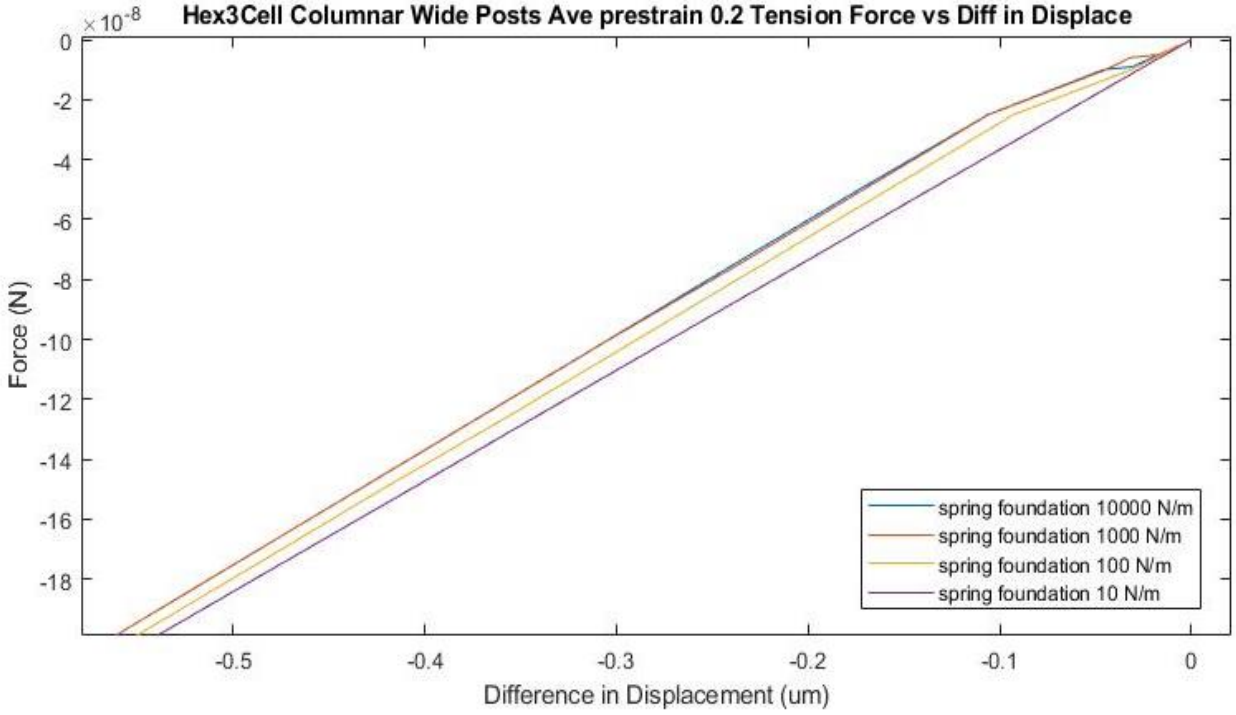
Hex3Cell Columnar Wide Posts Ave prestrain 0.2 Tension Force vs Diff in Displace
×10^-8
Force (N)
Difference in Displacement (um)
spring foundation 10000 N/m
spring foundation 1000 N/m
spring foundation 100 N/m
spring foundation 10 N/m

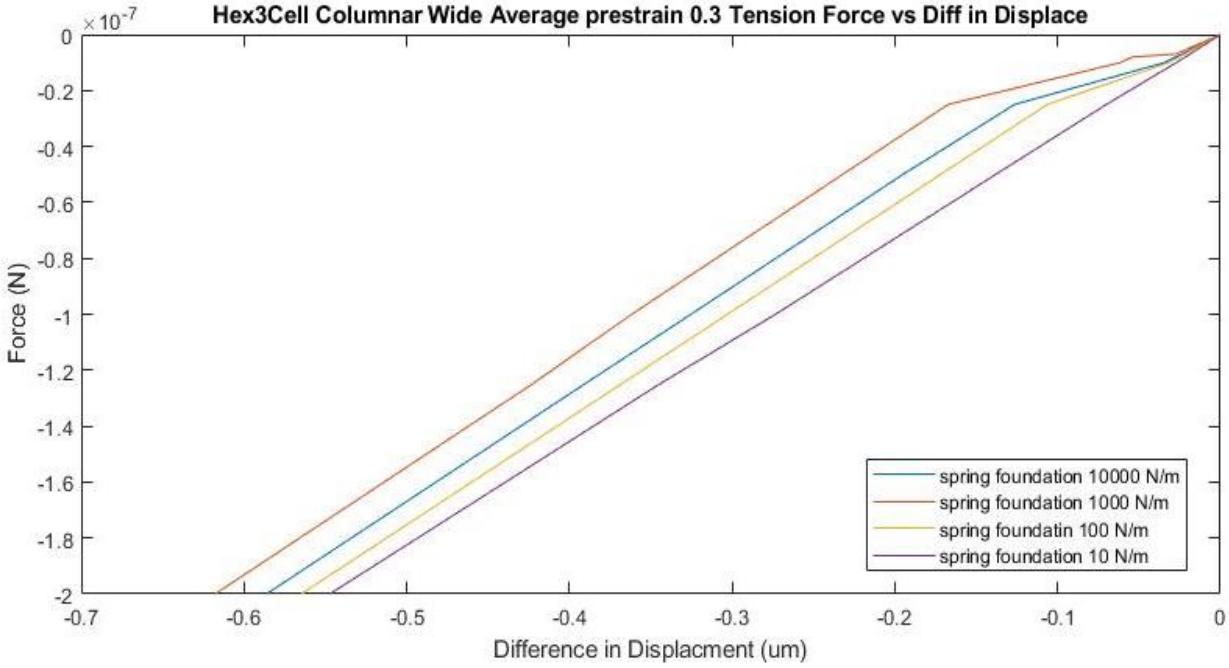
Hex3Cell Columnar Wide Average prestrain 0.3 Tension Force vs Diff in Displace
×10^-7
Force (N)
Difference in Displacment (um)
spring foundation 10000 N/m
spring foundation 1000 N/m
spring foundatin 100 N/m
spring foundation 10 N/m

Cuboidal or Medium Height Model with Top

The top is added strings across the hexagons

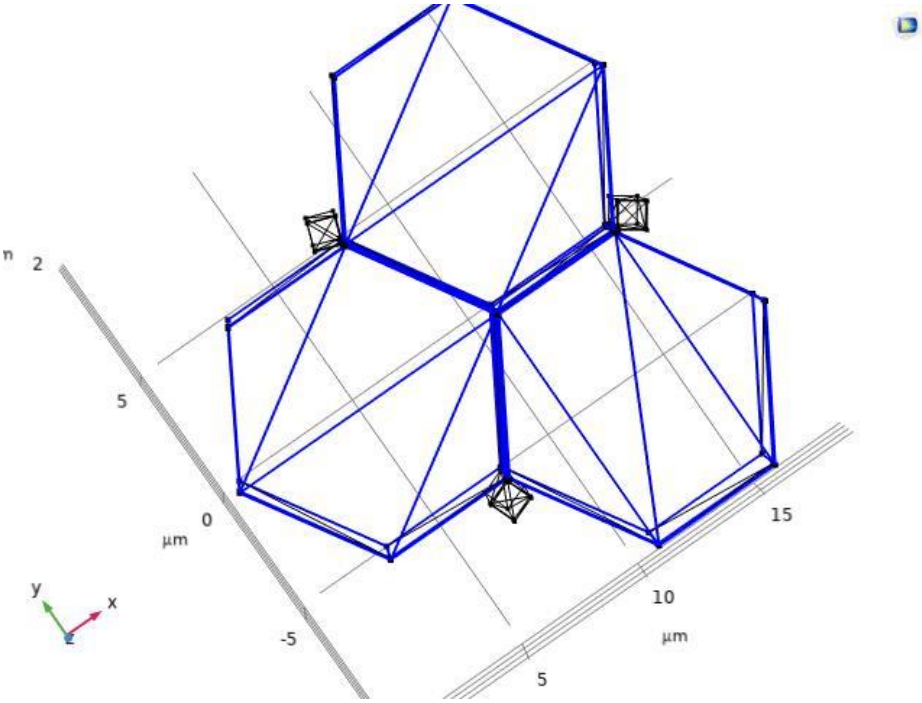

Top view of the Hexagon 3 Cell arrangement. The blue in the above image shows the strings or tension elements with the added strings across the hexagons.

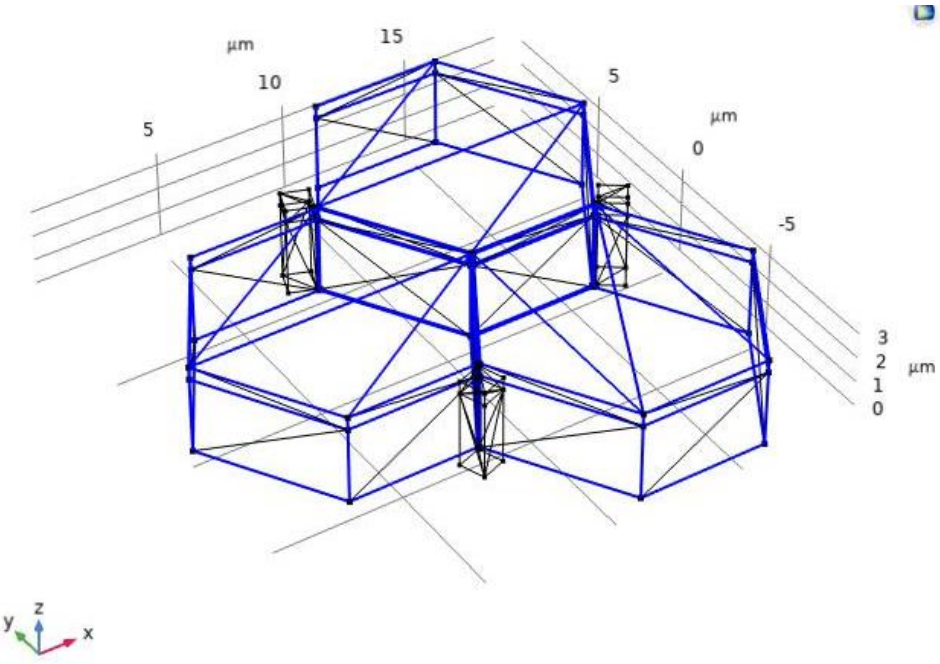

Side view of the cuboidal Medium Hexagon 3 Cell arrangement. The strings are shown in blue and the black lines are the rods or compression elements except for the posts.

Varying pre-strain

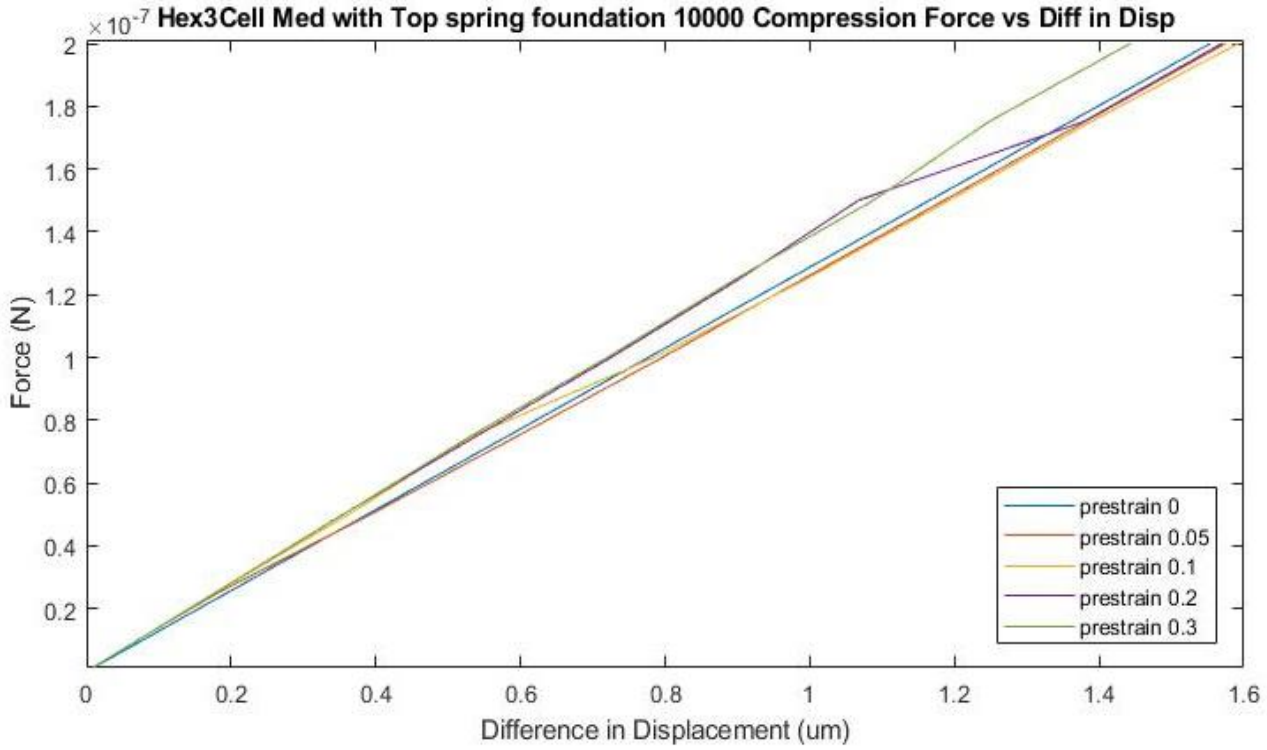

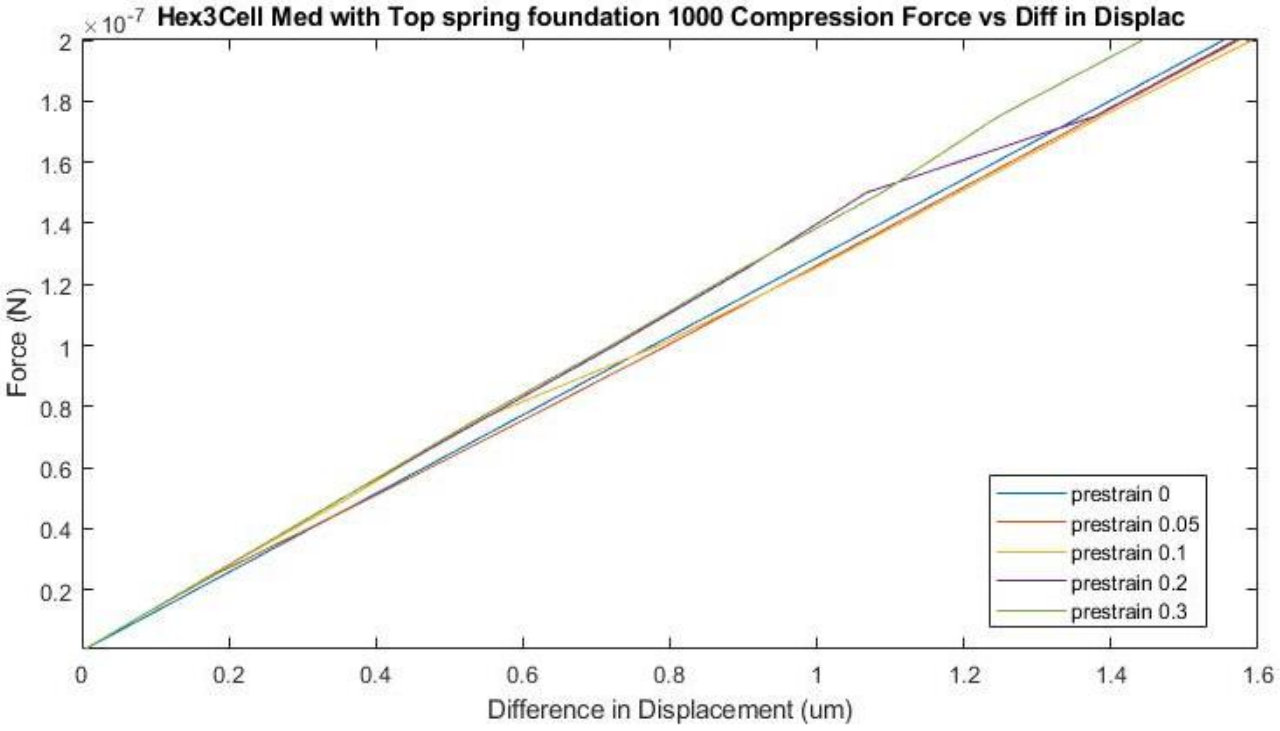

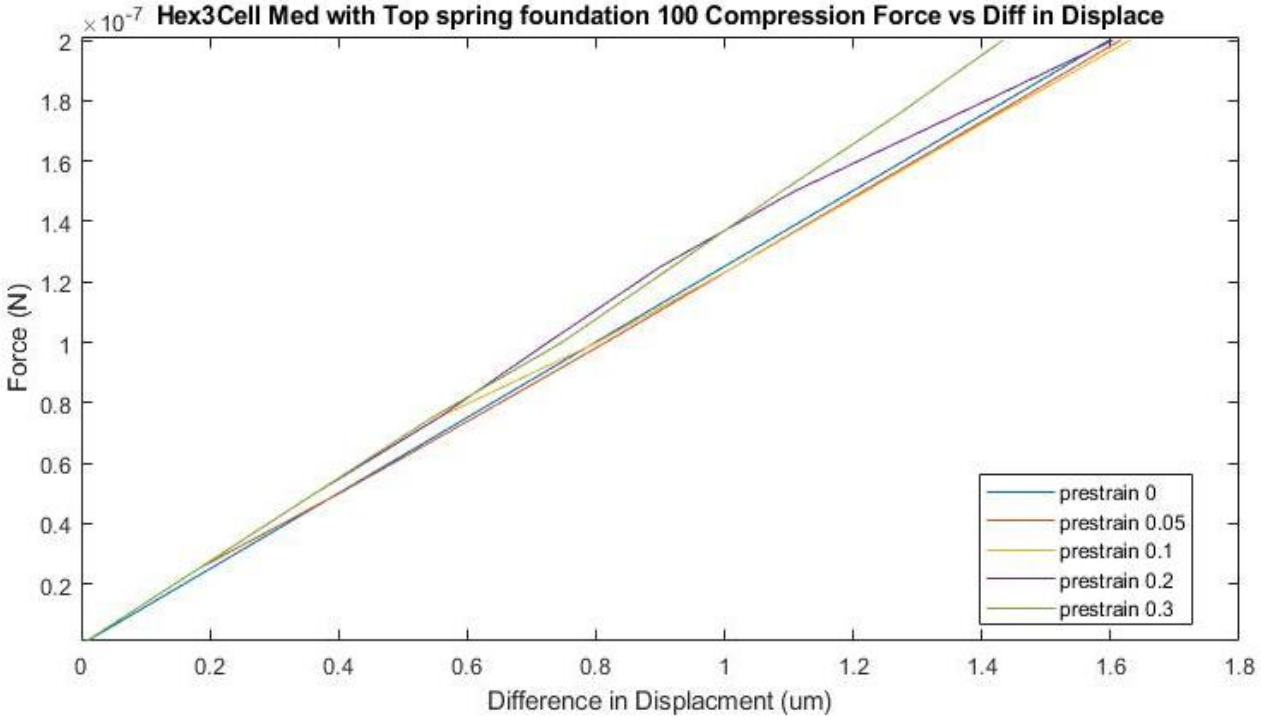
Hex3Cell Med with Top spring foundation 100 Compression Force vs Diff in Displace
×10^-7
Force (N)
Difference in Displacment (um)
prestrain 0
prestrain 0.05
prestrain 0.1
prestrain 0.2
prestrain 0.3

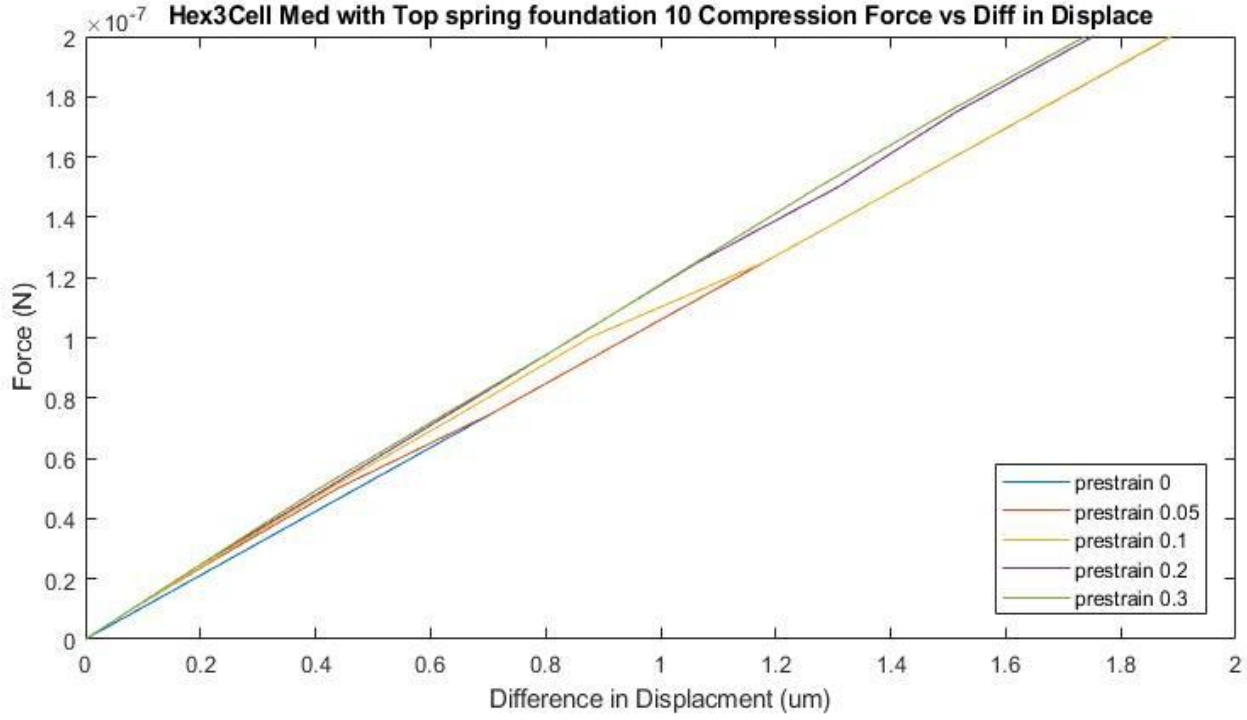
Hex3Cell Med with Top spring foundation 10 Compression Force vs Diff in Displace
×10^-7
Force (N)
Difference in Displacment (um)
prestrain 0
prestrain 0.05
prestrain 0.1
prestrain 0.2
prestrain 0.3

Varying spring foundations

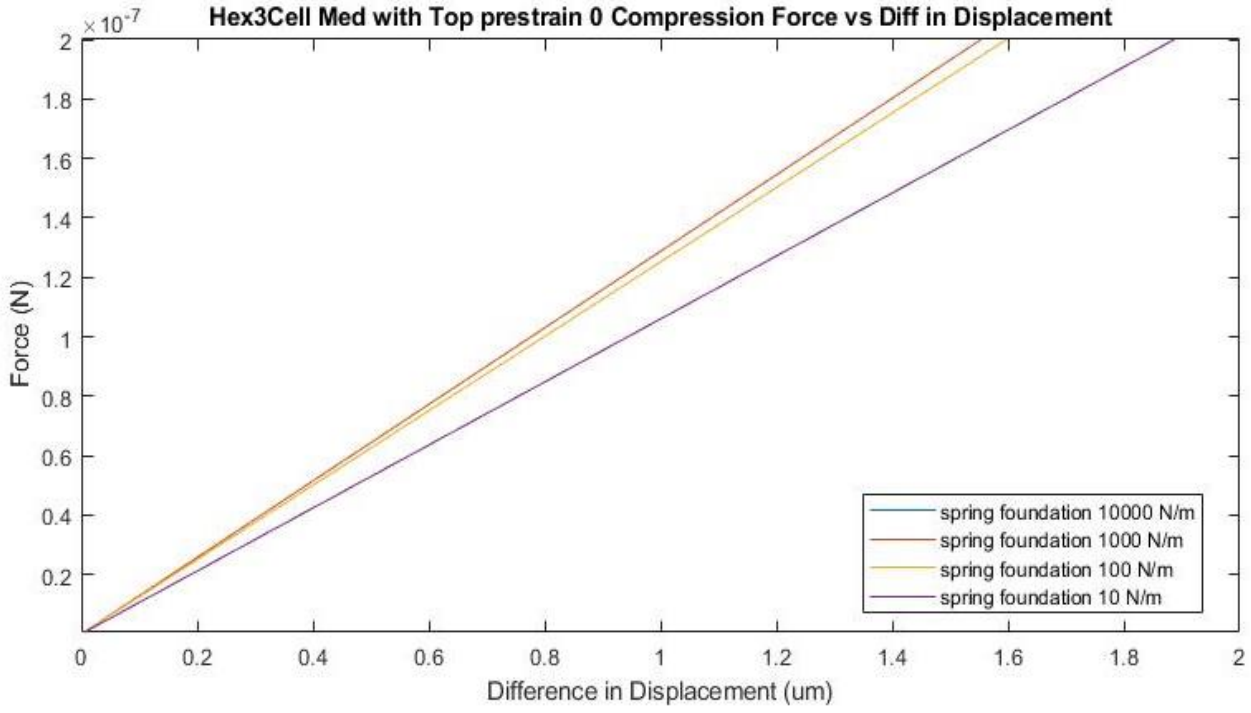

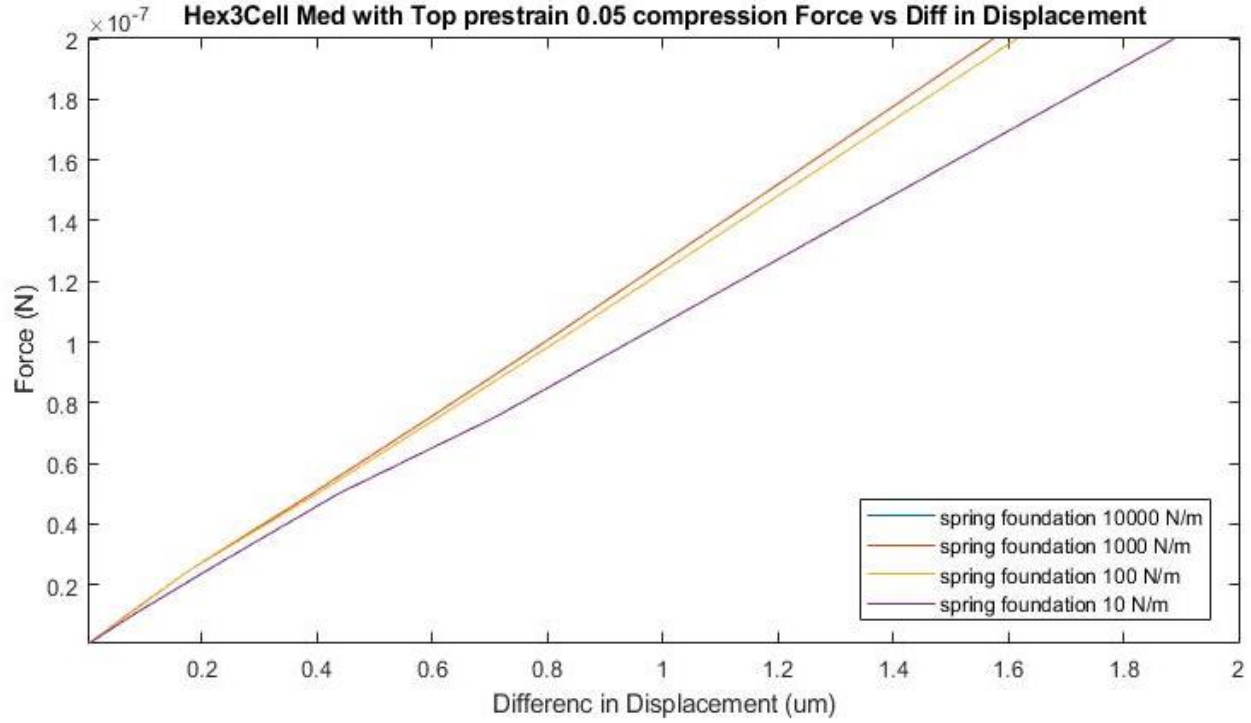

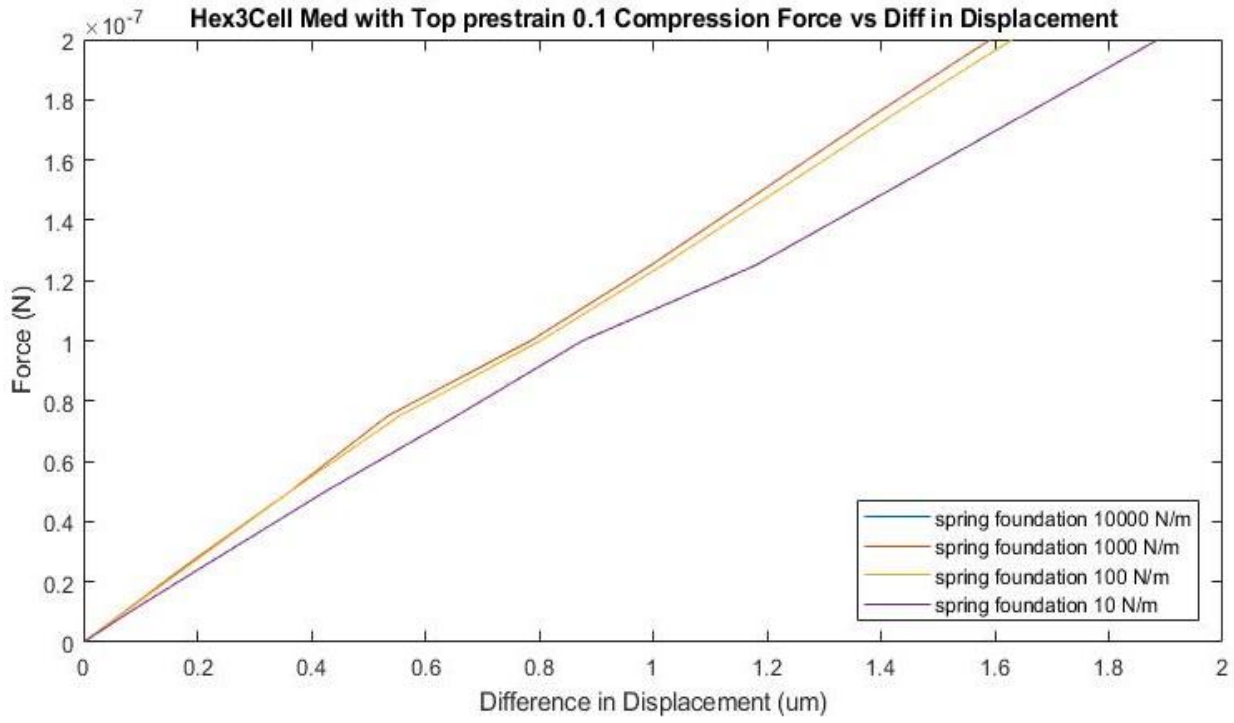
Hex3Cell Med with Top prestrain 0.1 Compression Force vs Diff in Displacement
×10^-7
Force (N)
Difference in Displacement (um)
spring foundation 10000 N/m
spring foundation 1000 N/m
spring foundation 100 N/m
spring foundation 10 N/m

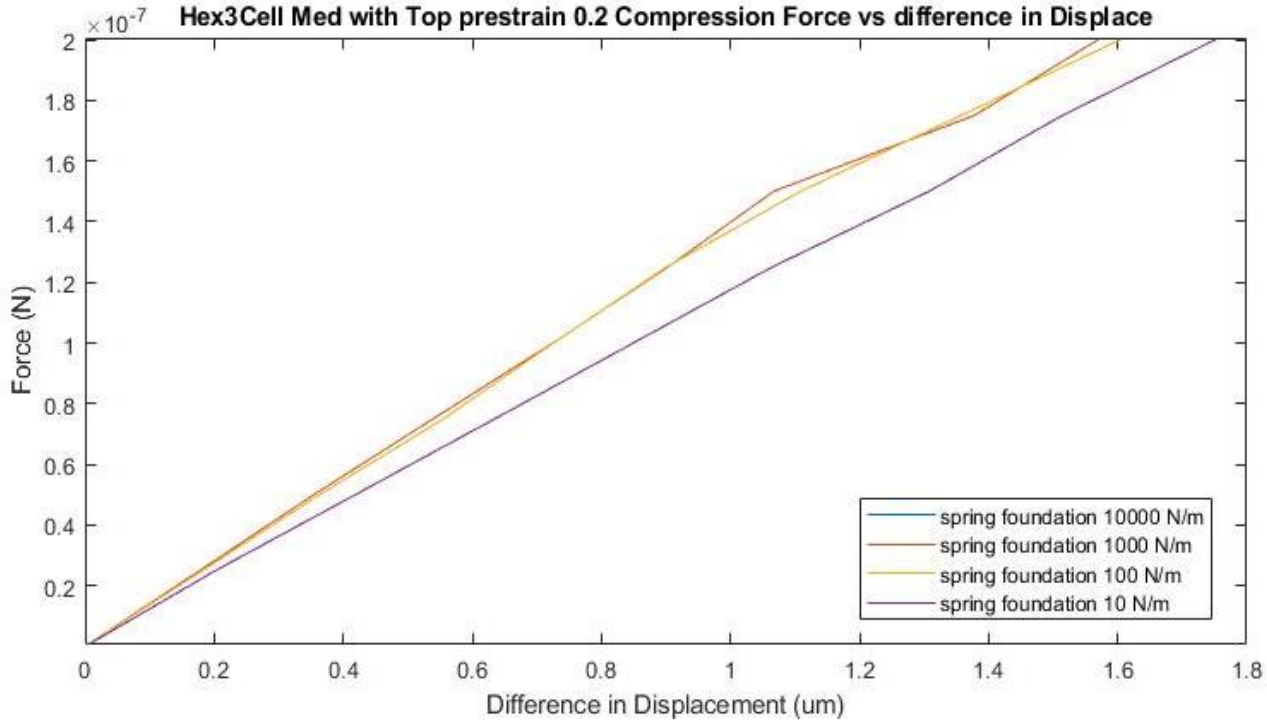
Hex3Cell Med with Top prestrain 0.2 Compression Force vs difference in Displace
×10^-7
Force (N)
Difference in Displacement (um)
spring foundation 10000 N/m
spring foundation 1000 N/m
spring foundation 100 N/m
spring foundation 10 N/m

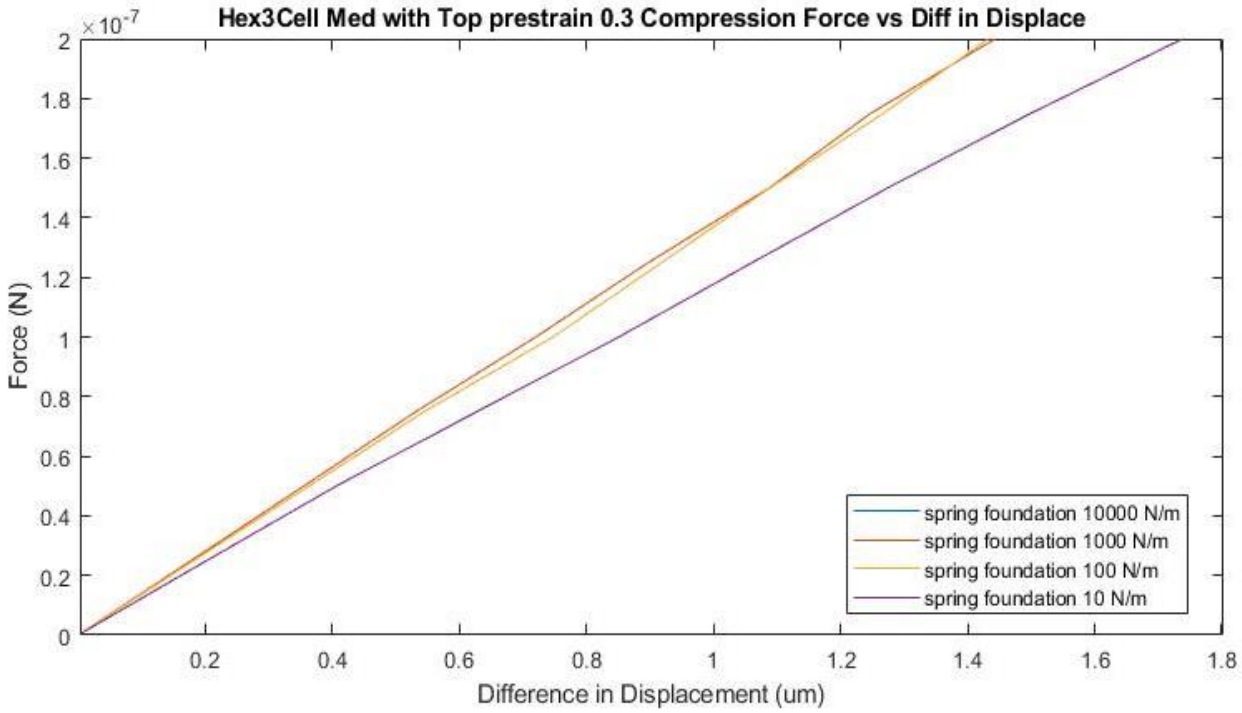

Tension graphs

Varying pre-strain

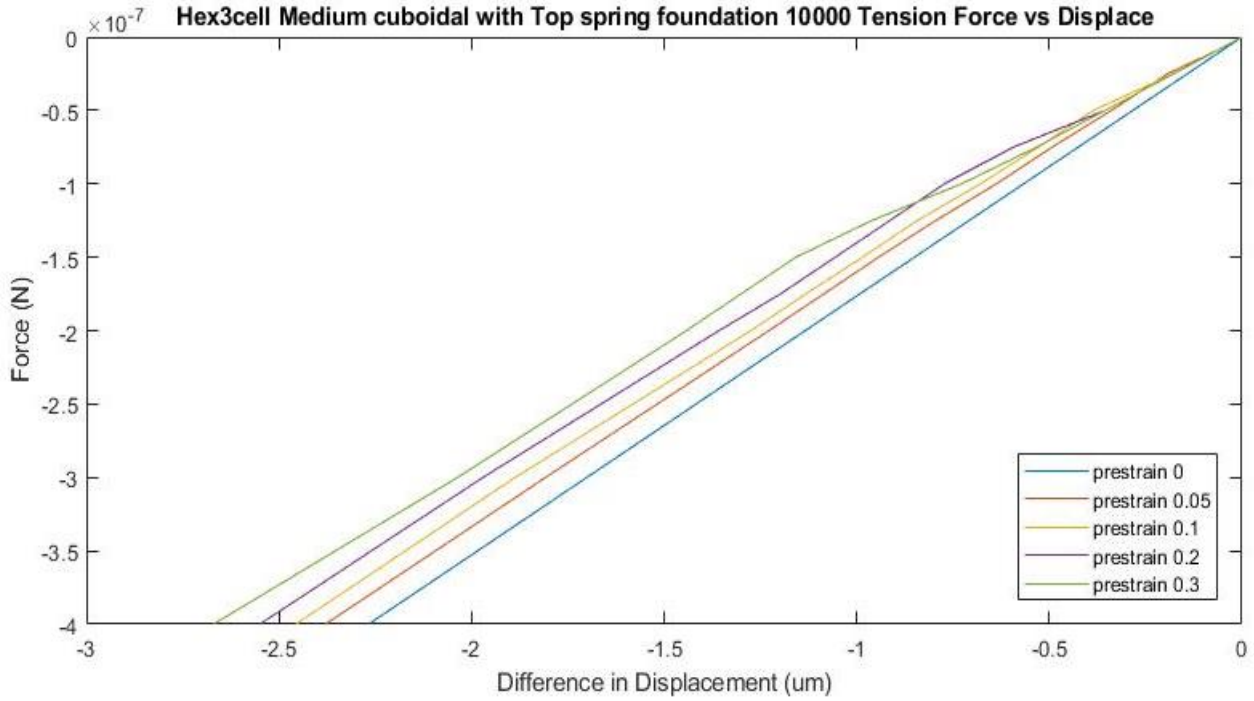

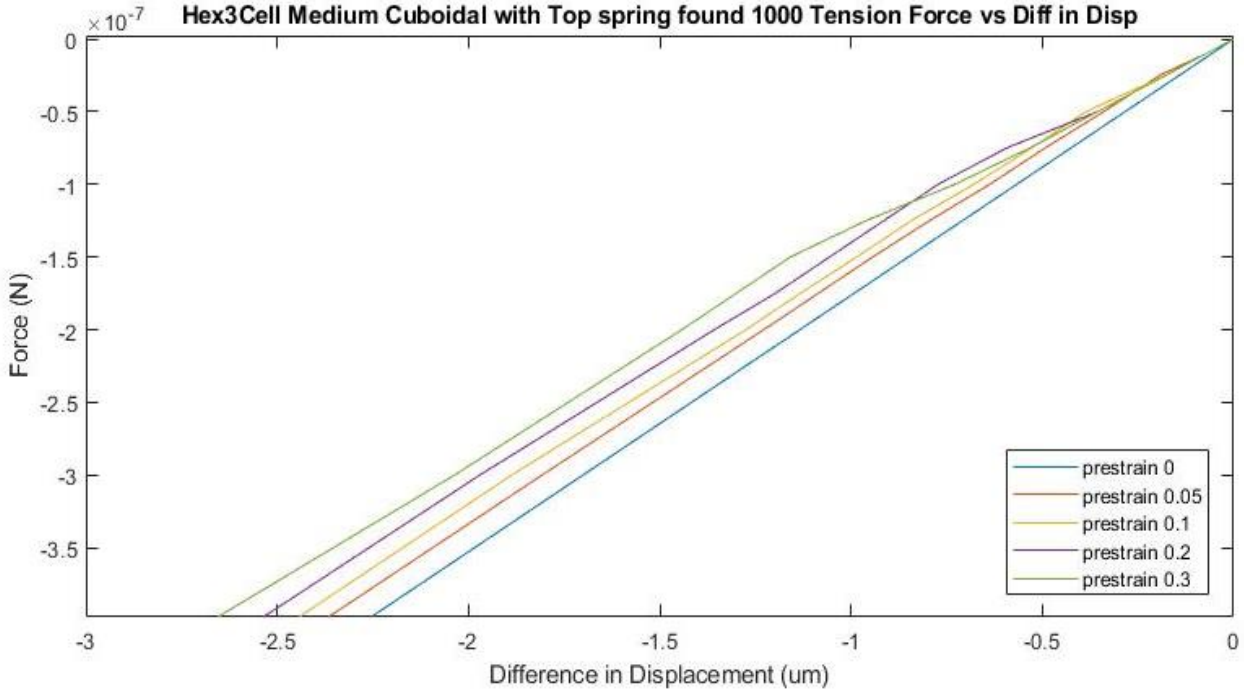
Hex3Cell Medium Cuboidal with Top spring found 1000 Tension Force vs Diff in Disp
×10^-7
Force (N)
Difference in Displacement (um)
prestrain 0
prestrain 0.05
prestrain 0.1
prestrain 0.2
prestrain 0.3

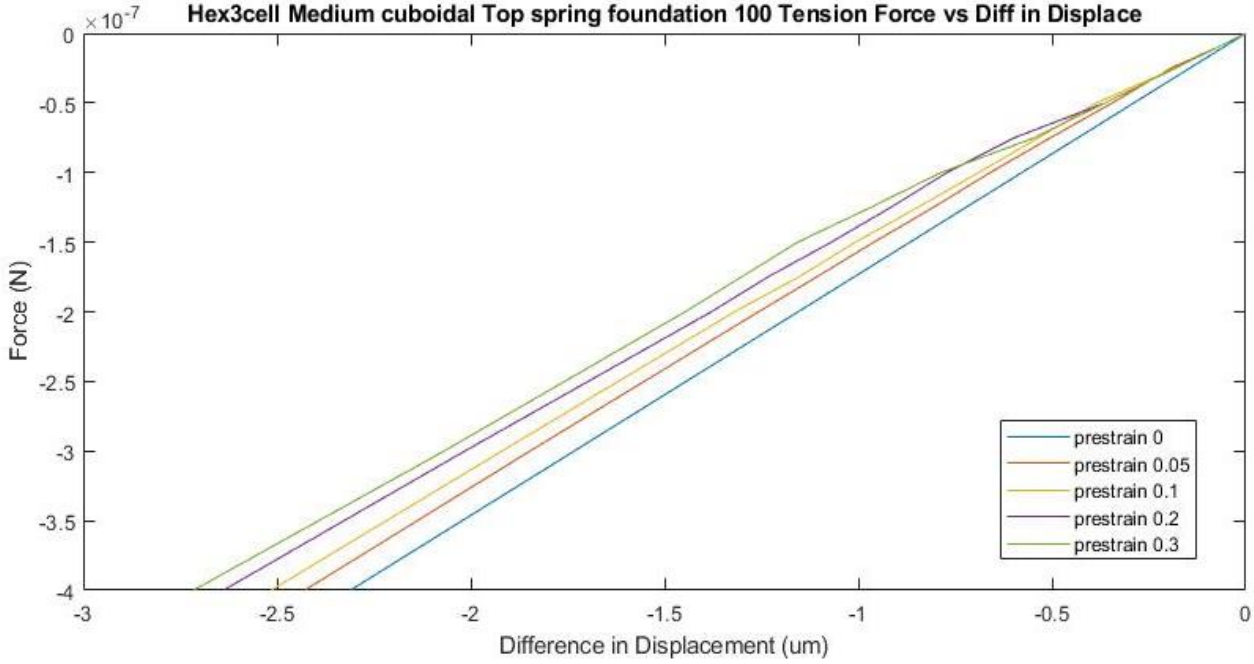
Hex3cell Medium cuboidal Top spring foundation 100 Tension Force vs Diff in Displace
×10^-7
Force (N)
Difference in Displacement (um)
prestrain 0
prestrain 0.05
prestrain 0.1
prestrain 0.2
prestrain 0.3

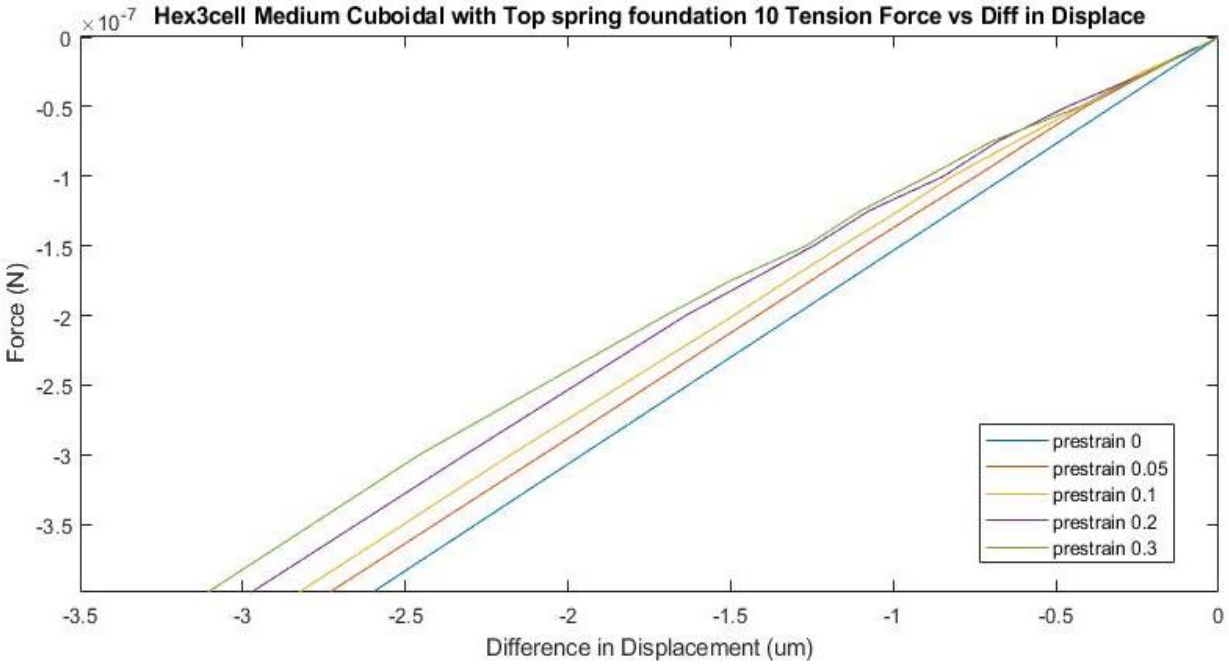

Varying spring foundation

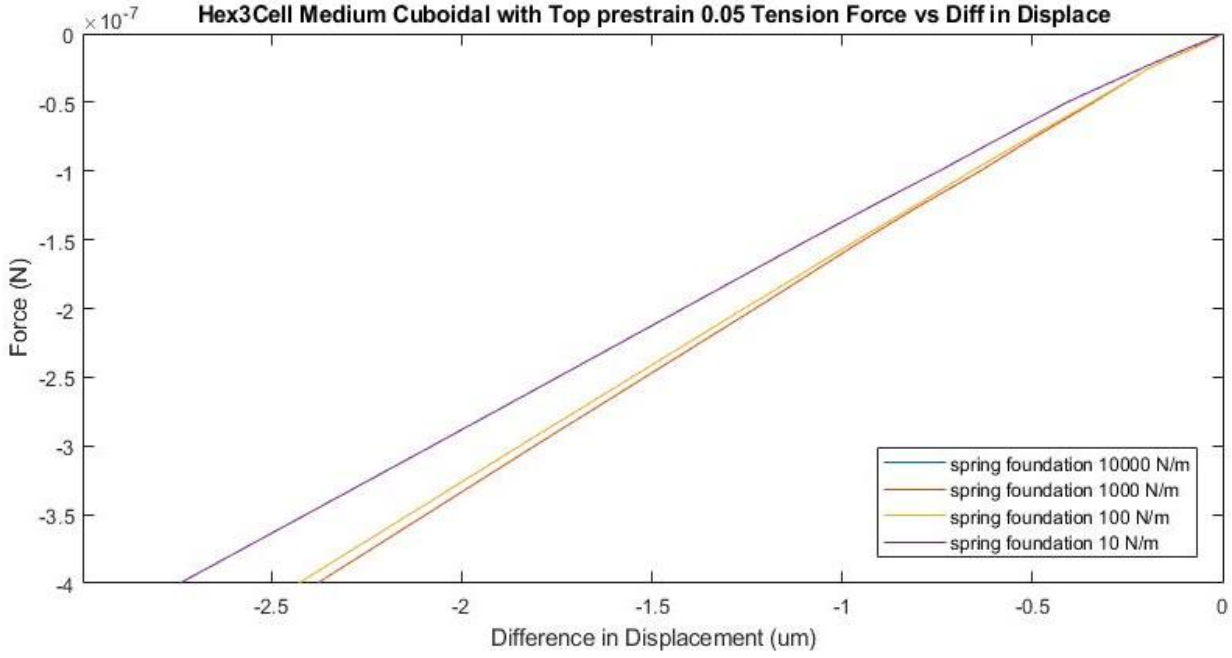

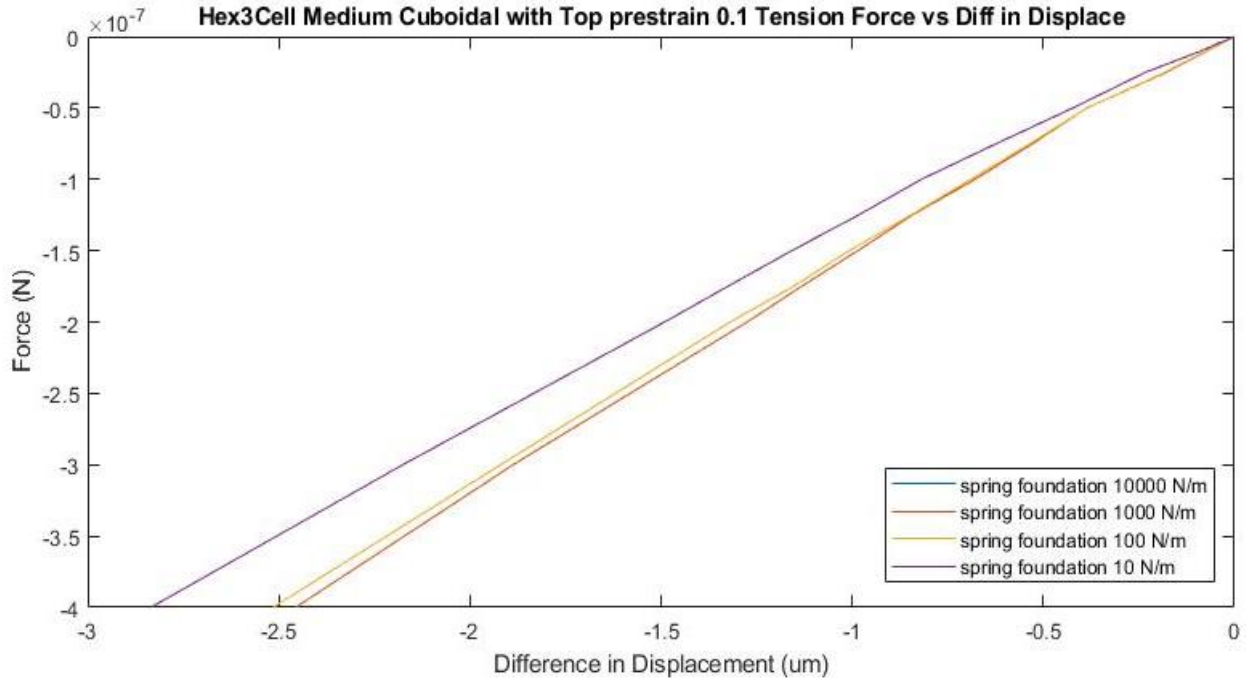

Cuboidal or Medium Height Model with Tensegrity Top

Compression varying pretrain

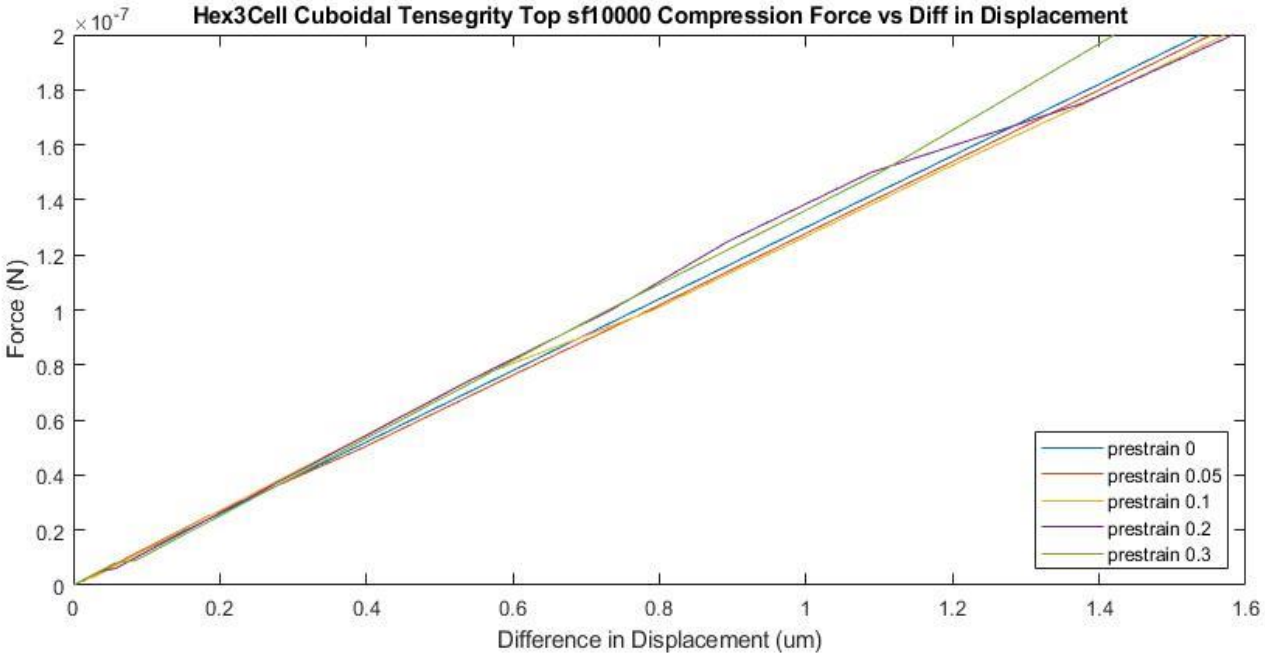

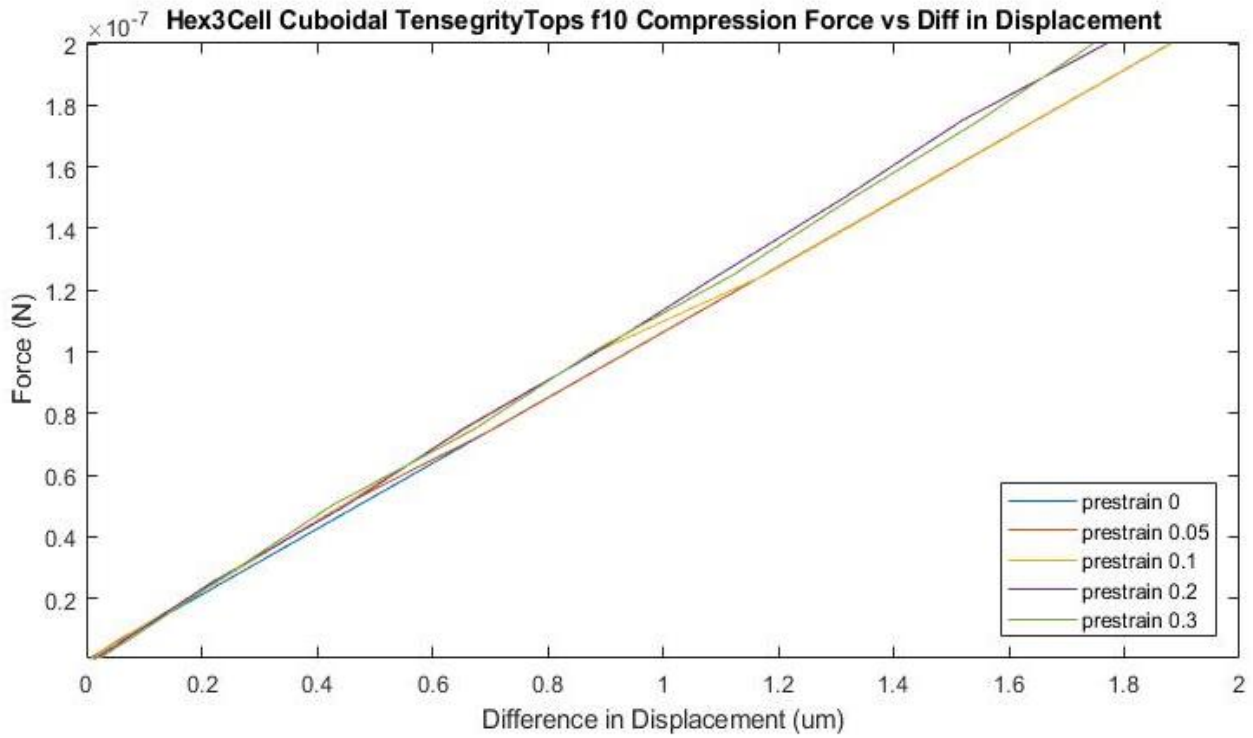

Tension Graphs

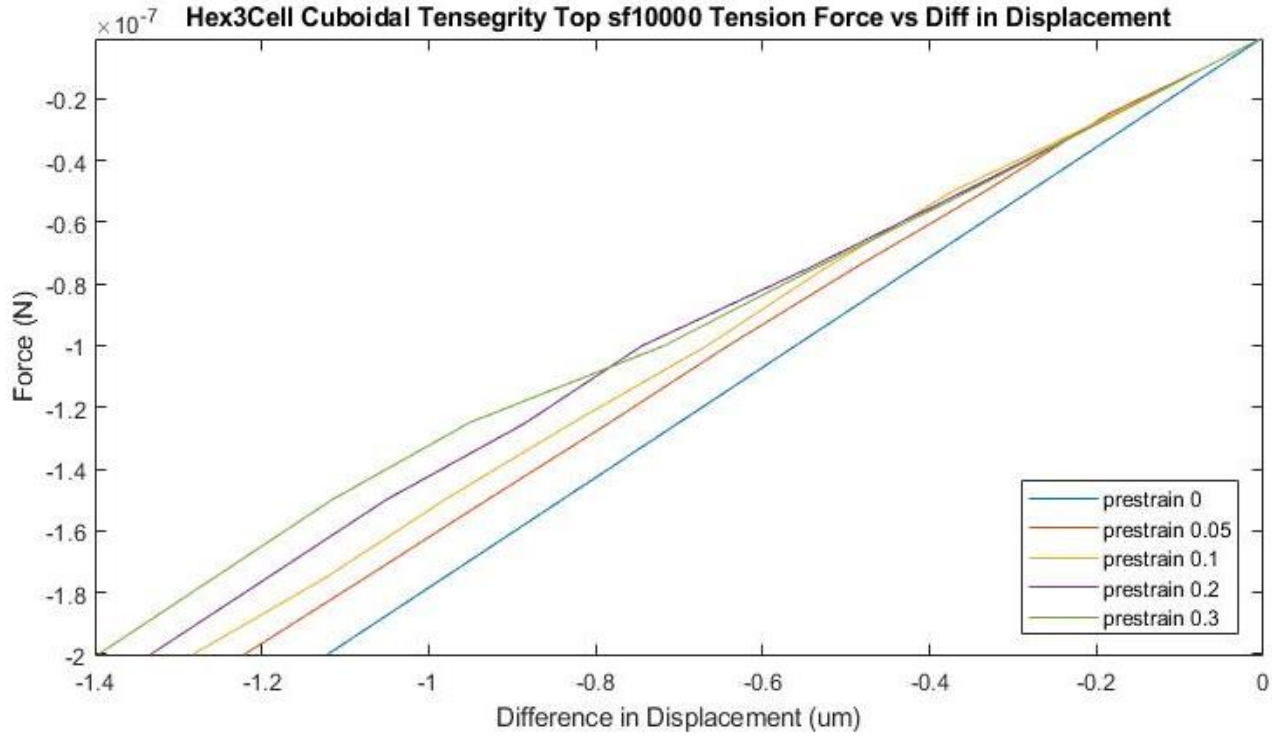

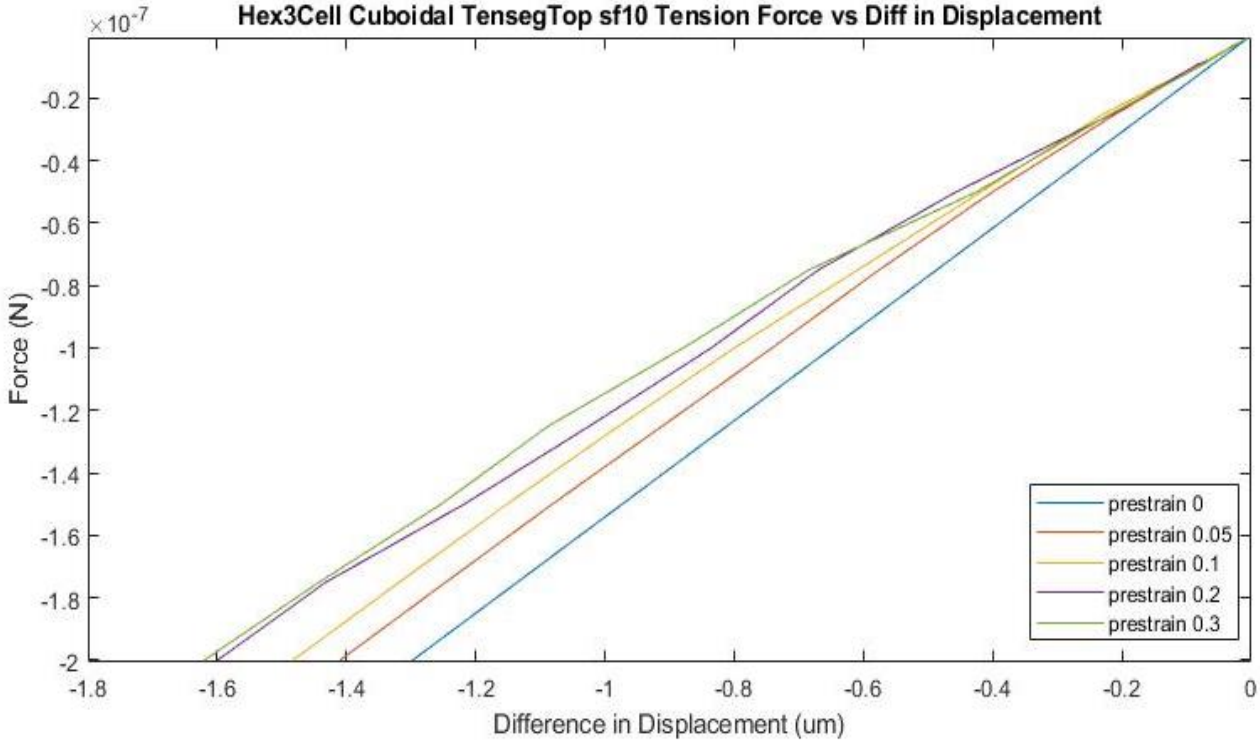
Hex3Cell Cuboidal TensegTop sf10 Tension Force vs Diff in Displacement
×10^-7
Force (N)
-0.2
-0.4
-0.6
-0.8
-1
-1.2
-1.4
-1.6
-1.8
-2
-1.8
-1.6
-1.4
-1.2
-1
-0.8
-0.6
-0.4
-0.2
0
Difference in Displacement (um)
prestrain 0
prestrain 0.05
prestrain 0.1
prestrain 0.2
prestrain 0.3

Cuboidal or Medium Height Model with Tensegrity Bottom

Compression Graphs

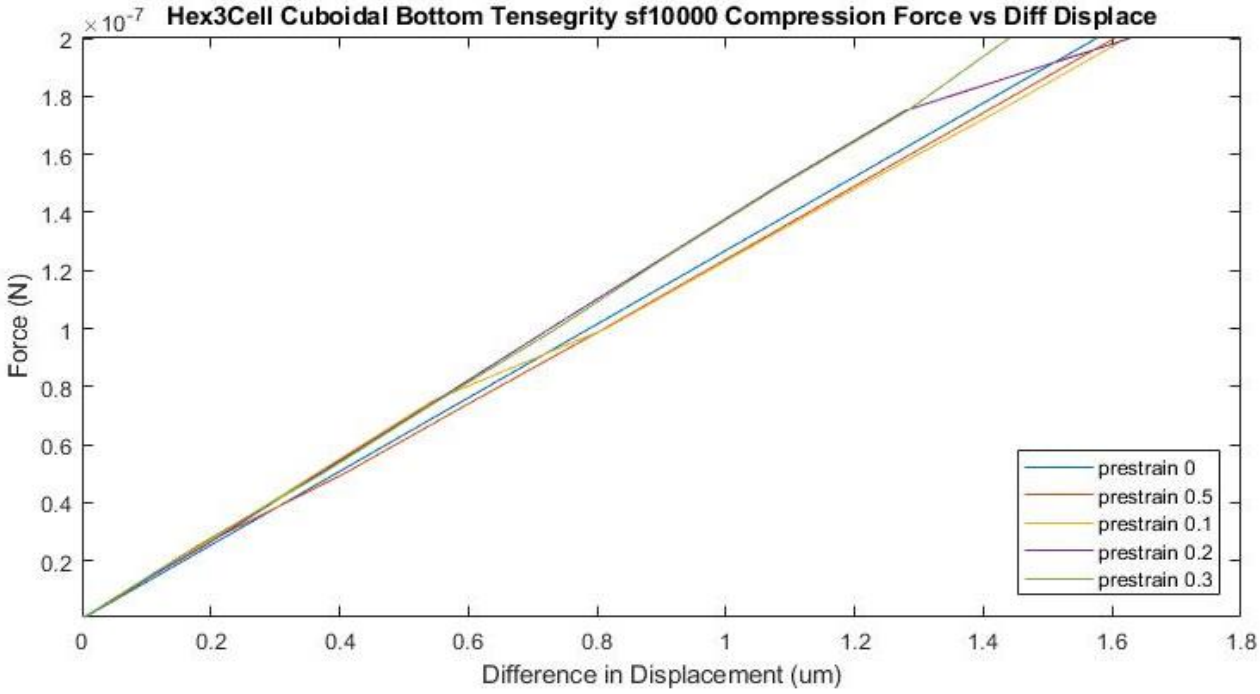

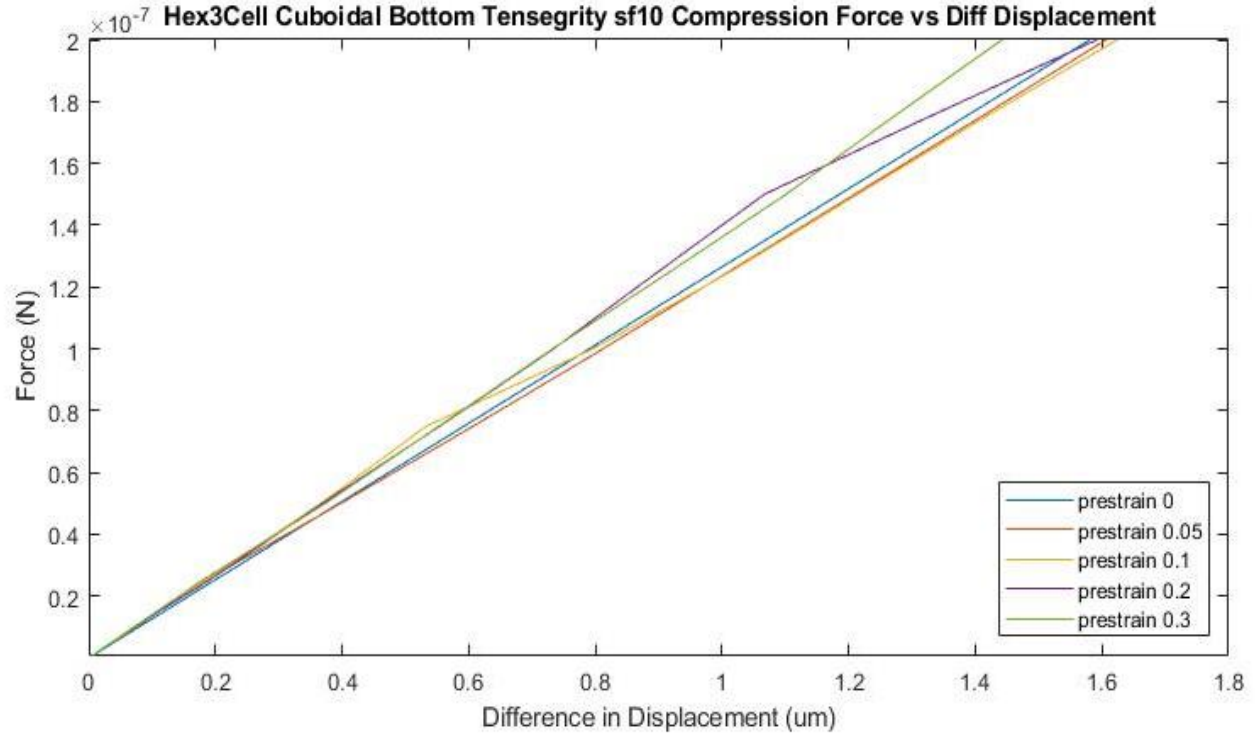

Tension Graphs

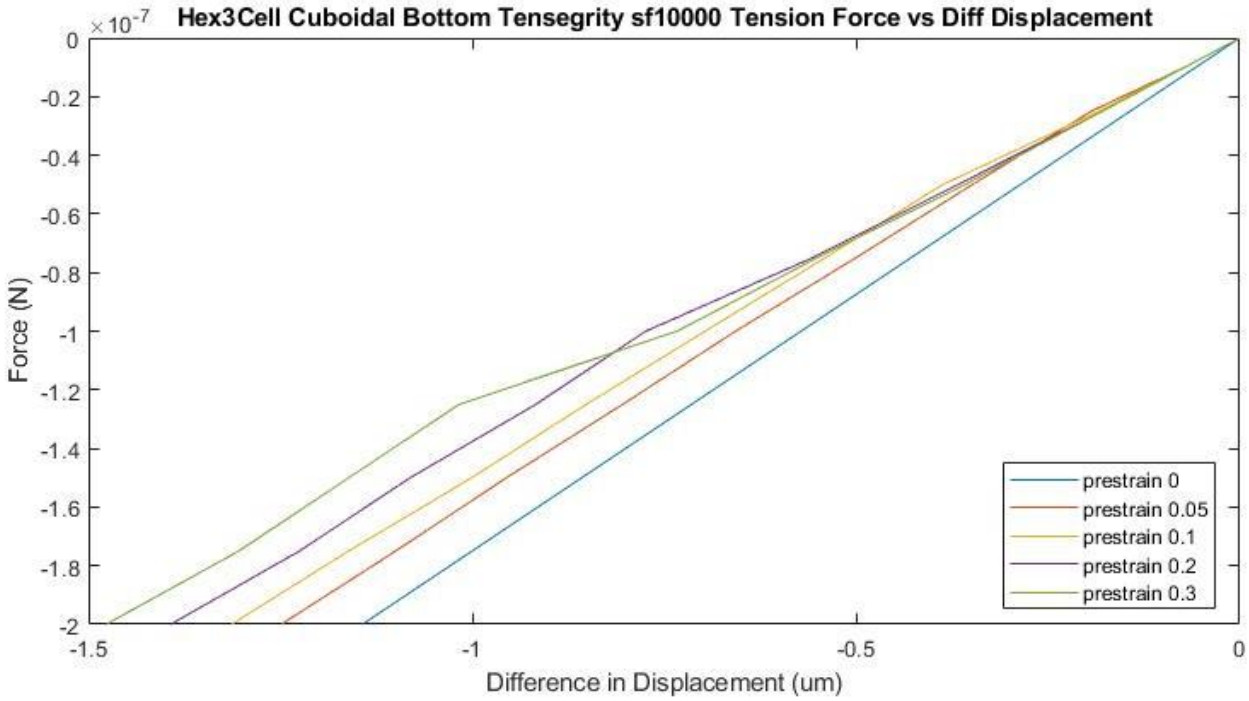

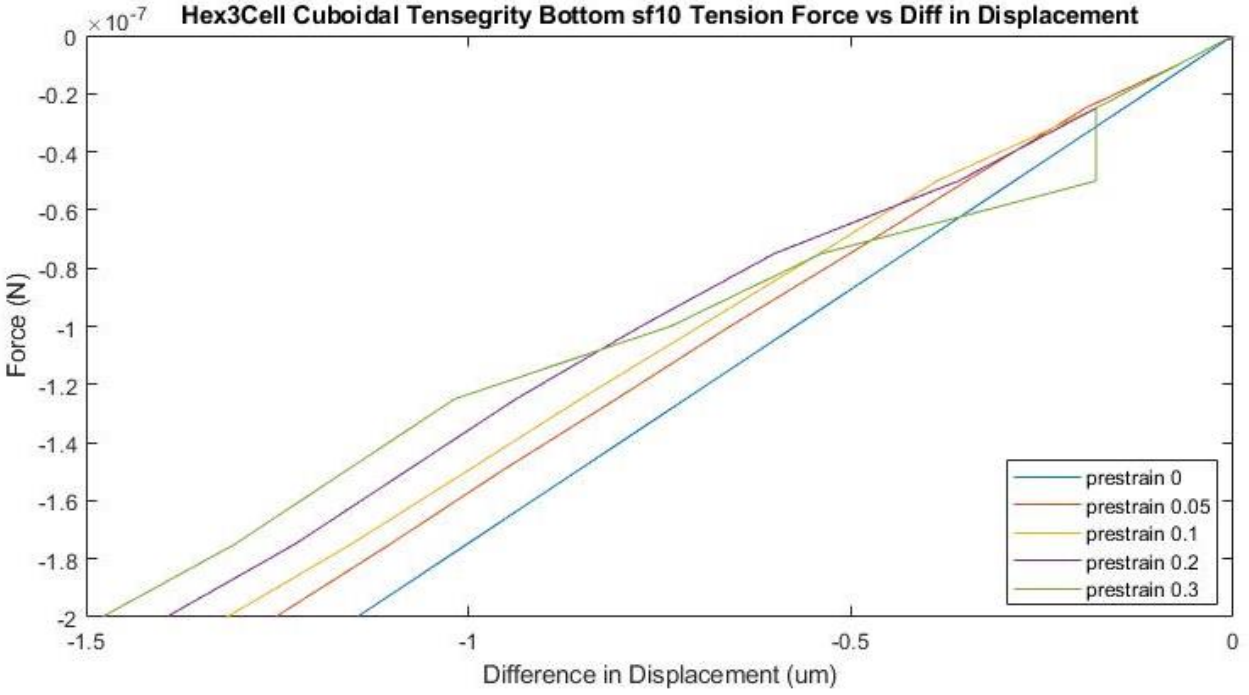

Cuboidal or Medium Height Model with k = 0.1

Compression Graphs

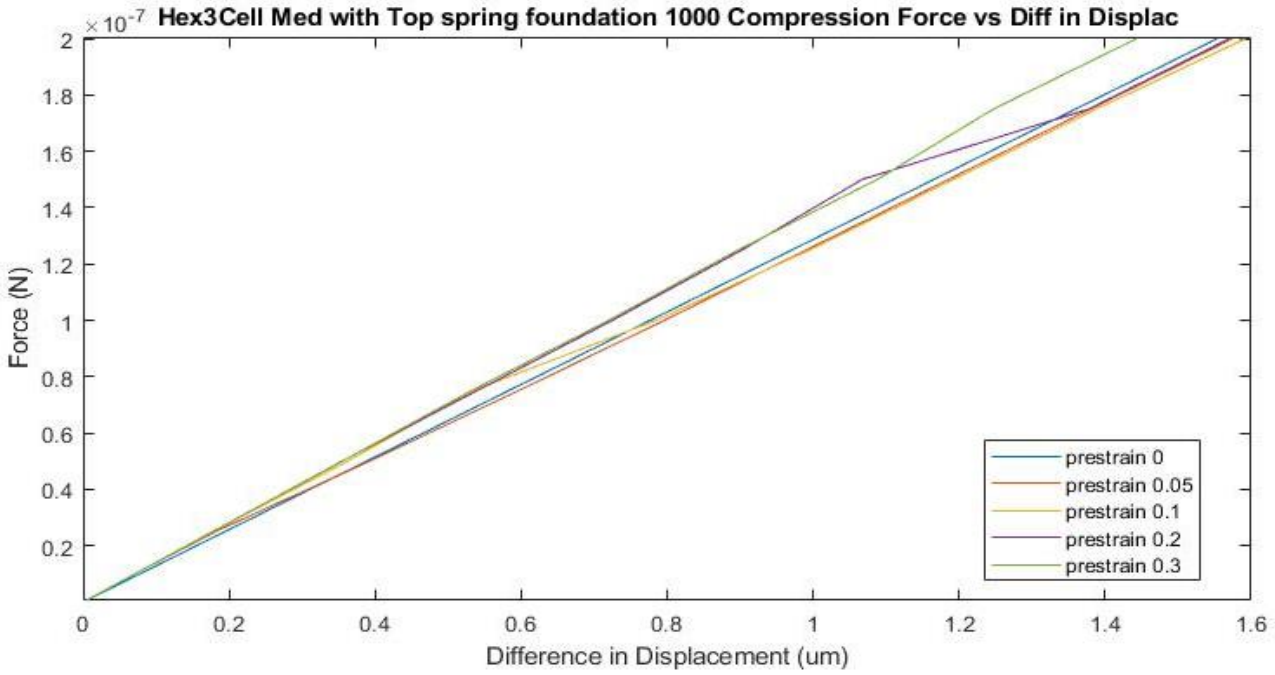

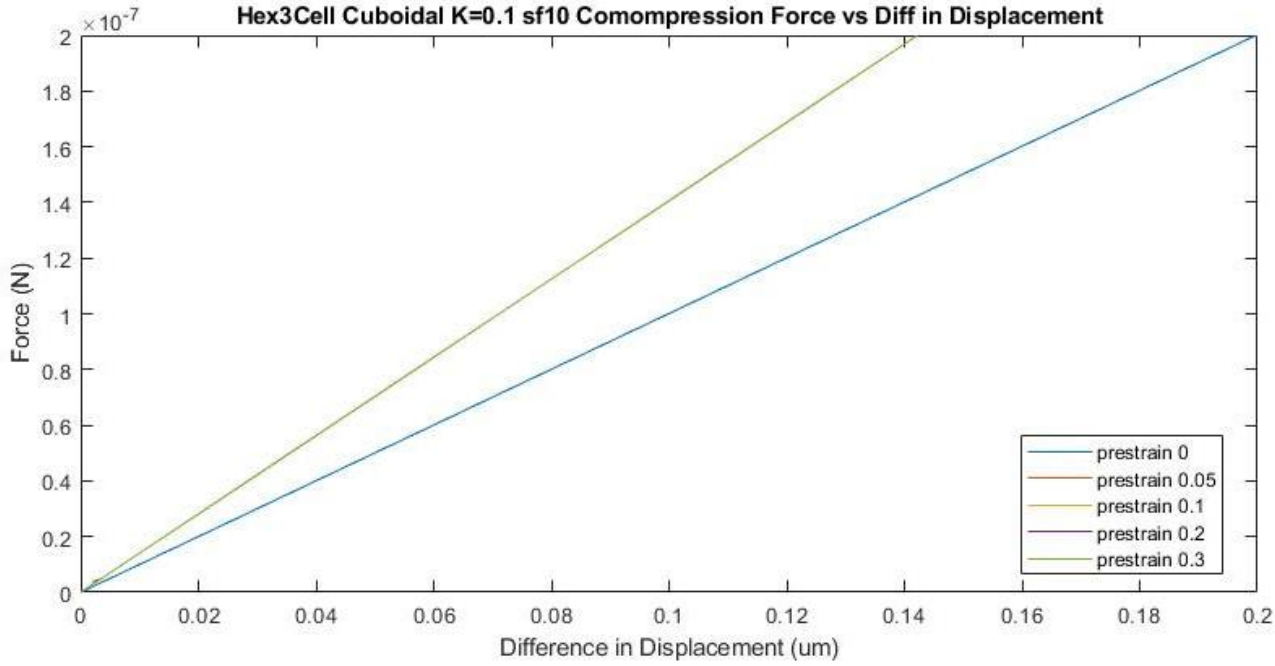

Tension Graphs